University of Thessaly
School of Engineering
Department of Mechanical Engineering

Diploma Thesis

Computational Non-local Plasticity of Porous Metals

by

SOCRATES D. XENOS

Submitted in Partial Fulfilment of the
Requirements for Diploma in Mechanical Engineering
2018

«οὐδέν τοῖς θαρροῦσιν ἀνάλωτον»
Μέγας Αλέξανδρος, 356-323 π.Χ.

Approved by the Three Members of the Advisory Committee:

First Member (Supervisor)

Professor Nikolaos Aravas
Department of Mechanical Engineering, University of Thessaly

Second Member

Assistant Professor Alexis Kermanidis
Department of Mechanical Engineering, University of Thessaly

Third Member

Assistant Professor Michalis Agoras
Department of Mechanical Engineering, University of Thessaly

Abstract

Computational Non-local Plasticity of Porous Metals

Socrates D. Xenos

Supervisor: Professor N. Aravas

This work is concerned with the formulation and the computational implementation of a rate-independent gradient plasticity anisotropic model for porous metals. The nonlocal effect is incorporated through the introduction of a nonlocal porosity variable, which is derived from the concurrent solution of an additional partial differential equation along with the classical equilibrium equations/equations of motion. This formulation is considered as 'implicit' in the sense that all higher gradients of the corresponding local variable are included and is proved to be equivalent to a fully nonlocal, internal format. The theoretical basis of the finite element method for the emerging mixed boundary value problem is examined thoroughly. The model is implemented through the 'user subroutine' UEL provided by the general purpose finite element program ABAQUS. A two-dimensional localization problem illustrating the ability to remove the pathological mesh-dependence of the corresponding local model and results from a series of finite element analyses for the investigation of the regularizing effect of the gradient model to the problem of ductile fracture of porous metals and the Charpy V-notch test are presented.

Keywords: Gradient Plasticity; Finite Element Method; Porous Metals; Localization;

Acknowledgements

If I had to describe my personal academic journey up to the point where this project has finally seen the day of light, I could do it with just 4 words: Easier said than done. Countless hours of hard work, intense study till very late at night, tremendous handwriting and constantly being on the move literally became a routine among short glimpses of relaxation with friends and family somewhere in between.

The first person I would deeply like to thank is no other than my supervisor, Professor Nikolaos Aravas, who entrusted me this intriguing and highly challenging topic. With his unique ability as a teacher to simplify and clearly present even the most difficult notions, he rendered attendance to his classes a pleasant experience and without his invaluable guidance during the latest years of my studies, I couldn't have come this far. It was an honor being his student and his personality, both as a person and as a teacher, will inspire me for the rest of my life. I would also like to express my deepest appreciation to Assistant Professors Alexis Kermanidis and Michalis Agoras for accepting being members of my advisory committee.

Undoubtedly, I'd like to recognize the assistance of all the faculty members, lab and teaching assistants that I had the chance to meet during these years who all contributed to me taking a first step into engineering. Among them, I would like to express my sincere gratitude to Professor Gregory N. Haidemenopoulos for his constant support and precious help concerning various critical issues throughout the years. Furthermore, I am deeply indebted to Assistant Professor Michalis Agoras, not only because he encouraged me in my decision to be engaged with computational mechanics in the first place, but also for our fruitful discussions regarding both scientific and social subjects. I also wish to thank Dr. Anna Zervaki especially for her moral support, during the last two years of my studies. The completion of this thesis would not, by any means, be possible without the immense support of Postdoctoral researcher Ioanna Papadioti, who not only introduced me to the finite element program ABAQUS but also contributed, with her crucial advise, to the completion of this project.

Moreover, I could not be more grateful to my parents, who patiently supported me in every way all of these years in this strenuous effort and to my older brother, for being the person I looked up to due his passion for evolution and excellence. Last but not least, I would like to thank from the depths of my heart my closest people namely, Giorgos, Kostas, Kostis, Apostolis, Stavros, Marina, Anna, Despoina and Dimitra, for their faith in me and for all the great moments we had together all of these years.

Contents

List of Figures

List of Tables

Introduction

In physical phenomena related to large plastic deformations, such as metal forming processes or failure of ductile materials, softening behavior eventually emerges at some region of the structure and deformation localizes severely into narrow zones of infinitesimal size. As is well known, computational modeling of such processes via conventional continuum (also known as local) elastic-plastic theories suffers from an insufficiency to provide an objective description of the corresponding failure mode in the sense that numerical results fail to converge to a unique solution as the discretization becomes more dense. This inherent problematic behavior can be attributed to the fact that, classical material models, which do not incorporate a characteristic material length, are invariant to spatial transformations which implies that material response is modeled in the same manner for all length scales. However, in order to accurately capture phenomena that take place in a microstructural level and alleviate the aforementioned deficiency, more information needs to be included in the corresponding numerical models.

In the context of plasticity theories, various approaches have been proposed in literature for the restoration of the well-posedness of the governing boundary value problem and the consequent regularization of the problem, all of which include an intrinsic material length scale and formulate the so-called nonlocal theories. An in-depth review and comparison of such models has been carried out by Rolshoven in [75]. In the recent years, in regard to metal materials, fundamental progress in the field of nonlocal plasticity models has been made, both from a theoretical and an applied point of view, as seen, for instance, in the works of Benallal and Tvergaard [11], de Borst *et al.* [24], Engelen *et al.* [26], Peerlings *et al.* [61], Pijaudier and Bažant [62], Ramaswamy and Aravas [68], [69], and Tvergaard and Needleman [83], [84]. Although the regularization procedures described by these models, which include enhancements both of an integral and of a gradient manner either of the kinematic or the constitutive equations, proved to be rather effective in the removal of the pathological mesh-dependancy of their local counterparts, the majority of them has, nonetheless, been tested in conjuction with material models that admit only isotropic macroscopic behavior.

The current endeavor focuses on the formulation of an implicit elastic-plastic anisotropic material model of the gradient type based on corresponding material model presented by Aravas and Ponte Castañeda in [7]. Computational implementation of the latter is realized through a 'user subroutine' that can be incorporated to the general purpose, commercial

finite element program ABAQUS, which is used as a solver for the discretized field equations that are involved. To be precise, the first two chapters serve as brief summary of the fundamental aspects of the classical continuum mechanics and finite deformation elastoplasticity theories, both of which build the general theoretical background necessary for the construction of the gradient anisotropic model. Chapter 3 offers an insight on the primary reasons behind the inobjective behavior of the local models with respect to discretization and also introduces the basic theoretical framework concerning the nonlocal theories. In Chapter 4, the nonlocal version of the anisotropic model is formulated, the corresponding 'tangent moduli' are derived and a mixed implicit-explicit scheme for the numerical integration of the constitutive equations is presented. Thereafter, the next chapter is devoted to the introduction of the finite element method, which is used for the solution of the mixed boundary value that emerges, and the calculation of the 'structural stiffness matrix' accounting for finite deformations. Finally, in Chapter 6, the results from finite element calculations that were carried out in order to investigate the effect of the regularization for a series of specific problems, are presented.

Standard notation is used throughout. Fraktur symbols $\mathfrak{B}$, $\mathfrak{P}$ denote body configurations and material points respectively while normal Lucida calligraphic symbols such as $\mathcal{E}$ are reserved for vector spaces. Boldface symbols denote tensors the orders of which are indicated by the context. All tensor components are written with respect to a fixed Cartesian coordinate system with base vectors $\mathbf{e}_i$ $(i = 1, 2, 3)$, and the summation convention is used for repeated Latin indices, unless otherwise indicated. The prefice det indicates the determinant, a superscript T the transpose, a superposed dot the material time derivative, and the superscripts *sym* and *skew*, enclosed in parentheses, the symmetric and anti-symmetric parts of a second order tensor. Let $\mathbf{a}$, $\mathbf{b}$ be vectors, $\mathbf{A}$, $\mathbf{B}$ second-order tensors, and $\boldsymbol{\mathcal{C}}$, $\boldsymbol{\mathcal{D}}$ two fourth-order tensors; the following products are used in the text: $(\mathbf{a}\,\mathbf{b})_{ij} = a_i\, b_j$, $\mathbf{A} : \mathbf{B} = A_{ij}\, B_{ij}$, $(\mathbf{A} \cdot \mathbf{B})_{ij} = A_{ik}\, B_{kj}$, $(\mathbf{A}\,\mathbf{B})_{ijkl} = A_{ij}\, B_{kl}$, $(\boldsymbol{\mathcal{C}} : \mathbf{A})_{ij} = \mathcal{C}_{ijkl}\, A_{kl}$, and $(\boldsymbol{\mathcal{C}} : \boldsymbol{\mathcal{D}})_{ijkl} = \mathcal{C}_{ijpq}\, \mathcal{D}_{pqkl}$. The inverse $\boldsymbol{\mathcal{C}}^{-1}$ of a fourth-order tensor $\boldsymbol{\mathcal{C}}$ that has the "minor" symmetries $\mathcal{C}_{ijkl} = \mathcal{C}_{jikl} = \mathcal{C}_{ijlk}$ is defined so that $\boldsymbol{\mathcal{C}} : \boldsymbol{\mathcal{C}}^{-1} = \boldsymbol{\mathcal{C}}^{-1} : \boldsymbol{\mathcal{C}} = \boldsymbol{\mathcal{I}}$, where $\boldsymbol{\mathcal{I}}$ is the symmetric fourth-order identity tensor with Cartesian components $\mathcal{I}_{ijkl} = (\delta_{ik}\, \delta_{jl} + \delta_{il}\, \delta_{jk})/2$, δ_{ij} being the Kronecker delta.

Chapter 1

Continuum Mechanics Theory

In this chapter, the fundamentals of continuum mechanics theory is presented. The first part of the chapter is concerned with the kinematics of deformation and more specifically with the general mathematical description of geometrical variations of a deformable body and the most general definition of the notion of strain. Thereinafter, various stress measures and their physical interpretation is summarized and the equations of motion are derived. In the final part, a brief reference is made on objectivity, objective rates of tensorial quantities and theory and purpose of constitutive equations. Most proofs are omitted but the reader is mostly referred to [10], [14], [15], [51] and [52] for further study[1].

1.1 Notion of a Continuum Medium

From a microscopic point of view, real *material objects* can be thought as an assemblage of discrete units of matter such as molecules, atoms etc. with gaps existing between them i.e. matter is not continuously distributed in space. Nevertheless, modeling of usual applications with the so called macroscopic theory, which neglects this kind of microscopic information, proves to be sufficiently accurate. Thus, in the context of macroscopic analysis of solids and fluids, also known as *continuum mechanics theory*, the notion of a hypothetical *continuum medium* is introduced, which is a material object whose mass is continuously distributed. This assumption allows the definition of material properties in every point $\mathbf{x}$ of the region of the Euclidean space $\mathcal{E}$ that the body currently occupies at time t.

Body and Configuration in Euclidian Space

Before one proceeds with the description of deformation in continuum bodies it would be useful, mostly for the sake of completeness, to qualitatively explain what in fact is a *continuum material body* what are the different *configurations* it can occupy at a certain time and how this material body is distinct from the region it is located in.

[1] Large portion of this chapter is also based on lecture notes from the Continuum Mechanics class of Prof. N. Aravas. Responsibility for any errors solely concerns the author.

Let $\mathcal{E}$ denote the geometric Euclidean space which is modeled by the set $\mathbb{R}^3$ of real numbers. One can assume that this space is made up of an infinite number of subregions $\mathcal{B}_i, i = 1, .., \infty$ such that the parent space can be constructed as the union of them:

$$\mathcal{B}_1 \cup \mathcal{B}_2 \cup \cdots \cup \mathcal{B}_\infty = \mathcal{E} \tag{1.1}$$

Consider now a continuum material object, which hereafter will simply be referred as *body* and denoted by $\mathfrak{B}$, that occupies a region $\mathcal{B}_i$ in space $\mathcal{E}$ at time t. The body $\mathfrak{B}$ can be thought to consist of an infinite number of "material points" (particles) $\mathfrak{P}_i, i = 1, ..., \infty$ each of which, due to the assumption of the continuum medium, corresponds to a unique position $\mathcal{P}_i$ in the region $\mathcal{B}_i$ of $\mathcal{E}$ at the moment t. Then, the notion of body can be qualitatively defined as a continuous particle distribution with the properties that each particle $\mathfrak{P}_i$ of $\mathfrak{B}$ occupies a unique position $\mathcal{P}_i$ of region $\mathcal{B}_i$ at time t and every position $\mathcal{P}_i$ of region $\mathcal{B}_i$ at time t is the position of a material point $\mathfrak{P}_i$ of body $\mathfrak{B}$ that occupies region $\mathcal{B}_i$. The last statement implies that, according to the continuum medium hypothesis, there exists a one-to-one mapping between the particles of a body and the geometric points of the region this body occupies at a given time t. This in turn leads to the conclusion that at *a specific time t* it is impossible for two particles $\mathfrak{P}_i$and$\mathfrak{P}_j$ to occupy the same point $\mathcal{P}$ in space and vice versa.

As suggested by (1.1) Euclidean space $\mathcal{E}$ can be subdivided into an infinite number of subregions $\mathcal{B}_i, i = 1, ..., \infty$. Moreover, as stated above, at a specific time t the body $\mathfrak{B}$ occupies the geometric region $\mathcal{B}_t$ and therefore as the continuum medium moves (deforms,translates and rotates) in $\mathcal{E}$ it then transitions from region $\mathcal{B}_t$ to $\mathcal{B}_{t'}$ i.e. it changes *configuration*. Consequently, the configuration of a body $\mathfrak{B}$ "evolves" with time so that a body can theoretically have an infinite number of configurations in space $\mathcal{E}$ which also means that, at different configurations, the same material point can correspond to a different position and thus have an infinite number of possible positions in $\mathcal{E}$. In this sense, it is possible to speak of *material points*, *material fibers*, *material areas* and *material volumes* of a body at a given time t (configuration) which coincide with the corresponding positions, curves etc. that they occupy in the specific subregion of $\mathcal{E}$.

In order to mathematically describe the motion and deformation of a body it is necessary to define an otherwise arbitrary configuration of the body, hereafter referred as *the reference configuration or undeformed*, which is naturally defined as the configuration of the body at the time t_0 when observation of the body begins. More specifically, results concerning the deformation of the body are deduced from the comparison of this reference state with any subsequent configuration of the body at a time $t > t_0$. In general, time t_0 is arbitrary but usually $t_0 = 0$ is chosen.

It is also worth noting that making use of the reference configuration one can define the "identity" of a material point $\mathfrak{P}$ as the position vector $\mathbf{X}$ of the particle at time t_0 in the

sense that at any given time a unique particle $\mathfrak{P}$ corresponds to a position $\mathcal{P}$ and since examination of the body begins from the undeformed configuration, $\mathbf{X}$ can only correspond to the specific particle $\mathfrak{P}$.

Motion and the Deformation Gradient

Using the notions introduced in Section 1.1 one can now describe the motion and subsequently the deformation of a body. Consider a body that at the reference configuration at time t_0 occupies a volume V_0 and at the current configuration at time t a volume V_t along with a material point A whose motion is examined, as shown in Figure 1.1:

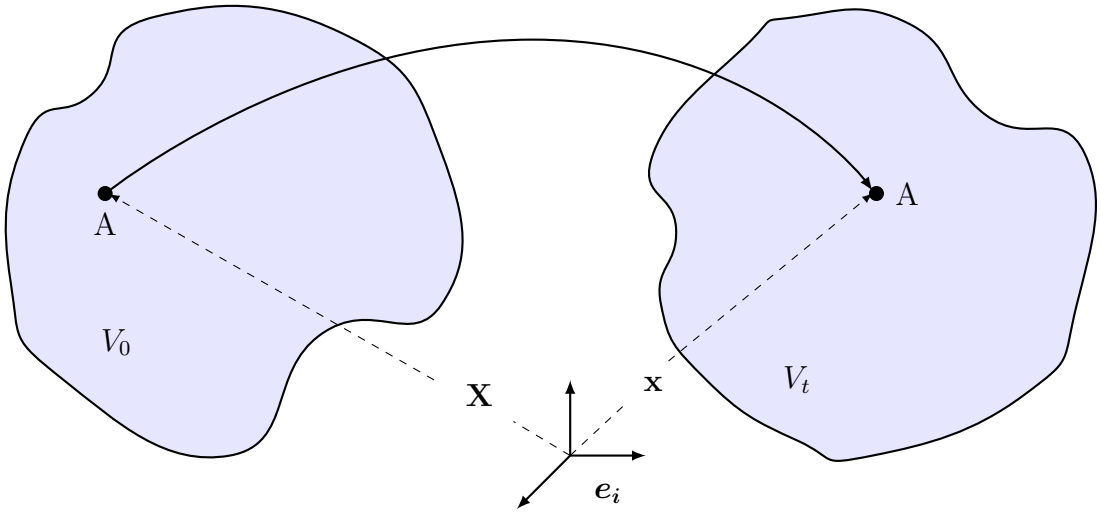

Figure 1.1: Mapping between reference and current configuration

If $\mathbf{X}$ is the position vector of A at $t = t_0$ then the position vector $\mathbf{x}$ in the current configuration will be a smooth function of the material point in the reference configuration ($\mathbf{X}$) and of the current state (i.e time t):

$$\mathbf{x} = \mathbf{x}(\mathbf{X}, t) \tag{1.2}$$

Since (1.2) holds for an arbitrary material point of the reference configuration then it should hold for any material point of the undeformed state. That is, (1.2) defines the position of all material points at a time $t > t_0$ and as a result it describes the motion of the body in space $\mathcal{E}$. As pointed out in Section 1.1, the mapping between the reference and the current configuration should be bijective which subsequently means that (1.2) is an invertible function in the sense that:

$$\mathbf{x} = \mathbf{x}(\mathbf{X}, t) \Rightarrow \mathbf{X} = \mathbf{X}(\mathbf{x}, t) \tag{1.3}$$

Description of motion of the body can be carried out using (1.2) either by following a specific material point as it moves through different configurations ($\mathbf{X} = ct$ and t is the independent variable) or by examining the variations of geometry of the body between the current and

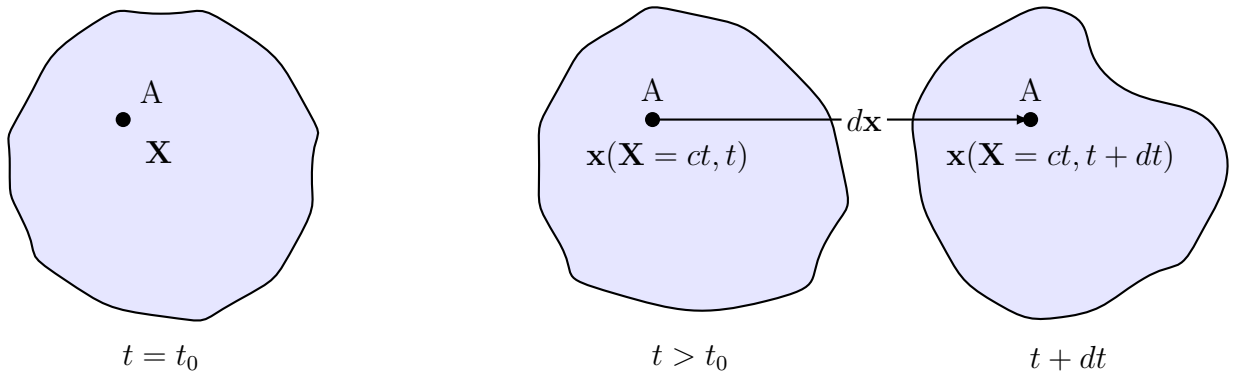

Figure 1.2: Variation of $\mathbf{x}$ for a specific material point A

the reference configuration ($t = ct$ and $\mathbf{X}$ are the independent variables).

In the former case, (1.2) is reduced to a vector-valued function of one variable:

$$\mathbf{x} = \mathbf{x}(\mathbf{X} = ct, t) = \mathbf{x}(t) \tag{1.4}$$

Consider now the variation of $\mathbf{x}$ due to the change of position of the specific material point from the current configuration to a configuration at time $t + dt$, as qualitatively depicted in Figure 1.2:

$$d\mathbf{x} = \frac{\partial \mathbf{x}}{\partial t}\, dt \equiv \boldsymbol{\upsilon}(\mathbf{X} = ct, t)\, dt \tag{1.5}$$

where $\boldsymbol{\upsilon}(\mathbf{X} = ct, t) \equiv \boldsymbol{\upsilon}(t)$ denotes the velocity of the material point under consideration. Assuming that $\mathbf{x}$ is twice differentiable, it is possible to also define the acceleration of a specific material point $\mathbf{a}(\mathbf{X} = ct, t) \equiv \mathbf{a}(t)$ as:

$$\mathbf{a}(t) = \frac{\partial \boldsymbol{\upsilon}(t)}{\partial t} = \frac{\partial^2 \mathbf{x}(t)}{\partial t^2} \tag{1.6}$$

where calculation of $\boldsymbol{\upsilon}(t)$ and $\mathbf{a}(t)$, when the expression of $\mathbf{x}$ is given, is carried out using the so called "material derivative" i.e. the rate of change of a scalar quantity $A(\mathbf{X}, t)$ with respect to t for a specific material point $\mathbf{X} = ct$.

In the latter case $\mathbf{x}$ is now a function of the position vector at the reference configuration, i.e:

$$\mathbf{x} = \mathbf{x}(\mathbf{X}, t = ct) = \mathbf{x}(\mathbf{X}) \tag{1.7}$$

Now, let $d\mathbf{X}$ denote an infinitesimal material fiber between points A ($\mathbf{X}$) and B ($\mathbf{X} + d\mathbf{X}$) at the reference configuration of the body. Then, the same material fiber AB at the deformed configuration $\mathfrak{B}_t$ is given as the variation of $d\mathbf{x}$ of position vector $\mathbf{x}$ as shown in Figure 1.3:

$$d\mathbf{x} = \frac{\partial \mathbf{x}(\mathbf{X}, t = ct)}{\partial \mathbf{X}} \cdot d\mathbf{X} \equiv \mathbf{F}(\mathbf{X}, t) \cdot d\mathbf{X} \tag{1.8}$$

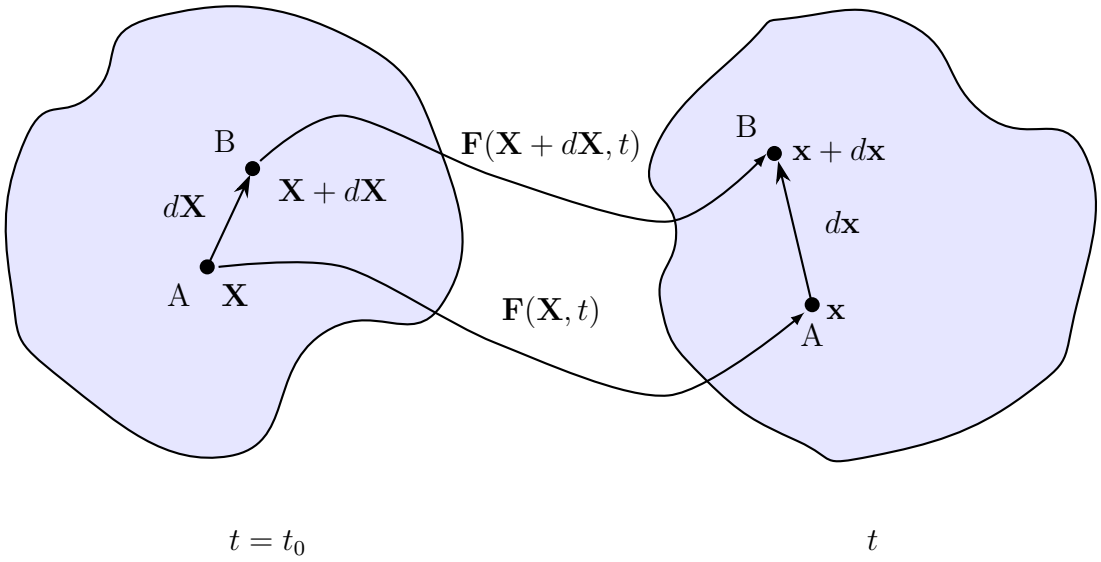

Figure 1.3: Mapping of a material fiber between reference and current configuration through the deformation gradient

where

$$\boxed{\mathbf{F}(\mathbf{X},t) \equiv \frac{\partial \mathbf{x}(\mathbf{X},t)}{\partial \mathbf{X}} = \mathbf{x}\boldsymbol{\nabla}_{\mathbf{X}} \quad \text{or} \quad F_{ij} = \frac{\partial x_i(\mathbf{X},t)}{\partial X_j} = x_i \nabla_{X_j}, \quad \nabla_{X_j} = \frac{\partial(.)}{\partial X_j}} \tag{1.9}$$

is a second order tensor known as *the deformation gradient*. It is important to note here that this quantity plays a fundamental role in the study of deformation of continuum bodies since, as suggested by the physical interpretation of 1.8, the deformation gradient relates the variation of any arbitrary material fiber $d\mathbf{X}$ at the reference configuration with the variation of the same fiber $d\mathbf{x}$ at the current configuration and thus one can assume that it is "embedded" with all the information concerning the deformation of the body. Indeed, it is possible to prove that geometrical variations of material fibers, material areas and material volumes all explicitly or implicitly depend on the deformation gradient $\mathbf{F}$. These results, along with some important remarks, are summarized in the following Section.

1.2 Description of Deformation in a Continuum Body

The concept of deformation in the context of continuum mechanics is associated with the variations of geometric characteristics of a continuum body between a reference configuration $\mathfrak{B}_0$ and any other subsequent configuration $\mathfrak{B}_t$ under consideration. More specifically, these variations could be referring to variations of length and relative orientation between two material fibers, variations of material areas and volumes. In general, the theory of such relations does not impose any constraints on the order of magnitude of displacements and thus also enables the kinematic description of finite deformations, with infinitesimal displacement

theory considered as a special linearized case. Fundamental results are summarized bellow, for the sake of completeness, without proof.

Change of Length and Angle

Consider the infinitesimal material fibers $d\mathbf{X}$ and $d\mathbf{x}$ of length ds_0 and ds which are in the direction of $\mathbf{N}$ and $\mathbf{n}$ in the undeformed and current configurations respectively as shown in Figure 1.4.

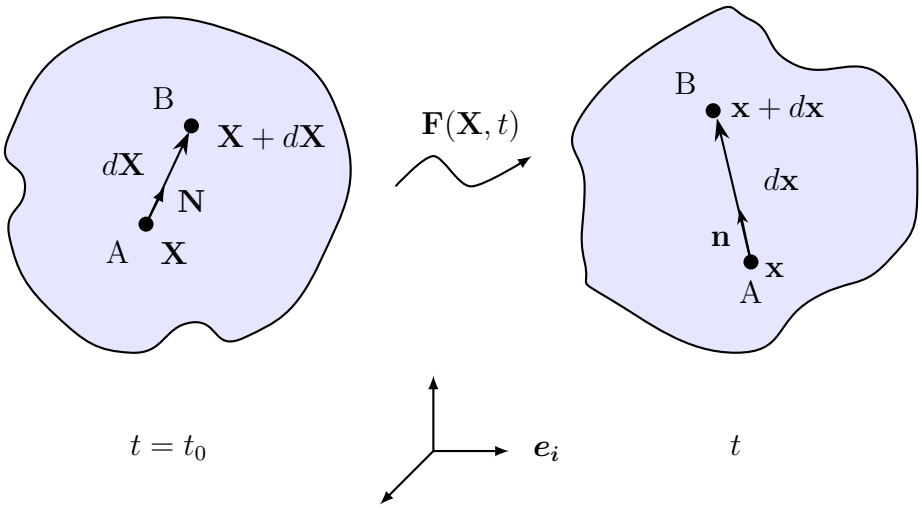

Figure 1.4: Variation of a material fiber between reference and current configuration.

where $d\mathbf{X} = ds_0\mathbf{N}$ and $d\mathbf{x} = ds\mathbf{n}$. Defining the symmetric and positive definite second order tensors $\mathbf{C}$ and $\mathbf{B}$ known as *right* and *left Cauchy-Green* tensors respectively as:

$$\boxed{\mathbf{C} = \mathbf{F}^T \cdot \mathbf{F}} \quad \text{and} \quad \boxed{\mathbf{B} = \mathbf{F} \cdot \mathbf{F}^T} \tag{1.10}$$

one can prove that the stretch and inverse stretch ratio between the two configurations can be given explicitly as:

$$\boxed{\lambda = \frac{ds}{ds_0} = \sqrt{\mathbf{N} \cdot \mathbf{C} \cdot \mathbf{N}}} \quad \text{and} \quad \boxed{\frac{1}{\lambda} = \frac{ds_0}{ds} = \sqrt{\mathbf{n} \cdot \mathbf{B}^{-1} \cdot \mathbf{n}}} \tag{1.11}$$

where $\mathbf{n}$ and $\mathbf{N}$ are related by the expression:

$$\boxed{\mathbf{n} = \frac{1}{|\mathbf{F} \cdot \mathbf{N}|}\mathbf{F} \cdot \mathbf{N}} \tag{1.12}$$

Equations (1.11) and (1.12) make clear that the stretch ratio (thus the deformed length) of an infinitesimal material fiber depends on the initial orientation of the material fiber in the reference configuration. Consequently, it is possible to state the optimization problem

of finding those directions $\mathbf{N}$ in the reference configuration for which the stretch ratio takes maximum and minimum values which can be solved by the means of mathematical programming. It can be proved that these maximum and minimum values correspond to the maximum and minimum eigenvalues of $\mathbf{C}$.

Concerning the variation of the relative orientation of two infinitesimal material fibers, consider the pairs $d\mathbf{X}^{(1)} = ds_0^{(1)}\mathbf{N}_1, d\mathbf{X}^{(2)} = ds_0^{(2)}\mathbf{N}_2$ and $d\mathbf{x}^{(1)} = ds^{(1)}\mathbf{n}_1, d\mathbf{x}^{(2)} = ds^{(2)}\mathbf{n}_2$ that form angles ϕ_0 and ϕ in the reference and deformed configurations respectively as depicted in Figure 1.5.

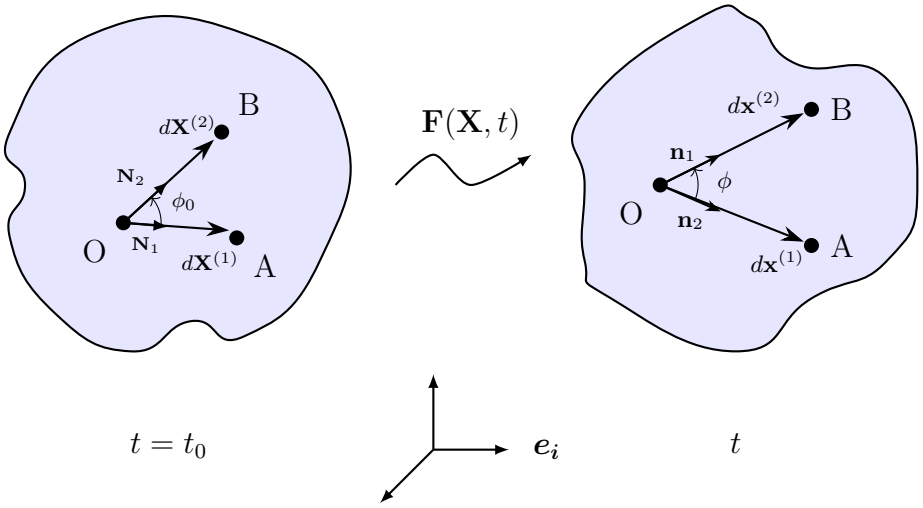

Figure 1.5: Variation of the relative orientation of two material fibers between reference and current configuration.

In this case, the relations for angles ϕ_0 and ϕ can be summarized as:

$$\boxed{cos\phi = \frac{\mathbf{N}_1 \cdot \mathbf{C} \cdot \mathbf{N}_2}{\lambda_1 \lambda_2}} \quad \text{with} \quad \lambda_i,\ i = 1, 2 \quad \text{from} \quad (1.11_a) \tag{1.13}$$

$$\boxed{cos\phi_0 = \lambda_1 \lambda_2 \mathbf{n}_1 \cdot \mathbf{B}^{-1} \cdot \mathbf{n}_2} \quad \text{with} \quad \frac{1}{\lambda_i},\ i = 1, 2 \quad \text{from} \quad (1.11_b) \tag{1.14}$$

Change of Surface and Volume

Let $d\mathbf{X}^{(1)}$, $d\mathbf{X}^{(2)}$, $d\mathbf{X}^{(3)}$ and $d\mathbf{x}^{(1)}$, $d\mathbf{x}^{(2)}$, $d\mathbf{x}^{(3)}$ be two triads of infinitesimal material fibers in the undeformed and current configuration forming infinitesimal material volumes dV_0 and dV_t respectively as shown in Figure 1.6, which are defined as:

$$dV_0 = d\mathbf{X}^{(3)} \cdot (d\mathbf{X}^{(1)} \times d\mathbf{X}^{(2)}) \quad \text{and} \quad dV = d\mathbf{x}^{(3)} \cdot (d\mathbf{x}^{(1)} \times d\mathbf{x}^{(2)}) \tag{1.15}$$

After some calculus it is readily proved that infinitesimal material volumes between reference and deformed configurations are related through the determinant of the deformation gradient

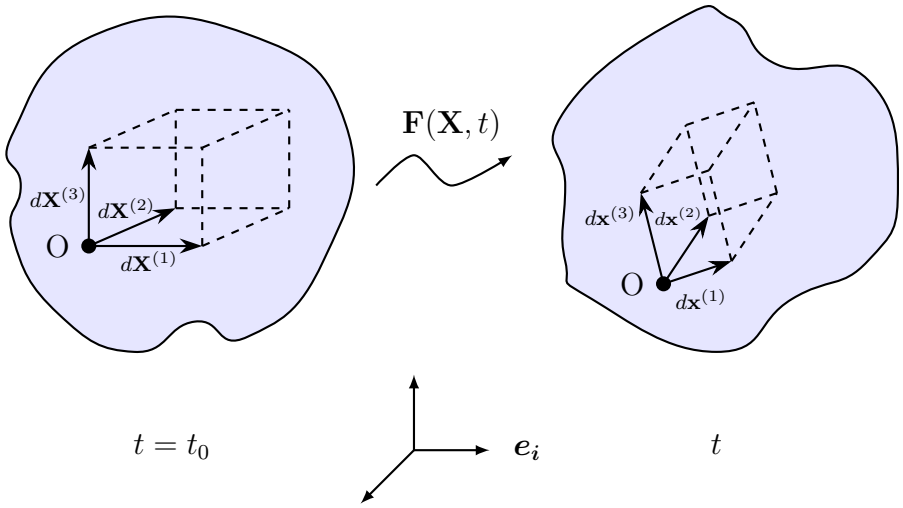

Figure 1.6: Variation of infinitesimal material volume between reference and current configuration.

as:

$$\boxed{dV = \det\mathbf{F}\, dV_0 = J\, dV_0} \tag{1.16}$$

It should be noted that examination of (1.16) reveals that if $J > 1$ then there is local expansion in the material whereas for values of $0 < J < 1$ material volume is locally reduced.

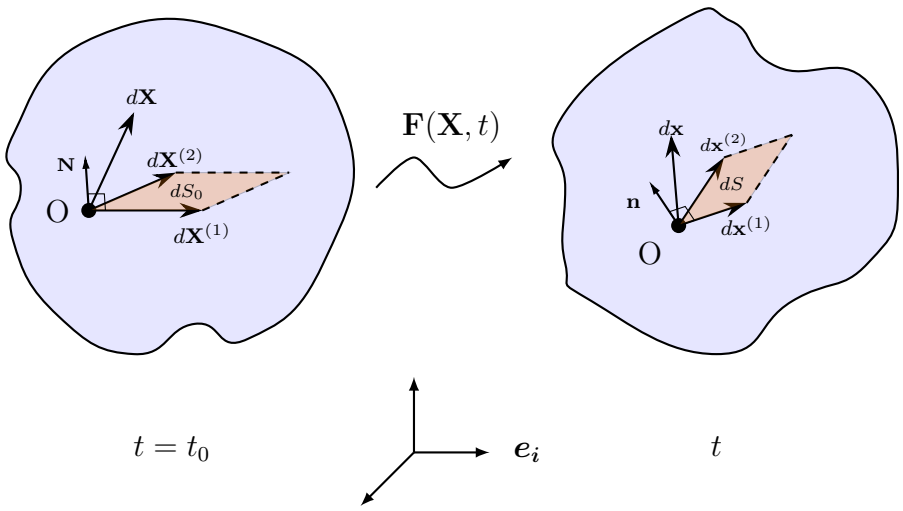

Figure 1.7: Variation of infinitesimal material area between reference and current configuration.

Finally, in the case of change of infinitesimal material areas, consider two pairs of infinitesimal fibers $d\mathbf{X}^{(1)}, d\mathbf{X}^{(2)}$ and $d\mathbf{x}^{(1)}, d\mathbf{x}^{(2)}$ that define the areas with vectors $\mathbf{dS_0}$ and $\mathbf{dS}$ in $\mathfrak{B}_0$ and $\mathfrak{B}_t$ respectively, as shown in Figure 1.7, in the sense that:

$$\mathbf{dS_0} = dS_0\mathbf{N} \quad \text{and} \quad \mathbf{dS} = dS\mathbf{n} \tag{1.17}$$

Additionally, if $d\mathbf{X}$ and $d\mathbf{x}$ are two arbitrary infinitesimal material fibers whose projection vectors $d\mathbf{X}_N = (d\mathbf{X}\cdot\mathbf{N})\mathbf{N}$, $d\mathbf{x}_n = (d\mathbf{x}\cdot\mathbf{n})\mathbf{n}$ form the infinitesimal volumes dV_0 and dV with the aforementioned pairs of fibers in the reference and deformed configurations respectively, then it is proved that the following relation, known as *Nanson's formula* holds:

$$\boxed{dS\mathbf{n} = J\, dS_0\mathbf{N}\cdot\mathbf{F}^{-1}} \tag{1.18}$$

Taking the absolute values of both sides and using the definitions of right and left Cauchy-Green tensors, one can find the expressions that relate dS_0, dS and $\mathbf{N}$, $\mathbf{n}$ are given as:

$$\boxed{\frac{dS}{dS_0} = J\sqrt{\mathbf{N}\cdot\mathbf{C}^{-1}\cdot\mathbf{N}} = J\sqrt{\mathbf{n}\cdot\mathbf{B}\cdot\mathbf{n}}} \tag{1.19}$$

and

$$\boxed{\mathbf{n} = \frac{1}{|\mathbf{N}\cdot\mathbf{F}^{-1}|}\,\mathbf{N}\cdot\mathbf{F}^{-1} = \frac{1}{|\mathbf{N}\cdot\mathbf{F}^{-T}|}\,\mathbf{F}^{-T}\cdot\mathbf{N}} \quad , \quad \boxed{\mathbf{N} = \frac{1}{|\mathbf{n}\cdot\mathbf{F}|}\,\mathbf{n}\cdot\mathbf{F}} \tag{1.20}$$

It should be emphasized here that, in the case of an infinitesimal material area, the unit vectors $\mathbf{N}$ and $\mathbf{n}$, even though they remain normal to the areas at all times, they are not attached to the corresponding material fibers whose directions momentarily coincide with them i.e. the material fiber $d\mathbf{X}_N$ in the direction $\mathbf{N}$ at $t = t_0$ is in general different from $d\mathbf{x}_n$ which is in the direction of $\mathbf{n}$ at the current time t. Moreover, expressions (1.16), (1.18) and (1.19) concerning variations of material areas and volumes are *local* in the sense that they do not hold for the whole area and volume of the continuum body but only in the vicinity of an arbitrary point with position vectors $\mathbf{X}$ and $\mathbf{x}$ in $\mathfrak{B}_0$ and $\mathfrak{B}_t$ respectively.

1.3 The Polar Decomposition Theorem

Let $\mathbf{A}$ be an invertible second order tensor. Then, it can be proved that $\mathbf{A}$ can be uniquely right or left multiplicatively decomposed into two tensors as :

$$\mathbf{A} = \mathbf{Q}\cdot\mathbf{U} = \mathbf{V}\cdot\mathbf{Q} \tag{1.21}$$

where $\mathbf{Q}$ is an orthoginal second order tensor[2] and $\mathbf{U}$, $\mathbf{V}$ are second order symmetric and positive definite tensors. Equation (1.21) is known as the *polar decomposition theorem*. The aforementioned symmetry and positive definiteness of $\mathbf{U}$ and $\mathbf{V}$ implies that they have real and positive eigenvalues which in turn means (by making use of their spectral representation with respect to the vector space defined by their respective eigenvectors) that :

$$\det\mathbf{U}, \det\mathbf{U}^{-1} > 0 \quad \text{and} \quad \det\mathbf{V}, \det\mathbf{V}^{-1} > 0 \tag{1.22}$$

[2]i.e. a second order tensor that when acting on a vector leaves its length unaffected and for which the relations $\mathbf{Q}^T\cdot\mathbf{Q} = \boldsymbol{\delta}$ and $\det\mathbf{Q} = \pm 1$ hold.

In continuum mechanics, the polar decomposition theorem is used to multiplicatevely decompose the deformation gradient $\mathbf{F}$ which can now be written as:

$$\mathbf{F} = \mathbf{Q} \cdot \mathbf{U} = \mathbf{V} \cdot \mathbf{Q} \tag{1.23}$$

Since $\det\mathbf{F} = J > 0$ then, solving for $\mathbf{Q}$ in (1.23) and calculating the corresponding determinant, one arrives at:

$$\det\mathbf{Q} = \det\mathbf{F}\,\det\mathbf{U}^{-1} \overset{(1.22)}{\Longrightarrow} \det\mathbf{Q} > 0 \tag{1.24}$$

Last equation suggests that $\mathbf{Q}$ is a proper orthogonal tensor i.e. $\mathbf{Q}$ is a rotation tensor which will hereafter be denoted as $\mathbf{R}$. Then (1.23) can be written as:

$$\boxed{\mathbf{F} = \mathbf{R} \cdot \mathbf{U} = \mathbf{V} \cdot \mathbf{R}} \tag{1.25}$$

where the tensors $\mathbf{U}$ and $\mathbf{V}$ are defined as:

$$\mathbf{U} = \sqrt{\mathbf{C}} \quad \text{and} \quad \mathbf{V} = \sqrt{\mathbf{B}} \tag{1.26}$$

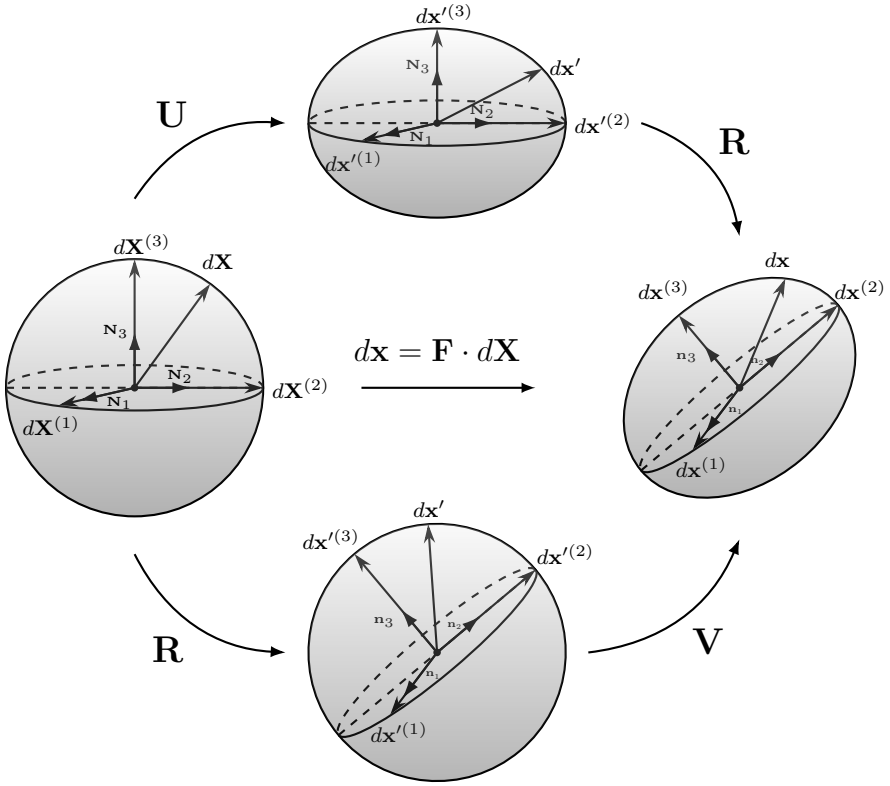

Figure 1.8: Geometric interpretation of polar decomposition of deformation gradient $\mathbf{F}$.

If λ_i^2 are the eigenvalues and $\mathbf{N}_i$, $\mathbf{n}_i$, $i = 1, 2, 3$, are the eigenvectors associated with the

tensors $\mathbf{C}$ and $\mathbf{B}$ respectively then, using the latter's spectral representations, (1.26) leads to:

$$\mathbf{U} = \sum_{i=1}^{3} \lambda_i \, \mathbf{N}_i \mathbf{N}_i \quad \text{and} \quad \mathbf{V} = \sum_{i=1}^{3} \lambda_i \, \mathbf{n}_i \mathbf{n}_i \tag{1.27}$$

where $\mathbf{n}_i = \mathbf{R} \cdot \mathbf{N}_i$ which consequently leads to the following expression for $\mathbf{R}$:

$$\mathbf{R} = \mathbf{n}_i \mathbf{N}_i \tag{1.28}$$

Since $\mathbf{N}_i$ and $\mathbf{n}_i$ express the principal directions of an arbitrary point in the reference and current configurations and λ_i is the stretch ratio of a material fiber in the principal direction i of the configuration considered, then (1.27) suggests that, in the context of continuum mechanics, tensors $\mathbf{U}$, $\mathbf{V}$ can be physically interpreted as the *stretch tensors* associated with undeformed and current configurations respectively. Furthermore, the triad of ($\mathbf{N}_i$,$\mathbf{C}$,$\mathbf{U}$) which is defined with respect to the reference configuration is usually referred to as a *Lagrangian triad* whereas the triad of ($\mathbf{n}_i$,$\mathbf{B}$,$\mathbf{V}$) which is defined with respect to the current configuration is called an *Eulerian triad*.

The polar decomposition of deformation gradient $\mathbf{F}$ is qualitatively presented in Figure 1.8 examining an infinitesimal sphere around an arbitrary point. Let $d\mathbf{X}$ be an infinitesimal material fiber in the reference configuration and $d\mathbf{x}$ be its mapping in the current configuration through $\mathbf{F}$. Then, using, without loss of generality, the right polar decomposition of $\mathbf{F}$, $d\mathbf{x}$ is given as:

$$d\mathbf{x} = \mathbf{R} \cdot \underbrace{\mathbf{U} \cdot d\mathbf{X}}_{d\mathbf{x}'} = \mathbf{R} \cdot d\mathbf{x}' \tag{1.29}$$

Equation (1.29) shows that transition of $d\mathbf{X}$ to $d\mathbf{x}$ can be decomposed and interpreted as a two step procedure where in the first phase material fibers in the reference principal directions are only stretched due to the action of $\mathbf{U}$ (although material fibers in arbitrary directions may be rotated as well) and in the second step all material fibers in the vicinity of the considered point undergo a rigid body rotation due to the effect of $\mathbf{R}$. An analogous interpretation may be derived by using the left polar decomposition of $\mathbf{F}$ where the described procedure takes place in a reversed manner.

Finally, it is important to mention here that the rotation tensor $\mathbf{R}$ derived from the polar decomposition of $\mathbf{F}$ has a key role in the description of constitutive modeling and will be used later on.

1.4 Generalized Strain Measures

It is well known from the classical theory of small strains that the (nominal) deformation of a material fiber with a reference length ds_0 that is stretched to a length ds in the deformed

state is simply given as the ratio of this variation and its initial length, i.e.:

$$\varepsilon = \frac{ds - ds_0}{ds_0} = \frac{ds}{ds_0} - 1 = \lambda - 1 \tag{1.30}$$

where λ is the stretch ratio defined in Section 1.2. While (1.30) is viable for small strain, one-dimensional deformations, it is desirable to deduce more general descriptions of deformation in the case of generalized finite three-dimensional geometrical variations. For this purpose, appropriate strain tensors have to be defined which whatsoever have to reduce to the description provided above in the infinitesimal strain case. In this sense, one can define general families of strain tensors either with respect to the reference or current configuration[3] as:

$$\mathbf{E}^{(m)}(\lambda_i) = \sum_{i=1}^{3} f^{(m)}(\lambda_i)\, \mathbf{N}_i\mathbf{N}_i \tag{1.31a}$$

$$\mathbf{e}^{(m)}(\lambda_i) = \sum_{i=1}^{3} f^{(m)}(\lambda_i)\, \mathbf{n}_i\mathbf{n}_i \tag{1.31b}$$

The only assumption made in (1.31a) and (1.31b) is that Lagrangian and Eulerian strain tensors are coaxial[4] to $\mathbf{U}$ and $\mathbf{V}$ respectively which one can think as viable choice taking into consideration the physical meaning of the aforementioned tensors. In general, the parametric scalar functions $f^{(m)}(\lambda_i)$ have to be chosen in such a manner so that for infinitesimal strains, tensorial definitions (1.31a),(1.31b) reduce to the small strain case but are otherwise arbitrary. Strictly speaking, small strains in one-dimension imply that:

$$\varepsilon = \lambda - 1 \approx 0 \Rightarrow \lambda - 1 = 0 \Rightarrow \lambda = 1 \tag{1.32}$$

Now using Taylor expansion of $f^{(m)}(\lambda)$ around $\lambda_0 = 1$ we get:

$$f^{(m)}(\lambda) = f^{(m)}(1) + \left.\frac{df^{(m)}(\lambda)}{d\lambda}\right|_{\lambda=1} (\lambda - 1) + O[(\lambda - 1)^2] \tag{1.33}$$

Again, for small strains $f^{(m)}(\lambda)$ needs comply with (1.32) suggesting, for a 1$^{\text{st}}$ order approximation, that the following mathematical restrictions are imposed on $f^{(m)}(\lambda)$:

$$\boxed{f^{(m)}(1) = 0} \quad \text{and} \quad \boxed{\left.\frac{df^{(m)}(\lambda)}{d\lambda}\right|_{\lambda=1} = 1} \tag{1.34}$$

In addition to these restrictions one can intuitevely postulate that some physical restrictions should also be imposed on $f^{(m)}(\lambda)$. Thus, it is natural to assume that as f increases

[3] Which are also known as Lagrangian and Eulerian strain tensors respectively

[4] i.e. Coaxiality of two arbitrary tensors $\mathbf{A}$ and $\mathbf{B}$ suggests that they have the same eigenvectors although this does not in any way imply that they are proportional to each other.

deformation also increases. Additionally, as stretch ratios approach zero and infinity deformation should approach $-\infty$ and ∞ respectively. Mathematically speaking these physical restrictions can be expressed as:

$$\boxed{\left.\frac{df^{(m)}(\lambda)}{d\lambda}\right|_{\lambda=1} > 0\ ,\ \forall\lambda\in\mathbb{R}} \quad \text{and} \quad \boxed{f^{(m)}(0)=-\infty\ ,\ f^{(m)}(\infty)=\infty} \tag{1.35}$$

A family of strains that satisfies restrictions (1.34) and (1.35) is defined as:

$$f^{(m)}(\lambda)=\begin{cases}\frac{1}{m}(\lambda^m-1) & ,\quad m\neq 0\\ \\ \ln(\lambda) & ,\quad m=0\end{cases} \qquad m\in\mathbb{Z} \tag{1.36}$$

Substituting (1.36) in (1.31a) it can be readily shown that $\mathbf{E}^{(m)}(\lambda)$ can be written in the following piecewise fashion:

$$\mathbf{E}^{(m)}=\begin{cases}\frac{1}{m}[(\mathbf{F}^T\cdot\mathbf{F})^n-\boldsymbol{\delta}] & ,\quad m=2n\\ \\ \frac{1}{m}[(\mathbf{F}^T\cdot\mathbf{F})^n\sqrt{\mathbf{F}^T\cdot\mathbf{F}}-\boldsymbol{\delta}] & ,\quad m=2n+1\end{cases} \qquad n\in\mathbb{Z} \tag{1.37}$$

This implies that if $m=2n$ is chosen then $\mathbf{E}^{(m)}$ is easily determined from $\mathbf{F}$ whereas for $m=2n+1$, (1.37) suggests that the calculation of the square root of the tensor $\mathbf{F}^T\cdot\mathbf{F}$ is needed which in general requires the solution of an eigenvalue problem.

Table 1.1: Commonly used strain tensors in continuum mechanics

	Strain	Definition
$m=2$	Green	$\mathbf{E}^G=\mathbf{E}^{(2)}=\frac{1}{2}\left(\mathbf{C}-\boldsymbol{\delta}\right)$
$m=1$	Biot	$\mathbf{E}^B=\mathbf{E}^{(1)}=\mathbf{U}-\boldsymbol{\delta}$
$m=0$	Henky (Logarithmic)	$\mathbf{E}^{\ln}=\mathbf{E}^{(0)}=\ln\mathbf{U}$ $\mathbf{e}^{\ln}=\mathbf{e}^{(0)}=\ln\mathbf{V}$
$m=-2$	Almansi	$\mathbf{e}^A=\mathbf{e}^{(-2)}=\frac{1}{2}(\boldsymbol{\delta}-\mathbf{B}^{-1})$

The most commonly used general strain measures are summarized in Table 1.1. Although there does not exist a single rule about the selection of a strain tensor for finite deformations

this choice should not be completely arbitrary in the sense that the physics of the problem and the behavior of the respective tensor for various values of λ have to be accounted for. Nevertheless, one could condone the use of Henky since it the only of the aforementioned strains that also satisfies the physical restrictions (1.35).

1.5 Rate of Deformation

Investigating the deformation of a continuum body often requires not only the determination of deformation at a specific moment in time but also the determination of how deformation evolves in time[5]. The whole analysis of the rate of deformation is carried out with respect to the current deformed configuration. Recalling the expressions for the definition of material velocity and motion of a body described by (1.5), (1.2), velocity can be expressed with respect to either the reference or the deformed configuration as:

$$\boldsymbol{v} = \frac{\partial \mathbf{x}(\mathbf{X}, t)}{\partial t} = \hat{\boldsymbol{v}}(\mathbf{X}, t) = \bar{\boldsymbol{v}}(\mathbf{x}, t) \tag{1.38}$$

Now, one is interested in the variation of deformation[6] between two particles which are connected by the infinitesimal fiber $d\mathbf{x}$ for a given time $t > t_0$ and hence for the variation of $\bar{\boldsymbol{v}}(\mathbf{x}, t)$. This variation of $\boldsymbol{v}$ in the vicinity of $\mathbf{x}$ is then calculated as:

$$d\boldsymbol{v} = \bar{\boldsymbol{v}}(\mathbf{x} + d\mathbf{x}, t) - \bar{\boldsymbol{v}}(\mathbf{x}, t) = \frac{\partial \boldsymbol{v}(\mathbf{x}, t)}{\partial \mathbf{x}} \cdot d\mathbf{x} \Rightarrow d\boldsymbol{v} = \mathbf{L} \cdot d\mathbf{x} \tag{1.39}$$

where

$$\boxed{\mathbf{L} = \frac{\partial \boldsymbol{v}(\mathbf{x}, t)}{\partial \mathbf{x}} = \boldsymbol{v} \boldsymbol{\nabla}_{\mathbf{x}}} \tag{1.40}$$

defines the spatial variation of the velocity known as the *velocity gradient* tensor. Additionally, it is important to also define the symmetric and skew parts of $\mathbf{L}$, known as *deformation rate* and *spin* tensors respectively, as:

$$\boxed{\mathbf{D} = \mathbf{L}^{(sym)} = \frac{1}{2}\left(\mathbf{L} + \mathbf{L}^T\right) \quad \text{or} \quad D_{ij} = \frac{1}{2}\left(\frac{\partial \boldsymbol{v}_i}{\partial \mathbf{x}_j} + \frac{\partial \boldsymbol{v}_i}{\partial \mathbf{x}_i}\right)} \tag{1.41a}$$

$$\boxed{\mathbf{W} = \mathbf{L}^{(skew)} = \frac{1}{2}\left(\mathbf{L} - \mathbf{L}^T\right) \quad \text{or} \quad W_{ij} = \frac{1}{2}\left(\frac{\partial \boldsymbol{v}_i}{\partial \mathbf{x}_j} - \frac{\partial \boldsymbol{v}_i}{\partial \mathbf{x}_i}\right)} \tag{1.41b}$$

so that

$$\mathbf{L} = \mathbf{D} + \mathbf{W} \tag{1.42}$$

[5] This urgency arises mostly in cases of non-linear material behavior such as plasticity where deformation history plays a part in the response of the material.

[6] i.e. the relative velocity

The physical meaning of $\mathbf{D}$, $\mathbf{W}$ is of great importance and will be explained in the following Subsections. Considering now the variation of $\boldsymbol{\upsilon}(\hat{\mathbf{X}}, t)$ in the reference configuration, i.e. :

$$\begin{aligned} d\boldsymbol{\upsilon} &= \boldsymbol{\upsilon}(\mathbf{X} \hat{+} d\mathbf{X}, t) - \boldsymbol{\upsilon}(\hat{\mathbf{X}}, t) = \frac{\partial \mathbf{x}(\mathbf{X} + d\mathbf{X}, t)}{\partial t} - \frac{\partial \mathbf{x}(\mathbf{X}, t)}{\partial t} \\ &= \frac{\partial}{\partial t}\Big[\mathbf{x}(\mathbf{X} + d\mathbf{X}, t) - \mathbf{x}(\mathbf{X}, t)\Big] = \frac{\partial}{\partial t}(d\mathbf{x}) = \frac{\partial}{\partial t}(\mathbf{F} \cdot \mathbf{X}) \Rightarrow \\ &\Rightarrow d\boldsymbol{\upsilon} = \dot{\mathbf{F}} \cdot d\mathbf{X} \end{aligned} \tag{1.43}$$

Equation (1.38) implies that variations (1.39) and (1.43) should be the same. Taking this into account and after some short calculations one arrives at an alternative expression of $\mathbf{L}$ in terms of $\mathbf{F}$ which is given as :

$$\boxed{\mathbf{L} = \dot{\mathbf{F}} \cdot \mathbf{F}^{-1}} \tag{1.44}$$

Now, calculation of the rate of change of an infinitesimal fiber $d\mathbf{x}$ of the current configuration leads to:

$$\dot{\overline{d\mathbf{x}}} = \mathbf{L} \cdot d\mathbf{x} \tag{1.45}$$

Equation (1.45) reveals the analogous to $\mathbf{F}$ physical interpretation of tensor $\mathbf{L}$ in the sense that the rate of change of an arbitrary infinitesimal fiber $d\mathbf{x}$ can be calculated if $\mathbf{L}$ is known. Then, one can intuitively address that the velocity gradient is embedded with all the information concerning the rate of change of all geometrical quantities between deformed configurations.

Finally, before one proceeds with the interpretation of $\mathbf{D}$ and $\mathbf{W}$ it is important to recall here the expression for the evolution equation of a vector with constant length. Let $\mathbf{m}(t = 0) \equiv \mathbf{m}_0$ be a vector of constant length and consider the linear transformation $\mathbf{A}(t)$ imposed on $\mathbf{m}_0$. Then, it can be easily proved that in order for $\mathbf{m}(t)$ to be a constant length vector at any time $t > 0$, $\mathbf{A}(t)$ needs to be an orthogonal tensor $\mathbf{Q}(t)$ so that:

$$\mathbf{m}(t) = \mathbf{Q}(t) \cdot \mathbf{m}_0 \tag{1.46}$$

Additionally, from the definition of orthogonal tensors one gets:

$$\begin{aligned} \mathbf{Q} \cdot \mathbf{Q}^T = \boldsymbol{\delta} \overset{\frac{\partial}{\partial t}}{\Rightarrow} \dot{\mathbf{Q}} \cdot \mathbf{Q}^T + \mathbf{Q} \cdot \dot{\mathbf{Q}}^T = \mathbf{0} \Rightarrow -\dot{\mathbf{Q}} \cdot \mathbf{Q}^T = \mathbf{Q} \cdot \dot{\mathbf{Q}}^T \\ \Rightarrow -\underbrace{\dot{\mathbf{Q}} \cdot \mathbf{Q}^T}_{\mathbf{W}^m} = (\dot{\mathbf{Q}} \cdot \mathbf{Q}^T)^T \Rightarrow -\mathbf{W}^m = (\mathbf{W}^m)^T \\ \Rightarrow \mathbf{W}^m(t) = \dot{\mathbf{Q}}(t) \cdot \mathbf{Q}^T(t) : \text{Antisymmetric} \end{aligned} \tag{1.47}$$

Then, using (1.46) and (1.47), the evolution equation of $\mathbf{m}(t)$ is given as:

$$\boxed{\dot{\mathbf{m}}(t) = \mathbf{W}^m(t) \cdot \mathbf{m} = \boldsymbol{\omega}(t) \times \mathbf{m}} \tag{1.48}$$

where $\boldsymbol{\omega}(t)$ is the axial vector of $\mathbf{W}^m$. Since $\mathbf{m}(t)$ has constant length then:

$$\mathbf{m}\cdot\mathbf{m}=ct \overset{\frac{\partial}{\partial t}}{\Rightarrow} \dot{\mathbf{m}}\cdot\mathbf{m}+\mathbf{m}\cdot\dot{\mathbf{m}}=0\Rightarrow \mathbf{m}\cdot\dot{\mathbf{m}}=0\Rightarrow \dot{\mathbf{m}}\perp\mathbf{m} \tag{1.49}$$

Equations (1.47-1.49) suggest that $\dot{\mathbf{m}}$ corresponds to a rotation of $\mathbf{m}$ around the axis defined by $\boldsymbol{\omega}$ and, considering the fact that $\dot{\mathbf{m}}$ is the rate of change of $\mathbf{m}$, then $\mathbf{W}^m(t)$ can be physically interpreted as the rate of rotation i.e. as the spin of the constant length vector $\mathbf{m}$ at time t.

1.5.1 Physical Interpretation of D

In the case of the deformation rate tensor $\mathbf{D}$, physical interpretation for its normal and shear components is carried out separately. To begin with, consider an infinitesimal material fiber $d\mathbf{X}=ds_0\mathbf{N}$ in the reference configuration that is mapped to $d\mathbf{x}=ds\mathbf{n}$ in direction $\mathbf{n}$ in the current state at $t>t_0$. Then, ds_0, ds are calculated as the magnitude of $d\mathbf{X}$ and $d\mathbf{x}$ respectively:

$$ds_0^2=d\mathbf{X}\cdot d\mathbf{X}\quad\text{and}\quad ds^2=d\mathbf{x}\cdot d\mathbf{x} \tag{1.50}$$

One is now interested with the rate of change of the length ds with time, i.e.:

$$\begin{aligned}\frac{\partial}{\partial t}(ds^2)=\frac{\partial}{\partial t}(d\mathbf{x}\cdot d\mathbf{x})\Rightarrow 2ds\frac{\partial}{\partial t}(ds)&=\underbrace{\frac{\partial}{\partial t}(d\mathbf{x})}_{d\mathbf{x}\cdot\mathbf{L}^T}\cdot d\mathbf{x}+d\mathbf{x}\cdot\underbrace{\frac{\partial}{\partial t}(d\mathbf{x})}_{\mathbf{L}\cdot d\mathbf{x}}=d\mathbf{x}\cdot\mathbf{L}^T\cdot d\mathbf{x}+d\mathbf{x}\cdot\mathbf{L}\cdot d\mathbf{x}\\
&=d\mathbf{x}\cdot\underbrace{(\mathbf{L}^T+\mathbf{L})}_{2\,\mathbf{D}}\cdot d\mathbf{x}=2\,d\mathbf{x}\cdot\mathbf{D}\cdot d\mathbf{x}=2\,ds^2\,\mathbf{n}\cdot\mathbf{D}\cdot\mathbf{n}\Rightarrow ds\frac{\partial}{\partial t}(ds)=ds^2\,\mathbf{n}\cdot\mathbf{D}\cdot\mathbf{n}\Rightarrow\\
\Rightarrow\mathbf{n}\cdot\mathbf{D}\cdot\mathbf{n}=D_{nn}=\frac{1}{ds}\frac{\partial}{\partial t}(ds)&=\frac{\partial}{\partial t}\left(\ln\frac{ds}{ds_0}\right)\overset{\lambda=\frac{ds}{ds_0}}{\Longrightarrow}\boxed{\mathbf{n}\cdot\mathbf{D}\cdot\mathbf{n}=D_{nn}=\frac{\dot{\lambda}}{\lambda}}\end{aligned} \tag{1.51}$$

Equation (1.51) implies that the normal components of $\mathbf{D}$ express the rate of the stretch ratio per unit length of a material fiber which, in the current configuration, is momentarily aligned with the direction of $\mathbf{n}$.

The physical meaning of the shear components can be explained according to the following syllogism. Firstly, let $\mathbf{m}$ be a unit vector (that remains unit during deformation) attached to a material fiber $d\mathbf{x}=ds\mathbf{m}$ in the current configuration. Then, as proved in the previous Section, $\dot{\mathbf{m}}$ can be written in the form (1.48), where $\mathbf{W}^m$ can now be explicitly calculated as:

$$\begin{aligned}\dot{\mathbf{m}}=\frac{\partial}{\partial t}\left(\frac{d\mathbf{x}}{ds}\right)&=\frac{1}{ds}\underbrace{\frac{\partial}{\partial t}(d\mathbf{x})}_{\mathbf{L}\cdot d\mathbf{x}}-\underbrace{\frac{d\mathbf{x}}{(ds)^2}}_{\mathbf{m}/ds}\underbrace{\frac{\partial}{\partial t}(ds)}_{ds\,\mathbf{m}\cdot\mathbf{D}\cdot\mathbf{m}}=\mathbf{L}\cdot\mathbf{m}-(\mathbf{m}\cdot\mathbf{D}\cdot\mathbf{m})\cdot\mathbf{m}\\
&\overset{(1.42)}{=}\mathbf{W}\cdot\mathbf{m}+\mathbf{D}\cdot\mathbf{m}-(\mathbf{m}\cdot\mathbf{D}\cdot\mathbf{m})\mathbf{m}=\mathbf{W}\cdot\mathbf{m}+\mathbf{D}\cdot\mathbf{m}\underbrace{\mathbf{m}\cdot\mathbf{m}}_{1}-\mathbf{m}(\mathbf{m}\cdot\mathbf{D}\cdot\mathbf{m})\end{aligned}$$

$$\Rightarrow \dot{\mathbf{m}} = \mathbf{W}^m \cdot \mathbf{m} = -\mathbf{m} \cdot \mathbf{W}^m \quad \text{with} \quad \boxed{\mathbf{W}^m = \mathbf{W} + \mathbf{D} \cdot \mathbf{mm} - \mathbf{mm} \cdot \mathbf{D}} \tag{1.52}$$

where $\mathbf{W}^m$ is a second order skew symmetric tensor. Consider now a pair of unit vectors $\mathbf{m}$ and $\mathbf{n}$ that are attached to two material fibers $\delta\mathbf{x}^{(1)}$ and $\delta\mathbf{x}^{(2)}$ that intersect forming an angle ϕ at the deformed state (see Figure 1.5). Taking the inner product of $\mathbf{m}$ and $\mathbf{n}$ and differentiating with respect to t yields:

$$\mathbf{m} \cdot \mathbf{n} = \cos\phi \overset{\frac{\partial}{\partial t}}{\Rightarrow} \dot{\phi} = -\frac{1}{\sin\phi} \frac{\partial}{\partial t}(\mathbf{m} \cdot \mathbf{n}) \tag{1.53}$$

Calculation of $\frac{\partial}{\partial t}(\mathbf{m} \cdot \mathbf{n})$ is as follows:

$$\begin{aligned}
\frac{\partial}{\partial t}(\mathbf{m} \cdot \mathbf{n}) &= \dot{\mathbf{m}} \cdot \mathbf{n} + \mathbf{m} \cdot \dot{\mathbf{n}} = -\dot{\mathbf{m}} \cdot \mathbf{W}^m \cdot \mathbf{n} + \mathbf{m} \cdot \mathbf{W}^n \cdot \mathbf{n} = \mathbf{m} \cdot (\mathbf{W}^n - \mathbf{W}^m) \cdot \mathbf{n} \\
&\overset{(1.52)}{=} \mathbf{m} \cdot (\mathbf{D} \cdot \mathbf{nn} - \mathbf{nn} \cdot \mathbf{D} - \mathbf{D} \cdot \mathbf{mm} + \mathbf{mm} \cdot \mathbf{D}) \cdot \mathbf{n} \\
&= \mathbf{m} \cdot \mathbf{D} \cdot \mathbf{n} - \cos\phi(D_{nn} - D_{mm}) + \mathbf{m} \cdot \mathbf{D} \cdot \mathbf{n} \\
&= 2\,\mathbf{m} \cdot \mathbf{D} \cdot \mathbf{n} - (D_{mm} + D_{nn})\,\cos\phi
\end{aligned} \tag{1.54}$$

Equations (1.53) and (1.54) lead to the desired expression for $\dot{\phi}$:

$$\boxed{\dot{\phi} = \frac{1}{\sin\phi}\Big[(D_{mm} + D_{nn}\,\cos\phi) - 2\,\mathbf{m} \cdot \mathbf{D} \cdot \mathbf{n}\Big]} \tag{1.55}$$

Although the general expression (1.55) reveals that the rate of change of the relative orientation between two material fibers will depend not only on their initial angle ϕ but also on their respective orientations, it is rather difficult, in this form, to deduce the physical meaning of the shear components of $\mathbf{D}$. Without loss of generality, let $\mathbf{m} = \mathbf{e}_1$ and $\mathbf{n} = \mathbf{e}_2$ so that $\cos\phi = 0$ and $\sin\phi = 1$ which imlies that (1.55) reduces to:

$$\dot{\phi} = -2\,\mathbf{e}_1 \cdot \mathbf{D} \cdot \mathbf{e}_2 = -2\,D_{12} \Rightarrow D_{12} = -\frac{1}{2}\dot{\phi} \tag{1.56}$$

Equation (1.56) suggests that the indirect components of the deformation rate tensor $\mathbf{D}$ express the rate of decrease of the angle between a pair of material fibers which, in the current configuration intersect at $\mathbf{x}$ and are momentarily aligned with the directions of $\mathbf{e}_i$ and $\mathbf{e}_j$ (i.e. perpendicular to each other). This observation also implies that the rate of change of the material fibers which, in the deformed configuration, are momentarily aligned with the principal directions of $\mathbf{D}$ is zero.

1.5.2 Physical Interpretation of W

In contrast to $\mathbf{D}$, the spin tensor $\mathbf{W}$ can be interpreted in more than one manners.

In the more usual approach, consider the special case where the unit vector $\mathbf{m}$ of (1.52) is momentarily aligned with the eigenvector $\mathbf{d}_i$, $i = 1, 2, 3$ of $\mathbf{D}$, i.e. $\mathbf{m} = \mathbf{d}_i$. Then, since $\mathbf{d}_i$ is an eigenvector of $\mathbf{D}$, the following should hold:

$$\mathbf{D} \cdot \mathbf{m} = \mathbf{m} \cdot \mathbf{D} = D_i \mathbf{m} \tag{1.57}$$

Substitution of (1.57) in (1.52) suggests that $\dot{\mathbf{m}}$ is of the form (1.48) with $\mathbf{W}^m = \mathbf{W}$. In the aforementioned context, this implies that $\mathbf{W}$ can be interpreted as the instantaneous rate of rotation (i.e spin) of the material fibers which, in the current configuration, are momentarily aligned with the principal directions of $\mathbf{D}$. An important remark here is that this spin is different from the spin of the eigenvectors themselves since the $\mathbf{d}_i$'s are along different material fibers at different moments.

Nevertheless, one can derive another important interpretation of $\mathbf{W}$ as described in [6] and is briefly summarized here. Consider the aforementioned unit vector $\mathbf{m}$ with respect to a Cartesian coordinate system with base vectors $\mathbf{e}_i$, $i = 1, 2, 3$ as shown in Figure 1.9:

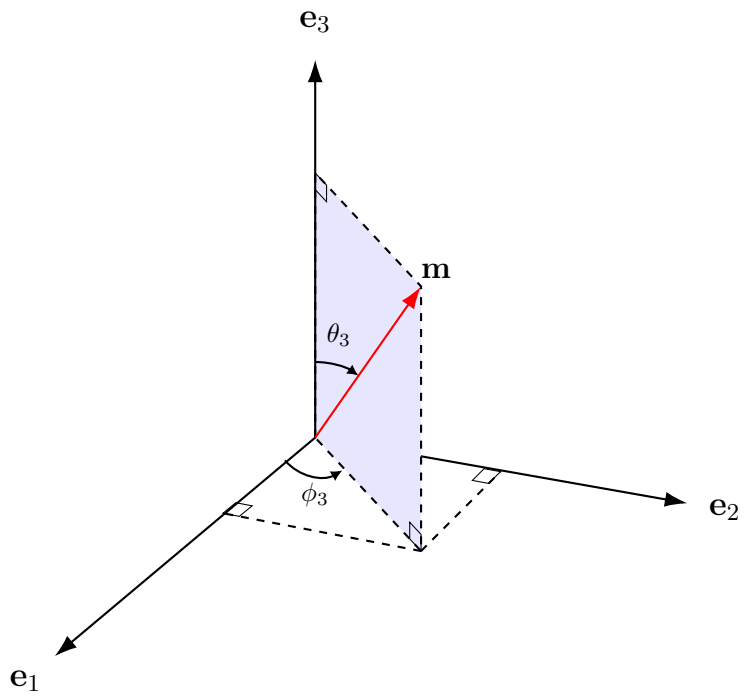

Figure 1.9: Unit vector $\mathbf{m}$ with the corresponding angles.

Then $\mathbf{m}$ can be written in the form:

$$\mathbf{m} = m_1\,\mathbf{e}_1 + m_2\,\mathbf{e}_2 + m_3\,\mathbf{e}_3 = \sin\theta_3\ \cos\phi_3\,\mathbf{e}_1 + \sin\theta_3\ \sin\phi_3\,\mathbf{e}_2 + \cos\theta_3\,\mathbf{e}_3 \tag{1.58}$$

Differentiating (1.58) with respect to t and comparing the second with the third side of the result obtained, one gets:

$$\dot{\phi}_3 = \frac{\cos\phi_3\,\dot{m}_2 - \sin\phi_3\,\dot{m}_1}{\sin\theta_3} \tag{1.59}$$

Evaluating $\dot{m}_1$ and $\dot{m}_2$ from (1.52), where $\mathbf{W}$ is a skew-symmetric tensor defined as:

$$\mathbf{W} = \omega_1 \left(-\mathbf{e}_2\mathbf{e}_3 + \mathbf{e}_3\mathbf{e}_2\right) + \omega_2 \left(\mathbf{e}_1\mathbf{e}_3 - \mathbf{e}_3\mathbf{e}_1\right) + \omega_3 \left(-\mathbf{e}_1\mathbf{e}_2 + \mathbf{e}_2\mathbf{e}_1\right)$$

and substituting in (1.59), $\dot{\phi}_3$ is then given by the expression:

$$\dot{\phi}_3 = \omega_3 - \frac{D_{11} - D_{22}}{2} \sin 2\phi_3 + D_{12} \cos 2\phi_3 + [(D_{23} - \omega_1) \cos \phi_3 - (D_{13} + \omega_2) \sin \phi_3] \cot \theta_3 \quad (1.60)$$

The average value of the rate of rotation of the arbitrary vector $\mathbf{m}$ around the axis 3 can then be proved to be :

$$\boxed{\langle \dot{\phi}_3 \rangle = \frac{1}{\pi} \int_{\theta_3=0}^{\pi} \left(\frac{1}{2\pi} \int_{\phi_3=0}^{2\pi} \dot{\phi}_3 \, d\phi_3 \right) d\theta_3 = \omega_3} \quad (1.61)$$

In a similar manner, one can prove that the average values about axes 1 and 2 are given as:

$$\boxed{\langle \dot{\phi}_1 \rangle = \omega_1 \quad \text{and} \quad \langle \dot{\phi}_2 \rangle = \omega_2} \quad (1.62)$$

Equations (1.61), (1.62) reveal that the spin tensor $\mathbf{W}$ can be thought as the average rate of rotation (spin) of all material fibers intersecting with the point considered, in the current configuration.

1.5.3 D and W in terms of $\dot{\mathbf{F}}$

In order to establish a connection between the analysis of deformation as physically described by the polar decomposition theorem in Section 1.3 and the aforementioned discussion, one would be interested to express $\mathbf{D}$ and $\mathbf{W}$ in terms of quantities that are embedded with the information of deformation of the body. For this purpose, recall equation (1.44) where $\dot{\mathbf{F}}$ and $\mathbf{F}^{-1}$ is readily calculated by (1.23) as:

$$\dot{\mathbf{F}} = \frac{\partial}{\partial t}(\mathbf{R} \cdot \mathbf{U}) \Rightarrow \dot{\mathbf{F}} = \dot{\mathbf{R}} \cdot \mathbf{U} + \mathbf{R} \cdot \dot{\mathbf{U}} \quad \text{and} \quad \mathbf{F}^{-1} = \mathbf{U}^{-1} \cdot \mathbf{R}^{-1} \overset{\mathbf{R}^{-1}=\mathbf{R}^T}{=} \mathbf{U}^{-1} \cdot \mathbf{R}^T \quad (1.63)$$

Substitution of (1.63) in (1.44) now yields:

$$\mathbf{L} = (\dot{\mathbf{R}} \cdot \mathbf{U} + \mathbf{R} \cdot \dot{\mathbf{U}}) \cdot \mathbf{U}^{-1} \cdot \mathbf{R}^{-1} = \underbrace{\dot{\mathbf{R}} \cdot \mathbf{R}^T}_{\boldsymbol{\Omega}} + \mathbf{R} \cdot \dot{\mathbf{U}} \cdot \mathbf{U}^{-1} \cdot \mathbf{R}^T$$

$$\Rightarrow \boxed{\mathbf{L} = \boldsymbol{\Omega} + \mathbf{R} \cdot \dot{\mathbf{U}} \cdot \mathbf{U}^{-1} \cdot \mathbf{R}^T} \quad (1.64)$$

where, since $\mathbf{R}$ is orthogonal, $\boldsymbol{\Omega} = \dot{\mathbf{R}} \cdot \mathbf{R}^T$ is an skew-symmetric tensor as a result of (1.47). Calculation of $\mathbf{D}$ and $\mathbf{W}$ using (1.64) leads to the following important results:

$$\boxed{\mathbf{D} = \frac{1}{2}(\mathbf{L}^T + \mathbf{L}) = \frac{1}{2}\,\mathbf{R}\cdot(\dot{\mathbf{U}}\cdot\mathbf{U}^{-1} + \mathbf{U}^{-1}\cdot\dot{\mathbf{U}})\cdot\mathbf{R}^T} \tag{1.65}$$

$$\boxed{\mathbf{W} = \frac{1}{2}(\mathbf{L}^T - \mathbf{L}) = \boldsymbol{\Omega} + \frac{1}{2}\,\mathbf{R}\cdot(\dot{\mathbf{U}}\cdot\mathbf{U}^{-1} - \mathbf{U}^{-1}\cdot\dot{\mathbf{U}})\cdot\mathbf{R}^T} \tag{1.66}$$

Since $\mathbf{D}$ and $\mathbf{W}$ express rates of deformation and rotation respectively, the question that naturally emerges consists in whether or not these quantities can be directly integrated[7] in order to receive the desired deformation and rotation at the specific moment of the deformation history. In this sense, consider the special case for which the eigenvectors $\mathbf{N}_i$ associated with the Lagrangian triad mentioned in Section 1.3 are independent of time[8]. Then, using the spectral representation of $\mathbf{U}$ and differentiating with respect to t, one gets:

$$\mathbf{U}(t) = \sum_{i=1}^{3}\lambda_i(t)\mathbf{N}_i\mathbf{N}_i\ ,\ \mathbf{U}^{-1}(t) = \sum_{i=1}^{3}\frac{1}{\lambda_i(t)}\mathbf{N}_i\mathbf{N}_i\ \text{ and }\ \dot{\mathbf{U}}(t) = \sum_{i=1}^{3}\dot{\lambda}_i(t)\mathbf{N}_i\mathbf{N}_i \tag{1.67}$$

Moreover, Table 1.1 suggests that the Lagrangian logarithmic strain tensor is given as:

$$\mathbf{E}^{\ln} = \ln\mathbf{U} = \sum_{i=1}^{3}\ln\lambda_i(t)\mathbf{N}_i\mathbf{N}_i \overset{\frac{\partial}{\partial t}}{\Rightarrow} \dot{\mathbf{E}}^{\ln} = \sum_{i=1}^{3}\frac{\dot{\lambda}_i(t)}{\lambda_i(t)}\mathbf{N}_i\mathbf{N}_i \tag{1.68}$$

and evaluation of $\dot{\mathbf{U}}\cdot\mathbf{U}^{-1} = \mathbf{U}^{-1}\cdot\dot{\mathbf{U}}$ also yields:

$$\dot{\mathbf{U}}\cdot\mathbf{U}^{-1} = \mathbf{U}^{-1}\cdot\dot{\mathbf{U}} = \sum_{i=1}^{3}\frac{\dot{\lambda}_i(t)}{\lambda_i(t)}\mathbf{N}_i\mathbf{N}_i = \dot{\mathbf{E}}^{\ln}$$

Substitution of last equation to $\mathbf{D}$ and $\mathbf{W}$ (1.66) finally leads to:

$$\boxed{\mathbf{D} = \mathbf{R}\cdot\dot{\mathbf{E}}^{\ln}\cdot\mathbf{R}^T \Rightarrow \dot{\mathbf{E}}^{\ln} = \mathbf{R}^T\cdot\mathbf{D}\cdot\mathbf{R}} \quad\text{and}\quad \boxed{\mathbf{W} = \boldsymbol{\Omega} = \dot{\mathbf{R}}\cdot\mathbf{R}^T} \tag{1.69}$$

It can be proved that a similar result can be obtained for the rate of the Green strain $\mathbf{E}^G$ (see Table 1.1):

$$\boxed{\dot{\mathbf{E}}^G = \mathbf{F}^T\cdot\mathbf{D}\cdot\mathbf{F}} \tag{1.70}$$

Equations (1.69), (1.70) reveal that, in general, nor a strain tensor neither an orthogonal tensor exist whose rate is equal to $\mathbf{D}$ and $\mathbf{W}$ respectively. This important remark suggests that $\mathbf{D}$ or $\mathbf{W}$ cannot be directly integrated unless (in the case of the logarithmic strain) they are modified to account for rigid body rotations.

[7] Using a numerical integration scheme in the general case such as backward Euler, forward Euler etc.
[8] i.e. as in the case of uniaxial tension.

1.6 Stresses and Equations of Motion

Until now fundamental aspects of the kinematics of deformation have been discussed thoroughly in the previous sections. That is, the relations describing the changes in geometry and orientation of continuum bodies have been summarized. Nevertheless, no reference to the external sources that actually bring about the aforementioned deformations has been considered. In the context of continuum mechanics, these external sources are categorized into *body* and *surface* forces[9]. Action of such forces on a deformable body results in the development of internal forces per unit of area known as *stresses* [10] which in turn leads to macroscopic geometrical variations that define the deformation of the body when compared to a reference state. The various stress measures commonly used in applications of continuum mechanics as well as the *equations of motion* that are used to determine them, are briefly recalled in the following subsections.

Stress Measures

Consider an arbitrary tetrahedron in the current configuration[11] with normal vectors $\mathbf{n}_i$ on the three lateral faces and define the respective surface tractions (stress vectors) $\mathbf{t}_i$ with respect to a Cartesian coordinate system as:

$$\mathbf{t}_i = \sigma_{i1}\mathbf{e}_1 + \sigma_{i2}\mathbf{e}_2 + \sigma_{i3}\mathbf{e}_3 = \sigma_{ij}\mathbf{e}_j \tag{1.71}$$

Then, if $\mathbf{n}$ and $\mathbf{t}$ are the normal and the stress vectors respectively of the oblique face of the tetrahedron, then it can be proved using Newton's 2$^{\text{nd}}$ law that $\mathbf{t}$ is fully defined by the components σ_{ij} as:

$$\mathbf{t} = \boldsymbol{\sigma} \cdot \mathbf{n} \quad \text{or} \quad t_i = \sigma_{ij} n_j \tag{1.72}$$

where, according to the quotient rule, σ_{ij} are the components of a second order tensor which is known as the *Cauchy stress* tensor:

$$\boxed{\boldsymbol{\sigma} = \sigma_{ij}\mathbf{e}_i\mathbf{e}_j} \tag{1.73}$$

The quantity σ_{ij} expresses the j-th component of force per unit of deformed area that is exerted on an infinitesimal surface in the current configuration whose normal vector $\mathbf{n}$ of the current configuration is in the i-th direction. The axiom of Conservation of Angular Momentum leads to the important result concerning the symmetry of $\boldsymbol{\sigma}$ in the sense that :

$$\boxed{\boldsymbol{\sigma}^T = \boldsymbol{\sigma} \quad \text{or} \quad \sigma_{ji} = \sigma_{ij}} \tag{1.74}$$

[9] i.e. forces that act on every material point and on surface points of the body respectively.
[10] In the general so called "micropolar" theories, moments per unit area are also considered.
[11] Sometimes referred to as the Cauchy tetrahedron

Even though in the remainder of this discussion the Cauchy or "true" stress measure will be used, for the sake of completeness, other important stress measures commonly used in theories and computational implementations of continuum mechanics are summarized as follows.

A widely used stress measure in metal plasticity, due to the isochoric nature of plastic deformation, that is also defined in the deformed configuration, is the *Kirchhoff stress* defined as:

$$\boxed{\boldsymbol{\tau} = J\boldsymbol{\sigma}} \tag{1.75}$$

One can also define a stress measure, known as the *nominal stress*, in a way such that two distinct stress vectors defined with respect to the reference and current configurations respectively result in the same total force vector[12], which is given in terms of $\boldsymbol{\sigma}$ or $\boldsymbol{\tau}$ as:

$$\boxed{\mathbf{T} = J\mathbf{F}^{-1} \cdot \boldsymbol{\sigma} = \mathbf{F}^{-1} \cdot \boldsymbol{\tau}} \tag{1.76}$$

The quantity T_{ij} is the j-th component of force per unit of reference area exerted on an infinitesimal surface on the current configuration whose normal vector $\mathbf{N}$ in the reference configuration was in the i-th direction. It should be noted here that, although use of $\mathbf{T}$ would allow for easier boundary conditions description since $\mathbf{N}$ is known in the reference configuration, $\mathbf{T}$ does not posses the convenient symmetric property of $\boldsymbol{\sigma}$ which would pose, among other issues, its computational implementation more difficult.

Finally, the so called *1st* and *2nd Piola-Kirhhoff stresses* (with the latter defined in the reference configuration) can be defined in terms of the aforementioned stress tensors as:

$$\boxed{\mathbf{P} = \mathbf{T}^T = J\boldsymbol{\sigma}^T \cdot \mathbf{F}^{-T}} \quad \text{and} \quad \boxed{\mathbf{S} = J\mathbf{F}^{-1} \cdot \boldsymbol{\sigma} \cdot \mathbf{F}^{-T} = \mathbf{F}^{-1} \cdot \boldsymbol{\tau} \cdot \mathbf{F}^{-T} = \mathbf{T} \cdot \mathbf{F}^{-1}} \tag{1.77}$$

Equations of Motion for Deformable Bodies

The equations of motion along with compatibility equations, constitutive equations and properly defined boundary conditions form a general Boundary Value Problem (BVP), solution of which leads to the calculation of displacements, deformations and stresses within the body, in the general case of a dynamic analysis. Their derivation, which in the rationale of continuum mechanics is based on the axiom of Conservation of Linear Momentum, is presented bellow. Let $\boldsymbol{l}$ denote the linear momentum of an arbitrary material volume $V \subset \mathfrak{B}$ bounded by a surface ∂V and of a mass density ρ, which is defined as:

$$\boldsymbol{l} = \int_V \rho\, \boldsymbol{v}\, dV \tag{1.78}$$

Then, using the Raynold's transport theorem[13] $\dot{\boldsymbol{l}}$ can be readily calculated as:

[12] Which is defined as stress vector multiplied by the respective area.

[13] Transport theorems are generalizations of Leibniz's rule for the calculation of the derivative of a curve, surface or volume integral expression with variable integration limits. Raynold's transport theorem is a

$$\dot{\boldsymbol{l}} = \int_V \rho\, \dot{\boldsymbol{\upsilon}}\, dV = \int_V \rho\, \mathbf{a}\, dV \tag{1.79}$$

Conservation of Linear Momentum suggests that the total forces acting on the considered volume V must be equal to the rate of change the volume's linear momentum, i.e. :

$$\Sigma\mathbf{F} = \dot{\boldsymbol{l}} = \int_V \rho\, \mathbf{a}\, dV \tag{1.80}$$

where, assuming pure mechanical behavior, the total forces consists only of surface traction and gravitational forces in the sense that:

$$\Sigma\mathbf{F} = \int_{\partial V} \mathbf{T}\, dS + \int_V \rho\, \mathbf{b}\, dV \tag{1.81}$$

Substituting (1.81) in (1.80) and carrying out some calculations one arrives at the following expression:

$$\int_V (\boldsymbol{\nabla} \cdot \boldsymbol{\sigma} + \rho\, \mathbf{b} - \rho\, \mathbf{a})\, dV = 0 \quad \forall\, V \tag{1.82}$$

Since last equation holds for any V then, using the so called localization theorem, one finally arrives at the desired system of partial differential equations of motion :

$$\boxed{\boldsymbol{\nabla} \cdot \boldsymbol{\sigma} + \rho\mathbf{b} = \rho\mathbf{a} \quad \text{or} \quad \sigma_{ij,j} + \rho b_i = \rho a_i} \tag{1.83}$$

In the case where acceleration of material particles can be considered small, the inertial term in the right hand side of (1.83) can be neglected resulting in the well known *static equilibrium equations*.

1.7 Principle of Objectivity and Objective Rates

An important axiom of the general theory of constitutive modeling demands constitutive behavior of materials to be independent of the *frame of reference* it is examined i.e. to *to be objective*. In a more abstract sense, one could think the notion of a frame of reference as an "obserever" who observes a phenomenon making measurements of positions and time either statically or while he translates and rotates in space. Mathematically speaking, let the Newtonian space time $\mathcal{N}_{st}$ denote the four-dimensional space where all real world events take place and consider the mathematical structure that models these events as the product space of $\mathcal{E}$ with the set of real numbers $\mathbb{R}$. A frame of reference f_r can then be defined as the mapping between the real world events and placement in a location of Euclidean space $(\mathbf{x})$ at a specific time (t) , i.e.:

$$f_r \;:\; \mathcal{N}_{st} \to \mathcal{E} \times \mathbb{R} \tag{1.84}$$

special case concerning volume integrals of the form $A = \int_V \rho\, f\, dV$

Consider now an event in $\mathcal{N}_{st}$ and two different observers f_r, $\overline{f_r}$ mapping this event into space positions and times $(\mathbf{x}, t)$ and $(\overline{\mathbf{x}}, \overline{t})$ respectively. A *change of frame* $f_{f_r \to \overline{f_r}}$ can then be introduced as a mapping relating $(\mathbf{x}, t)$ with $(\overline{\mathbf{x}}, \overline{t})$:

$$f_{f_r \to \overline{f_r}} \; : \; (\mathbf{x}, t) \to (\overline{\mathbf{x}}, \overline{t}) \tag{1.85}$$

Then, *Principle of Euclidean objectivity* demands that the change of frame must preserve relative distances and time between the two observers (material points) constant and thus the motion $\overline{\mathbf{x}}$ must differ, in the most general case, by a rigid body rotation plus a translation i.e. :

$$\overline{\mathbf{x}}(\mathbf{X}, \overline{t}) = \mathbf{Q}(t) \cdot \mathbf{x}(\mathbf{X}, t) + \mathbf{c}(t) \quad \text{with} \quad \overline{t} = t + c \tag{1.86}$$

where $\mathbf{Q}(t)$ is proper orthogonal with $\mathbf{Q}(0) = \boldsymbol{\delta}$, $\mathbf{c}(0) = 0$ and $c \in \mathbb{R}$ is equal to zero for simultaneous events (considered hereafter). If $\overline{\mathbf{Q}}$ is the mapping of any observable tensorial quantity g of order n (scalar, vector, second order tensor etc.) between the two observers due to the change of frame (1.86), then for g to be objective it has to express the exact same quantity in both frames, or symbolically speaking:

$$g(\overline{\mathbf{x}}, t) = \overline{\mathbf{Q}}[g(\mathbf{x}, t)] \tag{1.87}$$

More specifically, the arbitrary mapping $\overline{\mathbf{Q}}$ takes the following forms concerning 0^{th}, 1^{st} and 2^{nd} order Lagrangian and Eulerian tensors:

Scalar fields $\phi(\mathbf{X}, t)$, $\phi(\mathbf{x}, t)$, defined in $\mathfrak{B}_0$ and $\mathfrak{B}_t$ are considered Lagrangian and Eulerian objective respectively, if they transform according to :

$$\overline{\phi}(\mathbf{X}, t) = \phi(\mathbf{X}, t) \quad \text{and} \quad \overline{\phi}(\overline{\mathbf{x}}, t) = \phi(\mathbf{x}, t) \tag{1.88}$$

Tensors of 1^{st} and 2^{nd} order defined in $\mathfrak{B}_0$ are considered (Lagrangian) objective if they remain unaffected by the superposed rigid body rotation:

$$\overline{\mathbf{a}}(\mathbf{X}, t) = \mathbf{a}(\mathbf{X}, t) \quad \text{and} \quad \overline{\mathbf{A}}(\mathbf{X}, t) = \mathbf{A}(\mathbf{X}, t) \tag{1.89}$$

Tensors of 1^{st} and 2^{nd} order defined in $\mathfrak{B}_t$ are considered (Eulerian) objective if they transform according to:

$$\overline{\mathbf{a}}(\overline{\mathbf{x}}, t) = \mathbf{Q}(t) \cdot \mathbf{a}(\mathbf{x}, t) \quad \text{and} \quad \overline{\mathbf{A}}(\overline{\mathbf{x}}, t) = \mathbf{Q}(t) \cdot \mathbf{A}(\mathbf{x}, t) \cdot \mathbf{Q}^T(t) \tag{1.90}$$

Finally, 2^{nd} order tensors are called two-point objective if they transform according to:

$$\overline{\mathbf{A}} = \mathbf{Q}(t) \cdot \mathbf{A} \quad \text{or} \quad \overline{\mathbf{A}} = \mathbf{A} \cdot \mathbf{Q}^T(t) \tag{1.91}$$

It can be proved that $\boldsymbol{\sigma}$, $\boldsymbol{\tau}$ and $\mathbf{D}$ are Eulerian objective, $\mathbf{S}$, $\mathbf{t}$ and Lagrangian strain tensors

$\mathbf{E}$ are Lagrangian objective and $\mathbf{F}$ is a two-point objective tensor. Additionally, if $\mathbf{A}$ is Lagrangian objective then $\dot{\mathbf{A}}$ is also objective but if $\mathbf{A}$ is Eulerian objective then $\dot{\mathbf{A}}$ is *not* objective. This last remark can pose a serious problem in the case of finite deformation constitutive modeling (where rate formulation is used) since $\mathbf{D}$ requires a corresponding Eulerian objective stress rate while both $\dot{\boldsymbol{\sigma}}$ and $\dot{\boldsymbol{\tau}}$ are non-objective. For this purpose, one wants to define rates of quantities that are objective in order to tackle the aforementioned problem. In this direction, consider a time varying basis $\mathbf{e}_i^\star(t)$, where $\mathbf{e}_i^\star$ are in general neither unit nor orthogonal, and let their evolution equations be:

$$\dot{\mathbf{e}}_i^\star(t) = \mathbf{A}(t) \cdot \mathbf{e}_i^\star = \mathbf{e}_i^\star \cdot \mathbf{A}^T(t) \tag{1.92}$$

Any vector $\mathbf{a}(t)$ and second order tensor $\boldsymbol{\sigma}(t)$ can be written with respect to the basis (1.92) as:

$$\mathbf{a}(t) = a_i(t)\, \mathbf{e}_i^\star(t) \quad \text{and} \quad \boldsymbol{\sigma}(t) = \sigma_{ij}(t)\, \mathbf{e}_i^\star(t)\mathbf{e}_i^\star(t)$$

Then, the rates of $\mathbf{a}(t)$ and $\boldsymbol{\sigma}(t)$ as seen by an observer who is attached to the evolving base $\mathbf{e}_i^\star(t)$, which are known as *corodeformational rates* (or *corotational* if $\mathbf{A}$ is skew-symmetric) and denoted by $\overset{\square}{\mathbf{a}}$ and $\overset{\square}{\boldsymbol{\sigma}}$ respectively, are proved to be given by :

$$\boxed{\overset{\square}{\mathbf{a}} = \dot{\mathbf{a}} - \mathbf{A} \cdot \mathbf{a}} \quad \text{and} \quad \boxed{\overset{\square}{\boldsymbol{\sigma}} = \dot{\boldsymbol{\sigma}} - \mathbf{A} \cdot \boldsymbol{\sigma} - \boldsymbol{\sigma} \cdot \mathbf{A}^T} \tag{1.93}$$

For, $\overset{\square}{\mathbf{a}}$ and $\overset{\square}{\boldsymbol{\sigma}}$ to be Eulerian objective in the sense of (1.90) then, in both cases, $\mathbf{A}$ has to transform according to:

$$\boxed{\overline{\mathbf{A}} = \mathbf{Q} \cdot \mathbf{A} \cdot \mathbf{Q}^T + \dot{\mathbf{Q}} \cdot \mathbf{Q}^T} \tag{1.94}$$

The most commonly used objectives rates for special choices of $\mathbf{A}(t)$ are summarized in Table 1.2 :

Table 1.2: Eulerian objective rates of vectors and 2nd order tensors.

Rate	Choice of $\mathbf{A}$	Definition
Jaumann	$\mathbf{A} = \mathbf{W}$	$\overset{\triangledown}{\mathbf{a}} = \dot{\mathbf{a}} - \mathbf{W} \cdot \mathbf{a}$, $\overset{\triangledown}{\boldsymbol{\sigma}} = \dot{\boldsymbol{\sigma}} - \mathbf{W} \cdot \boldsymbol{\sigma} - \boldsymbol{\sigma} \cdot \mathbf{W}^T$
Green-Naghdi	$\mathbf{A} = \dot{\mathbf{R}} \cdot \mathbf{R}^T = \boldsymbol{\Omega}$	$\overset{\circ}{\mathbf{a}} = \dot{\mathbf{a}} - \boldsymbol{\Omega} \cdot \mathbf{a}$, $\overset{\circ}{\boldsymbol{\sigma}} = \dot{\boldsymbol{\sigma}} - \boldsymbol{\Omega} \cdot \boldsymbol{\sigma} - \boldsymbol{\sigma} \cdot \boldsymbol{\Omega}^T$
Truesdell	$\mathbf{A} = \mathbf{L}$	$\overset{*}{\mathbf{a}} = \dot{\mathbf{a}} - \mathbf{L} \cdot \mathbf{a}$, $\overset{*}{\boldsymbol{\sigma}} = \dot{\boldsymbol{\sigma}} - \mathbf{L} \cdot \boldsymbol{\sigma} - \boldsymbol{\sigma} \cdot \mathbf{L}^T$
Cotter-Rivlin	$\mathbf{A} = -\mathbf{L}^T$	$\overset{\triangle}{\mathbf{a}} = \dot{\mathbf{a}} + \mathbf{L}^T \cdot \mathbf{a}$, $\overset{\triangle}{\boldsymbol{\sigma}} = \dot{\boldsymbol{\sigma}} + \mathbf{L}^T \cdot \boldsymbol{\sigma} + \boldsymbol{\sigma} \cdot \mathbf{L}$

In constitutive model for gradient plasticity developed in Chapter 4 the Jaumann derivative of the quantities involved is chosen due to its easier computational implementation.

Chapter 2

Finite Deformation Elastoplasticity

Herein, aspects of the theory of finite deformation elastoplasticity that are used in the constitutive modeling presented in Chapter 4 are summarized. More specifically, based on the theory of the previous chapter, important relations concerning the kinematics of finite deformation elastoplasticity which depend on the concept of the multiplicative decomposition of $\mathbf{F}$ are described. Thereafter, general theory of rate-independent constitutive modeling for the elastic and plastic part of deformation, the so-called consistency condition, the loading-unloading criterion and hardening are also briefly presented.

2.1 Kinematics of Finite Deformation Plasticity

As outlined in [32], [50], [53] and in several other references in the relevant literature, in the classical theories of infinitesimal elastoplastic deformations, the fundamental assumption adopted imposes the restriction that both elastic and plastic strains are small approximately of order $O(10^{-3})$ so one does not have to explicitly make a distinction between the reference and deformed configurations. This simplifying hypothesis allows for the constitutive modeling of the material to be based on the additive decomposition of the total strain tensor into an elastic and plastic part, assuming uncoupled elastic-plastic behavior. Even though this theory might be viable for usual structural analysis applications (where design to prevent plastic flow is desired), in cases where finite plastic and/or elastic deformations are introduced (such as metal forming processes, explosive forming etc.) another approach has to be considered. The first consistent analysis of an general kinematic description of finite deformations was presented by Lee [50], who proposed the introduction of an *intermediate unstressed configuration*[1] $\mathfrak{B}_i$. This assumption resulted in the well known multiplicative decomposition of the deformation gradient $\mathbf{F}$ into an elastic part $\mathbf{F}^e$ and plastic part $\mathbf{F}^p$:

$$\boxed{\mathbf{F} = \mathbf{F}^e \cdot \mathbf{F}^p} \tag{2.1}$$

[1] Which in the general case, as mentioned in [8], is a fictitious one since in a material that exhibits a Bauschinger effect such that unloading to $\mathfrak{B}_i$ may cause additional plastic deformation, residual stressed may be introduced in the intermediate configuration, thus violating its definition.

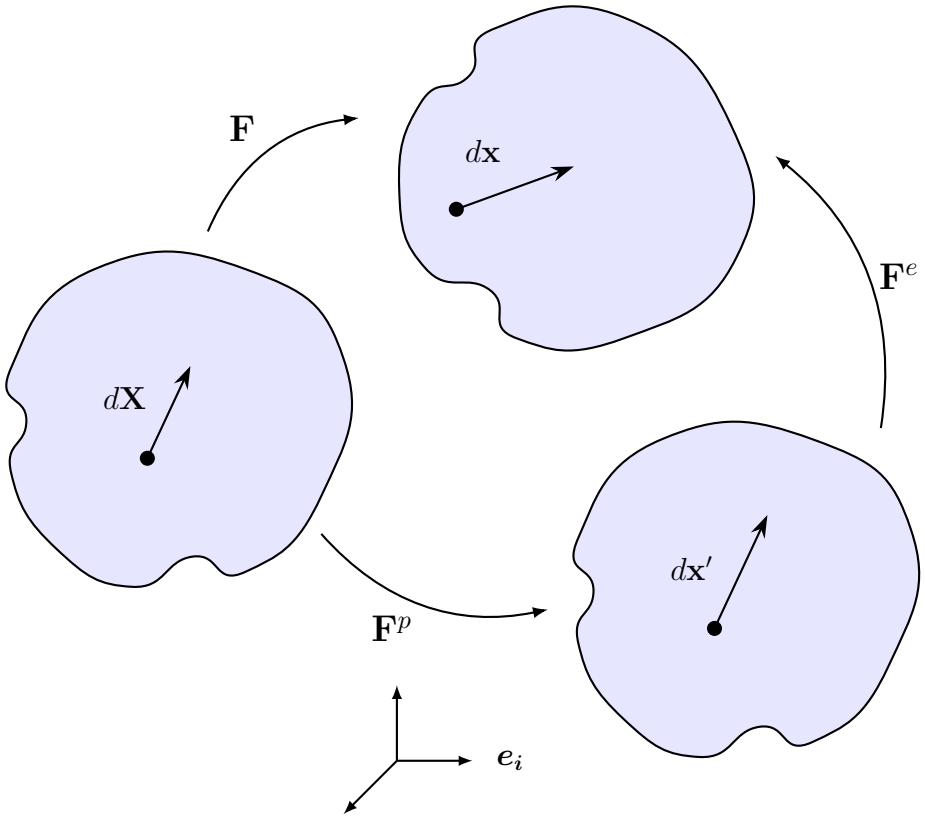

Figure 2.1: Multiplicative decomposition of deformation gradient $\mathbf{F}$.

Schematic representation of (2.1) is illustrated in Figure 2.1.

Using (2.1) one would be interested to derive expressions of the tensors $\mathbf{L}$, $\mathbf{D}$ and $\mathbf{W}$ introduced in Section 1.5 in terms of $\mathbf{F}^e$ and $\mathbf{F}^p$. Substituting (2.1) in (1.44) one arrives at the following additive decomposition of the velocity gradient tensor:

$$\begin{aligned}\mathbf{L} = \dot{\mathbf{F}} \cdot \mathbf{F}^{-1} = (\dot{\mathbf{F}}^e \cdot \mathbf{F}^p + \mathbf{F}^e \cdot \dot{\mathbf{F}}^p) \cdot \mathbf{F}^{p-1} \cdot \mathbf{F}^{e-1} \Rightarrow \\ \Rightarrow \mathbf{L} = \dot{\mathbf{F}}^e \cdot \mathbf{F}^{e-1} + \mathbf{F}^e \cdot \dot{\mathbf{F}}^p \cdot \mathbf{F}^{p-1} \cdot \mathbf{F}^{e-1} \Rightarrow \boxed{\mathbf{L} = \mathbf{L}^e + \mathbf{L}^p}\end{aligned} \tag{2.2}$$

where

$$\boxed{\mathbf{L}^e = \dot{\mathbf{F}}^e \cdot \mathbf{F}^{e-1}} \quad , \quad \boxed{\mathbf{L}^p = \mathbf{F}^e \cdot \mathbf{L}_i^p \cdot \mathbf{F}^{e-1}} \quad \text{and} \quad \boxed{\mathbf{L}_i^p = \dot{\mathbf{F}}^p \cdot \mathbf{F}^{p-1}} \tag{2.3}$$

It should be noted here that both $\mathbf{L}^p$ and $\mathbf{L}^e$ are defined at the current with respect to the reference configuration whereas $\mathbf{L}_i^p$ is defined in the fictitious isoclinic with respect to the undeformed configuration. Additionally, one can decompose $\mathbf{L}_i^p$ into symmetric and antisymmetric parts respectively as:

$$\mathbf{L}_i^p = \mathbf{D}_i^p + \mathbf{W}_i^p \text{ where } \mathbf{D}_i^p = \frac{1}{2}(\mathbf{L}_i^p + (\mathbf{L}_i^p)^T) \quad \text{and} \quad \mathbf{W}_i^p = \frac{1}{2}(\mathbf{L}_i^p - (\mathbf{L}_i^p)^T) \tag{2.4}$$

Finally, using the right polar decomposition for the elastic part of the deformation gradient i.e. $\mathbf{F}^e = \mathbf{R} \cdot \mathbf{U}^e$, the property $\mathbf{R}^{-1} = \mathbf{R}^T$ due to the proper orthogonality of $\mathbf{R}$ and equations

(2.2), (2.3), one can get the general expressions for the additive decompositions of $\mathbf{D}$ and $\mathbf{W}$ as thoroughly described in [6]:

$$\boxed{\mathbf{D} = \mathbf{D}^e + \mathbf{D}^p} \quad \text{and} \quad \boxed{\mathbf{W} = \boldsymbol{\Omega} + \mathbf{W}^e + \mathbf{W}^p} \tag{2.5}$$

with

$$\boxed{\mathbf{D}^e = (\mathbf{L}^e)^{(sym)} = \mathbf{R} \cdot [\dot{\mathbf{U}}^e \cdot (\mathbf{U}^e)^{-1}]^{(sym)} \cdot \mathbf{R}^T} \tag{2.6}$$

$$\boxed{\mathbf{D}^p = (\mathbf{L}^p)^{(sym)} = \mathbf{R} \cdot [\mathbf{U}^e \cdot \mathbf{L}_i^p \cdot (\mathbf{U}^e)^{-1}]^{(sym)} \cdot \mathbf{R}^T} \tag{2.7}$$

$$\boxed{\boldsymbol{\Omega} = \dot{\mathbf{R}} \cdot \mathbf{R}^T, \quad \mathbf{W}^e = (\mathbf{L}^e)^{(skew)} = \mathbf{R} \cdot [\dot{\mathbf{U}}^e \cdot (\mathbf{U}^e)^{-1}]^{(skew)} \cdot \mathbf{R}^T} \tag{2.8}$$

$$\boxed{\mathbf{W}^p = (\mathbf{L}^p)^{(skew)} = \mathbf{R} \cdot [\mathbf{U}^e \cdot \mathbf{L}_i^p \cdot (\mathbf{U}^e)^{-1}]^{(skew)} \cdot \mathbf{R}^T} \tag{2.9}$$

where it is be proved, in the context of crystal plasticity, that $\boldsymbol{\Omega}$ expresses the spin of all slip systems i.e. it can be thought as the spin of the microstructure of the material. Relations (2.6-2.9) consist the general kinematic description of large strain elastoplasticity and will be used, with appropriate simplifying assumptions, in the description of the general framework of rate-independent plasticity which in turn is the basis for the development of the nonlocal model of Chapter 4.

2.2 Constitutive Theory of Rate - Independent Elastoplasticity

As mentioned in Section 1.6, the general BVP of elastoplasticity is associated to the solution of a system of, in principle, nonlinear system of partial differential equations for the calculation of the displacement, strain and stress fields of the continuum body. However, although the equations of motion and kinematic equations are valid for all materials regardless of their physical nature[2] (solids, fluids etc.), constitutive equations are *material dependent* in the sense that, naturally, distinct materials can respond quite differently to the same external stimulus. Even though this last remark implies that constitutive modeling has to be carried out solely for the material under consideration, this procedure in not as arbitrary as it seems since a general constitutive framework can be constructed and then, with the appropriate assumptions, be applied for the material examined.

Then, as described in [29], [32] and [53] one can group the constitutive modeling of elastoplactic material into two major approaches, both having the multiplicative decomposition of $\mathbf{F}$ given by (2.1) as a starting point. In the first approach, the material is modeled as hyperelastic[3] where additionally elastic-plastic behavior is treated in terms of Helmholtz free

[2] As long the continuum hypothesis holds.

[3] i.e. as one for which the stress-strain relation can be derived from a *strain energy density potential*.

energy density. The second approach, which is also adopted in the context of this diploma thesis, uses a hypoelastic description of the material[4], the additive decompositions of (2.5) and objective rates. In the latter case, elastic and plastic behavior are treated separately and then they can be combined in order to describe the total elastoplastic constitutive behavior.

Before one proceeds with the mathematical description of the aforementioned theory, it is important to remember that in the description of constitutive equations, pairs of stress and strain rates cannot be arbitrarily selected in the sense their product has to correspond to a *stress power* which is produced or dissipated due to the external forces. It can be proved (see [58]) that the stress power per unit volume is by definition given in terms of the Cauchy or Kirchhoff stresses as:

$$\dot{W}_{int} = \mathrm{tr}(\boldsymbol{\sigma} \cdot \mathbf{D}) = \frac{1}{J}\,\mathrm{tr}(\boldsymbol{\tau} \cdot \mathbf{D}) \tag{2.10}$$

Such stress-strain rate pairs are mentioned in the literature as *work-conjugate*. Work - conjugate strain rate pairs for stress measures other than the ones mentioned above can be found using (2.10).

2.2.1 Elastic Regime

In general, since elastic deformation is fully reversible after unloading, one would naturally postulate that hyperelastic behavior is more of a sensible choice for the description of a material that can possibly exhibit large elastic strains. Then, for the work-conjugate pair of the 2$^{\text{nd}}$ Piola-Kirhhoff stress $\mathbf{S}$ and Green strain $\mathbf{E}^G$, the hyperelastic constitutive equation for the elastic behavior of the material can be written, if one postulates the existence of an elastic stress potential per unit volume W^e, as ([8], [10] and [53]):

$$\mathbf{S}^e = \frac{\partial W^e(\mathbf{E}^e)}{\partial \mathbf{E}^e} \tag{2.11}$$

where $\mathbf{E}^e$ is the elastic part of $\mathbf{E}^G$ and $\mathbf{S}^e$ corresponds to $\mathbf{E}^e$. One would be interested in the rate form of the hyperelastic equation (2.11) so differentiation with respect to time yields:

$$\dot{\mathbf{S}}^e = \hat{\boldsymbol{\mathcal{L}}}^e : \dot{\mathbf{E}}^e \quad \text{with} \quad \hat{\boldsymbol{\mathcal{L}}}^e = \frac{\partial^2 W^e}{\partial \mathbf{E}^e \partial \mathbf{E}^e} \tag{2.12}$$

On the other hand, the hypoelastic, corotational constitutive formulation assumes that a linear relation between the corotational Cauchy stress rate and the elastic part of $\mathbf{D}$ can be established, in the sense that:

$$\overset{\circ}{\boldsymbol{\sigma}} = \boldsymbol{\mathcal{L}}^e : \mathbf{D}^e \tag{2.13}$$

[4]Materials considered hypoelastic are such that the work during a closed loading cycle is not zero even in the absence of inelastic deformation and so, a stress-strain relationship *cannot* be derived from a potential function.

Where $\mathring{\boldsymbol{\sigma}}$ is the Green-Naghdi objective rate which is corotational with the spin of the microstructure $\boldsymbol{\Omega}$ of the material. Taking into consideration that applications of the model described in Chapter 4 concern modeling of materials for which plastic strains are orders of magnitude larger than elastic strains, then, one can assume small elastic strains. In this case, as proved in Aravas [8] and Fish [29], the hyperelastic formulation (2.12) can be reduced, in leading order, to the hypoelastic one of (2.13) with:

$$\mathcal{L}^e_{ijkl} = R_{ip}R_{jq}R_{kr}R_{ls}\hat{\mathcal{L}}^e_{pqrs}$$

Additionally, for small elastic strains, it can be proved that $\mathbf{W}^e = O(\varepsilon^2)$, $\varepsilon << 1$, so that $\mathbf{W}$ is approximately equal to:

$$\mathbf{W} = \boldsymbol{\Omega} + \mathbf{W}^p \tag{2.14}$$

Using (2.13), (2.14) and the definitions of the Green-Naghdi and Jaumann objective rates one can arrive to an alternative rate formulation of the hypoelastic model expressed in terms of the Jaumann rate:

$$\boxed{\overset{\nabla}{\boldsymbol{\sigma}} = \mathring{\boldsymbol{\sigma}} + \boldsymbol{\sigma}\cdot\mathbf{W}^p - \mathbf{W}^p\cdot\boldsymbol{\sigma} = \boldsymbol{\mathcal{L}}^e : \mathbf{D}^e + \boldsymbol{\sigma}\cdot\mathbf{W}^p - \mathbf{W}^p\cdot\boldsymbol{\sigma}} \tag{2.15}$$

2.2.2 Plastic Regime

It is well known from the theory of infinitesimal deformations that for the inelastic (or plastic in the context of metal plasticity) part of the deformation, one cannot develop a constitutive equation that is bijective in stress and strain as in linear elasticity in the sense the one-to-one correspondence of stress and strain is no longer valid. The latter can be made clear in the case of uniaxial tension where, given a value for the final stress (strain) state of the material in the plastic region there exists an infinite number of possible corresponding strain (stress) states i.e. the final state of the material is path dependent.

To begin with, this implies that additional information is necessary in order to establish a relation between stress and strain in the plastic regime and this information is provided through the so-called *state* or *internal variables*, hereafter denoted as $\mathbf{s} = \{s_1, s_2, ...s_n\}$. The physical nature of these variables generally depends on the material under consideration. Nevertheless, one could imagine that these variables describe the necessary *deformation history* of the material which in turn depends, for real heterogeneous materials, on their *microstructure* i.e. the structural distribution of the material in length scales orders of magnitude smaller than the visible, macroscopic one. Moreover, what one identifies as macroscopic deformation is due to the transformation or *evolution* of the underlying microstructure of the material and in order to describe this evolution, it is necessary to calculate the rate of change of the state variables which are known as the *evolution equations* of $\mathbf{s}$.

Another important result of the non bijective nature of the plastic deformation is that

one should approach its description incrementally and thus the plastic behavior will be described by a rate constitutive equation. In this procedure, at every loading increment, one first needs a criterion to determine whether or not the material point under consideration is plastically deformed and, in case that it is, a criterion is needed in order to determine if this point continuous to deform plastically or if it unloads elastically during the increment. This is achieved by the introduction of the so-called *yield function*[5] and the *loading-unloading criterion*.

Yield Condition and Normality Rule

As mentioned above, one wishes to know for a given state of the loading program (i.e. given $\boldsymbol{\sigma} = \boldsymbol{\sigma}^*$ and $\mathbf{s} = \mathbf{s}^*$) whether the material point under consideration is in the elastic or plastic region in order for the appropriate constitutive approach to be implemented. Then, this leads to the definition of the yield function $\Phi = \Phi(\boldsymbol{\sigma}, \mathbf{s})$ which is used to define the *yield condition*:

$$\Phi(\boldsymbol{\sigma}^*, \mathbf{s}^*) \begin{cases} < 0 & \Rightarrow \quad \text{Elastic response} \\ \\ \geq 0 & \Rightarrow \quad \text{Plastic Response} \end{cases} \tag{2.16}$$

The yield function Φ can in principle be any multivariable function of $\boldsymbol{\sigma}$ and $\mathbf{s}$ although experimental observations and the physics of the material class under consideration have to be taken into account in order to derive an accurate closed form. In the most general case, one can write Φ in the form:

$$\boxed{\Phi(\boldsymbol{\sigma}, s^{\alpha}) = \sigma_e(\boldsymbol{\sigma}, s^{\beta}) - \sigma_y(s^{\gamma})} \tag{2.17}$$

where σ_e is a properly defined *equivalent stress*, σ_y is the *yield curve* of the material derived from the uniaxial tension test and generally $\beta \neq \gamma$.

Using the notion of the yield function one is now able to define the constitutive relation for the plastic part $\mathbf{D}^p$ of deformation. In the case of small elastic deformations, it is proved in [53] using the postulate of maximum plastic dissipation that $\mathbf{D}^p$ for finite plastic deformations is given by a "normality rule" in terms of Kirchhoff stress, which is analogous to the one of the corresponding infinitesimal theory:

$$\mathbf{D}^p = \varphi \, \frac{\partial g}{\partial \boldsymbol{\tau}} \tag{2.18}$$

where φ is a scalar quantity and g is the so-called plastic potential. For metal plasticity, the plastic potential g is selected to coincide with the yield function Φ and deformation is also isochoric (i.e. $J = 1$). Furthermore, for *rate independent plasticity*, ϕ is equal to the so-called *plastic multiplier* $\dot{\lambda}$ which can be implicitly calculated by the consistency condition

[5] Although there exist general plasticity theories that do not define a yield function

described in the following subsection. With all these in mind, (2.18) can be written in the form:

$$\boxed{\mathbf{D}^p = \dot{\lambda}\,\mathbf{N} \quad \text{where} \quad \mathbf{N} = \frac{\partial \Phi}{\partial \boldsymbol{\sigma}}\ ,\ \ \dot{\lambda} \geq 0} \tag{2.19}$$

As in the case of infinitesimal deformations and due to the symmetry of the Cauchy tensor, Φ is proved to be convex in the six-dimensional stress space and $\mathbf{D}^p$ can be interpreted as being an outward-pointing normal vector to the yield surface in the direction of $\mathbf{N}$.

The Consistency Condition

In the case of rate-independent plasticity, one imposes the restriction, for ongoing plastic deformation, that any variation of the internal variables $d\mathbf{s}$ (which are the set of *parameters* that determine the variation of Φ) is such that the yield criterion is satisfied in the new state described by $\mathbf{s} + d\mathbf{s}$. The aforementioned statement is known as the consistency condition and can be generally defined (see Dafalias [19]) as:

$$\boxed{\dot{\Phi} = \frac{\partial \Phi}{\partial \boldsymbol{\sigma}} : \dot{\boldsymbol{\sigma}} + \frac{\partial \Phi}{\partial \mathbf{s}} \cdot \dot{\mathbf{s}} = \frac{\partial \Phi}{\partial \boldsymbol{\sigma}} : \overset{\triangledown}{\boldsymbol{\sigma}} + \frac{\partial \Phi}{\partial \mathbf{s}} \cdot \overset{\triangledown}{\mathbf{s}} = \frac{\partial \Phi}{\partial \boldsymbol{\sigma}} : \overset{\circ}{\boldsymbol{\sigma}} + \frac{\partial \Phi}{\partial \mathbf{s}} \cdot \overset{\circ}{\mathbf{s}} = 0} \tag{2.20}$$

Moreover, for the constitutive model to be rate independent, the corotational evolution equations of $\mathbf{s}$ have to be homogeneous function of degree one with respect to $\mathbf{D}^p$, i.e.:

$$\overset{\circ}{\mathbf{s}} = \mathbf{G}(\boldsymbol{\sigma}, \mathbf{s}, \mathbf{D}^p) = \dot{\lambda}\,\mathbf{g}(\boldsymbol{\sigma}, \mathbf{s}) \tag{2.21}$$

where $\mathbf{g}$ is a properly defined function set depending on the state variable choice.

Using the fact that $\mathbf{D}^e = \mathbf{D} - \mathbf{D}^p$ due to (2.5) and taking into consideration (2.13), (2.19) and (2.21), one can calculate $\dot{\lambda}$ from the consistency condition (2.20) as follows:

$$\begin{aligned}
&\frac{\partial \Phi}{\partial \boldsymbol{\sigma}} : \overset{\circ}{\boldsymbol{\sigma}} + \frac{\partial \Phi}{\partial \mathbf{s}} \cdot \overset{\circ}{\mathbf{s}} = \frac{\partial \Phi}{\partial \boldsymbol{\sigma}} : \boldsymbol{\mathcal{L}}^e : (\mathbf{D} - \dot{\lambda}\,\mathbf{N}) + \dot{\lambda}\,\frac{\partial \Phi}{\partial \mathbf{s}} \cdot \mathbf{g} = \\
&= \mathbf{N} : \boldsymbol{\mathcal{L}}^e : \mathbf{D} - \dot{\lambda}\left(H + \mathbf{N} : \boldsymbol{\mathcal{L}}^e : \mathbf{D}\right) = 0 \\
&\Rightarrow \boxed{\dot{\lambda} = \frac{1}{L}\,\mathbf{N} : \boldsymbol{\mathcal{L}}^e : \mathbf{D}}
\end{aligned} \tag{2.22}$$

where H, which is known the *hardening modulus*, and the quantity L are given by:

$$\boxed{H = -\frac{\partial \Phi}{\partial \mathbf{s}} \cdot \mathbf{g}} \quad \text{and} \quad \boxed{L = H + \mathbf{N} : \boldsymbol{\mathcal{L}}^e : \mathbf{N}} \tag{2.23}$$

Finally, since definition of H, which can be either positive or negative, suggests that it is order of magnitude of yield stress ($O(\sigma_0)$), $\boldsymbol{\mathcal{L}}^e$ is by definition a positive definite tensor of the same order as the elastic modulus ($O(E)$), $\mathbf{N}$ is of order 1 (i.e. $\frac{O(\sigma_0)}{O(\sigma_0)} \to 1$) and for metals

$O(\sigma_0) << O(E)$, then (2.23) implies that L is always positive.

Hardening and Loading-Unloading Criterion

The hardening modulus H defined in the previous subsection can be readily proved to be associated with the *local hardening* or *softening* of the material point under consideration. In this direction, let $\boldsymbol{\sigma}^A$ and $\mathbf{s}$ define the current state in the vicinity a material point A and $d\mathbf{s}$ be the variation of the state variables that leads to the new state which is characterized by the yield surface $\Phi(\boldsymbol{\sigma}, \mathbf{s}+d\mathbf{s})$. Then, one can decide if the material has undergone hardening or softening depending on whether the stress $\boldsymbol{\sigma}^A$ that caused this incremental variation lies on the interior or the exterior of the new yield surface or mathematically speaking:

$$\Phi(\boldsymbol{\sigma}^A, \mathbf{s}+d\mathbf{s}) \begin{cases} < 0 & \Rightarrow \quad \text{Hardening} \\ \\ > 0 & \Rightarrow \quad \text{Softening} \end{cases} \tag{2.24}$$

Using the Taylor expansion of $\Phi(\boldsymbol{\sigma}^A, \mathbf{s}+d\mathbf{s})$ one gets:

$$\begin{aligned} &\Phi(\boldsymbol{\sigma}^A, \mathbf{s}+d\mathbf{s}) = \Phi(\boldsymbol{\sigma}^A, \mathbf{s}) + \left.\frac{\partial \Phi}{\partial \mathbf{s}}\right|_{(\boldsymbol{\sigma}^A, \mathbf{s})} \cdot d\mathbf{s} + O(d\mathbf{s}^2) \overset{\substack{\Phi(\boldsymbol{\sigma}^A,\mathbf{s})=0 \\ d\mathbf{s}=d\lambda\,\mathbf{g}}}{\Longrightarrow} \\ &\Phi(\boldsymbol{\sigma}^A, \mathbf{s}+d\mathbf{s}) \approx d\lambda \underbrace{\left.\frac{\partial \Phi}{\partial \mathbf{s}}\right|_{(\boldsymbol{\sigma}^A, \mathbf{s})} \cdot \mathbf{g}}_{-H} = -d\lambda\, H \end{aligned} \tag{2.25}$$

Equations (2.24) and (2.25) imply that $H > 0$ corresponds to hardening while $H < 0$ corresponds to softening around point A.

One can derive the condition for plastic loading from the fact that $\dot{\lambda}$ has to be positive for further plastic deformation to take place. This observation, along with (2.22) lead to the following restriction:

$$\dot{\lambda} > 0 \overset{L>0}{\Longrightarrow} \mathbf{N} : \underbrace{\boldsymbol{\mathcal{L}}^e : \mathbf{D}}_{\dot{\boldsymbol{\sigma}}^e} > 0 \Rightarrow \mathbf{N} : \dot{\boldsymbol{\sigma}}^e > 0 \Rightarrow \boxed{\mathbf{N} : \Delta\boldsymbol{\sigma}^e > 0} \tag{2.26}$$

The quantity $\Delta\boldsymbol{\sigma}^e$ is known as the *elastic predictor* and can be thought as the increment in stress if the corresponding total deformation increment $\Delta\mathbf{E}$ was thought to be purely elastic. In the context of computational plasticity, given a $\Delta\mathbf{E}$, $\Delta\boldsymbol{\sigma}^e = \boldsymbol{\mathcal{L}}^e : \Delta\mathbf{E}$ is calculated and the the yield condition is examined; if $\Phi(\Delta\boldsymbol{\sigma}^e) > 0$, plastic deformation occurs during the increment and consequently the elastoplastic constitutive formulation is implemented whereas $\Phi(\Delta\boldsymbol{\sigma}^e) < 0$ means that elastic unloading takes place and elasticity is used.

Chapter 3

Instabilities, Bifurcations and Nonlocal Theories

Having described the general theoretical framework that will be used for the development of the model in Chapter 4, it would be useful at this point to address the issue concerning the necessity of the introduction of an enhanced model in order to deal with computational simulation difficulties due to instabilities that can possibly arise in elastoplastic mediums. To be precise, the most commonly encountered instabilities and the corresponding bifurcation theory, which are closely related to, are briefly presented first. Thereafter, techniques for the examination and analysis of post-critical behavior as well as a review of the methods that can be used to tackle the aforementioned numerical difficulties are also summarized.

3.1 Instabilities in Elastic-Plastic Mediums

From a mathematical perspective, the notion of *stability* is usually associated with the qualitative behavior of the solutions of differential equations and the evolution of dynamical systems under infinitesimal disturbances. More specifically, stability theory addresses the question of whether or not, small variations of the initial data of a problem will lead to small variations of its solution. However, in the context of mechanics of materials, a variety of definitions for stability exist each associated with different conditions under which the corresponding stability is lost. When examining the behavior of a material undergoing large inelastic deformations, the corresponding non-linearities involved may result in a number of instabilities, the most common of which include the so-called *geometrical, material* and *structural instabilities* [12]. The basic characteristics concerning the aforementioned classes of instabilities are described in the following.

Geometrical and Material Instabilities

A typical example of a geometrical instability appears in the *buckling of an elastic-plastic structural member*. As is well known, in principle, when a structural member (e.g. a column

or a beam) is subjected to compressive external loads[1], there exists a load level (which actually consists the lower bound for the buckling critical load) in which the member deviates from the fundamental deformation pattern and deflects even though this load level may be considerably less than the required load for complete loss of stress capacity of the member. At the latter critical load, the system becomes unstable and buckling occurs. Any further increase in load may result in different deformation modes corresponding to different critical loads which can be determined by solving an eigenvalue problem in the sense of ordinary differential equations. Nevertheless, the aforementioned procedure is only valid under the assumption of a "perfect" member in the sense that neither initial imperfections[2] nor deviation from the linear elastic response are taken into account. In such cases, the nonlinearities introduced result in critical loads lower than the theoretical ones predicted by the classical theory, with this observation being of utmost importance when designing large scale structures against buckling instabilities. In this direction, more sophisticated (mostly numerical) techniques are used for the stability analysis of systems involving geometrical nonlinearities and severe "snap-back - snap-through" behavior such as the so-called "arc-length" method ([73], [17]). For the sake of completeness, it should be mentioned that instabilities in elastic-plastic buckling considering initial imperfections have extensively been examined by Hutchinson in [41], [42] and [43].

On the other hand, material instabilities in the mechanical context are related, from a phenomenological point of view, to the so-called *localization phenomena* that can emerge, under certain conditions, within a structure. The term "localization" in the sense of Rice [72] refers to the emergence of regions of specific size where all further deformation of the structure tends to concentrate (i.e., localize) regardless of the fact that the loading program may remain unaltered. In this case, the rest of the structure usually unloads elastically and thus exhibits a rigid-like behavior. Classical examples of material instabilities in metals include the formation of *shear bands* and the procedure of *void nucleation, growth and coalescence* both of which are related to the well-known failure mechanism of *ductile fracture* and actually pose restrictions to the ductility of the corresponding material, i.e. to the margin of plastic deformation that can be imposed before the material starts to its lose stress carrying capacity and fail. The latter mechanisms involved in ductile fracture are examined and compared in a unified manner in [76] and consist in the following:

- Shear bands can emerge in clean single crystals, polycrystalline materials, non-porous materials, or porous metals due to excessive localization of deformation in narrow zones which can be a result of different mechanisms in the corresponding materials. For instance, in the first two cases, due to absence of void nucleating sites or for high pressure conditions, at some point of the loading, the homogeneous deformation switches to a highly localized deformation mode, without the occuring of damage

[1] Although there are cases where buckling is caused by tensile loadings.

[2] Such imperfections may be of geometrical nature (e.g., initial curvature of the member), of material nature (e.g. inhomogeneous material) or they may even be associated with the loading conditions (e.g. eccentric loading).

(emergence of voids) prior or after the localization. In the third case, localization of deformation is due to various softening mechanisms at the scale of the microstructure of the material and for ongoing plastic deformation, the formation of shear bands is followed by the nucleation, growth and subsequent coalescence of voids within the bands. Finally, for porous metals shear bands may appear either due to growth of voids which imply softening of the material and localization of deformation or the emergence of shear bands and growth and coalescence of voids may happen simultaneously.

- The mechanism of void nucleation, growth and coalescence emerges in the context of ductile fracture in more than one ways either prior, after or simultaneously with the localization of deformation described above. One scenario has microvoids that exist in a number of polycrystalline metals to act as nucleation sites for new voids driven by the deformation of the material, a procedure which gives rise to softening in the material due to the growth and coalescence mechanism, which leads to localization of deformation into shear bands that engulf the aforementioned voids. Alternatively, especially in the cases where two scale voids[3] exist in the material, microvoids nucleate[4], grow and coalesce in the ligaments between larger voids while, at the same time, this procedure also marks the initiation of localization of deformation in the ligament area.

Nonetheless, it should be mentioned that distinction of the latter mechanisms involved in ductile fracture is ambiguous in the sense that a number of parameters (such as stress triaxiality) affect the procedure and it is not clear in all cases which mechanism takes place before the other or whether they develop in a concurrent manner. Material instabilities, as described above, have been extensively investigated for instance by Tvergaard in [78], [79], [80], [81] and by Hutchinson and Tvergaard in [40] for the case of metals and by Bažant [13] for the case of concrete.

Structural Instabilities

Structural instabilities, occuring as a result of widespread geometric or material instabilities, lead to *plastic flow localization*, i.e., concentration of stresses and strain rates in a such a portion of the material, which ultimately results in the total collapse of the structure. Probably, the most well known instability of this kind is the so-called *necking* of a tensile metal test specimen that signals the point of the corresponding deformation program after which all deformation and stresses localize into a specific region of the material known as the "neck region". Another example of a structural instability is that of *buckling localization*, due to which, when plastic buckling takes place, the classical periodical pattern of the eigenmodes is replaced by the growth of localized buckles in some region of the structure ([12]).

Although the latter phenomenological descriptions may provide an insight on the qualitative perspective of the various instabilities that may emerge in a material at some point of

[3] In the sense that existing voids in the material originating from the presence of inclusions are significantly larger than the voids that may nucleate due to localization.

[4] The free surfaces of the larger voids most of the times act as nucleation sites of smaller voids.

its deformation, it would be useful for the sake of completeness to outline the fundamental stability criteria that are related to the mathematical conditions under which such instabilities may occur. To begin with, a condition concerning material stability was first proposed by Hill [36] and later was restated by Drucker [25], which states that a material is stable if the incremental inner product of stress and strain is strictly positive or in other words that the incremental work of internal forces always increases i.e.,

$$dW^{in} = d\boldsymbol{\sigma} : d\boldsymbol{\varepsilon} > 0 \tag{3.1}$$

where, with no loss of generality, small strain notation is adopted. Substitution of $d\boldsymbol{\sigma}$ from the corresponding incremental constitutive equation[5] characterizing the behavior of the material in (3.1) leads in the following inequality:

$$d\boldsymbol{\varepsilon}^T : \boldsymbol{\mathcal{L}}^{ep} : d\boldsymbol{\varepsilon} > 0 \ \forall \ d\boldsymbol{\varepsilon} \ \neq \ \mathbf{0} \tag{3.2}$$

where $\boldsymbol{\mathcal{L}}^{ep}$ denotes the material tangent modulus of the incremental constitutive equation. In view of the latter and the symmetry of the strain tensor, an instability occurs whenever $\boldsymbol{\mathcal{L}}^{ep}$ loses its positive-definiteness, i.e. when ([24]):

$$\boxed{\det[\boldsymbol{\mathcal{L}}^{ep} + (\boldsymbol{\mathcal{L}}^{ep})^T] = 0} \tag{3.3}$$

Equation (3.3) suggests only a *local* condition of stability in the sense that it is a sufficient condition for an instability in the vicinity of an arbitrary material point of the medium. However, especially in the context of finite element analysis, one is interested to be aware of the conditions under which a structural instability might take place. Such a condition may be derived by considering the integral form of the stability criterion (3.1) for a material occupying a volume V ([36]):

$$\int_V \dot{\boldsymbol{\sigma}} : \dot{\boldsymbol{\varepsilon}} dV > 0 \tag{3.4}$$

Introduction of the finite element approximation in the last equation leads to the conclusion that, structural stability is lost if and only if at least one eigenvalue of the matrix $\Big[K\Big] + \Big[K\Big]^T$ vanishes, i.e., when ([24]):

$$\boxed{\det\left(\Big[K\Big] + \Big[K\Big]^T\right) = 0} \tag{3.5}$$

where $\Big[K\Big]$ is the Jacobian "stiffness matrix" of the structure resulting from the discretization of the corresponding weak formulation of the BVP of elastoplasticity[6]. It should be noted here that (3.5) is a necessary and sufficient condition for the rise of a structural instability even if $\Big[K\Big]$ is not symmetric[7] ([23]). In the latter case, (3.5) reduces to the classical condition

[5] This constitutive equation can, in principle, be very general but reducible to a "linear-like" form with the use of the so-called tangential material modulus.

[6] The general concepts of the Finite Element Method are thoroughly discussed in Chapter 5.

[7] As is usually the case in finite deformations.

that structural stability is lost if and only if $\left[K\right]$ loses its positive-definiteness.

3.2 Bifurcations and Ill-Posedness of the Elastoplastic BVP

The instabilities described in the previous section are usually associated in practice with the transition of the solution of the problem from the primary equilibrium path to one or more alternative equilibrium paths or, in other words, with the introduction of one or more *bifurcations*. As it widely remarked, numerical investigation of the post-bifurcation behavior with the methods provided by classical continuum models results in serious computational issues and this can be mathematically explained by the fact that the conditions under which such bifurcations can emerge coincide with the conditions under which the classical BVP that models the physical problem is no longer well-posed. In this direction, the conditions for the occurrence and detection of bifurcations[8] and the association of the former with the ill-posedness are established in the following in order to justify the corresponding modifications that are introduced later on.

3.2.1 Bifurcation Criteria and Detection Methods

Generally speaking, bifurcations can be categorized, as *local* or *global* depending on whether the corresponding conditions under which they may take place are expressed in terms of quantities related to the constitutive or the structural behavior of the material respectively.

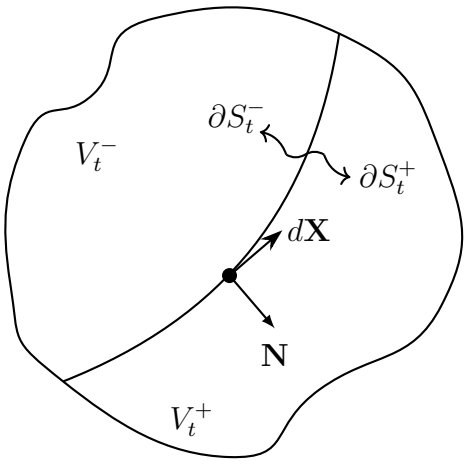

Figure 3.1: Surface discontinuity with outward-pointing normal vector $\mathbf{N}$ in an elastic-plastic medium occupying volume V at time t, which splits the body into two subregions V_t^+ and V_t^-.

[8]It should be mentioned that the relevant discussion focuses on bifurcations related to material and structural instabilities only. A detailed analysis on geometric bifurcations can be found in the works of Hutchinson [41], [42].

Starting with former ones, assuming a rate-independent material with no initial imperfections, one wants to determine when the constitutive behavior of the material allows the bifurcation from a homogeneous to a highly localized deformation pattern at some region in the vicinity of an arbitrary point of the medium. The latter is equivalent to permit the emergence of a stationary surface discontinuity[9] in the material such as the one presented in Figure 3.1. Compatibility conditions force all infinitesimal material fibers $d\mathbf{X}$ in the reference configuration, which belong to the plane tangential to the surface discontinuity, to be uniquely mapped into the corresponding fibers $d\mathbf{x}$ in the current configuration, so that:

$$d\mathbf{x}^+ = d\mathbf{x}^- \equiv d\mathbf{x} = \mathbf{F}^+ \cdot d\mathbf{X} = \mathbf{F}^- \cdot d\mathbf{X} \;\Rightarrow\; (\mathbf{F}^+ - \mathbf{F}^-) \cdot d\mathbf{X} = \mathbf{0} \tag{3.6}$$

Now, setting $\mathbf{F}^+ - \mathbf{F}^- \equiv \mathbf{G}$ and writing (3.6) in indicial notation one gets:

$$G_{ij}dX_j = 0 \;\Rightarrow\; \begin{cases} G_{1j}dX_j = 0 \\ G_{2j}dX_j = 0 \\ G_{3j}dX_j = 0 \end{cases} \Rightarrow\; G_{1j},\, G_{2j},\, G_{3j} \perp dX_j \;\forall\, d\mathbf{X} \tag{3.7}$$

Last equation suggests that since the (row) vectors G_{1j}, G_{2j}, G_{3j} are perpendicular to the arbitrary fibers dX_j then it can be deduced that they are parallel to the normal vector N_j of the discontinuity surface so they can be written as:

$$G_{1j} = a_1 N_j,\; G_{2j} = a_2 N_j,\; G_{3j} = a_3 N_j \;\Rightarrow\; G_{ij} = a_i N_j \text{ or } \mathbf{G} = \mathbf{aN} \tag{3.8}$$

where $\mathbf{a}$ is an arbitrary vector. In view of these, the jump condition in the deformation gradient can then be written as:

$$[\![\mathbf{F}]\!] = \mathbf{F}^+ - \mathbf{F}^- = \mathbf{aN} \quad \text{or} \quad \dot{\mathbf{F}}^+ = \dot{\mathbf{F}}^- + \dot{\mathbf{a}}\mathbf{N} \tag{3.9}$$

where "$[\![\square]\!]$" denotes the jump in the quantity $\square$. Using (3.9), the traction equilibrium condition across the surface expressed in terms of the Cauchy stress and the constitutive law in terms of the tangent modulus $\boldsymbol{\mathcal{L}}^{ep}$, it can be proved that (see [56], [72]) a local bifurcation can occur if there exists a vector $\mathbf{N}$ such as:

$$\boxed{\begin{array}{c} \det(\mathbf{N} \cdot \boldsymbol{\mathcal{L}}^{ep} \cdot \mathbf{N} + \mathbf{A}) = 0 \\ \text{with} \quad \mathbf{A} = -\dfrac{1}{2}[\boldsymbol{\sigma} - \boldsymbol{\sigma}\mathbf{NN} - (\mathbf{N} \cdot \boldsymbol{\sigma} \cdot \mathbf{N})\boldsymbol{\delta} + \mathbf{NN} \cdot \boldsymbol{\sigma}] \end{array}} \tag{3.10}$$

What is important to remember here is that in the derivation of (3.10), no assumptions where made concerning this localization region[10] and thus one may postulate that it can be

[9] As defined by Hill in [37]

[10] Which, in the context of material instabilities considered here, could refer for example to the thickness of the shear bands that emerge.

of arbitrarily small size.

On the other hand, deduction of global conditions for the occurence of a bifurcation at a structural (global) level is based on the the works of Hill ([35], [36]) concerning the uniqueness of solution of the corresponding BVP. As proved in [23], [24] a necessary and sufficient condition for the existence of more than one solutions is that the structural stiffness matrix $\left[K\right]$ is not invertible, i.e.,

$$\boxed{\det\left(\left[K\right]\right) = 0} \tag{3.11}$$

It should be pointed out that for structures characterized by a symmetric stiffness matrix, loss of material stability coincides with the loss of uniqueness of solution of the governing BVP while for non-symmetric stiffness matrices, loss of stability can precede the emergence of a bifurcation in the sense that (3.5) may be satisfied prior to (3.11) ([24]).

Detection of bifurcation points and analysis of the post-bifurcation behavior is of great interest, for instance in the numerical determination of limit points in the context of forming limit analysis. As mentioned in [12], the methods that are usually implemented for the latter purpose can be briefly categorized as follows:

- The first class of methods[11] is based on the calculation of eigenvalues and eigenvectors of the structural stiffness matrix. In this case, one or more negative eigenvalues indicate that a possible bifurcation point may have been crossed. Although this method is straightforward numerical issues related to heavy computational cost and ill-conditioned stiffness matrix close to bifurcation point may appear.

- Another common method for the examination of bifurcations includes the introduction of *initial imperfections*, which can be of material or geometrical type[12], and the determination of possible directions for which (3.10) is satisfied. Naturally, this kind of analysis seems more realistic since real structures cannot be, in any sense, perfect. Nevertheless, with this method, the results depend on the choice and the magnitude of the initial imperfection and thus they correspond to a specific bifurcation mode, excluding other possible bifurcation types.

- Finally, *phenomenological models* may also be introduced to enhance the underlying constitutive model for the investigation of possible bifurcations.

3.2.2 Mathematical Insufficiency of Classical (Local) Models

While the stability and bifurcation detection conditions developed in the previous sections can be used for the determination of the bifurcation points and the corresponding load levels,

[11] Also known as *"direct" methods*.

[12] In the first case, a slight inhomogeneity of some property is introduced for a specific part of the structure while in the second case, usually a small dimensional imperfection is introduced.

post-peak numerical simulations of various related problems (such as damage or strain localization problems) using the classical continuum mechanics theory, usually leads to bizarre results, both from a physical and from a mathematical perspective. For instance, as it is pointed out by Pijaudier *et al.* in [62], implementation of damage and crack propagation simulations using the standard continuum mechanics theory results in unrealistic failure predictions in the sense that the corresponding material fails immediately slightly after peak load with zero energy dissipation and with deformation localized in a zone of zero width. On the other hand, from a mathematical point of view, the one-dimensional example presented by Jirásek and Bažant in [44] is illustrative of the underlying loss of well posedness of the problem. More specifically, in the case of uniaxial tension of a perfect homogeneous bar, it is proved that, since in the post peak region an infinite number of strain states corresponds to a unique stress, deformation needs not to be uniform and, at complete unloading, the final displacement of the bar depends on the size of the softening region which is in fact undetermined. In the context of the finite element analysis of the same bar with a small strength imperfection, last sentence then implies that, for a well established numerical algorithm, the softening region extends over a single element and thus its corresponding size depends on the number of elements, i.e., on the discretization of the problem. These computational ambiguities are a result of the fact that, the condition for the emergence of a local bifurcation (related to a material instability such as localization of deformation) coincide with so-called *loss of ellipticity* of the classical BVP that governs the physical problem, leading to the loss of the well-posedness of the problem. This can be proved in the following manner.

To begin with, consider the rate of equilibrium equations derived from (1.83) in terms of the nominal stress tensor $\mathbf{T}$, which, in absence of body forces, can be written as:

$$\boldsymbol{\nabla}_{\mathbf{X}} \cdot \dot{\mathbf{T}}^T = \mathbf{0} \quad \text{or} \quad \frac{\partial \dot{T}_{ji}}{\partial X_j} = 0 \tag{3.12}$$

With no loss of generality, assuming that the reference configuration coincides with the instantaneous (current) one, it is proved in [36] that the material derivative of the nominal stress and its transpose are given, in terms of the Cauchy stress, as:

$$\dot{\mathbf{T}} = \dot{\boldsymbol{\sigma}} - \mathbf{L} \cdot \boldsymbol{\sigma} + \boldsymbol{\sigma} \mathrm{tr}(\mathbf{L}) \quad \text{and} \quad \dot{\mathbf{T}}^T = \dot{\boldsymbol{\sigma}} - \boldsymbol{\sigma} \cdot \mathbf{L}^T + \boldsymbol{\sigma} \mathrm{tr}(\mathbf{L}) \tag{3.13}$$

Moreover, using the definition of Jaumann stress rate from Table 1.2, the definition of the spin tensor $\mathbf{W}$ from (1.41) and assuming that the total elastoplastic behavior of the material can be expressed in terms of the tangent modulus $\boldsymbol{\mathcal{L}}^{ep}$, one has:

$$\begin{aligned} \dot{\boldsymbol{\sigma}} &= \overset{\nabla}{\boldsymbol{\sigma}} - \frac{1}{2}\boldsymbol{\sigma} \cdot (\mathbf{L} - \mathbf{L}^T) + \frac{1}{2}(\mathbf{L} - \mathbf{L}^T) \cdot \boldsymbol{\sigma} \\ \text{where} \quad \overset{\nabla}{\boldsymbol{\sigma}} &= \boldsymbol{\mathcal{L}}^{ep} : \mathbf{D} = \boldsymbol{\mathcal{L}}^{ep} : \mathbf{L} \end{aligned} \tag{3.14}$$

Using $(3.13)_2$ and (3.14), (3.12) leads to the following form of the equilibrium equations:

$$\boldsymbol{\nabla}_{\mathbf{X}} \cdot \left[\left(\boldsymbol{\mathcal{L}}^{ep} + \bar{\boldsymbol{\Sigma}} \right) : \mathbf{L} \right]^T = \mathbf{0}$$

$$\text{where} \quad \bar{\Sigma}_{ijkl} = \frac{1}{2}(\delta_{jl}\sigma_{ik} - \delta_{jk}\sigma_{il} - \sigma_{il}\delta_{kj} - \sigma_{ik}\delta_{jl}) + \delta_{kl}\sigma_{ij} \tag{3.15}$$

The ellipticity property can be investigated by examining the so-called principal symbol of the PDE in the sense of Agmon (see [3]). The can be done by substituting the higher order derivative of the differential operator (i.e., the differential operator of the principal part of the PDE) with arbitrary polynomials of the same degree as the order of the corresponding derivatives. In the context of the tensorial expression (3.15), the principal symbol takes the form:

$$\mathbf{P}_s(\mathbf{N}) = \mathbf{N} \cdot \left(\boldsymbol{\mathcal{L}}^{ep} + \bar{\boldsymbol{\Sigma}} \right) \cdot \mathbf{N} = \mathbf{N} \cdot \boldsymbol{\mathcal{L}}^{ep} \cdot \mathbf{N} + \underbrace{\mathbf{N} \cdot \bar{\boldsymbol{\Sigma}} \cdot \mathbf{N}}_{\mathbf{A}} = \mathbf{N} \cdot \boldsymbol{\mathcal{L}}^{ep} \cdot \mathbf{N} + \mathbf{A} \tag{3.16}$$

where $\mathbf{A}$ is given by $(3.10)_2$. Then, the corresponding PDE is said to lose ellipticity[13] if there exists a vector $\mathbf{N}$ such that the determinant of the principal symbol is zero, i.e.,

$$\boxed{\det(\mathbf{P}_s) \equiv \det(\mathbf{N} \cdot \boldsymbol{\mathcal{L}}^{ep} \cdot \mathbf{N} + \mathbf{A}) = 0} \tag{3.17}$$

Comparison of (3.17) with condition (3.10), which marks the onset of a local bifurcation into a mode of highly localized strain, reveals that the emergence of a surface discontinuity of arbitrary size in the vicinity of a material point of the body coincides with the loss of ellipticity of the BVP characterizing the physical problem. From a qualitative point of view, since the corresponding localization area is practically undetermined in view of the classical formulations, the mathematical model admits an infinite number of failure modes in the sense that, any failure mode with a pre-failure localized area between the real one[14] and the one that corresponds to immediate post-peak load collapse with zero size and dissipation, is mathematically accepted which contradicts the physical existence of a unique final failure pattern.

From this discussion, it is obvious that, in order to tackle the problems described above, additional information must be taken into account concerning the size of the localization area so as to express the real failure process. This size, also known as the *characteristic length* of the material, is an intrinsic material property which acts as *localization limiter*, i.e., it establishes a lower bound to the possible size of the various localized phenomena. Among other ways to incorporate such a material length to the problem, a solution is to extend the classical (local) continuum model using the so-called *nonlocal theories*, the basic ideas of which are described in the following section. For instance, as proved in [11], the addition of a

[13] Strictly speaking the property of ellipticity actually refers to the corresponding differential operator.

[14] This refers to the observable one, the one that would take place if the corresponding experiment was carried out.

nonlocal enhancement in a classical formulation allows the restoration of the well posedness of the mathematical problem, although ellipticity may still be lost if the elastic moduli $\boldsymbol{\mathcal{L}}^e$ lose ellipticity, a condition which is unlikely to happen in real situations since that would require very high stress rates which rarely occur in practice.

3.3 Fundamentals of Nonlocal Theories

As described in [75], classical continuum models, i.e., models that do not incorporate an intrinsic material length, can be considered *local* in the sense that they exclude long-distance material point interactions accepting force interactions at finite distance only in the form of body forces. Indeed, the formulation of continuum mechanics theory is based on the assumption that the stress state at any material point of the body depends solely on the strain history at that point. The corresponding deformation history of the material at any point in time is then characterized by the current values of the state variables alone as described in the previous chapter, excluding any higher order gradients that would imply nonlocal effects. In this rationale, mechanical behavior is modeled in the same manner for both the macro and the micro scale. As proved in practice, the latter consideration poses no problems in the continuum model as long as strain distribution is smooth and no discontinuities are present[15]. However, since all real materials posses heterogeneous properties as the length scale of observation becomes smaller, it becomes a necessity, in order to accurately describe the effects that take place at such a micro level, for the underlying microstructural properties not to be neglected. For example, these effects become of utmost importance when highly nonlinear (inelastic) material behavior is exhibited (as in the case of strain localization due to severe plastic deformation, examined in the previous sections). In this case, classical continuum models, which to not include a characteristic length, prove to be inadequate, lose their ellicptic[16] character and fail to correctly produce meaningful results.

In the context of plasticity, a solution to overcoming the aforementioned difficulties can be achieved by enhancing the classical models so as to include long-range interactions at all material points, where the precise distance of these interactions is dictated by the characteristic length ℓ of the material. In general, one can divide such enhancement into two major groups (see [75] for more details on each topic):

- Models that enhance the *kinematic equations*, in the sense that they incorporate higher order gradients or nonlocal averages of the strain field.
- Models that enhance the *constitutive equations* by considering gradients or nonlocal averages of the internal variables such as the class of models described for example by Ramaswamy and Aravas in [68], [69].

[15] This is usually the case in classical elasticity theory where stress and strain fields remain homogeneous.
[16] Or hyperbolic character in the case of dynamics.

Even though, both methods have been extensively used throughout the literature, the latter seems more computationally attractive and is favored in this thesis in the form of the gradient model described in Chapter 4 since it can be implemented in such a way so as the elastic part of the formulation may still be described by the classical model and the nonlocal effect be activated only in the plastic part of the constitutive equations.

At this point, for the sake of completeness, it is important to give the definition of the nonlocal of a local variable. For this purpose, consider the local field $\mathbf{a}(\mathbf{x})$ that may represent any quantity of the local problem that is meaningful to define a corresponding nonlocal quantity (i.e., it may refer to strain or any other scalar, vector or tensor internal variable). Then, the weighted spatial, or nonlocal average, $\bar{\mathbf{a}}(\mathbf{x})$, of the field $\mathbf{a}(\mathbf{x})$ is defined as ([26], [61], [75]):

$$\boxed{\bar{\mathbf{a}}(\mathbf{x}) = \frac{1}{W(\mathbf{x})} \int_V w(\mathbf{x},\mathbf{y})\mathbf{a}(\mathbf{y})dV(\mathbf{y}) \quad \text{with} \quad W(\mathbf{x}) = \int_V w(\mathbf{x},\mathbf{y})dV(\mathbf{y})} \tag{3.18}$$

where w is a properly selected weight function and $\mathbf{y}$ is the position vector of the infinitesimal material volume $dV(\mathbf{y})$. It should be noted here that, the normalising factor W is defined in such a way so that as $\ell \to 0$ or for a homogeneous local field variable, the nonlocal formulation reduces to the local one. Nonlocal models that fit in the formalism defined by (3.18) are considered *strongly nonlocal* from the mathematical perspective in the sense that the nonlocal variable is calculated using information from all material points included in the domain V of integration. Finally, the intrinsic material length is introduced through the weight function w, which is usually of the Gaussian type in the sense that it can be stated in the general form:

$$w(\mathbf{x},\mathbf{y}) = \frac{1}{c^G}\exp\left(-\frac{|\mathbf{x}-\mathbf{y}|^2}{2\ell^2}\right) \quad \text{where} \quad c^G = \begin{cases} (2\pi)^{1/2}\ell & \text{for 1D} \\ 2\pi\ell^2 & \text{for 2D} \\ (2\pi)^{-3/2}\ell^3 & \text{for 3D} \end{cases} \tag{3.19}$$

3.3.1 Constitutive Model Enhancement of the Gradient Type

As mentioned in the previous section, a subclass of methods for the enrichment of the constitutive equations consists in the introduction of gradients of local internal variables. In principle, this can be done either explicitly or implicitly depending on the way gradients enter the model. To begin with, with no loss of generality, let $a(\mathbf{x})$ be a scalar local internal variable. Then. both approaches depend on the evaluation of the nonlocal counterpart of a which can be found by expanding the latter quantity into a Taylor series and substituting in (3.18), a procedure that ultimately yields ([26], [61]):

$$\bar{a}(\mathbf{x}) = a(\mathbf{x}) + c(\ell)\nabla^2 a(\mathbf{x}) + d(\ell)\nabla^4 a(\mathbf{x}) + \cdots \tag{3.20}$$

where the parameters $c(\ell), d(\ell)$ both have dimensions of length to an even power. If the nonlocal variable is chosen to be directly calculated from (3.20) then the corresponding enhancement is called *explicit* in the sense that gradients of the local variable are directly utilized in the nonlocal enrichment. However, even though the latter expression, which is a a simple algebraic equation, seems appealing from a computational point of view one should, nonetheless, observe that its actual evaluation requires the truncation of the series, a procedure which from a mathematical point of view imposes restriction on the accuracy of the approach. From a physical point of view, reduction of higher order gradients in the calculation of the nonlocal variable diminishes the desirable long-distance effects and thus renders this method *weakly nonlocal* in the sense that the response of the material at any point depends only on the infinitesimal neighborhood of that point only. On the other hand, if one considers the calculation of $\bar{a}$ from the PDE of the Helmholtz type that is constructed by subtracting the Laplacian of (3.20) premultiplied by $c(\ell)$ from itself, i.e.,

$$\bar{a}(\mathbf{x}) - c(\ell)\nabla^2\bar{a}(\mathbf{x}) = a(\mathbf{x}) \tag{3.21a}$$

$$\text{where} \quad \nabla^2\bar{a}(\mathbf{x}) = \nabla^2 a(\mathbf{x}) + c(\ell)\nabla^4 a(\mathbf{x}) + \cdots \tag{3.21b}$$

then, since (3.21b) incorporates an infinite series of higher order terms, truly long distance interactions are included . Unique determination of $\bar{a}$ requires appropriate boundary conditions which, in view of the desired behavior in the limiting cases of small ℓ and/or homogeneous local fields, are defined by using the homogeneous Neumann boundary conditions ([26], [75]):

$$\boldsymbol{\nabla}\bar{a}\cdot\mathbf{n} = 0 \quad \text{on } \partial V \tag{3.22}$$

where $\mathbf{n}$ is the outward normal to the external boundary of the solution domain V. Such models that involve an additional field equation for the nonlocal variable are known as *implicit* in the sense that this nonlocal variable is not directly evaluated from the gradients of the local variable but it is instead the solution of BVP of the general form (3.21a), (3.22). As proved by Peerlings *et al.* in [61], the mathematical strong nonlocal character of implicit gradient models is verified due to the fact that this additional BVP is equivalent to the nonlocal average operation described by (3.18), if Green's function is used as the corresponding weight function and $c(\ell)$ is defined as:

$$c(\ell) = \ell^2 \tag{3.23}$$

With all these in mind, and by taking into account the computational simplicity of the implementation of a gradient compared to an integral model, an implicit gradient model of the form (3.21a)-(3.23) has been developed, which is described in the ensuing chapter.

Chapter 4

Gradient Anisotropic Model for Porous Materials

In this chapter the *gradient anisotropic model for two-phase porous materials* which builds on the work of Aravas and Ponte Castañeda [7] is presented. More specifically, a brief discussion about the physical aspects and modeling of the material and its microstructure is carried out. Thereafter, the general notions developed in Chapter 2 are specified for the development of the elastic and plastic constitutive behavior of the material which are then combined for the derivation of the total elastoplastic, rate constitutive equation and the so-called "material tangent moduli", which are used in the finite element method presented in Chapter 5. A mixed implicit-explicit numerical procedure for the integration of the aforementioned rate equations is also introduced.

4.1 Description of the Model

As described in [21] and [63], two-phase porous materials are a special case of two-phase composites with so-called *"particulate" microstructures*[1] where the inclusion phase (the phase with the smaller concentration or volume fraction) is considered vacuous, i.e. fully compressible. As suggested by Ponte Castañeda and Willis [65] and Kailasam *et al.*[45], [46], the special class of "particulate" microstructures for which ellipsoidal inclusions are spatially distributed with the so-called "ellipsoidal symmetry"[2] can, in the most general case, be described by considering that the "shape" and "orientation" of the distribution is different from the actual shape and orientation of the voids. Nonetheless, for porous materials, the effect of the spatial distribution of the voids is proved to be insignificant and can be

[1] "Particulate" microstructures can be thought as a generalized form of the dilute ellipsoidal inclusion microstructure described in the monumental work of Eshelby [27] where no restriction on the concentration of the inclusions is imposed.

[2] The notion of *"ellipsoidal symmetry"* is of statistical nature and can be interpreted as follows; if $\mathbf{x}$ is the center of an inclusion or the distribution of inclusion r in space then "ellipsoidal symmetry" expresses the probability of the center $\mathbf{x}'$ of another inclusion/distribution s to be located on the circumference of an ellipsoid with center $\mathbf{x}$.

neglected which consequently leads to the assumption that microstructure and its evolution will solely depend on the shape and orientation of the voids which will be assumed to be the same as their distribution's. The aforementioned simplifying hypothesis for identical shape and orientation between the pores and their spatial distribution, allowed the use of the theory for linear elastic two-phase composites presented in [86], [87] in the development of the anisotropic model of [7] which is the basis for the nonlocal model suggested herein. In this context, one can introduce a *"Representative Local Ellipsoidal Void"* (RLEV), as depicted in Figure 4.1, which characterizes the behavior at every point homogenized (effective) material.

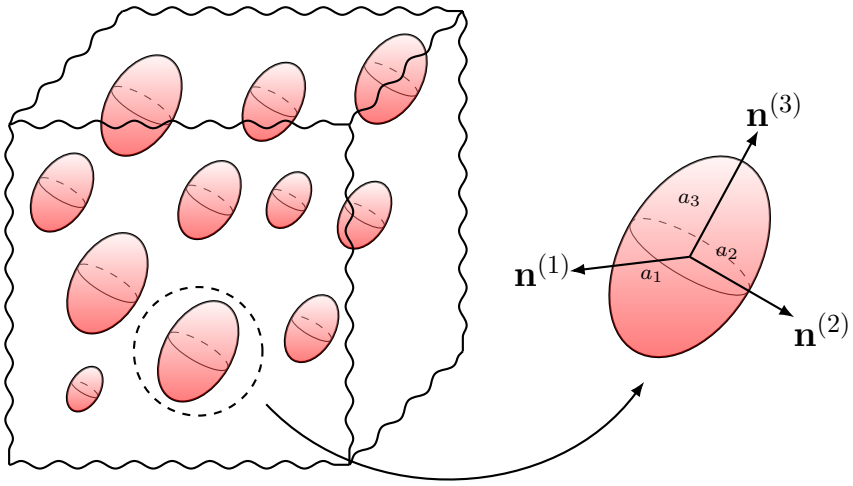

Figure 4.1: The "Representative Local Ellipsoidal Void"

The RLEV can be fully determined by the triad of unit vectors ($\mathbf{n}^{(1)}$, $\mathbf{n}^{(2)}$, $\mathbf{n}^{(3)} = \mathbf{n}^{(1)} \times \mathbf{n}^{(2)}$) in the direction of its principal axes along with the corresponding principal lengths ($2a_1$, $2a_2$, $2a_3$) or equivalently the local ellipsoid's aspect ratios defined as $w_1 = a_3/a_1$ and $w_2 = a_3/a_2$. In the beginning, the pores are assumed to be ellipsoidal and they are uniformly distributed in the matrix phase and during the deformation program they remain ellipsoidal but change their shape, volume and orientation. This implies that, in the most general case, *the homogenized material exhibits a locally orthotropic behavior* and retains this material symmetry throughout its deformation with the corresponding axes of orthotropy coinciding with the principal axes of the RLEV. As a special case of the latter generalization one can consider the case of spherical voids (i.e. $a_1 = a_2 = a_3$) for which the effective material behavior is initially isotropic. Additionally, if V_{v} is the volume of the voids and V is the total material volume, then one can define the local volume fraction or *local porosity* f_{loc} as:

$$\boxed{f_{\mathrm{loc}} = \frac{V_{\mathrm{v}}}{V}} \tag{4.1}$$

In the original formulations of the classical (local) anisotropic model first described in [66] and later extended in [7] and [47], the microstructure of the porous material is characterized by the equivalent plastic strain $\bar{\varepsilon}^p$ of the matrix material, the aspect ratios w_α, $\alpha = 1, 2$, the

orientation vectors $\mathbf{n}^{(i)}$, $i = 1, 2, 3$ and the local porosity f_{loc}, i.e., the state variable vector $\mathbf{s}$ is given as:

$$\boxed{\mathbf{s} = \{\bar{\varepsilon}^p, f_{\text{loc}}, w_1, w_2, \mathbf{n}^{(1)}, \mathbf{n}^{(2)}, \mathbf{n}^{(3)}\}} \tag{4.2}$$

Moreover, the effective yield function $\tilde{\Phi}$ and the normalized effective fourth order viscous compliance tensor $\tilde{\boldsymbol{m}}$ for the linear comparison porous material, which was first derived using the variational method proposed in [64], depend on the aforementioned internal variables (see also [21]):

$$\tilde{\Phi} = \tilde{\Phi}(\boldsymbol{\sigma}, \mathbf{s}) \quad \text{and} \quad \tilde{\boldsymbol{m}} = \tilde{\boldsymbol{m}}(f_{\text{loc}}, w_1, w_2, \mathbf{n}^{(1)}, \mathbf{n}^{(2)}, \mathbf{n}^{(3)}) \tag{4.3}$$

In the context of the gradient anisotropic constitutive model proposed in this thesis, a *nonlocal porosity* variable f is introduced for the regularization of the aforementioned local model. The nonlocal porosity f is determined from the solution of a BVP of the form presented in Chapter 3 for an implicit gradient constitutive enhancement, i.e.:

$$\boxed{\begin{aligned} f - \ell^2 \nabla^2 f &= f_{\text{loc}} \quad \text{in} \quad V \\ \text{B.C.}: \quad \frac{\partial f}{\partial n} &= 0 \quad \text{on} \quad \partial V \end{aligned}} \tag{4.4}$$

where ∂V is the boundary, with outward-pointing vector $\mathbf{n}$, of the solution domain V and ℓ is the characteristic length of the material[3] which acts as a localization limiter and thus allows the restoration of the well-posedness of the fundamental elastoplastic BVP. Furthermore, it is now assumed that $\tilde{\Phi}$ and $\tilde{\boldsymbol{m}}$ depend on the nonlocal porosity f instead of f_{loc} so they are of the form:

$$\tilde{\Phi} = \tilde{\Phi}(\boldsymbol{\sigma}, \bar{\varepsilon}^p, f, w_1, w_2, \mathbf{n}^{(1)}, \mathbf{n}^{(2)}, \mathbf{n}^{(3)}) \quad \text{and} \quad \tilde{\boldsymbol{m}} = \tilde{\boldsymbol{m}}(f, w_1, w_2, \mathbf{n}^{(1)}, \mathbf{n}^{(2)}, \mathbf{n}^{(3)}) \tag{4.5}$$

where explicit expressions for $\tilde{\Phi}$ and $\tilde{\boldsymbol{m}}$ are given in the sections that follow. Finally, in order to ensure that more accurate predictions are attained for the homogenized response and the evolution of the microstructure for low as well as high stress triaxiallities, the aforementioned tensor $\tilde{\boldsymbol{m}}$ is substituted by a modified version proposed by Danas and Aravas in [22] which is given as:

$$\boxed{\tilde{\boldsymbol{m}}^{\text{mvar}} = \tilde{\boldsymbol{m}} + (q_{\mathcal{J}}^2 - 1)\, \boldsymbol{\mathcal{J}} : \tilde{\boldsymbol{m}} : \boldsymbol{\mathcal{J}} \quad , \quad q_{\mathcal{J}} = \frac{1 - f}{\sqrt{f}\ln(1/f)}} \tag{4.6}$$

where $\boldsymbol{\mathcal{J}}$ is the fourth order hydrostatic (spherical) "projection" tensor (defined in Eq. 4.11) and $q_{\mathcal{J}}$ is introduced as a correction factor for more realistic predictions in purely hydrostatic loadings.

[3] In polycrystalline materials the characteristic length is of the same order as the size of a grain.

4.1.1 Elastic Constitutive Behavior

As mentioned in Subsection 2.2.1, for finite (plastic) deformations with small elastic strains, a hypoelastic constitutive equation for the elastic part of the rate of deformation can be adopted in the sense of the inverse of (2.13):

$$\boxed{\mathbf{D}^e = \widetilde{\boldsymbol{\mathcal{M}}}^e : \mathring{\boldsymbol{\sigma}}} \tag{4.7}$$

where $\widetilde{\boldsymbol{\mathcal{M}}}^e$ is the macroscopic elastic compliance tensor of the porous material and $\mathring{\boldsymbol{\sigma}}$ is the rate of the true stress which is corotational with the spin of the voids, i.e.,

$$\mathring{\boldsymbol{\sigma}} = \dot{\boldsymbol{\sigma}} - \boldsymbol{\omega} \cdot \boldsymbol{\sigma} + \boldsymbol{\sigma} \cdot \boldsymbol{\omega} \tag{4.8}$$

with $\boldsymbol{\omega}$[4] being the spin of the voids relative to a fixed frame of reference which can be mathematically expressed by the rate equations of the orientation vectors $\mathbf{n}^{(i)}$, i.e., $\dot{\mathbf{n}}^{(i)} = \boldsymbol{\omega} \cdot \mathbf{n}^{(i)}$, $i = 1, 2, 3$. The skew-symmetric, second order tensor $\boldsymbol{\omega}$ is calculated in the context of the evolution of the shape and orientation of the representative local ellipsoid presented later in this section. Taking into consideration the simplifications about the shape and orientation of the voids and their spatial distribution discussed in the previous section, one arrives at the following expression for the effective elastic compliance tensor ([21], [86]):

$$\boxed{\widetilde{\boldsymbol{\mathcal{M}}}^e = \boldsymbol{\mathcal{M}} + \frac{f}{1-f}\boldsymbol{\mathcal{Q}}^{-1}} \tag{4.9}$$

In (4.9), $\boldsymbol{\mathcal{M}}$ is the elastic compliance tensor of the matrix, which is defined as the inverse of the matrix material's elasticity tensor $\boldsymbol{\mathcal{L}}$:

$$\boldsymbol{\mathcal{M}} = \boldsymbol{\mathcal{L}}^{-1} = \frac{1}{2\mu}\boldsymbol{\mathcal{K}} + \frac{1}{3\kappa}\boldsymbol{\mathcal{J}} = \frac{1}{2\mu}\left(\boldsymbol{\mathcal{K}} + \frac{1-2\nu}{1+\nu}\boldsymbol{\mathcal{J}}\right) \quad , \quad \boldsymbol{\mathcal{L}} = 2\mu\boldsymbol{\mathcal{K}} + 3\kappa\boldsymbol{\mathcal{J}} \tag{4.10}$$

where μ, κ and ν denote the shear modulus, bulk modulus and Poisson's ratio of the matrix material respectively and $\boldsymbol{\mathcal{K}}$, $\boldsymbol{\mathcal{J}}$ are the fourth order "shear" and "hydrostatic" projection tensors given as:

$$\boldsymbol{\mathcal{J}} = \frac{1}{3}\boldsymbol{\delta}\boldsymbol{\delta} \quad \text{and} \quad \boldsymbol{\mathcal{K}} = \boldsymbol{\mathcal{I}} - \boldsymbol{\mathcal{J}} \tag{4.11}$$

with $\boldsymbol{\delta}$, $\boldsymbol{\mathcal{I}}$ being the second and fourth order symmetric identity tensors with Cartesian components δ_{ij} and $\mathcal{I}_{ijkl} = (\delta_{ik}\delta_{jl} + \delta_{il}\delta_{jk})/2$ respectively. Moreover, f is now the nonlocal porosity defined by 4.4 and $\boldsymbol{\mathcal{Q}}$ is a fourth order tensor concerning the microstructure of the material, which is related to the so-called Eshelby tensor $\boldsymbol{\mathcal{S}}$ ([27], [28]) as :

$$\boldsymbol{\mathcal{Q}} = \boldsymbol{\mathcal{L}} : (\boldsymbol{\mathcal{I}} - \boldsymbol{\mathcal{S}}) \tag{4.12}$$

[4] Which corresponds to the spin of the microstructure generally denoted as $\boldsymbol{\Omega}$ in Chapter 2.

It is important to note here that $\boldsymbol{\mathcal{S}}$ depends on the Poisson's ratio ν of the matrix, the aspect ratios (w_1, w_2) and the orientation vectors $(\mathbf{n}^{(1)}, \mathbf{n}^{(2)}, \mathbf{n}^{(3)})$ while $\boldsymbol{\mathcal{Q}}$ is proportional to μ and also depends on ν, (w_1, w_2) and $(\mathbf{n}^{(1)}, \mathbf{n}^{(2)}, \mathbf{n}^{(3)})$. Furthermore, $\boldsymbol{\mathcal{S}}$ posses the minor symmetries (i.e., $\mathcal{S}_{ijkl} = \mathcal{S}_{jikl} = \mathcal{S}_{ijlk}$) whereas the fourth order tensor $\boldsymbol{\mathcal{Q}}$ posses both the "major" ($\mathcal{Q}_{ijkl} = \mathcal{Q}_{klij}$) and the minor symmetries of the elasticity tensor. Explicit expressions for the tensors $\boldsymbol{\mathcal{Q}}$ and $\boldsymbol{\mathcal{S}}$ are presented in Appendix A.

In any case, one should also bear in mind that the components of $\widetilde{\boldsymbol{\mathcal{M}}}^e$ depend on the non-local porosity, the shape and orientation of the voids which change as the material deforms and thus they are not constant.

4.1.2 Plastic Constitutive Behavior

The development of the plastic part of the constitutive behavior is based on the works of Ponte Castañeda [64] and Ponte Castañeda and Willis [65] who used the results of the classical Hashin-Shtrikman estimates as the properties of the so-called "linear comparison composite" (LCC) in order to derive estimates for the macroscopic behavior of the nonlinear porous material via an optimization procedure. Using the original expression derived in [21], [47] and [66] and the modification proposed in [22], the macroscopic yield function for the porous material is now given as:

$$\boxed{\tilde{\Phi} = \tilde{\sigma}_e^2(\boldsymbol{\sigma}, f, w_1, w_2, \mathbf{n}^{(1)}, \mathbf{n}^{(2)}, \mathbf{n}^{(3)}) - \sigma_y^2(\bar{\varepsilon}^p) = \frac{1}{1-f}\boldsymbol{\sigma} : \tilde{\boldsymbol{m}}^{\mathrm{mvar}} : \boldsymbol{\sigma} - \sigma_y^2(\bar{\varepsilon}^p)} \tag{4.13}$$

where $\tilde{\sigma}_e$ is the effective equivalent stress of the LCC and $\sigma_y(\bar{\varepsilon}^p)$ is the yield strength of the matrix, which is assumed to exhibit isotropic hardening. The modified normalized viscous compliance tensor $\tilde{\boldsymbol{m}}^{\mathrm{mvar}}$ is given by (4.6) where $\tilde{\boldsymbol{m}}$ is the effective viscous compliance tensor for the LCC derived in the classical model:

$$\tilde{\boldsymbol{m}} = \tilde{\boldsymbol{m}}(f, w_1, w_2, \mathbf{n}^{(1)}, \mathbf{n}^{(2)}, \mathbf{n}^{(3)}) = 3\mu\widetilde{\boldsymbol{\mathcal{M}}}^e|_{\nu\to 1/2} = \frac{3}{2}\boldsymbol{\mathcal{K}} + \frac{3}{1-f}\mu\boldsymbol{\mathcal{Q}}^{-1}|_{\nu\to 1/2} \tag{4.14}$$

In the latter expression, $\widetilde{\boldsymbol{\mathcal{M}}}^e$ is the same as in (4.9) with the difference that it is calculated for $\nu \to 1/2$, taking into consideration the incompressibility of the matrix. However, it is more convenient to calculate $\tilde{\boldsymbol{m}}$ from the second expression in (4.14) by considering the corresponding the limits from the explicit expressions of $\boldsymbol{\mathcal{Q}}$ presented in Appendix A. Moreover, it should be mentioned here that the effective yield function $\tilde{\Phi}$ of the material exhibits orthotropic symmetry with symmetry axes coinciding with the orientation vectors, $\mathbf{n}^{(i)}$, $i = 1, 2, 3$, of the RLEV. In the special case of spherical voids (i.e., $w_1 = w_2 = 1$) the porous material is macroscopically isotropic and the yield function reduces to:

$$\tilde{\Phi} = \tilde{\Phi}(\boldsymbol{\sigma}, \bar{\varepsilon}^p, f) = \left(1 + \frac{2}{3}f\right)\left(\frac{\sigma_e^M}{1-f}\right)^2 + \frac{9}{4}f\left(\frac{p}{1-f}\right)^2 - \sigma_y^2(\bar{\varepsilon}^p) \tag{4.15}$$

where $\sigma_e^M = \sqrt{3\boldsymbol{\sigma}^{\mathrm{d}} : \boldsymbol{\sigma}^{\mathrm{d}}/2}$ is the von Mises equivalent stress, $\boldsymbol{\sigma}^{\mathrm{d}}$ is the deviatoric stress tensor and $p = \sigma_{ii}/3$ is the hydrostatic or average stress.

Finally, for the plastic $\mathbf{D}^p$ of the rate of deformation, the normality rule given by (2.19) can be used to characterize the corresponding plastic behavior. Thus, taking into account (4.13), one can arrive at the following expression:

$$\boxed{\mathbf{D}^p = \dot{\lambda}\mathbf{N} \quad \text{with} \quad \mathbf{N} = \frac{\partial \tilde{\Phi}}{\partial \boldsymbol{\sigma}} = \frac{2}{1-f}\tilde{\mathbb{m}}^{\mathrm{mvar}} : \boldsymbol{\sigma}} \tag{4.16}$$

with $\dot{\lambda} \geq 0$ being the plastic multiplier, an explicit expression of which is later derived for the case of the gradient anisotropic model presented herein.

4.1.3 Evolution Equations of State Variables

Finite (plastic) deformation inevitably lead to changes in the microstructure of the heterogeneous material which in turn is mathematically expressed by the so called evolution or rate of change of the state variables that model the microstructure, i.e, the evolution equations of $\mathbf{s}$ defined by (4.2). In the case of porous metals, a viable assumption that can be adopted (since elastic deformation is negligible compared to plastic deformation) is that all changes in the microstructure are solely a consequence of plastic deformation of the matrix, which leads to variations in the shape, volume and orientation of the voids. Then, with the latter hypothesis, one can determine the desired evolution equations of the state variables from the kinematics of deformation presented in Chapter 2 and, assuming that the evolution of the state variables concerning the RLEV can be characterized by the average plastic rate of deformation and spin of the pores, by using the corresponding homogenization procedure developed in [47] and [66].

4.1.3.1 Evolution Equations for $\bar{\varepsilon}^p$ and Local Porosity f_{loc}

In the classical formulation, considering the physics of the problem, one can derive the evolution equation of the equivalent plastic strain $\bar{\varepsilon}^p$ by postulating that the macroscopic plastic power developed in the material has to be microscopically dissipated for the plastic deformation of the matrix. Mathematically speaking, this can be expressed as follows:

$$\dot{W}^p_{\mathrm{macro}} = \dot{W}^p_{\mathrm{micro}} \Rightarrow V(\boldsymbol{\sigma} : \mathbf{D}^p) = V_m(\sigma_y(\bar{\varepsilon}^p)\,\dot{\bar{\varepsilon}}^p) \Rightarrow \boldsymbol{\sigma} : \mathbf{D}^p = \frac{V - V_{\mathrm{v}}}{V}(\sigma_y(\bar{\varepsilon}^p)\,\dot{\bar{\varepsilon}}^p) \Rightarrow$$
$$\overset{(4.1)}{\Longrightarrow} \boldsymbol{\sigma} : \mathbf{D}^p = (1 - f_{\mathrm{loc}})\,\sigma_y(\bar{\varepsilon}^p)\,\dot{\bar{\varepsilon}}^p \overset{(4.16)}{\Longrightarrow} \dot{\bar{\varepsilon}}^p = \dot{\lambda}\,\frac{\boldsymbol{\sigma} : \mathbf{N}}{(1 - f_{\mathrm{loc}})\sigma_y(\bar{\varepsilon}^p)}$$

In the gradient formulation, f_{loc} is substituted by the regularized nonlocal porosity f in the last expression so the rate of change of $\bar{\varepsilon}^p$ is now given as:

$$\boxed{\dot{\bar{\varepsilon}}^p = \dot{\lambda}\,\frac{\boldsymbol{\sigma} : \mathbf{N}}{(1-f)\sigma_y(\bar{\varepsilon}^p)} \equiv \dot{\lambda}\, g_1(\boldsymbol{\sigma}, \bar{\varepsilon}^p, f, w_1, w_2, \mathbf{n}^{(1)}, \mathbf{n}^{(2)}, \mathbf{n}^{(3)})} \tag{4.17}$$

On the other hand, the evolution equation for the local porosity, i.e., the volume fraction of the pores, is derived in the original model, by starting from its definition (4.1) and considering the incopressibility of the matrix ($\dot{V}_m = 0$), as follows:

$$f_{\text{loc}} = \frac{V_{\text{v}}}{V} \Rightarrow \dot{f}_{\text{loc}} = \frac{\dot{V}_{\text{v}}}{V_{\text{v}}} - \frac{V_{\text{v}}}{V^2}\dot{V} \xrightarrow{\dot{V}_{\text{v}} = \dot{V}} \dot{f}_{\text{loc}} = \frac{\dot{V}}{V} - f_{\text{loc}}\frac{\dot{V}}{V} = (1 - f_{\text{loc}})\frac{\dot{V}}{V} \tag{4.18}$$

An expression for the quantity $\dot{V}/V$ can be found using (1.16) and the fact that $\dot{J} = J\, D_{kk}$:

$$dV = J\, dV_0 \Rightarrow d\dot{V} = \dot{J}\, dV_0 = J\, D_{kk}\, dV_0 \overset{\int}{\Rightarrow} \frac{\dot{V}}{V} = D_{kk} \tag{4.19}$$

As mentioned before, elastic strains are small and fully recoverable (during unloading) thus, one can assume that any changes in f_{loc} are due to the plastic part of the volumetric deformation rate, i.e., D^p_{kk}. With this in mind, substitution of (4.19) in (4.18) yields:

$$\dot{f}_{\text{loc}} = (1 - f_{\text{loc}})D^p_{kk} = \dot{\lambda}(1 - f_{\text{loc}})N_{kk} \tag{4.20}$$

As with the equivalent plastic strain, in the nonlocal case, f_{loc} in (4.20) is substituted with the nonlocal porosity f. Moreover, in general, one needs to consider not only the evolution of porosity due to growth of existing voids, which is expressed by (4.20), but also the increase in porosity with nucleation of new pores as the material deforms due to cracking or interfacial decohesion of inclusion or precipitate particles. This effect can be introduced using the strain-driven nucleation term, $\mathcal{T}(\bar{\varepsilon}^p)\dot{\bar{\varepsilon}}^p$, proposed by Chu and Needleman [16], where the nucleation parameter $\mathcal{T}(\bar{\varepsilon}^p)$ is given as:

$$\mathcal{T}(\bar{\varepsilon}^p) = \frac{f_N}{s_n\sqrt{2\pi}} \exp\left[-\frac{1}{2}\left(\frac{\bar{\varepsilon}^p - \varepsilon_N}{s_N}\right)^2\right] \tag{4.21}$$

where f_N is the volume fraction of the void nucleating particles and $\mathcal{T}$ is selected so that the nucleation strain follows a normal distribution with mean value ε_N and standard deviation s_N. Using the aforementioned ideas, one can finally arrive at the general evolution equation for the total porosity in the material, i.e.,

$$\boxed{\dot{f}_{\text{loc}} = \dot{f}^{(\text{growth})}_{\text{loc}} + \dot{f}^{(\text{nucl})}_{\text{loc}} = (1-f)D^p_{kk} + \mathcal{T}(\bar{\varepsilon}^p)\dot{\bar{\varepsilon}}^p = \dot{\lambda}[(1-f)N_{kk} + \mathcal{T}(\bar{\varepsilon}^p)g_1]} \tag{4.22}$$

It should be emphasized here that, selection of $f_N = 0$ implies that nucleation of new voids is neglected and the evolution equation for local porosity reduces to (4.20) with $f_{\text{loc}} \to f$.

4.1.3.2 Evolution of the Shape and Orientation of the RLEV

As mentioned in Subsection 4.1.3, for the local formulation, the evolution of the internal variables concerning the RLEV is based on the average rate of deformation and spin developed in the voids. Using the variational procedure proposed by Ponte Casteñeda in [64], one can determine expression the average deformation rate and the average spin of the local ellipsoid in terms of the macroscopic plastic deformation rate $\mathbf{D}^p$ and the macroscopic spin of the continuum body $\mathbf{W}$. More specifically, it has been shown in [47] and [66] (see also [21]) that the average deformation rate $\mathbf{D}^{\mathrm{v}}$ and average spin $\mathbf{W}^{\mathrm{v}}$ in the RLEV are given as:

$$\mathbf{D}^{\mathrm{v}} = \boldsymbol{\mathcal{A}} : \mathbf{D}^p \quad \text{and} \quad \mathbf{W}^{\mathrm{v}} = \mathbf{W} - \boldsymbol{\mathcal{C}} : \mathbf{D}^p \tag{4.23}$$

where $\boldsymbol{\mathcal{A}}$ and $\boldsymbol{\mathcal{C}}$ are the so called deformation and spin fourth order "concentration tensors" of the vacuous phase, which are defined as:

$$\boldsymbol{\mathcal{A}} = [\boldsymbol{\mathcal{I}} - (1 - f_{\mathrm{loc}})\boldsymbol{\mathcal{S}}|_{\nu=1/2}]^{-1} \quad \text{and} \quad \boldsymbol{\mathcal{C}} = -(1 - f_{\mathrm{loc}})\boldsymbol{\Pi} : \boldsymbol{\mathcal{A}} \tag{4.24}$$

Here $\boldsymbol{\Pi}$ denotes the fourth order Eshelby ([27], [28]) rotation tensor that determines the spin of an isolated void in an infinite, linear viscous matrix. Once again, in the nonlocal model, f_{loc} is substituted by its nonlocal counterpart f so (4.24) now yields:

$$\boldsymbol{\mathcal{A}} = [\boldsymbol{\mathcal{I}} - (1 - f)\boldsymbol{\mathcal{S}}|_{\nu=1/2}]^{-1} \quad \text{and} \quad \boldsymbol{\mathcal{C}} = -(1 - f)\boldsymbol{\Pi} : \boldsymbol{\mathcal{A}} \tag{4.25}$$

It should be noted here that tensor $\boldsymbol{\Pi}$ is antisymmetric with respect to the first two indices and symmetric with respect to the last two, i.e., $\Pi_{ijkl} = -\Pi_{jikl} = \Pi_{ijlk}$ and depends on the aspect ratios (w_1, w_2) and the orientation vectors $(\mathbf{n}^{(1)}, \mathbf{n}^{(2)}, \mathbf{n}^{(3)})$. On the other hand, the "concentration tensors" $\boldsymbol{\mathcal{A}}$ and $\boldsymbol{\mathcal{C}}$ have the symmetries and antisymmetries of $\boldsymbol{\mathcal{S}}$ and $\boldsymbol{\Pi}$ respectively, both depend on $(f, w_1, w_2, \mathbf{n}^{(1)}, \mathbf{n}^{(2)}, \mathbf{n}^{(3)})$ and in the limiting case of $f \to 0$ their expressions reduce to the corresponding formulae of Eshelby ([27], [28]) for the case of an isolated void in an infinite, incompressible matrix. Expressions for the evaluation of tensor $\boldsymbol{\Pi}$ are given in Appendix A.

Using the aforementioned ideas, one can calculate the evolution equations of the aspect ratios (w_1, w_2) in the following manner. At first, considering the definition of w_1 and differentiating with respect to time one receives:

$$\begin{aligned} w_1 = \frac{a_3}{a_1} \Rightarrow \dot{w}_1 = \frac{\dot{a}_3 a_1 - a_3 \dot{a}_1}{a_1^2} = \frac{a_3}{a_1}\frac{a_1}{a_3}\left(\frac{\dot{a}_3}{a_1} - \frac{a_3 \dot{a}_1}{a_1^2}\right) = w_1\left(\frac{\dot{a}_3}{a_3} - \frac{\dot{a}_1}{a_1}\right) \overset{(1.51)}{\Longrightarrow} \\ \Rightarrow \dot{w}_1 = w_1(\mathbf{n}^{(3)} \cdot \mathbf{D}^{\mathrm{v}} \cdot \mathbf{n}^{(3)} - \mathbf{n}^{(1)} \cdot \mathbf{D}^{\mathrm{v}} \cdot \mathbf{n}^{(1)}) = w_1(\mathbf{n}^{(3)}\mathbf{n}^{(3)} - \mathbf{n}^{(1)}\mathbf{n}^{(1)}) : \mathbf{D}^{\mathrm{v}} \end{aligned} \tag{4.26}$$

where $2a_i$ is the length of the ith principal axis of the local representative ellipsoid. Additionally, taking into account (4.16) and (4.23) for the plastic and average rate of deformation and plugging them into (4.26), one can arrive at the following expression for the rate of change

of w_1:

$$\boxed{\dot{w}_1 = \dot{\lambda} w_1(\mathbf{n}^{(3)}\mathbf{n}^{(3)} - \mathbf{n}^{(1)}\mathbf{n}^{(1)}) : \boldsymbol{\mathcal{A}} : \mathbf{N} \equiv \dot{\lambda} g_2(\boldsymbol{\sigma}, f, w_1, w_2, \mathbf{n}^{(1)}, \mathbf{n}^{(2)}, \mathbf{n}^{(3)})} \tag{4.27}$$

In a similar fashion, it can be readily proved that the evolution equation for w_2 is given as:

$$\boxed{\dot{w}_2 = \dot{\lambda} w_2(\mathbf{n}^{(3)}\mathbf{n}^{(3)} - \mathbf{n}^{(2)}\mathbf{n}^{(2)}) : \boldsymbol{\mathcal{A}} : \mathbf{N} \equiv \dot{\lambda} g_3(\boldsymbol{\sigma}, f, w_1, w_2, \mathbf{n}^{(1)}, \mathbf{n}^{(2)}, \mathbf{n}^{(3)})} \tag{4.28}$$

Although equations (4.27) and (4.28) are not directly numerically integrated in the formulation presented herein for the incremental update of w_1 and w_2 they are, nonetheless, utilized in the calculations involved in the consistency condition for the evaluation of $\dot{\lambda}$, which is carried out in Section 4.2. In particular, due to numerical difficulties that rose during the implementation of the gradient anisotropic model for the set of applications presented in Chapter 6, an alternative approach to the one presented in [7], based on the average kinematic description of the local ellipsoidal void, is used in the following for the description of evolution of the shape and orientation of the voids.

To begin with, one can imagine that the RLEV develops during plastic flow from a "reference spherical void" of radius a_0. In this sense, if $\mathfrak{B}_0$ denotes the reference configuration and $\bar{\mathfrak{B}}$, $\mathfrak{B}_t$ denote the the instantaneous initial and the current configurations of the void at any time of the deformation program, then, the deformation gradient of the ellipsoidal void $\mathbf{F}^{\mathrm{v}}(t)$ relative to the reference spherical void can be written as:

$$\mathbf{F}^{\mathrm{v}}(t) = \frac{\partial \mathbf{x}_t}{\partial \mathbf{x}_0} = \frac{\partial \mathbf{x}_t}{\partial \bar{\mathbf{x}}} \cdot \frac{\partial \bar{\mathbf{x}}}{\partial \mathbf{x}_0} \equiv \bar{\mathbf{F}}^{\mathrm{v}}(t) \cdot \mathbf{F}_0^{\mathrm{v}} \tag{4.29}$$

where $\mathbf{F}_0^{\mathrm{v}}$ is the deformation gradient of the initial representative void relative to the reference spherical void and $\bar{\mathbf{F}}^{\mathrm{v}}(t)$ is the deformation gradient of the evolving ellipsoidal relative to its initial shape. In the special case where the voids are initially spherical, $\mathfrak{B}_0$ and $\bar{\mathfrak{B}}$ coincide, suggesting that $\mathbf{F}_0^{\mathrm{v}} = \boldsymbol{\delta}$. In general however, the voids can be initially ellipsoidal , i.e., $\mathbf{F}_0^{\mathrm{v}} \neq \boldsymbol{\delta}$ and the procedure that follows is valid for both cases. Using (4.29), one can prove that the corresponding average velocity of the RLEV $\mathbf{L}^{\mathrm{v}}$ can be written as:

$$\mathbf{L}^{\mathrm{v}} = \mathbf{D}^{\mathrm{v}} + \mathbf{W}^{\mathrm{v}} = \dot{\mathbf{F}}^{\mathrm{v}} \cdot \mathbf{F}^{\mathrm{v}-1} = \dot{\bar{\mathbf{F}}}^{\mathrm{v}} \cdot \bar{\mathbf{F}}^{\mathrm{v}-1} \tag{4.30}$$

Now, substitution of the expressions of (4.23) for $\mathbf{D}^{\mathrm{v}}$ and $\mathbf{W}^{\mathrm{v}}$ in (4.30) yields:

$$\boxed{\dot{\mathbf{F}}^{\mathrm{v}} \cdot \mathbf{F}^{\mathrm{v}-1} = (\boldsymbol{\mathcal{A}} - \boldsymbol{\mathcal{C}}) : \mathbf{D}^p + \mathbf{W}} \tag{4.31}$$

which is the differential equation that, together with the initial condition $\mathbf{F}^{\mathrm{v}}(0) = \mathbf{F}_0^{\mathrm{v}}$, defines the deformation gradient, $\mathbf{F}^{\mathrm{v}}(t)$, of the local representative ellipsoid. Moreover, introducing the so called "rotation neutralized" ([55]) version of $\mathbf{F}^{\mathrm{v}}$ as:

$$\hat{\mathbf{F}}^{\mathrm{v}}(t) = \mathbf{R}^T(t) \cdot \mathbf{F}^{\mathrm{v}}(t) \tag{4.32}$$

solution[5] of (4.31) leads now to the derivation of an expression for $\hat{\mathbf{F}}^{\mathrm{v}}$ which can then be used for the calculation of the aspect ratios w_α and the rotation neutralized orientation vectors $\hat{\mathbf{n}}^{(i)}$ (see (4.50)), at the end of the increment.

4.2 The Elastoplastic Material Behavior

In the previous sections, a detailed description of the separate elastic and plastic constitutive behavior of the material model under consideration has been presented. As mentioned in Section 2.2, in the context of classical (local) rate-independent incremental plasticity, one wants to derive a combined elastic-plastic constitutive equation relating the objective rate of a suitably selected stress measure to a corresponding total rate of deformation in the sense that the aforementioned pair has to belong in the same objectivity class (i.e. both Eulerian or Lagrangian objective) and simultaneously express a work-conjugate pair. However, in the case of nonlocal plasticity, the casual Elastoplastic BVP is enhanced with an additional partial differential equation (and a relevant boundary condition) for the nonlocal porosity f which now suggests a primary unknown along with the displacement field. Thus, except from the so called "tangent modulus" of the material, the need for the calculation of the variation of stress and local porosity with respect to the unknowns of the problem arises in the finite element method, as will be proved in Chapter 5. The derivation of the aforementioned relations is as follows.

To begin with, assuming that plastic loading occurs (i.e., $\dot{\lambda} > 0$), then, considering the fact that $\mathbf{D}^e = \mathbf{D} - \mathbf{D}^p = \mathbf{D} - \dot{\lambda}\mathbf{N}$ as suggested by (2.5), (4.16) and using (2.15), one gets:

$$\begin{aligned} \overset{\nabla}{\boldsymbol{\sigma}} &= \boldsymbol{\mathcal{L}}^e : \mathbf{D}^e + \boldsymbol{\sigma} \cdot \mathbf{W}^p - \mathbf{W}^p \cdot \boldsymbol{\sigma} = \boldsymbol{\mathcal{L}}^e : (\mathbf{D} - \dot{\lambda}\mathbf{N}) + \boldsymbol{\sigma} \cdot \mathbf{W}^p - \mathbf{W}^p \cdot \boldsymbol{\sigma} = \\ &= \boldsymbol{\mathcal{L}}^e : \mathbf{D} - \dot{\lambda}\boldsymbol{\mathcal{L}}^e : \mathbf{N} + \boldsymbol{\sigma} \cdot \mathbf{W}^p - \mathbf{W}^p \cdot \boldsymbol{\sigma} \end{aligned} \tag{4.33}$$

Furthermore, it is proved in [7] (see also [18], [19]) that the so-called "plastic spin" $\mathbf{W}^p$ can be written in the form:

$$\mathbf{W}^p = \dot{\lambda}\boldsymbol{\Omega}^p \tag{4.34}$$

where $\boldsymbol{\Omega}^p = \boldsymbol{\Omega}^p(f, w_1, w_2, \mathbf{n}^{(1)}, \mathbf{n}^{(2)}, \mathbf{n}^{(3)})$ is a second order tensor, which is given as:

$$\boldsymbol{\Omega}^p = \boldsymbol{\mathcal{C}} : \mathbf{N} - \frac{1}{2} \sum_{\substack{i,j=1 \\ i \neq j \\ w_i \neq w_j}} \frac{w_i^2 + w_j^2}{w_i^2 - w_j^2} [(\mathbf{n}^{(i)}\mathbf{n}^{(j)} + \mathbf{n}^{(j)}\mathbf{n}^{(i)}) : \mathcal{A} : \mathbf{N}]\mathbf{n}^{(i)}\mathbf{n}^{(j)}, \quad (w_3 = 1) \tag{4.35}$$

Substitution of (4.35) in (4.34) now yields:

[5] The solution procedure of the first order ordinary differential equation (ODE) for $\hat{\mathbf{F}}^{\mathrm{v}}$ is presented in detail in Appendix B

$$\overset{\triangledown}{\boldsymbol{\sigma}} = \overset{\circ}{\boldsymbol{\sigma}} + \dot{\lambda}(\boldsymbol{\sigma}\cdot\boldsymbol{\Omega}^p - \boldsymbol{\Omega}^p\cdot\boldsymbol{\sigma}) \quad \text{with} \quad \overset{\circ}{\boldsymbol{\sigma}} = \boldsymbol{\mathcal{L}}^e : \mathbf{D} - \dot{\lambda}\boldsymbol{\mathcal{L}}^e : \mathbf{N} \tag{4.36}$$

One now needs to derive an explicit expression of the unknown plastic multiplier $\dot{\lambda}$. In this sense, following the generalized rationale developed in Subsection 2.2.2 and taking into consideration (4.16), (4.17), (4.27), (4.28), the consistency condition $\dot{\tilde{\Phi}}$ for the effective yield function is of the form of (2.20):

$$\dot{\tilde{\Phi}} = \underbrace{\frac{\partial\tilde{\Phi}}{\partial\boldsymbol{\sigma}} : \overset{\circ}{\boldsymbol{\sigma}}}_{\mathbf{N}:\overset{\circ}{\boldsymbol{\sigma}}} + \frac{\partial\tilde{\Phi}}{\partial\bar{\varepsilon}^p}\underbrace{\dot{\bar{\varepsilon}}^p}_{\dot{\lambda}g_1} + \frac{\partial\tilde{\Phi}}{\partial f}\dot{f} + \frac{\partial\tilde{\Phi}}{\partial w_1}\underbrace{\dot{w}_1}_{\dot{\lambda}g_2} + \frac{\partial\tilde{\Phi}}{\partial w_2}\underbrace{\dot{w}_2}_{\dot{\lambda}g_3} + \frac{\partial\tilde{\Phi}}{\partial\mathbf{n}^{(i)}}\cdot\overset{\circ}{\mathbf{n}}^{(i)} = 0 \tag{4.37}$$

Since $\mathbf{n}^{(i)}$'s are corotational with the spin of the voids $\boldsymbol{\omega}$ then $\overset{\circ}{\mathbf{n}}^{(i)} = \dot{\mathbf{n}}^{(i)} - \boldsymbol{\omega}\cdot\mathbf{n}^{(i)} = 0$ and so, substitution of $\overset{\circ}{\boldsymbol{\sigma}}$ from (4.36) to (4.37) leads to:

$$\begin{aligned}
\dot{\tilde{\Phi}} &= \mathbf{N} : (\boldsymbol{\mathcal{L}}^e : \mathbf{D} - \dot{\lambda}\boldsymbol{\mathcal{L}}^e : \mathbf{N}) - \dot{\lambda}\underbrace{\left(\frac{\partial\tilde{\Phi}}{\partial\bar{\varepsilon}^p}g_1 + \frac{\partial\tilde{\Phi}}{\partial w_1}g_2 + \frac{\partial\tilde{\Phi}}{\partial w_2}g_3\right)}_{-H} + \frac{\partial\tilde{\Phi}}{\partial f}\dot{f} = \\
&= \mathbf{N} : (\boldsymbol{\mathcal{L}}^e : \mathbf{D} - \dot{\lambda}\boldsymbol{\mathcal{L}}^e : \mathbf{N}) - \dot{\lambda}H + \frac{\partial\tilde{\Phi}}{\partial f}\dot{f} = \\
&= -\dot{\lambda}(H + \mathbf{N} : \boldsymbol{\mathcal{L}}^e : \mathbf{N}) + \mathbf{N} : \boldsymbol{\mathcal{L}}^e : \mathbf{D} + \frac{\partial\tilde{\Phi}}{\partial f}\dot{f} = 0 \Rightarrow \\
\Rightarrow \boxed{\dot{\lambda} = \frac{1}{L}\left(\mathbf{N} : \boldsymbol{\mathcal{L}}^e : \mathbf{D} + \frac{\partial\tilde{\Phi}}{\partial f}\dot{f}\right)} \quad &\text{where} \quad \boxed{L = H + \mathbf{N} : \boldsymbol{\mathcal{L}}^e : \mathbf{N}}
\end{aligned} \tag{4.38}$$

Using expression (4.38) for $\dot{\lambda}$, $\overset{\circ}{\boldsymbol{\sigma}}$ is now given as[6]

$$\overset{\circ}{\boldsymbol{\sigma}} = \boldsymbol{\mathcal{L}}^e : \mathbf{D} - \frac{1}{L}\left(\mathbf{N} : \boldsymbol{\mathcal{L}}^e : \mathbf{D} + \frac{\partial\tilde{\Phi}}{\partial f}\dot{f}\right)\boldsymbol{\mathcal{L}}^e : \mathbf{N} = \left(\boldsymbol{\mathcal{L}}^e - \frac{1}{L}\boldsymbol{\mathcal{L}}^e : \mathbf{N}\mathbf{N} : \boldsymbol{\mathcal{L}}^e\right) : \mathbf{D} - \frac{1}{L}\frac{\partial\tilde{\Phi}}{\partial f}\boldsymbol{\mathcal{L}}^e : \mathbf{N}\dot{f}$$

Plugging this last equation into (4.36), one gets the following for the Jaumann stress rate $\overset{\triangledown}{\boldsymbol{\sigma}}$:

$$\overset{\triangledown}{\boldsymbol{\sigma}} = \overset{\circ}{\boldsymbol{\sigma}} + \dot{\lambda}(\boldsymbol{\sigma}\cdot\boldsymbol{\Omega}^p - \boldsymbol{\Omega}^p\cdot\boldsymbol{\sigma}) = \overset{\circ}{\boldsymbol{\sigma}} + \frac{1}{L}(\boldsymbol{\sigma}\cdot\boldsymbol{\Omega}^p - \boldsymbol{\Omega}^p\cdot\boldsymbol{\sigma})\left(\mathbf{N} : \boldsymbol{\mathcal{L}}^e : \mathbf{D} + \frac{\partial\tilde{\Phi}}{\partial f}\dot{f}\right) \Rightarrow$$

$$\overset{\triangledown}{\boldsymbol{\sigma}} = \left(\boldsymbol{\mathcal{L}}^e - \frac{1}{L}\boldsymbol{\mathcal{L}}^e : \mathbf{N}\mathbf{N} : \boldsymbol{\mathcal{L}}^e\right) : \mathbf{D} - \frac{1}{L}\frac{\partial\tilde{\Phi}}{\partial f}\boldsymbol{\mathcal{L}}^e : \mathbf{N}\dot{f} + \frac{1}{L}(\boldsymbol{\sigma}\cdot\boldsymbol{\Omega}^p - \boldsymbol{\Omega}^p\cdot\boldsymbol{\sigma})\left(\mathbf{N} : \boldsymbol{\mathcal{L}}^e : \mathbf{D} + \frac{\partial\tilde{\Phi}}{\partial f}\dot{f}\right) \Rightarrow$$

$$\overset{\triangledown}{\boldsymbol{\sigma}} = \left[\boldsymbol{\mathcal{L}}^e - \frac{1}{L}(\boldsymbol{\mathcal{L}}^e : \mathbf{N})(\boldsymbol{\mathcal{L}}^e : \mathbf{N}) + \frac{1}{L}(\boldsymbol{\sigma}\cdot\boldsymbol{\Omega}^p - \boldsymbol{\Omega}^p\cdot\boldsymbol{\sigma})(\boldsymbol{\mathcal{L}}^e : \mathbf{N})\right] : \mathbf{D} + \frac{1}{L}\frac{\partial\tilde{\Phi}}{\partial f}(\boldsymbol{\sigma}\cdot\boldsymbol{\Omega}^p - \boldsymbol{\Omega}^p\cdot\boldsymbol{\sigma} + \boldsymbol{\mathcal{L}}^e : \mathbf{N})\dot{f} \Rightarrow$$

$$\overset{\triangledown}{\boldsymbol{\sigma}} = \left[\boldsymbol{\mathcal{L}}^e - \frac{1}{L}(\boldsymbol{\mathcal{L}}^e : \mathbf{N} - \boldsymbol{\sigma}\cdot\boldsymbol{\Omega}^p + \boldsymbol{\Omega}^p\cdot\boldsymbol{\sigma})\boldsymbol{\mathcal{L}}^e : \mathbf{N}\right] : \mathbf{D} - \frac{1}{L}\frac{\partial\tilde{\Phi}}{\partial f}(\boldsymbol{\mathcal{L}}^e : \mathbf{N} - \boldsymbol{\sigma}\cdot\boldsymbol{\Omega}^p + \boldsymbol{\Omega}^p\cdot\boldsymbol{\sigma})\dot{f} \Rightarrow$$

[6] Here the property $(\mathbf{A} : \mathbf{B})\mathbf{C} = (\mathbf{C}\mathbf{A}) : \mathbf{B}$, that holds for any triad of second order tensors $\mathbf{A}$, $\mathbf{B}$, $\mathbf{C}$, is taken into account.

$$\Rightarrow \quad \boxed{\overset{\nabla}{\boldsymbol{\sigma}} = \left[\boldsymbol{\mathcal{L}}^e - \mathbf{A}(\boldsymbol{\mathcal{L}}^e : \mathbf{N})\right] : \mathbf{D} - \frac{\partial \tilde{\Phi}}{\partial f}\mathbf{A}\dot{f}} \quad , \quad \mathbf{A} = \frac{1}{L}(\boldsymbol{\mathcal{L}}^e : \mathbf{N} - \boldsymbol{\sigma}\cdot\boldsymbol{\Omega}^p + \boldsymbol{\Omega}^p\cdot\boldsymbol{\sigma}) \tag{4.39}$$

Equation (4.39) can now be used to approximate the aforementioned variations[7] of stress with respect to strain and nonlocal porosity as:

$$\boxed{\frac{\partial \boldsymbol{\sigma}}{\partial \mathbf{E}} = \boldsymbol{\mathcal{L}}^e - \mathbf{A}(\boldsymbol{\mathcal{L}}^e : \mathbf{N})} \quad \text{and} \quad \boxed{\frac{\partial \boldsymbol{\sigma}}{\partial f} = -\frac{\partial \tilde{\Phi}}{\partial f}\mathbf{A}} \tag{4.40}$$

Furthermore, substituting $\dot{\lambda}$ from (4.38) into (4.22), one also gets:

$$\dot{f}_{\text{loc}} = \dot{\lambda}[(1-f)N_{kk} + \mathcal{T}(\bar{\varepsilon}^p)g_1] = \frac{1}{L}[(1-f)N_{kk} + \mathcal{T}(\bar{\varepsilon}^p)g_1]\left(\mathbf{N} : \boldsymbol{\mathcal{L}}^e : \mathbf{D} + \frac{\partial \tilde{\Phi}}{\partial f}\dot{f}\right) \Rightarrow$$

$$\Rightarrow \boxed{\dot{f}_{\text{loc}} = B\mathbf{N} : \boldsymbol{\mathcal{L}}^e : \mathbf{D} + B\frac{\partial \tilde{\Phi}}{\partial f}\dot{f}} \quad , \quad B = \frac{1}{L}[(1-f)N_{kk} + \mathcal{T}(\bar{\varepsilon}^p)g_1] \tag{4.41}$$

Using (4.41), variations of f_{loc} with respect to strain and the nonlocal porosity are approximated as:

$$\boxed{\frac{\partial f_{\text{loc}}}{\partial \mathbf{E}} = B\mathbf{N} : \boldsymbol{\mathcal{L}}^e} \quad \text{and} \quad \boxed{\frac{\partial f_{\text{loc}}}{\partial f} = B\frac{\partial \tilde{\Phi}}{\partial f}} \tag{4.42}$$

The total elastoplastic behavior of the model can now be described in a conveniently unified manner by introducing a binary plasticity parameter α^{p}, such that $\mathbf{A}$ and B are modified as:

$$\boxed{\mathbf{A} = \frac{\alpha^{\text{p}}}{L}(\boldsymbol{\mathcal{L}}^e : \mathbf{N} - \boldsymbol{\sigma}\cdot\boldsymbol{\Omega}^p + \boldsymbol{\Omega}^p\cdot\boldsymbol{\sigma})} \quad , \quad \boxed{B = \frac{\alpha^{\text{p}}}{L}[(1-f)N_{kk} + \mathcal{T}(\bar{\varepsilon}^p)g_1]} \tag{4.43}$$

If $\alpha^{\text{p}} = 1$, then elastic-plastic behavior occurs and the total response of the material is described by (4.39) - (4.42). On the contrary, $\alpha^{\text{p}} = 0$ implies that $\mathbf{A} = \mathbf{0}$ and $B = 0$, elasticity takes place, and the constitutive behavior is described by the reduced versions of (4.39), (4.40) and (4.42) :

$$\boxed{\overset{\nabla}{\boldsymbol{\sigma}} = \boldsymbol{\mathcal{L}}^e : \mathbf{D}} \tag{4.44}$$

and

$$\boxed{\frac{\partial \boldsymbol{\sigma}}{\partial \mathbf{E}} = \boldsymbol{\mathcal{L}}^e \ , \ \frac{\partial \boldsymbol{\sigma}}{\partial f} = \mathbf{0} \ , \ \frac{\partial f_{\text{loc}}}{\partial \mathbf{E}} = \mathbf{0} \ , \ \frac{\partial f_{\text{loc}}}{\partial f} = 0} \tag{4.45}$$

[7] In general however, such variations actually depend on the integration scheme that is implemented to integrate the constitutive equations. In the latter procedure, the corresponding variations also known as "linearization moduli" are deduced, which are consistent with integration algorithm that is used for the integration of the constitutive equations.

4.3 Numerical Integration of the Constitutive Model

In the previous sections, the total response of the material and the evolution of the microstructure, as the deformation progresses, has been described in detail. In the context of finite element analysis, which is used for the numerical implementation of the model presented herein, the solution of the corresponding BVP is developed incrementally and the constitutive equations that model the problem have to be integrated numerically at the local Gauss integration points of each finite element. To be more precise, at the part of the computations where material behavior is examined, at a given Gauss point, the solution $(\mathbf{F}_n,\ \boldsymbol{\sigma}_n,\ \mathbf{s}_n)$ at time t_n as well as the deformation gradient $\mathbf{F}_{n+1}$ at time t_{n+1} are known and the problem is to determine the solution $(\boldsymbol{\sigma}_{n+1},\ \mathbf{s}_{n+1})$ along with the "moduli" $\frac{\partial \boldsymbol{\sigma}}{\partial \mathbf{E}}|_{n+1}$, $\frac{\partial \boldsymbol{\sigma}}{\partial f}|_{n+1}$, $\frac{\partial f_{\text{loc}}}{\partial \mathbf{E}}|_{n+1}$, $\frac{\partial f_{\text{loc}}}{\partial f}|_{n+1}$ at the end of the time increment. For this purpose, following [7], a combination of backward (implicit) and forward (explicit) Euler schemes are used for the aforementioned numerical integration, with the procedure being as follows.

Let $\mathbf{F}$ be the deformation gradient, which is defined relative to the configuration at the beginning of the time increment under consideration. Then, the time variation of $\mathbf{F}$ during the corresponding time increment $[t_n, t_{n+1}]$ can be written as :

$$\mathbf{F}(t) = \Delta\mathbf{F}(t) \cdot \mathbf{F}_n = \mathbf{R}(t) \cdot \mathbf{U}(t) \cdot \mathbf{F}_n \ , \quad t \in [t_n, t_{n+1}] \tag{4.46}$$

where $\mathbf{R}(t)$, $\mathbf{U}(t)$ are the rotation and stretch tensors of the right polar decomposition associated with $\Delta\mathbf{F}(t)$. Using (1.44) and (4.46) , one can now define the deformation rate $\mathbf{D}(t)$ and spin $\mathbf{W}(t)$ tensors as the symmetric and skew-symmetric parts of the velocity gradient, i.e.:

$$\mathbf{D}(t) \equiv [\dot{\mathbf{F}}(t) \cdot \mathbf{F}^{-1}(t)]^{(sym)} = [\Delta\dot{\mathbf{F}}(t) \cdot \Delta\mathbf{F}^{-1}(t)]^{(sym)} \tag{4.47}$$

and

$$\mathbf{W}(t) \equiv [\dot{\mathbf{F}}(t) \cdot \mathbf{F}^{-1}(t)]^{(skew)} = [\Delta\dot{\mathbf{F}}(t) \cdot \Delta\mathbf{F}^{-1}(t)]^{(skew)} \tag{4.48}$$

If the assumption that the Lagrangian triad associated with $\Delta\mathbf{F}(t)$ (i.e., the eigenvectors of $\mathbf{U}(t)$) remains constant in the time interval $[t_n, t_{n+1}]$ is adopted[8] then, as proved in Section 1.5.3, $\mathbf{D}(t)$ and $\mathbf{W}(t)$ can be given in terms of the logarithmic strain $\mathbf{E}^{\ln}(t) \equiv \mathbf{E}(t)$ by (1.69):

$$\mathbf{D}(t) = \mathbf{R}(t) \cdot \dot{\mathbf{E}}(t) \cdot \mathbf{R}^T(t) \quad \text{and} \quad \mathbf{W}(t) = \dot{\mathbf{R}}(t) \cdot \mathbf{R}^T(t) \tag{4.49}$$

where $\mathbf{E}(t) = \ln\mathbf{U}(t)$ is defined relative to the configuration at time t_n. With all these in mind, one can now define the "rotation neutralized" versions of $\boldsymbol{\sigma}$ and $\mathbf{n}^{(i)}$, as:

$$\hat{\boldsymbol{\sigma}}(t) = \mathbf{R}^T(t) \cdot \boldsymbol{\sigma}(t) \cdot \mathbf{R}(t) \quad \text{and} \quad \hat{\mathbf{n}}^{(i)}(t) = \mathbf{R}^T \cdot \mathbf{n}^{(i)}(t) \tag{4.50}$$

[8] An alternative assumption is that of constant strain rate over the increment ([55], [57]) which could be considered less "computationally safe", in the sense that accuracy of the numerical solution may deteriorate severely depending *both* on the nature of deformation and the size of the increment.

Additionally, one can readily show using (4.49) and (4.50) that, the Jaumman stress rate is related to $\hat{\boldsymbol{\sigma}}$ by the expression:

$$\overset{\nabla}{\boldsymbol{\sigma}}(t) = \mathbf{R}(t) \cdot \dot{\hat{\boldsymbol{\sigma}}}(t) \cdot \mathbf{R}^T(t) \tag{4.51}$$

It should be noted here that at the start of the increment ($t = t_n$), the following relations hold:

$$\mathbf{F}_n = \mathbf{R}_n = \mathbf{U}_n = \boldsymbol{\delta} \ , \ \hat{\boldsymbol{\sigma}}_n = \boldsymbol{\sigma}_n \ , \ \hat{\mathbf{n}}_n^{(i)} = \mathbf{n}_n^{(i)} \quad \text{and} \quad \mathbf{E}_n = \mathbf{0} \tag{4.52}$$

whereas at the end of the increment ($t = t_{n+1}$) one has:

$$\begin{gathered} \Delta\mathbf{F}_{n+1} = \mathbf{F}_{n+1} \cdot \mathbf{F}_n = \mathbf{R}_{n+1} \cdot \mathbf{U}_{n+1} = \text{known} \\ \mathbf{U}_{n+1} = \sum_{i=1}^{3} \lambda_i^{(\Delta\mathbf{F})} \mathbf{N}_i^{(\Delta\mathbf{F})} \mathbf{N}_i^{(\Delta\mathbf{F})} = \text{known} \ , \ \mathbf{R}_{n+1} = \Delta\mathbf{F}_{n+1} \cdot \mathbf{U}_{n+1}^{-1} = \text{known} \\ \text{and} \quad \mathbf{E}_{n+1} = \ln\mathbf{U}_{n+1} = \text{known} \end{gathered} \tag{4.53}$$

where $\lambda_i^{(\Delta\mathbf{F})}$, $\mathbf{N}_i^{(\Delta\mathbf{F})}$ correspond to the eigenvalues and eigenvectors of $\Delta\mathbf{F}$ respectively. Taking into account that $\tilde{\Phi}$, $\mathbf{N}$, g_j ($j = 1, 2, 3$), and $\boldsymbol{\Omega}^p$ are isotropic functions of their arguments, i.e., they are such that:

$$\tilde{\Phi}(\mathbf{R} \cdot \boldsymbol{\sigma} \cdot \mathbf{R}^T, \bar{\varepsilon}^p, f, w_\alpha, \mathbf{R} \cdot \mathbf{n}^{(i)}) = \tilde{\Phi}(\boldsymbol{\sigma}, \bar{\varepsilon}^p, f, w_\alpha, \mathbf{n}^{(i)}) \tag{4.54}$$

$$\mathbf{N}(\mathbf{R} \cdot \boldsymbol{\sigma} \cdot \mathbf{R}^T, f, w_\alpha, \mathbf{R} \cdot \mathbf{n}^{(i)}) = \mathbf{R} \cdot \mathbf{N}(\boldsymbol{\sigma}, f, w_\alpha, \mathbf{n}^{(i)}) \cdot \mathbf{R}^T \tag{4.55}$$

$$g_j(\mathbf{R} \cdot \boldsymbol{\sigma} \cdot \mathbf{R}^T, \bar{\varepsilon}^p, f, w_\alpha, \mathbf{R} \cdot \mathbf{n}^{(i)}) = g_j(\boldsymbol{\sigma}, \bar{\varepsilon}^p, f, w_\alpha, \mathbf{n}^{(i)}) \tag{4.56}$$

$$\boldsymbol{\Omega}^p(\mathbf{R} \cdot \boldsymbol{\sigma} \cdot \mathbf{R}^T, f, w_\alpha, \mathbf{R} \cdot \mathbf{n}^{(i)}) = \mathbf{R} \cdot \boldsymbol{\Omega}^p(\boldsymbol{\sigma}, f, w_\alpha, \mathbf{n}^{(i)}) \cdot \mathbf{R}^T \tag{4.57}$$

the constitutive equations (2.5), (4.13), (4.16), (4.17), (4.22), (4.31) and (4.36) and the evolution equations (4.27), (4.28) can now be written in the rotation neutralized form as:

$$\dot{\mathbf{E}} = \dot{\mathbf{E}}^e + \dot{\mathbf{E}}^p \tag{4.58}$$

$$\tilde{\Phi}(\hat{\boldsymbol{\sigma}}, \hat{\bar{\mathbf{s}}}) = 0 \tag{4.59}$$

$$\dot{\mathbf{E}}^p = \dot{\lambda}\mathbf{N}(\hat{\boldsymbol{\sigma}}, \hat{\bar{\mathbf{s}}}) \tag{4.60}$$

$$\dot{\bar{\varepsilon}}^p = \dot{\lambda} g_1(\hat{\boldsymbol{\sigma}}, \hat{\bar{\mathbf{s}}}) = \frac{\hat{\boldsymbol{\sigma}} \cdot \dot{\mathbf{E}}^p}{(1-f)\sigma_y(\bar{\varepsilon}^p)} \tag{4.61}$$

$$\dot{f}_{\text{loc}} = \dot{\lambda}[(1-f)N_{kk} + \mathcal{T}(\bar{\varepsilon}^p) g_1(\hat{\boldsymbol{\sigma}}, \hat{\bar{\mathbf{s}}})] = (1-f)\Delta E_{kk}^p + \mathcal{T}(\bar{\varepsilon}^p)\dot{\bar{\varepsilon}}^p \tag{4.62}$$

$$\dot{\hat{\mathbf{F}}}^{\text{v}} \cdot \hat{\mathbf{F}}^{\text{v}-1} = (\hat{\boldsymbol{\mathcal{A}}} - \hat{\boldsymbol{\mathcal{C}}}) : \dot{\mathbf{E}}^p \tag{4.63}$$

$$\dot{\hat{\boldsymbol{\sigma}}} = \hat{\boldsymbol{\mathcal{L}}}^e \cdot \dot{\mathbf{E}} - \dot{\lambda}\hat{\boldsymbol{\mathcal{L}}}^e : \dot{\mathbf{E}}^p + \dot{\lambda}[\hat{\boldsymbol{\sigma}} \cdot \boldsymbol{\Omega}^p(\hat{\boldsymbol{\sigma}}, \hat{\bar{\mathbf{s}}}) - \boldsymbol{\Omega}^p(\hat{\boldsymbol{\sigma}}, \hat{\bar{\mathbf{s}}}) \cdot \hat{\boldsymbol{\sigma}}] \tag{4.64}$$

and

$$\dot{w}_1 = \dot{\lambda} g_2(\hat{\boldsymbol{\sigma}}, \hat{\bar{\mathbf{s}}}) = (\hat{\mathbf{n}}^{(3)}\hat{\mathbf{n}}^{(3)} - \hat{\mathbf{n}}^{(1)}\hat{\mathbf{n}}^{(1)}) : \hat{\boldsymbol{\mathcal{A}}} : \dot{\mathbf{E}}^p \tag{4.65}$$

$$\dot{w}_2 = \dot{\lambda} g_3(\hat{\boldsymbol{\sigma}}, \hat{\bar{\mathbf{s}}}) = (\hat{\mathbf{n}}^{(3)}\hat{\mathbf{n}}^{(3)} - \hat{\mathbf{n}}^{(2)}\hat{\mathbf{n}}^{(2)}) : \hat{\boldsymbol{\mathcal{A}}} : \dot{\mathbf{E}}^p \tag{4.66}$$

where $\hat{\mathcal{A}}_{ijpq} = R^T_{ik}R^T_{jl}R^T_{pm}R^T_{qn}\mathcal{A}_{klmn}$ and $\hat{\mathcal{C}}_{ijpq} = R^T_{ik}R^T_{jl}R^T_{pm}R^T_{qn}\mathcal{C}_{klmn}$ (i.e., $\boldsymbol{\mathcal{A}}$, $\boldsymbol{\mathcal{C}}$ are isotropic functions of their arguments), $\hat{\mathcal{L}}^e_{ijkl} = R_{mi}R_{nj}R_{pk}R_{ql}\mathcal{L}^e_{mnpq}$, and $\hat{\bar{\mathbf{s}}} = \{\bar{\varepsilon}^p, f, w_1, w_2, \hat{\mathbf{n}}^{(1)}, \hat{\mathbf{n}}^{(2)}, \hat{\mathbf{n}}^{(3)}\}$. Equations (4.58)-(4.64) can now be integrated in order to receive the desired solution at the end of the increment.

First of all, equation (4.58) can be integrated exactly to yield:

$$\Delta\mathbf{E} = \Delta\mathbf{E}^e + \Delta\mathbf{E}^p \quad \Rightarrow \quad \Delta\mathbf{E}^e = \Delta\mathbf{E} - \Delta\mathbf{E}^p \tag{4.67}$$

where the notation $\Delta\square = \square_{n+1} - \square_n$ ($\square$ being a scalar, vector or tensor quantity) is used and from (4.52), (4.53), $\Delta\mathbf{E} = \mathbf{E}_{n+1} =$ known. Moreover, $\Delta\mathbf{E}^p$ is calculated by numerically integrating the flow rule (4.60) using a backward Euler scheme, i.e.,

$$\Delta\mathbf{E}^p = \Delta\lambda\mathbf{N}_{n+1} \ , \ \mathbf{N}_{n+1} \equiv \hat{\mathbf{N}}_{n+1} = \mathbf{N}(\hat{\boldsymbol{\sigma}}_{n+1}, f, w_\alpha|_{n+1}, \hat{\mathbf{n}}^{(i)}_{n+1}) \tag{4.68}$$

In contrast to [7], a backward Euler scheme is also implemented for the numerical integration of the evolution equations (4.61), (4.62) for $\bar{\varepsilon}^p$ and f_{loc}:

$$\bar{\varepsilon}^p_{n+1} = \bar{\varepsilon}^p_n + \Delta\bar{\varepsilon}^p \quad , \quad \Delta\bar{\varepsilon}^p \equiv \Delta\bar{\varepsilon}^p_{n+1} = \frac{\hat{\boldsymbol{\sigma}}_{n+1} : \Delta\mathbf{E}^p}{(1-f)\sigma_y(\bar{\varepsilon}^p_{n+1})} \equiv \mathbf{R}_2 : \Delta\mathbf{E}^p \tag{4.69}$$

$$f_{\text{loc}}|_{n+1} = f_{\text{loc}}|_n + \Delta f_{\text{loc}} \quad , \quad \Delta f_{\text{loc}} \equiv \Delta f_{\text{loc}}|_{n+1} = (1-f)\Delta E^p_{kk} + \mathcal{T}(\bar{\varepsilon}^p_{n+1})\Delta\bar{\varepsilon}^p \tag{4.70}$$

Furthermore, assuming a constant plastic strain rate over the corresponding increment, i.e., $\dot{\mathbf{E}}^p = ct$, (4.63) can be integrated exactly (see Appendix B) to get an explicit expression for $\hat{\mathbf{F}}^{\text{v}}$ at the end of the increment:

$$\hat{\mathbf{F}}^{\text{v}}_{n+1} = (\exp\mathbf{M}) \cdot \hat{\mathbf{F}}^{\text{v}}_n \quad \text{where} \quad \mathbf{M} = (\mathcal{A}_n - \mathcal{C}_n) : \Delta\mathbf{E}^p \tag{4.71}$$

Then, using (4.71) one can calculate the aspect ratios $w_\alpha|_{n+1}$, $\alpha = 1, 2$ and the orientation vectors $\hat{\mathbf{n}}^{(i)}_{n+1}$, $i = 1, 2, 3$ from the eigenvalues and eigenvectors of the left Cauchy-Green tensor $\hat{\mathbf{B}}^{\text{v}}_{n+1}$ associated with $\hat{\mathbf{F}}^{\text{v}}_{n+1}$:

$$\hat{\mathbf{B}}^{\text{v}}_{n+1} = \hat{\mathbf{F}}^{\text{v}}_{n+1} \cdot (\hat{\mathbf{F}}^{\text{v}}_{n+1})^T = a^2_{n+1}\hat{\mathbf{n}}^{(1)}_{n+1}\hat{\mathbf{n}}^{(1)}_{n+1} + b^2_{n+1}\hat{\mathbf{n}}^{(2)}_{n+1}\hat{\mathbf{n}}^{(2)}_{n+1} + c^2_{n+1}\hat{\mathbf{n}}^{(3)}_{n+1}\hat{\mathbf{n}}^{(3)}_{n+1}$$

$$\text{and} \qquad w_1|_{n+1} = \frac{c_{n+1}}{a_{n+1}} \quad , \quad w_2|_{n+1} = \frac{c_{n+1}}{b_{n+1}} \tag{4.72}$$

Equation (4.64) for the stress at the end of the increment is integrated numerically using

forward Euler:

$$\hat{\boldsymbol{\sigma}}_{n+1} = \boldsymbol{\sigma}_n + \boldsymbol{\mathcal{L}}_n^e : \Delta\mathbf{E} - \boldsymbol{\mathcal{L}}_n^e : \Delta\mathbf{E}^p + \Delta\lambda(\boldsymbol{\sigma}_n \cdot \boldsymbol{\Omega}_n^p - \boldsymbol{\Omega}_n^p \cdot \boldsymbol{\sigma}_n) \equiv \boldsymbol{\sigma}^e + \boldsymbol{\sigma}^{pc} + \Delta\lambda\mathbf{R}_1 \quad (4.73)$$

where $\boldsymbol{\sigma}^e = \boldsymbol{\sigma}_n + \boldsymbol{\mathcal{L}}_n^e : \Delta\mathbf{E}$ is the elastic predictor and $\boldsymbol{\sigma}^{pc} = -\boldsymbol{\mathcal{L}}_n^e : \Delta\mathbf{E}^p$ is the so called "plastic corrector", which, in the six-dimensional space of symmetric tensors (e.g. in stress space) can be thought as the "return" to the yield surface in the direction of $\mathbf{N}$. As pointed out in [7], use of backward Euler for the numerical integration of $\Delta\mathbf{E}^p$ ensures that a $\Delta\lambda$ such that the yield condition at t_{n+1} is satisfied always exists thus allowing for larger strain increments $\Delta\mathbf{E}$ compared to the yield strain ([59]). Also, in (4.73) use has been made of the fact that $\hat{\boldsymbol{\sigma}}_n = \boldsymbol{\sigma}_n$, $\hat{\bar{\mathbf{s}}}_n = \bar{\mathbf{s}}_n$ and $\hat{\boldsymbol{\mathcal{L}}}_n^e = \boldsymbol{\mathcal{L}}_n^e$. Finally, the evolution equations (4.65) and (4.66) are also integrated using forward Euler, yielding:

$$\Delta w_\alpha = w_\alpha|_n(\mathbf{n}_n^{(3)}\mathbf{n}_n^{(3)} - \mathbf{n}_n^{(\alpha)}\mathbf{n}_n^{(\alpha)}) : \boldsymbol{\mathcal{A}}_n : \Delta\mathbf{E}^p \equiv \mathbf{R}_{3\alpha} : \Delta\mathbf{E}^p \ , \quad \alpha = 1, 2 \quad (4.74)$$

taking into consideration that $\hat{\mathbf{n}}_n^{(i)} = \mathbf{n}_n^{(i)}$ and $\hat{\boldsymbol{\mathcal{A}}}_n = \boldsymbol{\mathcal{A}}_n$ also hold.

The algorithm that has been developed for the update of stresses, state variables and the "tangent moduli" using (4.67) through (4.74), in case the increment under consideration is an elastoplastic increment, i.e., $\tilde{\Phi}(\boldsymbol{\sigma}^e, \bar{\mathbf{s}}_n) \geq 0$, is presented bellow. To begin with, the quantities $\Delta\lambda$ and $\Delta\mathbf{E}^p$ are now chosen as primary unknowns of the problem which are determined from the system of nonlinear equations involving the yield function at t_{n+1} and (4.68):

$$\begin{cases} \tilde{\Phi}(\Delta\lambda, \Delta\mathbf{E}^p) = 0 \\ \\ \mathbf{G} = \Delta\mathbf{E}^p - \Delta\lambda\mathbf{N}(\Delta\lambda, \Delta\mathbf{E}^p) = \mathbf{0} \end{cases} \quad \text{or} \quad \underset{(n+1)\times 1}{\begin{Bmatrix} \tilde{\Phi}(\Delta\lambda, \Delta E^p) \\ \\ \{G(\Delta\lambda, \Delta E^p)\} \end{Bmatrix}} = \underset{(n+1)\times 1}{\begin{Bmatrix} 0 \\ \\ \{0\} \end{Bmatrix}} \quad (4.75)$$

where $n = 1, 4, 6$ for one-,two- and three-dimensional problems respectively. Since (4.75) are nonlinear, they are solved numerically using the iterative Newton-Raphson method, which is implemented in the following manner. Assuming that at any iteration of the method $\Delta\lambda$ and $\Delta\mathbf{E}^p$ are known from the previous, non-converged, iteration, and that all quantities at the beginning of the increment are known as well, one can calculate $\hat{\boldsymbol{\sigma}}_{n+1}$, $\bar{\varepsilon}_{n+1}^p$, $w_\alpha|_{n+1}$ and $\hat{\mathbf{n}}_{n+1}^{(i)}$ from (4.73) (4.69) and (4.72) respectively and check for convergence. If convergence is not achieved in the current iteration, then, in order to to determine the corrections of $\Delta\lambda$ and $\Delta\mathbf{E}^p$, it is proved that the following linear system has to be solved:

$$\underset{(n+1)\times 1}{\begin{Bmatrix} \Delta(\Delta\lambda) \\ \\ \{\Delta(\Delta E^p)\} \end{Bmatrix}} = -\underset{(n+1)\times(n+1)}{\begin{bmatrix} \frac{\partial\tilde{\Phi}}{\partial(\Delta\lambda)} & \left[\frac{\partial\tilde{\Phi}}{\partial(\Delta E^p)}\right] \\ \\ \left\{\frac{\partial G}{\partial(\Delta\lambda)}\right\} & \left[\frac{\partial G}{\partial(\Delta E^p)}\right] \end{bmatrix}^{-1}} \underset{(n+1)\times 1}{\begin{Bmatrix} \tilde{\Phi}(\Delta\lambda, \Delta E^p) \\ \\ \{G(\Delta\lambda, \Delta E^p)\} \end{Bmatrix}} \Leftrightarrow \quad (4.76)$$

$$\left\{\begin{array}{c} \underset{1\times 1}{\Delta(\Delta\lambda)} \\ \underset{n\times 1}{\left\{\Delta(\Delta E^p)\right\}} \\ \underset{(n+1)\times 1}{} \end{array}\right\} = -\underset{(n+1)\times(n+1)}{\left[\ J\ \right]}^{-1} \left\{\begin{array}{c} \underset{1\times 1}{\tilde{\Phi}(\Delta\lambda,\Delta E^p)} \\ \underset{n\times 1}{\left\{G(\Delta\lambda,\Delta E^p)\right\}} \\ \underset{(n+1)\times 1}{} \end{array}\right\} \tag{4.77}$$

where $\left[\ J\ \right]$ is the Jacobian of the system and $\left[\frac{\partial\tilde{\Phi}}{\partial(\Delta E^p)}\right]$, $\left\{\frac{\partial G}{\partial(\Delta\lambda)}\right\}$, $\left[\frac{\partial G}{\partial(\Delta E^p)}\right]$, $\left\{\Delta(\Delta E^p)\right\}$, $\left\{G(\Delta\lambda, E^p)\right\}$ denote the matrix representations of the corresponding tensorial quantities (for a relevant discussion on tensor to matrix mappings see [54]). Explicit expressions for the quantities $\frac{\partial\tilde{\Phi}}{\partial(\Delta\lambda)}$, $\frac{\partial\tilde{\Phi}}{\partial(\Delta\mathbf{E}^p)}$, $\frac{\partial\mathbf{G}}{\partial(\Delta\lambda)}$ and $\frac{\partial\mathbf{G}}{\partial(\Delta\mathbf{E}^p)}$ that appear in the calculation of the Jacobian in (4.77) can be derived by taking into account the analytical expressions for all involved quantities and by using the chain rule on $\tilde{\Phi}$ and $\mathbf{G}$ as follows:

$$\begin{aligned}\frac{\partial\tilde{\Phi}}{\partial(\Delta\lambda)} &= \frac{\partial\tilde{\Phi}}{\partial\hat{\boldsymbol{\sigma}}_{n+1}} : \frac{\partial\hat{\boldsymbol{\sigma}}_{n+1}}{\partial(\Delta\lambda)} + \frac{\partial\tilde{\Phi}}{\partial\bar{\varepsilon}^p_{n+1}}\underbrace{\frac{\partial\bar{\varepsilon}^p_{n+1}}{\partial(\Delta\lambda)}}_{0} + \frac{\partial\tilde{\Phi}}{\partial w_\alpha|_{n+1}}\underbrace{\frac{\partial w_\alpha|_{n+1}}{\partial(\Delta\lambda)}}_{0} + \frac{\partial\tilde{\Phi}}{\partial\hat{\mathbf{n}}^{(i)}_{n+1}}\cdot\frac{\partial\hat{\mathbf{n}}^{(i)}_{n+1}}{\partial(\Delta\lambda)} = \\ &= \frac{\partial\tilde{\Phi}}{\partial\hat{\boldsymbol{\sigma}}_{n+1}} : \frac{\partial\hat{\boldsymbol{\sigma}}_{n+1}}{\partial(\Delta\lambda)} + \underbrace{\frac{\partial\tilde{\Phi}}{\partial\hat{\mathbf{n}}^{(i)}_{n+1}}}_{\approx\mathbf{0}}\cdot\frac{\partial\hat{\mathbf{n}}^{(i)}_{n+1}}{\partial(\Delta\lambda)} \overset{(4.73)}{\underset{(4.16)}{\Longrightarrow}} \boxed{\frac{\partial\tilde{\Phi}}{\partial(\Delta\lambda)} \approx \mathbf{N}_{n+1} : \mathbf{R}_1}\end{aligned} \tag{4.78}$$

$$\begin{aligned}\frac{\partial\tilde{\Phi}}{\partial(\Delta\mathbf{E}^p)} &= \frac{\partial\tilde{\Phi}}{\partial\hat{\boldsymbol{\sigma}}_{n+1}} : \frac{\partial\hat{\boldsymbol{\sigma}}_{n+1}}{\partial(\Delta\mathbf{E}^p)} + \frac{\partial\tilde{\Phi}}{\partial\bar{\varepsilon}^p_{n+1}}\frac{\partial\bar{\varepsilon}^p_{n+1}}{\partial(\Delta\mathbf{E}^p)} + \frac{\partial\tilde{\Phi}}{\partial w_\alpha|_{n+1}}\frac{\partial w_\alpha|_{n+1}}{\partial(\Delta\mathbf{E}^p)} + \frac{\partial\tilde{\Phi}}{\partial\hat{\mathbf{n}}^{(i)}_{n+1}}\cdot\underbrace{\frac{\partial\hat{\mathbf{n}}^{(i)}_{n+1}}{\partial(\Delta\mathbf{E}^p)}}_{\mathbf{0}} = \\ &= \frac{\partial\tilde{\Phi}}{\partial\hat{\boldsymbol{\sigma}}_{n+1}} : \frac{\partial\hat{\boldsymbol{\sigma}}_{n+1}}{\partial(\Delta\mathbf{E}^p)} + \frac{\partial\tilde{\Phi}}{\partial\bar{\varepsilon}^p_{n+1}}\frac{\partial\bar{\varepsilon}^p_{n+1}}{\partial(\Delta\mathbf{E}^p)} + \frac{\partial\tilde{\Phi}}{\partial w_\alpha|_{n+1}}\frac{\partial w_\alpha|_{n+1}}{\partial(\Delta\mathbf{E}^p)} \overset{(4.73)}{\underset{(4.16)}{\Longrightarrow}} \\ &\Rightarrow \boxed{\frac{\partial\tilde{\Phi}}{\partial(\Delta\mathbf{E}^p)} = -\mathbf{N}_{n+1} : \boldsymbol{\mathcal{L}}^e_n + \frac{\partial\tilde{\Phi}}{\partial\bar{\varepsilon}^p_{n+1}}\frac{\partial\bar{\varepsilon}^p_{n+1}}{\partial(\Delta\mathbf{E}^p)} + \frac{\partial\tilde{\Phi}}{\partial w_\alpha|_{n+1}}\frac{\partial w_\alpha|_{n+1}}{\partial(\Delta\mathbf{E}^p)}}\end{aligned} \tag{4.79}$$

$$\begin{aligned}\frac{\partial\mathbf{G}}{\partial(\Delta\lambda)} &= \frac{\partial(\Delta\mathbf{E}^p)}{\partial(\Delta\lambda)} - \Delta\lambda\left(\frac{\partial\mathbf{N}_{n+1}}{\partial\hat{\boldsymbol{\sigma}}_{n+1}} : \frac{\partial\hat{\boldsymbol{\sigma}}_{n+1}}{\partial(\Delta\lambda)} + \frac{\partial\mathbf{N}_{n+1}}{\partial w_\alpha|_{n+1}}\underbrace{\frac{\partial w_\alpha|_{n+1}}{\partial(\Delta\lambda)}}_{0} + \frac{\partial\mathbf{N}_{n+1}}{\partial\hat{\mathbf{n}}^{(i)}_{n+1}}\cdot\frac{\partial\hat{\mathbf{n}}^{(i)}_{n+1}}{\partial(\Delta\lambda)}\right) = \\ &\overset{(4.68)}{=} -\mathbf{N}_{n+1} - \Delta\lambda\left(\frac{\partial\mathbf{N}_{n+1}}{\partial\hat{\boldsymbol{\sigma}}_{n+1}} : \frac{\partial\hat{\boldsymbol{\sigma}}_{n+1}}{\partial(\Delta\lambda)} + \underbrace{\frac{\partial\mathbf{N}_{n+1}}{\partial\hat{\mathbf{n}}^{(i)}_{n+1}}}_{\approx\mathbf{0}}\cdot\frac{\partial\hat{\mathbf{n}}^{(i)}_{n+1}}{\partial(\Delta\lambda)}\right) \overset{(4.73)}{\Longrightarrow} \\ &\Rightarrow \boxed{\frac{\partial\mathbf{G}}{\partial(\Delta\lambda)} \approx -\mathbf{N}_{n+1} - \Delta\lambda\frac{\partial\mathbf{N}_{n+1}}{\partial\hat{\boldsymbol{\sigma}}_{n+1}} : \mathbf{R}_1}\end{aligned} \tag{4.80}$$

and

$$\frac{\partial \mathbf{G}}{\partial(\Delta\mathbf{E}^p)} = \frac{\partial(\Delta\mathbf{E}^p)}{\partial(\Delta\mathbf{E}^p)} - \Delta\lambda\left(\frac{\partial \mathbf{N}_{n+1}}{\partial\hat{\boldsymbol{\sigma}}_{n+1}} : \frac{\partial\hat{\boldsymbol{\sigma}}_{n+1}}{\partial(\Delta\mathbf{E}^p)} + \frac{\partial \mathbf{N}_{n+1}}{\partial w_\alpha|_{n+1}}\frac{\partial w_\alpha|_{n+1}}{\partial(\Delta\mathbf{E}^p)} + \frac{\partial \mathbf{N}_{n+1}}{\partial\hat{\mathbf{n}}^{(i)}_{n+1}} \cdot \underbrace{\frac{\partial\hat{\mathbf{n}}^{(i)}_{n+1}}{\partial(\Delta\mathbf{E}^p)}}_{\mathbf{0}}\right) =$$

$$\overset{(4.68)}{=} -\boldsymbol{\mathcal{I}} - \Delta\lambda\left(\frac{\partial \mathbf{N}_{n+1}}{\partial\hat{\boldsymbol{\sigma}}_{n+1}} : \frac{\partial\hat{\boldsymbol{\sigma}}_{n+1}}{\partial(\Delta\mathbf{E}^p)} + \frac{\partial \mathbf{N}_{n+1}}{\partial w_\alpha|_{n+1}}\frac{\partial w_\alpha|_{n+1}}{\partial(\Delta\mathbf{E}^p)}\right) \overset{(4.73)}{\Longrightarrow}$$

$$\Rightarrow \boxed{\frac{\partial \mathbf{G}}{\partial(\Delta\mathbf{E}^p)} = -\boldsymbol{\mathcal{I}} - \Delta\lambda\left(-\frac{\partial \mathbf{N}_{n+1}}{\partial\hat{\boldsymbol{\sigma}}_{n+1}} : \boldsymbol{\mathcal{L}}^e_n + \frac{\partial \mathbf{N}_{n+1}}{\partial w_\alpha|_{n+1}}\frac{\partial w_\alpha|_{n+1}}{\partial(\Delta\mathbf{E}^p)}\right)} \tag{4.81}$$

where variations of $\tilde{\Phi}$ and $\mathbf{N}_{n+1}$ with respect to $\hat{\mathbf{n}}^{(i)}_{n+1}$ have been previously found to be small, from a computational point of view, and thus can be neglected (see [20]). Furthermore, since f is now a nodal unknown the corresponding derivatives do not appear in the equations presented above. Using the results for the derivatives of $\tilde{m}$ from the classical variational procedure derived in [7], one can calculate the derivatives necessary in the latter calculations. More precisely, (4.13) and (4.16) lead to:

$$\frac{\partial\tilde{\Phi}}{\partial\bar{\varepsilon}^p_{n+1}} = \frac{\partial}{\partial\bar{\varepsilon}^p_{n+1}}\left(-\sigma_y^2(\bar{\varepsilon}^p_{n+1})\right) \Rightarrow \boxed{\frac{\partial\tilde{\Phi}}{\partial\bar{\varepsilon}^p_{n+1}} = -2\sigma_y(\bar{\varepsilon}^p_{n+1})\frac{d\sigma_y}{d\bar{\varepsilon}^p_{n+1}}} \tag{4.82}$$

$$\boxed{\frac{\partial\tilde{\Phi}}{\partial w_\alpha|_{n+1}} = \frac{1}{1-f}\hat{\boldsymbol{\sigma}}_{n+1} : \frac{\partial\tilde{\boldsymbol{m}}^{\text{mvar}}}{\partial w_\alpha|_{n+1}} : \hat{\boldsymbol{\sigma}}_{n+1}} \tag{4.83}$$

$$\boxed{\frac{\partial \mathbf{N}_{n+1}}{\partial\hat{\boldsymbol{\sigma}}_{n+1}} = \frac{2}{1-f}\tilde{\boldsymbol{m}}^{\text{mvar}} : \hat{\boldsymbol{\sigma}}_{n+1}} \tag{4.84}$$

and

$$\boxed{\frac{\partial \mathbf{N}_{n+1}}{\partial w_\alpha|_{n+1}} = \frac{2}{1-f}\frac{\partial\tilde{\boldsymbol{m}}^{\text{mvar}}}{\partial w_\alpha|_{n+1}} : \hat{\boldsymbol{\sigma}}_{n+1}} \tag{4.85}$$

where

$$\frac{\partial\tilde{\boldsymbol{m}}^{\text{mvar}}}{\partial w_\alpha|_{n+1}} = \frac{\partial\tilde{\boldsymbol{m}}}{\partial w_\alpha|_{n+1}} + (q^2_{\mathcal{J}} - 1)\boldsymbol{\mathcal{J}} : \frac{\partial\tilde{\boldsymbol{m}}}{\partial w_\alpha|_{n+1}} : \boldsymbol{\mathcal{J}} \tag{4.86}$$

$$\text{with} \quad \frac{\partial\tilde{\boldsymbol{m}}}{\partial w_\alpha|_{n+1}} = -\frac{3f}{1-f}\mu\left(\boldsymbol{\mathcal{Q}}^{-1} : \frac{\partial\boldsymbol{\mathcal{Q}}}{\partial w_\alpha|_{n+1}} : \boldsymbol{\mathcal{Q}}^{-1}\right)\Big|_{\nu=\frac{1}{2}} \tag{4.87}$$

and the quantity $\frac{\partial\boldsymbol{\mathcal{Q}}}{\partial w_\alpha|_{n+1}}$ is calculated numerically. Also, from (4.69) and (4.74) one gets:

$$\frac{\partial\bar{\varepsilon}^p_{n+1}}{\partial(\Delta\mathbf{E}^p)} = \frac{\partial}{\partial(\Delta\mathbf{E}^p)}\left(\bar{\varepsilon}^p_n + \Delta\bar{\varepsilon}^p\right) = \frac{\partial(\Delta\bar{\varepsilon}^p)}{\partial(\Delta\mathbf{E}^p)} \Rightarrow \boxed{\frac{\partial\bar{\varepsilon}^p_{n+1}}{\partial(\Delta\mathbf{E}^p)} = \frac{\hat{\boldsymbol{\sigma}}_{n+1}}{(1-f)\sigma_y(\bar{\varepsilon}^p_{n+1})} \equiv \mathbf{R}_2} \tag{4.88}$$

and

$$\frac{\partial w_\alpha|_{n+1}}{\partial(\Delta\mathbf{E}^p)} = \frac{\partial}{\partial(\Delta\mathbf{E}^p)}\Big(w_\alpha|_n + \Delta w_\alpha\Big) = \frac{\partial(\Delta w_\alpha)}{\partial(\Delta\mathbf{E}^p)} \Rightarrow$$

$$\Rightarrow \boxed{\frac{\partial w_\alpha|_{n+1}}{\partial(\Delta\mathbf{E}^p)} = w_\alpha|_n(\mathbf{n}_n^{(3)}\mathbf{n}_n^{(3)} - \mathbf{n}_n^{(\alpha)}\mathbf{n}_n^{(\alpha)}) : \boldsymbol{\mathcal{A}}_n \equiv \mathbf{R}_{3\alpha}} \tag{4.89}$$

Table 4.1: The Newton-Raphson algorithm for the iterative calculation of $\Delta\lambda$ and $\Delta\mathbf{E}^p$

1. Set $k = 0$.

2. Given $(\Delta\lambda)^{(k)}$, $(\Delta\mathbf{E}^p)^{(k)}$ calculate $(\hat{\boldsymbol{\sigma}}_{n+1})^{(k)}$, $(\bar{\varepsilon}^p_{n+1})^{(k)}$, $(f_{\rm loc}|_{n+1})^{(k)}$, $(w_\alpha|_{n+1})^{(k)}$ and $(\hat{\mathbf{n}}^{(i)}_{n+1})^{(k)}$ from (4.69), (4.70), (4.72) and (4.73).

3. Calculate $(\tilde{\Phi}_{n+1})^{(k)}$ and $(\mathbf{G}_{n+1})^{(k)}$ from (4.75).

4. If $(\tilde{\Phi}_{n+1})^{(k)} \leq$ YTOL and $(G_j|_{n+1})^{(k)} \leq$ ETOL, $\forall\, j$, then GOTO **5.** Else GOTO **i.**

- **i.** Calculate $(\frac{\partial\tilde{\Phi}}{\partial(\Delta\lambda)})^{(k)}$, $(\frac{\partial\tilde{\Phi}}{\partial(\Delta\mathbf{E}^p)})^{(k)}$, $(\frac{\partial\mathbf{G}}{\partial(\Delta\lambda)})^{(k)}$ and $(\frac{\partial\mathbf{G}}{\partial(\Delta\mathbf{E}^p)})^{(k)}$ from (4.78)-(4.81).
- **ii.** Solve the linear system (4.77) for the corrections $\Delta(\Delta\lambda)$ and $\Delta(\Delta\mathbf{E}^p)$.
- **iii.** Calculate $(\Delta\lambda)^{(k+1)} = (\Delta\lambda)^{(k)} + \Delta(\Delta\lambda)$ and $(\Delta\mathbf{E}^p)^{(k+1)} = (\Delta\mathbf{E}^p)^{(k)} + \Delta(\Delta\mathbf{E}^p)$.
- **iv.** Set $k \leftarrow k+1$ and GOTO **2.**

5. Solution has converged. Set $\square_{n+1} = (\square_{n+1})^{(k)}$, where $(\square_{n+1})^{(k)}$ is any quantity (scalar, vector or tensor) calculated at the converged iteration k, and exit.

After convergence of (4.77) is achieved, $\bar{\varepsilon}^p_{n+1}$, $f_{\rm loc}|_{n+1}$ and $w_\alpha|_{n+1}$ are known, $\boldsymbol{\sigma}_{n+1}$, $\mathbf{n}^{(i)}_{n+1}$ can be calculated from (4.50):

$$\boxed{\boldsymbol{\sigma}_{n+1} = \mathbf{R}_{n+1}\cdot\hat{\boldsymbol{\sigma}}_{n+1}\cdot\mathbf{R}^T_{n+1}} \quad \text{and} \quad \boxed{\mathbf{n}^{(i)}_{n+1} = \mathbf{R}_{n+1}\cdot\hat{\mathbf{n}}^{(i)}_{n+1}} \tag{4.90}$$

and the "tangent moduli" needed for the finite element calculations can now be evaluated at t_{n+1} using (4.40) and (4.42), where $\frac{\partial\tilde{\Phi}}{\partial f}$ is given as:

$$\boxed{\frac{\partial\tilde{\Phi}}{\partial f} = \frac{1}{(1-f)^2}\boldsymbol{\sigma}_{n+1} : \left[\tilde{\boldsymbol{m}}^{\rm mvar} + (1-f)\frac{\partial\tilde{\boldsymbol{m}}^{\rm mvar}}{\partial f}\right] : \boldsymbol{\sigma}_{n+1}} \tag{4.91}$$

with

$$\frac{\partial\tilde{\boldsymbol{m}}^{\rm mvar}}{\partial f} = \frac{\partial\tilde{\boldsymbol{m}}}{\partial f} + \boldsymbol{\mathcal{J}} : \left[2q_{\mathcal{J}}\frac{\partial q_{\mathcal{J}}}{\partial f} + (q^2_{\mathcal{J}} - 1)\frac{\partial\tilde{\boldsymbol{m}}}{\partial f}\right], \quad \frac{\partial q_{\mathcal{J}}}{\partial f} = \frac{2 - 2f - (1+f)\ln(\frac{1}{f})}{2f^{3/2}\left[\ln(\frac{1}{f})\right]}$$

$$\text{and} \quad \frac{\partial \tilde{\mathfrak{m}}}{\partial f} = \frac{3}{(1-f)^2}\mu \boldsymbol{\mathcal{Q}}^{-1}|_{\nu=\frac{1}{2}} \tag{4.92}$$

The Newton-Raphson algorithm described above is summarized in Table 4.1. Closing this section, it is worth pointing out some important remarks concerning the integration algorithm presented herein.

- In general, at every iteration of the Newton-Raphson method, $\Delta\lambda$ and $\Delta\mathbf{E}^p$ are evaluated using the incremental form of (4.38) and (4.60) respectively, i.e.,

$$\Delta\lambda = \frac{1}{L}\left(\mathbf{N} : \boldsymbol{\mathcal{L}}^e : \Delta\mathbf{E} + \frac{\partial\tilde{\Phi}}{\partial f}\Delta f\right) \quad \text{and} \quad \Delta\mathbf{E}^p = \Delta\lambda\mathbf{N} \tag{4.93}$$

  where Δf is known from the finite element solution. Moreover, integration of a slightly modified version of (4.38) and equation (4.60) using forward Euler, yields first estimates for $\Delta\lambda$ and $\Delta\mathbf{E}^p$:

$$\Delta\lambda = \frac{1}{L_n}(\mathbf{N}_n : \boldsymbol{\mathcal{L}}^e_n : \Delta\mathbf{E}) \quad \text{and} \quad \Delta\mathbf{E}^p = \Delta\lambda\mathbf{N}_n \tag{4.94}$$

- As mentioned earlier, an implicit integration scheme is used herein for the update of $\bar{\varepsilon}^p$ and f_{loc} which implies that equation (4.69) is now non-linear in $\Delta\bar{\varepsilon}^p$. Thus, an iterative Newton-Raphson method is implemented for the respective calculation which is presented in detail in Appendix B.

- As in the original classical anisotropic model presented in [7], the so-called "B-bar" method introduced by Hughes in [39] for nearly-incompressible media, is also used in the computational implementation of the gradient model.

- In the special case of a two-dimensional problem where the motion is taking place in the $x_1 - x_2$ plane, the $\mathbf{n}^{(i)}$'s can be written as:

$$\mathbf{n}^{(1)} = \cos\theta\mathbf{e}_1 + \sin\theta\mathbf{e}_2 \ , \ \mathbf{n}^{(2)} = -\sin\theta\mathbf{e}_1 + \cos\theta\mathbf{e}_2 \ \text{ and } \ \mathbf{n}^{(3)} = \mathbf{n}^{(1)} \times \mathbf{n}^{(2)} \tag{4.95}$$

  where ($\mathbf{e}_1$,$\mathbf{e}_2$) are the unit vectors along x_1- and x_2- axes. In this case, one can substitute the orientation vectors $\mathbf{n}^{(i)}_{n+1}$ at the end of every increment with a corresponding angle θ_{n+1}, which can be calculated from equations (4.95), thus making the computations more efficient. Furthermore, in this case, $\boldsymbol{\Omega}^p$ can also be written in the following simplified form:

$$\boldsymbol{\Omega}^p = \omega^p(-\mathbf{e}_1\mathbf{e}_2 + \mathbf{e}_2\mathbf{e}_1) = \omega^p(-\mathbf{n}^{(1)}\mathbf{n}^{(2)} + \mathbf{n}^{(2)}\mathbf{n}^{(1)}) \tag{4.96a}$$

$$\text{with} \quad \omega^p = -\mathbf{e}_1 \cdot \boldsymbol{\Omega}^p \cdot \mathbf{e}_2 = -\mathbf{n}^{(1)} \cdot \boldsymbol{\Omega}^p \cdot \mathbf{n}^{(2)} \tag{4.96b}$$

Using (4.35), (4.96b) yields:

$$\omega^p = \begin{cases} -\mathbf{e}_1 \cdot (\boldsymbol{\mathcal{C}} : \mathbf{N}) \cdot \mathbf{e}_2 + \dfrac{1}{2}\dfrac{w_1^2 + w_2^2}{w_1^2 - w_2^2}(\mathbf{n}^{(1)}\mathbf{n}^{(2)} + \mathbf{n}^{(2)}\mathbf{n}^{(1)}) : \boldsymbol{\mathcal{A}} : \mathbf{N}\,, & \text{when } w_1 \neq w_2 \\ 0\,, \quad \text{when } w_1 = w_2 \end{cases} \tag{4.97}$$

Chapter 5

Computational Implementation: FEM

The gradient anisotropic model describing the constitutive behavior of the porous metal, which was developed in the previous chapter, can now be combined with the equations of motion derived in Chapter 1 to form the BVP which is solved numerically using the finite element method (FEM), the formulation of which is presented in the following. More precisely, the corresponding equations consisting the general BVP are summarized first and the *weak (or integral)* formulation of the problem is then derived. Furthermore, the finite element approximation is introduced resulting in a system of nonlinear equations which are then solved via the Newton-Raphson method. The latter requires the calculation of a Jacobian matrix, known as the "structural stiffness matrix", which is calculated in a separate section. Finally, the fundamental ideas concerning the *User MATerial (UMAT)* and *User ELement (UEL)* subroutines, which are used for the implementation of the FEM in the general purpose finite element program ABAQUS, are briefly discussed.

5.1 Weak Formulation of the General BVP

Consider a continuum body, which in the reference configuration $\mathfrak{B}_0$ at $t = t_0 = 0$ occupies volume V_0 bounded by a surface ∂V_0 with a mass density ρ_0. Imagine now that this body is subjected to external body forces $\mathbf{b}$ per unit mass, surface (traction) forces $\hat{\mathbf{t}}$ on part ∂V_t of its surface and known displacements $\hat{\mathbf{u}}$ on its remaining surface ∂V_u[1]. Consequently, the body is deformed and at a subsequent time $t > t_0$ it occupies volume V bounded by a surface ∂V with a density ρ. Then, the stress field developed in the body in terms of the true stress can generally be determined by the equations of motion, which are given by (1.83) and are recalled here for convenience:

$$\boldsymbol{\nabla} \cdot \boldsymbol{\sigma} + \rho \mathbf{b} = \rho \mathbf{a} \quad \text{or} \quad \frac{\partial \sigma_{ij}}{\partial x_j} + \rho b_i = \rho a_i \quad \text{with} \quad \mathbf{a} = \ddot{\mathbf{u}} \tag{5.1}$$

Furthermore, one needs to introduce the kinematic (or compatibility) relations

[1] Recall that $\partial V_t \cup \partial V_u = \partial V$ while $\partial V_t \cap \partial V_u = \varnothing$.

$$\mathbf{D} = \frac{1}{2}\left(\boldsymbol{\upsilon}\boldsymbol{\nabla} + \boldsymbol{\nabla}\boldsymbol{\upsilon}\right) \quad \text{or} \quad D_{ij} = \frac{1}{2}\left(\frac{\partial \upsilon_i}{\partial x_j} + \frac{\partial \upsilon_j}{\partial x_i}\right) \tag{5.2}$$

which correlate, in general, the deformation rate tensor $\mathbf{D}$ to the velocity field $\boldsymbol{\upsilon}$ and the constitutive equations, which are of the form:

$$\overset{\nabla}{\boldsymbol{\sigma}} = \overset{\nabla}{\boldsymbol{\sigma}}(\mathbf{D}) \tag{5.3}$$

are in general nonlinear, and describe the total elastoplastic response of the material due the external stimulus. The classical BVP is completed with the addition of prescribed displacement and traction boundary conditions on the corresponding parts of the total boundary:

$$\mathbf{u} = \hat{\mathbf{u}} = \text{known}\,, \quad \text{on } \partial V_u \tag{5.4}$$

$$\mathbf{t} = \boldsymbol{\sigma}\cdot\mathbf{n} = \hat{\mathbf{t}} = \text{known}\,, \quad \text{on } \partial V_t \tag{5.5}$$

In the context of the implicit gradient formulation developed in this thesis, the total BVP is a two-field one in the sense that a second field equation, in the form of a Helmholtz PDE for the nonlocal porosity, is introduced, i.e.,

$$f - \ell^2\nabla^2 f = f_{\text{loc}} \tag{5.6}$$

with the corresponding Neumann boundary conditions on the external boundary ∂V for the unique determination of f being:

$$\boldsymbol{\nabla} f\cdot\mathbf{n} = 0 \quad \text{or} \quad \frac{\partial f}{\partial n} = 0 \quad \text{on } \partial V \tag{5.7}$$

The constitutive behavior is now enhanced in order to include the dependance of the fields $\boldsymbol{\sigma}$ and f_{loc} on the unknown field f and so the constitutive equations (5.3) are now of the form:

$$\overset{\nabla}{\boldsymbol{\sigma}} = \overset{\nabla}{\boldsymbol{\sigma}}(\mathbf{D}, f) \quad \text{and} \quad \dot{f}_{\text{loc}} = \dot{f}_{\text{loc}}(\mathbf{D}, f) \tag{5.8}$$

Thus, the so-called *strong formulation* of the BVP of nonlocal (gradient) elastoplasticity involves the field equations (5.1), (5.6), the kinematic relations (5.2), the constitutive equations (5.8) and the boundary conditions (5.4), (5.5) and (5.7). As pointed out in Section 4.2, constitutive equations (5.8) are nonlinear and thus the latter BVP has to be solved numerically. For this purpose, the BVP has to be written in a variational form[2], a procedure which is carried out in the following. For convenience matters, the problems described above are treated separately and then they are combined to yield the coupled, equivalent variational formulation.

[2]Which, as proved by the theory of Calculus of Variations, is completely equivalent with the strong formulation of the problem since no approximations are introduced so far.

I. Variational Formulation of the Classical (Local) Problem

In this case, the variational formulation of the BVP (5.1)-(5.5) is strictly described by the following statement:
Find $\mathbf{u}(\mathbf{x},t) \in H^2$ *satisfying (5.4) such that for all* $\boldsymbol{\upsilon}^\star, \mathbf{v}^\star \in L^2$ *satisfying the homogeneous B.C.'s* $\boldsymbol{\upsilon}^\star = \mathbf{0}, \mathbf{v}^\star = \mathbf{0}$ *on* ∂V_u*:*

$$W_1(\mathbf{u}, f) = \int\limits_{V(t)} (\boldsymbol{\nabla} \cdot \boldsymbol{\sigma} + \rho\mathbf{b} - \rho\mathbf{a}) \cdot \boldsymbol{\upsilon}^\star dV + \int\limits_{\partial V_t(t)} (\boldsymbol{\sigma} \cdot \mathbf{n} - \hat{\mathbf{t}}) \cdot \mathbf{v}^\star dS = 0 \tag{5.9}$$

where H^k denotes the (Sobolev) space of functions with square-integrable derivatives through order k, L^p denotes the (Lebesgue) space of p-integrable functions and the test functions $\boldsymbol{\upsilon}^\star, \mathbf{v}^\star$ are also known as "virtual velocities". Taking advantage of the chain rule, the Gauss theorem and the symmetry of the Cauchy stress, one can readily prove that

$$\int\limits_{V(t)} (\boldsymbol{\nabla} \cdot \boldsymbol{\sigma}) \cdot \boldsymbol{\upsilon}^\star dV = \int\limits_{\partial V_t(t)} (\boldsymbol{\sigma} \cdot \mathbf{n}) \cdot \boldsymbol{\upsilon}^\star dS - \int\limits_{V(t)} \boldsymbol{\sigma} : \mathbf{D}^\star dV \tag{5.10}$$

Substituting the latter expression into (5.9) and taking into consideration that $\boldsymbol{\upsilon}^\star, \mathbf{v}^\star$ are arbitrary functions satisfying the B.C's described above, one can derive the following general expression of the functional W_1:

$$\boxed{W_1(\mathbf{u}, f) = \int\limits_{V(t)} \rho\mathbf{b} \cdot \boldsymbol{\upsilon}^\star dV + \int\limits_{\partial V_t(t)} \hat{\mathbf{t}} \cdot \boldsymbol{\upsilon}^\star dS - \int\limits_{V(t)} \boldsymbol{\sigma} : \mathbf{D}^\star dV - \int\limits_{V(t)} \rho\ddot{\mathbf{u}} \cdot \boldsymbol{\upsilon}^\star dV = 0} \tag{5.11}$$

where $\boldsymbol{\sigma} = \boldsymbol{\sigma}(\mathbf{u}, f)$ and $\mathbf{D}^\star = (\boldsymbol{\upsilon}^\star \boldsymbol{\nabla} + \boldsymbol{\nabla}\boldsymbol{\upsilon}^\star)/2$.

II. Variational Formulation of Nonlocal Problem

The formulation of the BVP (5.6)-(5.7) can equivalently be described by the following variational statement:
Find $f(\mathbf{x},t) \in H^2$ *satisfying (5.7) such that for all* $f^\star, \gamma^\star \in L^2$ *:*

$$W_2(\mathbf{u}, f) = \int\limits_{V(t)} (f - \ell^2\nabla^2 f - f_{\text{loc}}) f^\star dV + \int\limits_{\partial V(t)} (\boldsymbol{\nabla} f \cdot \mathbf{n}) \gamma^\star dS = 0 \tag{5.12}$$

The latter functional can be simplified as follows. Firstly, using the product rule for the second term one gets:

$$\nabla^2 f f^\star = (\boldsymbol{\nabla} \cdot \boldsymbol{\nabla} f) f^\star = \boldsymbol{\nabla} \cdot (\boldsymbol{\nabla} f f^\star) - \boldsymbol{\nabla} f \cdot \boldsymbol{\nabla} f^\star \tag{5.13}$$

Now, substitution of last expression into (5.12) and use of the Gauss theorem, leads to :

$$
\begin{aligned}
W_2(\mathbf{u},f) &= \int\limits_{V(t)} [(f-f_{\text{loc}})f^\star + \ell^2 \boldsymbol{\nabla} f \cdot \boldsymbol{\nabla} f^\star] dV - \ell^2 \int\limits_{V(t)} \boldsymbol{\nabla} \cdot (\boldsymbol{\nabla} f f^\star) dV + \int\limits_{\partial V(t)} (\boldsymbol{\nabla} f \cdot \mathbf{n}) \gamma^\star dS \\
&= \int\limits_{V(t)} [(f-f_{\text{loc}})f^\star + \ell^2 \boldsymbol{\nabla} f \cdot \boldsymbol{\nabla} f^\star] dV - \ell^2 \int\limits_{\partial V_t(t)} (\boldsymbol{\nabla} f \cdot \mathbf{n}) f^\star dS + \int\limits_{\partial V(t)} (\boldsymbol{\nabla} f \cdot \mathbf{n}) \gamma^\star dS \\
&= \int\limits_{V(t)} [(f-f_{\text{loc}})f^\star + \ell^2 \boldsymbol{\nabla} f \cdot \boldsymbol{\nabla} f^\star] dV + \int\limits_{\partial V(t)} (\boldsymbol{\nabla} f \cdot \mathbf{n}) (\gamma^\star - \ell^2 f^\star) dS = 0
\end{aligned}
$$

Since $\gamma^\star, f^\star$ are arbitrary, choosing $\gamma^\star = \ell^2 f^\star$ and substituting this in the latter expression, one ends up with the following for the functional W_2:

$$
\boxed{W_2(\mathbf{u},f) = \int\limits_{V(t)} [(f-f_{\text{loc}})f^\star + \ell^2 \boldsymbol{\nabla} f \cdot \boldsymbol{\nabla} f^\star] dV = 0} \tag{5.14}
$$

where $f_{\text{loc}} = f_{\text{loc}}(\mathbf{u}, f)$.

Having derived the corresponding equivalent formulation of the local and nonlocal BVP's, one can know combine (5.11) and (5.14) into a single variational statement:
Find $\mathbf{u}(\mathbf{x},t) \in H^2$ *satisfying (5.4) and* $f(\mathbf{x},t) \in H^1$ *satisfying (5.7) such that for all* $\boldsymbol{\upsilon}^\star \in H^1$ *satisfying the homogeneous B.C.* $\boldsymbol{\upsilon}^\star = \mathbf{0}$ *on* ∂V_u *and for all* $f^\star \in H^1$*:*

$$
\boxed{\begin{aligned}
W(\mathbf{u},f) = &- \int\limits_{V(t)} \rho \ddot{\mathbf{u}} \cdot \boldsymbol{\upsilon}^\star dV + \int\limits_{V(t)} \rho \mathbf{b} \cdot \boldsymbol{\upsilon}^\star dV + \int\limits_{\partial V_t(t)} \hat{\mathbf{t}} \cdot \boldsymbol{\upsilon}^\star dS \\
&- \int\limits_{V(t)} [\boldsymbol{\sigma} : \mathbf{D}^\star + (f-f_{\text{loc}})f^\star + \ell^2 \boldsymbol{\nabla} f \cdot \boldsymbol{\nabla} f^\star] dV = 0
\end{aligned}} \tag{5.15}
$$

where $\boldsymbol{\sigma} = \boldsymbol{\sigma}(\mathbf{u}, f)$, $f_{\text{loc}} = f_{\text{loc}}(\mathbf{u}, f)$ and $\mathbf{D}^\star = (\boldsymbol{\upsilon}^\star \boldsymbol{\nabla} + \boldsymbol{\nabla} \boldsymbol{\upsilon}^\star)/2$. The latter statement suggests the so-called *weak formulation* of the mixed BVP, which can now be used to introduce the finite element approximation.

5.2 Finite Element Formulation

In the context of the FEM, the continuous domain of solution V is discretized into finite elements and the primary unknown fields of the problem, i.e., $\mathbf{u}$ and f, are approximated within each element using appropriately selected interpolation functions[3]. The problem is also discretized in time and is solved incrementally and so the solution of the initial BVP is reduced to the solution of an algebraic system of nonlinear equations in each increment. More precisely, in every element at every time instant, one can write the following interpolations:

[3]Which are known as "shape functions". Since these are selected a priori, they are considered known in the following.

$$\underset{M\times 1}{\Big\{u(\mathbf{x})\Big\}} = \underset{M\times n}{\Big[N_u(\mathbf{x})\Big]}\underset{n\times 1}{\Big\{d^e\Big\}} \;,\; \underset{M\times 1}{\Big\{\ddot{u}(\mathbf{x})\Big\}} = \underset{M\times n}{\Big[N_u(\mathbf{x})\Big]}\underset{n\times 1}{\Big\{\ddot{d}^e\Big\}} \;,\; \underset{M\times 1}{\Big\{v^\star(\mathbf{x})\Big\}} = \underset{M\times n}{\Big[N_u(\mathbf{x})\Big]}\underset{n\times 1}{\Big\{d^{e^\star}\Big\}}$$

$$\text{and} \qquad f(\mathbf{x}) = \underset{1\times n}{\lfloor N_f(\mathbf{x})\rfloor}\underset{n\times 1}{\Big\{d^e\Big\}} \;,\; f^\star(\mathbf{x}) = \underset{1\times n}{\lfloor N_f(\mathbf{x})\rfloor}\underset{n\times 1}{\Big\{d^{e^\star}\Big\}} \tag{5.16}$$

so that

$$\underset{N\times 1}{\Big\{D(\mathbf{x})\Big\}} = \underset{N\times n}{\Big[B_u(\mathbf{x})\Big]}\underset{n\times 1}{\Big\{d^e\Big\}} \quad , \quad \underset{N\times 1}{\Big\{D^\star(\mathbf{x})\Big\}} = \underset{N\times n}{\Big[B_u(\mathbf{x})\Big]}\underset{n\times 1}{\Big\{d^{e^\star}\Big\}}$$

$$\text{and} \qquad \underset{M\times 1}{\Big\{\nabla f(\mathbf{x})\Big\}} = \underset{M\times n}{\Big[B_f(\mathbf{x})\Big]}\underset{n\times 1}{\Big\{d^e\Big\}} \quad , \quad \underset{M\times 1}{\Big\{\nabla f^\star(\mathbf{x})\Big\}} = \underset{M\times n}{\Big[B_f(\mathbf{x})\Big]}\underset{n\times 1}{\Big\{d^{e^\star}\Big\}} \tag{5.17}$$

where $M = 1, N = 1$, for one dimensional problems, $M = 2, N = 4$ for two-dimensional, $M = 3, N = 6$ for three-dimensional problems and n is the number of the total nodal unknowns of the element. In the latter expressions, $\Big[N_u(\mathbf{x})\Big]$, $\lfloor N_f(\mathbf{x})\rfloor$ contain the interpolation functions and $\Big[B_u(\mathbf{x})\Big]$, $\Big[B_f(\mathbf{x})\Big]$ are the matrices of the spatial derivatives, with the former being defined by accounting for the symmetric form of $\Big\{D(\mathbf{x})\Big\}$ vector. Furthermore, the vectors $\Big\{d^e\Big\}$, $\Big\{\ddot{d}^e\Big\}$ and $\Big\{d^{e^\star}\Big\}$ contain the nodal unknowns, the accelerations and the virtual nodal unknowns respectively and can be written as:

$$\begin{aligned}
\underset{1\times n}{\lfloor d^e\rfloor} &= \underset{n\times 1}{\Big\{d^e\Big\}}^T = \Big\lfloor\; u_1^1 \;\; \cdots \;\; u_M^1 \;\; f^1 \;\; \cdots\cdots \;\; u_1^n \;\; \cdots \;\; u_M^n \;\; f^n \;\Big\rfloor \\
\underset{1\times n}{\Big\lfloor \ddot{d}^e\Big\rfloor} &= \underset{n\times 1}{\Big\{\ddot{d}^e\Big\}}^T = \Big\lfloor\; \ddot{u}_1^1 \;\; \cdots \;\; \ddot{u}_M^1 \;\; 0 \;\; \cdots\cdots \;\; \ddot{u}_1^n \;\; \cdots \;\; \ddot{u}_M^n \;\; 0 \;\Big\rfloor \\
\underset{1\times n}{\Big\lfloor d^{e^\star}\Big\rfloor} &= \underset{n\times 1}{\Big\{d^{e^\star}\Big\}}^T = \Big\lfloor\; u_1^{1^\star} \;\; \cdots \;\; u_M^{1^\star} \;\; f^{1^\star} \;\; \cdots\cdots \;\; u_1^{n^\star} \;\; \cdots \;\; u_M^{n^\star} \;\; f^{n^\star} \;\Big\rfloor
\end{aligned} \tag{5.18}$$

Introducing now the vector $\lfloor D^\star\rfloor$ of global virtual unknowns, the matrix mappings of the rest of the quantities in the weak formulation (5.15), i.e.,

$$\boldsymbol{\sigma} \rightarrow \underset{N\times 1}{\Big\{\sigma\Big\}} \quad , \quad \hat{\mathbf{t}} \rightarrow \underset{M\times 1}{\Big\{\hat{t}\Big\}} \quad , \quad \mathbf{b} \rightarrow \underset{M\times 1}{\Big\{b\Big\}} \tag{5.19}$$

and substituting (5.16)-(5.19) into (5.15) which is calculated at the end of the current increment, one gets the following expression:

$$W = \lfloor D^\star\rfloor \bigwedge_e \Bigg\{ -\int\limits_{V_{n+1}^e} \Big(\rho\,\Big[N_u\Big]_{n+1}^T\Big[N_u\Big]_{n+1}\,dV\Big)\Big\{\ddot{d}^e\Big\}_{n+1} + \int\limits_{V_{n+1}^e}\Big[N_u\Big]_{n+1}^T\Big\{b\Big\}_{n+1}\,dV + \\ + \int\limits_{\partial V_{n+1}^e}\Big[N_u\Big]_{n+1}^T\Big\{\hat{t}\Big\}_{n+1}dS -$$

$$-\int\limits_{V^e_{n+1}}\left[\left[B_u\right]^T_{n+1}\left\{\sigma\right\}_{n+1}+(f-f_{\text{loc}}|_{n+1})\left\{N_f\right\}_{n+1}+\ell^2\left[B_f\right]_{n+1}\left\{\nabla f\right\}_{n+1}\right]dV\Bigg\}=0 \quad (5.20)$$

where "A_e" denotes the assembly operator. Since the latter expression holds $\forall\,\lfloor D^\star\rfloor$, then

$$\begin{aligned}\mathop{\mathrm{A}}_{e}\Bigg\{&-\int\limits_{V^e_{n+1}}\left(\rho\left[N_u\right]^T_{n+1}\left[N_u\right]_{n+1}dV\right)\left\{\ddot{d}^e\right\}_{n+1}+\int\limits_{V^e_{n+1}}\left[N_u\right]^T_{n+1}\left\{b\right\}_{n+1}dV+\\&+\int\limits_{\partial V^e_{n+1}}\left[N_u\right]^T_{n+1}\left\{\hat{t}\right\}_{n+1}dS-\\&-\int\limits_{V^e_{n+1}}\left[\left[B_u\right]^T_{n+1}\left\{\sigma\right\}_{n+1}+(f-f_{\text{loc}}|_{n+1})\left\{N_f\right\}_{n+1}+\ell^2\left[B_f\right]_{n+1}\left\{\nabla f\right\}_{n+1}\right]dV\Bigg\}=0\end{aligned} \quad (5.21)$$

must hold. Furthermore, defining the mass matrix, external and internal load vectors respectively as:

$$\begin{aligned}\left[M\right]_{n+1}&=\mathop{\mathrm{A}}_{e}\left[m^e\right]_{n+1}\\\left[m^e\right]_{n+1}&=\int\limits_{V^e_{n+1}}\rho\left[N_u\right]^T_{n+1}\left[N_u\right]_{n+1}dV\end{aligned} \quad (5.22)$$

$$\begin{aligned}\left\{F_{\text{ext}}\right\}_{n+1}&=\mathop{\mathrm{A}}_{e}\left\{f^e_{\text{ext}}\right\}_{n+1}\\\left\{f^e_{\text{ext}}\right\}_{n+1}&=\int\limits_{V^e_{n+1}}\left[N_u\right]^T_{n+1}\left\{b\right\}_{n+1}dV+\int\limits_{\partial V^e_{n+1}}\left[N_u\right]^T_{n+1}\left\{\hat{t}\right\}_{n+1}dS\end{aligned} \quad (5.23)$$

$$\begin{aligned}\left\{F_{\text{int}}\right\}_{n+1}&=\mathop{\mathrm{A}}_{e}\left\{f^e_{\text{int}}\right\}_{n+1}\\\left\{f^e_{\text{int}}\right\}_{n+1}&=\int\limits_{V^e_{n+1}}\left[\left[B_u\right]^T_{n+1}\left\{\sigma\right\}_{n+1}+(f-f_{\text{loc}}|_{n+1})\left\{N_f\right\}_{n+1}+\ell^2\left[B_f\right]_{n+1}\left\{\nabla f\right\}_{n+1}\right]dV\end{aligned} \quad (5.24)$$

one can now write (5.21) in the compact form:

$$\boxed{\begin{aligned}\left\{R_{\text{D}}(\left\{D\right\})\right\}_{n+1}&=\mathop{\mathrm{A}}_{e}\left\{r^e_{\text{D}}(\left\{d^e\right\})\right\}_{n+1}=\left\{0\right\}\\\left\{r^e_{\text{D}}(\left\{d^e\right\})\right\}_{n+1}&=-\left[m^e\right]_{n+1}\left\{\ddot{d}^e(\left\{d^e\right\})\right\}_{n+1}+\left\{r^e_{\text{S}}(\left\{d^e\right\})\right\}_{n+1}\\\left\{r^e_{\text{S}}(\left\{d^e\right\})\right\}_{n+1}&=\left\{f^e_{\text{ext}}\right\}_{n+1}-\left\{f^e_{\text{int}}(\left\{d^e\right\})\right\}_{n+1}\end{aligned}} \quad (5.25)$$

In (5.25), $\left\{R_{\mathrm{D}}\right\}$ denotes the dynamic residual of the global problem, while $\left\{r^e_{\mathrm{D}}\right\}$ and $\left\{r^e_{\mathrm{S}}\right\}$ correspond to the dynamic and static residuals respectively in any element e of the finite element mesh. Equation $(5.25)_1$ suggests, due to the nonlinearity of the constitutive equations, a system of nonlinear, algebraic equations for the nodal unknowns $\left\{d^e\right\}$, which is numerically solved in each increment using the Newton-Raphson iterative method. For simplicity reasons and with no loss of generality, for the remainder of this chapter, inertial effects will be neglected[4] (i.e., $\ddot{\mathbf{u}} = \mathbf{0}$ in (5.11) and (5.15)). In this case, (5.25) reduces to the classical static formulation found in [60], i.e.,

$$\boxed{\begin{aligned}\left\{R_{\mathrm{S}}(\left\{D\right\})\right\}_{n+1} &= \mathop{\mathbf{A}}_{e}\left\{r^e_{\mathrm{S}}(\left\{d^e\right\})\right\}_{n+1} = \left\{0\right\}\\ \left\{r^e_{\mathrm{S}}(\left\{d^e\right\})\right\}_{n+1} &= \left\{f^e_{\mathrm{ext}}\right\}_{n+1} - \left\{f^e_{\mathrm{int}}(\left\{d^e\right\})\right\}_{n+1}\end{aligned}} \tag{5.26}$$

If, for any iteration of the Newton method, (5.26) does not converge, it is proved that the following system has to be solved for the corrections $\left\{\Delta D\right\}$ of the global unknown vector:

$$\boxed{\left[K_{\mathrm{S}}\right]_{n+1}\left\{\Delta D\right\} = \left\{R_{\mathrm{S}}\right\}_{n+1}} \tag{5.27}$$

Solution of (5.27) requires the calculation of the so-called Jacobian "stiffness" matrix $\left[K_{\mathrm{S}}\right]$ evaluated at the end of the current increment, which is defined as:

$$\begin{aligned}\left[K_{\mathrm{S}}\right]_{n+1} = -\frac{\partial\left\{R_{\mathrm{S}}\right\}_{n+1}}{\partial\left\{D\right\}_{n+1}} = \frac{\partial\left\{F_{\mathrm{int}}\right\}_{n+1}}{\partial\left\{D\right\}_{n+1}} &= \mathop{\mathbf{A}}_{e}\left[k^e_{\mathrm{S}}\right]_{n+1}\\ \left[k^e_{\mathrm{S}}\right]_{n+1} &= \frac{\partial\left\{f^e_{\mathrm{int}}\right\}_{n+1}}{\partial\left\{d^e\right\}_{n+1}}\end{aligned} \tag{5.28}$$

where $\left\{D\right\}$ is the global unknown vector. Although (5.28) can, at least in principle, be used, along with (5.24), for the determination of the Jacobian of the global system, nonetheless, an alternative approach is usually adopted. More specifically, using (5.26), (5.20) can be written as:

$$W = \lfloor D^\star \rfloor \left\{R_{\mathrm{S}}\right\}_{n+1} = 0 \tag{5.29}$$

Then the differential of W is calculated as:

[4]The formulation of the FEM and the corresponding solution procedure which is implemented for nonlinear dynamic problems is examined in Appendix C

$$dW = \lfloor D^\star \rfloor \frac{\partial \left\{R_{\mathrm{S}}\right\}_{n+1}}{\partial \left\{D\right\}_{n+1}} d\left\{D\right\} = -\lfloor D^\star \rfloor \left[K_{\mathrm{S}}\right]_{n+1} d\left\{D\right\} \equiv -\lfloor D^\star \rfloor \bigwedge_e \left[k_{\mathrm{S}}^e\right]_{n+1} d\left\{D\right\} \tag{5.30}$$

Thus, the Jacobian matrix of the system can be evaluated by comparing an analytic expression for the differential dW with (5.30), a procedure which is carried out in the following section.

5.3 Calculation of the Jacobian Stiffness Matrix

To begin with the derivation of the exact Jacobian in the general case of finite deformations, recalling (5.11) and (5.14), expression (5.15) and its corresponding differential can be written as:

$$W = W_1 - W_2 \;\Rightarrow\; dW = dW_1 - dW_2 \tag{5.31}$$

Equation (5.31) suggests that the differential of the weak formulation of the mixed BVP can be derived by separately calculating the differentials dW_1 and dW_2 of the constituent problems and then combining them together. In both situations, since finite deformations are taken into account, all integrals expressed with respect to the current configuration are transformed into integrals with respect to the reference configuration in order to avoid considering variations of the non-constant integration limits, differentiation of the corresponding functional is carried out and then the finite element discretization is introduced. Also, for the rest of this section, all quantities are assumed to be evaluated at time t_{n+1} unless indicated otherwise.

Calculation of dW_1 :

In view of the aforementioned procedure, using (1.16)[5], the functional W_1 can be rewritten as:

$$W_1 = \int_{V_0} \rho_0 \mathbf{b} \cdot \boldsymbol{\upsilon}^\star dV_0 + \int_{\partial V_{t0}} \hat{\mathbf{t}}_0 \cdot \boldsymbol{\upsilon}^\star dS_0 - \int_{V_0} \mathrm{tr}\left(\boldsymbol{\sigma} \cdot \frac{\partial \boldsymbol{\upsilon}^\star}{\partial \mathbf{x}} \cdot \frac{\partial \mathbf{x}}{\partial \mathbf{X}}\right) J dV_0 \tag{5.32}$$

where ρ_0 is the initial mass density of the material at time $t = 0$. Assuming that applied external forces are independent of the body's motion, it can be proved (see Papatriantafillou [60]) that the differential dW_1 of (5.32) is given as[6]

$$dW_1 = -\int_V \mathrm{tr}[\mathbf{L}^\star \cdot (-d\mathbf{L} \cdot \boldsymbol{\sigma} + d\boldsymbol{\sigma} + \boldsymbol{\sigma} dL_{kk})] dV = -\int_V \mathbf{L}^\star : (d\boldsymbol{\sigma} - \boldsymbol{\sigma} \cdot d\mathbf{L}^T + \boldsymbol{\sigma} dL_{kk}) dV \tag{5.33}$$

In order to proceed with the evaluation of dW_1 from (5.33), one needs to derive an explicit

[5] And due to the fact that the force vector $d\mathbf{Q}$ on an infinitesimal area in the current configuration can be expressed as $d\mathbf{Q} = \hat{\mathbf{t}} dS = \hat{\mathbf{t}}_0 dS_0$ where $\hat{\mathbf{t}}_0$ is the nominal traction vector at time $t = 0$.

[6] Recall here that, for any second order tensors $\mathbf{A}$, $\mathbf{B}$, the property $\mathrm{tr}(\mathbf{A} \cdot \mathbf{B}) = \mathbf{A} : \mathbf{B}^T$ holds.

expression for the differential of stress $d\boldsymbol{\sigma}$. In principle, this is not a trivial calculation since the latter variation depends both on the underlying constitutive model and on the numerical integration scheme used for the integration of the corresponding constitutive equations. However, an approximate expression for $d\boldsymbol{\sigma}$, for the case of the gradient anisotropic model developed in the previous chapter, can be derived as follows.

To begin with, defining the variation $d\mathbf{L} = (d\mathbf{u})\boldsymbol{\nabla} = \partial(d\mathbf{u})/\partial\mathbf{x}$ and adopting once again the assumption that the Lagrangian triad associated with $\Delta\mathbf{F}$ defined by (4.46) is fixed over the time increment under consideration, it can be proved that:

$$d\mathbf{D} = \frac{1}{2}(d\mathbf{L} + d\mathbf{L}^T) = \mathbf{R}\cdot d\mathbf{E}\cdot\mathbf{R}^T \ , \ d\mathbf{W} = \frac{1}{2}(d\mathbf{L} - d\mathbf{L}^T) = d\mathbf{R}\cdot\mathbf{R}^T = -\mathbf{R}\cdot d\mathbf{R}^T \quad (5.34)$$

so that, starting from the relation of $\boldsymbol{\sigma}$ in terms of $\hat{\boldsymbol{\sigma}}$, one has the following:

$$\boldsymbol{\sigma} = \mathbf{R}\cdot\hat{\boldsymbol{\sigma}}\cdot\mathbf{R}^T \ \Rightarrow \ d\boldsymbol{\sigma} = d\mathbf{R}\cdot\hat{\boldsymbol{\sigma}}\cdot\mathbf{R}^T + \mathbf{R}\cdot d\hat{\boldsymbol{\sigma}}\cdot\mathbf{R}^T + \mathbf{R}\cdot\hat{\boldsymbol{\sigma}}\cdot d\mathbf{R}^T \overset{(4.50)_1}{\Longrightarrow}$$

$$\Rightarrow d\boldsymbol{\sigma} = \underbrace{\mathbf{R}\cdot\mathbf{R}^T}_{d\mathbf{W}}\cdot\boldsymbol{\sigma} + \mathbf{R}\cdot d\hat{\boldsymbol{\sigma}}\cdot\mathbf{R}^T + \boldsymbol{\sigma}\cdot\underbrace{\mathbf{R}\cdot d\mathbf{R}^T}_{-d\mathbf{W}} = d\mathbf{W}\cdot\boldsymbol{\sigma} + \mathbf{R}\cdot d\hat{\boldsymbol{\sigma}}\cdot\mathbf{R}^T - \boldsymbol{\sigma}\cdot d\mathbf{W} \Rightarrow$$

$$\Rightarrow d\boldsymbol{\sigma} = d^J\boldsymbol{\sigma} - \frac{1}{2}\boldsymbol{\sigma}\cdot(d\mathbf{L} - d\mathbf{L}^T) + \frac{1}{2}(d\mathbf{L} - d\mathbf{L}^T)\cdot\boldsymbol{\sigma} \quad (5.35)$$

where $d^J\boldsymbol{\sigma} \equiv \mathbf{R}\cdot d\hat{\boldsymbol{\sigma}}\cdot\mathbf{R}^T = d\boldsymbol{\sigma} + \boldsymbol{\sigma}\cdot d\mathbf{W} - d\mathbf{W}\cdot\boldsymbol{\sigma}$ denotes the differential associated with the Jaumann derivative of $\boldsymbol{\sigma}$. Using the chain rule, $d^J\boldsymbol{\sigma}$ can be evaluated as:

$$d^J\boldsymbol{\sigma} \equiv \mathbf{R}\cdot d\hat{\boldsymbol{\sigma}}\cdot\mathbf{R}^T = \mathbf{R}\cdot\left(\frac{\partial\hat{\boldsymbol{\sigma}}}{\partial\mathbf{E}} : d\mathbf{E} + \frac{\partial\hat{\boldsymbol{\sigma}}}{\partial f}df\right)\cdot\mathbf{R}^T \overset{(5.34)}{=}$$

$$= \mathbf{R}\cdot\left[\frac{\partial\hat{\boldsymbol{\sigma}}}{\partial\mathbf{E}} : (\mathbf{R}^T\cdot d\mathbf{D}\cdot\mathbf{R}) + \frac{\partial\hat{\boldsymbol{\sigma}}}{\partial f}df\right]\cdot\mathbf{R}^T =$$

$$= \mathbf{R}\cdot\left[\frac{\partial\hat{\boldsymbol{\sigma}}}{\partial\mathbf{E}} : (\mathbf{R}^T\cdot d\mathbf{D}\cdot\mathbf{R})\right]\cdot\mathbf{R}^T + \left(\mathbf{R}\cdot\frac{\partial\hat{\boldsymbol{\sigma}}}{\partial f}\cdot\mathbf{R}^T\right)df \Rightarrow$$

$$\Rightarrow d^J\boldsymbol{\sigma} = \frac{\partial\boldsymbol{\sigma}}{\partial\mathbf{E}} : d\mathbf{D} + \frac{\partial\boldsymbol{\sigma}}{\partial f}df \equiv \frac{\partial\boldsymbol{\sigma}}{\partial\mathbf{E}} : d\mathbf{L} + \frac{\partial\boldsymbol{\sigma}}{\partial f}df \quad (5.36)$$

where

$$\frac{\partial\sigma_{ij}}{\partial E_{kl}} = R_{im}R_{jn}R_{kp}R_{lq}\frac{\partial\hat{\sigma}_{mn}}{\partial E_{pq}} \quad \text{and} \quad \frac{\partial\sigma_{ij}}{\partial f} = R_{im}R_{jn}\frac{\partial\hat{\sigma_{mn}}}{\partial f} \quad (5.37)$$

Plugging (5.36) into (5.35), one gets the following explicit expression for $d\boldsymbol{\sigma}$:

$$d\boldsymbol{\sigma} = \frac{\partial\boldsymbol{\sigma}}{\partial\mathbf{E}} : d\mathbf{L} + \frac{\partial\boldsymbol{\sigma}}{\partial f}df - \frac{1}{2}\boldsymbol{\sigma}\cdot(d\mathbf{L} - d\mathbf{L}^T) + \frac{1}{2}(d\mathbf{L} - d\mathbf{L}^T)\cdot\boldsymbol{\sigma} \quad (5.38)$$

Now, substitution of the latter into (5.33), yields the desired expression for dW_1, i.e.,

$$dW_1 = -\int_V \mathbf{L}^\star : \left[\left(\frac{\partial \boldsymbol{\sigma}}{\partial \mathbf{E}} + \boldsymbol{\Sigma} + \boldsymbol{\sigma}\boldsymbol{\delta}\right) : d\mathbf{L} + \frac{\partial \boldsymbol{\sigma}}{\partial f} df\right] dV \tag{5.39}$$

where the components of the forth order tensor $\boldsymbol{\Sigma}$ are given as[7]:

$$\Sigma_{ijkl} = \Sigma_{klij} = \frac{1}{2}(\delta_{ik}\sigma_{jl} - \delta_{il}\sigma_{jk} - \sigma_{ik}\delta_{jl} - \sigma_{il}\delta_{jk}) \tag{5.40}$$

Next, consider the introduction of the following finite element approximation:

$$\underset{\bar{N}\times 1}{\Big\{dL(\mathbf{x})\Big\}} = \underset{\bar{N}\times n}{\Big[B_L(\mathbf{x})\Big]}\underset{n\times 1}{\Big\{d^e\Big\}} \quad \text{and} \quad \underset{\bar{N}\times 1}{\Big\{L^\star(\mathbf{x})\Big\}} = \underset{\bar{N}\times n}{\Big[B_L(\mathbf{x})\Big]}\underset{n\times 1}{\Big\{d^{e\star}\Big\}} \tag{5.41}$$

where $\bar{N} = 1, 5, 9$ for one-, two- and three-dimensional problems respectively and $\Big[B_L(\mathbf{x})\Big]$ is different from $\Big[B_u(\mathbf{x})\Big]$ in the sense that it is defined by taking into account that the matrix representation of $d\mathbf{L}$ contains all components of the corresponding tensor. Furthermore, using (5.16) for the interpolation of f and introducing the matrix forms of $\frac{\partial \boldsymbol{\sigma}}{\partial \mathbf{E}}$, $\frac{\partial \boldsymbol{\sigma}}{\partial f}$ and $\boldsymbol{\Sigma}$ as:

$$\frac{\partial \boldsymbol{\sigma}}{\partial \mathbf{E}} \rightarrow \underset{\bar{N}\times\bar{N}}{\left[\frac{\partial \sigma}{\partial E}\right]} \quad , \quad \frac{\partial \boldsymbol{\sigma}}{\partial f} \rightarrow \underset{\bar{N}\times 1}{\left[\frac{\partial \sigma}{\partial f}\right]} \quad , \quad \boldsymbol{\Sigma} \rightarrow \underset{\bar{N}\times\bar{N}}{\Big[\Sigma\Big]} \tag{5.42}$$

equation (5.39) can finally be written as

$$dW_1 = -\lfloor D^\star \rfloor \underset{e}{\mathbf{A}} \left\{ \int_{V^e} \left[\Big[B_L\Big]^T \left(\left[\frac{\partial \sigma}{\partial E}\right] + \Big[\Sigma\Big] + \Big\{\sigma\Big\}\lfloor\delta\rfloor \right) \Big[B_L\Big] + \Big[B_L\Big]^T \left\{\frac{\partial \sigma}{\partial f}\right\} \lfloor N_f \rfloor \right] dV \right\} d\Big\{D\Big\} \tag{5.43}$$

It should be noted here that, if the symmetries of the corresponding tensors are taken into account, one can substitute $\Big[B_L\Big]$ with $\Big[B_u\Big]$ and $\bar{N}$ with N in expressions (5.42) and (5.43).

Calculation of dW_2 :

In order to proceed with the calculation of dW_2, it is convenient to restate (5.14) in the following manner:

$$W_2 = \int_V \left[(f - f_{\text{loc}}) f^\star + \ell^2 \frac{\partial f}{\partial \mathbf{x}} \cdot \frac{\partial f^\star}{\partial \mathbf{x}} \right] dV \tag{5.44}$$

Yet again, the latter integral needs to be "pushed-back" from the current to the reference configuration which can be achieved by utilizing (1.16) and by noting that

$$\frac{\partial f}{\partial \mathbf{x}} = \frac{\partial f}{\partial \mathbf{X}} \cdot \frac{\partial \mathbf{X}}{\partial \mathbf{x}} = \frac{\partial f}{\partial \mathbf{X}} \cdot \mathbf{F}^{-1} = \mathbf{F}^{-T} \cdot \frac{\partial f}{\partial \mathbf{X}}$$

[7] For explicit expressions concerning this tensor see Appendix D of [60].

$$\frac{\partial f^\star}{\partial \mathbf{x}} = \frac{\partial f^\star}{\partial \mathbf{X}} \cdot \frac{\partial \mathbf{X}}{\partial \mathbf{x}} = \frac{\partial f^\star}{\partial \mathbf{X}} \cdot \mathbf{F}^{-1} = \mathbf{F}^{-T} \cdot \frac{\partial f^\star}{\partial \mathbf{X}} \tag{5.45}$$

Consequently, (5.44) can be rewritten as:

$$W_2 = \int_{V_0} \left[(f - f_{\text{loc}}) f^\star + \ell^2 \frac{\partial f}{\partial \mathbf{X}} \cdot \mathbf{F}^{-1} \cdot \mathbf{F}^{-T} \cdot \frac{\partial f^\star}{\partial \mathbf{X}} \right] J dV_0 \tag{5.46}$$

The functional W_1 is now in appropriate form, so differentiation of (5.46) yields:

$$\begin{aligned} dW_2 = \int_{V_0} \Bigg\{ & (df - df_{\text{loc}}) f^\star + \\ & + \ell^2 \left[\frac{\partial df}{\partial \mathbf{X}} \cdot \mathbf{F}^{-1} \cdot \mathbf{F}^{-T} + \frac{\partial f}{\partial \mathbf{X}} \cdot d(\mathbf{F}^{-1}) \cdot \mathbf{F}^{-T} + \frac{\partial f}{\partial \mathbf{X}} \cdot \mathbf{F}^{-1} \cdot d(\mathbf{F}^{-T}) \right] \cdot \frac{\partial f^\star}{\partial \mathbf{X}} \Bigg\} J dV_0 + \\ & + \int_{V_0} \left[(f - f_{\text{loc}}) f^\star + \ell^2 \frac{\partial f}{\partial \mathbf{X}} \cdot \mathbf{F}^{-1} \cdot \mathbf{F}^{-T} \cdot \frac{\partial f^\star}{\partial \mathbf{X}} \right] dJ dV_0 \end{aligned} \tag{5.47}$$

Moreover, it can be readily proved that (see [60]) the following relations hold:

$$d\mathbf{L} = \frac{\partial (d\mathbf{u})}{\partial \mathbf{x}} \quad , \quad d(\mathbf{F}^{-1}) = -\mathbf{F}^{-1} \cdot d\mathbf{L} \quad \text{and} \quad d(\mathbf{F}^{-T}) = -d\mathbf{L}^T \cdot \mathbf{F}^{-T} \tag{5.48}$$

Thus, substituting the corresponding quantities from (5.48) into (5.47), and taking into account the fact that $dJ = J dD_{kk}$, one now gets:

$$\begin{aligned} dW_2 = & \int_{V_0} (df - df_{\text{loc}}) f^\star J dV_0 + \\ & + \int_{V_0} \ell^2 \left[\frac{\partial df}{\partial \mathbf{X}} \cdot \mathbf{F}^{-1} \cdot \mathbf{F}^{-T} - \frac{\partial f}{\partial \mathbf{X}} \cdot \mathbf{F}^{-1} \cdot d\mathbf{L} \cdot \mathbf{F}^{-T} - \frac{\partial f}{\partial \mathbf{X}} \cdot \mathbf{F}^{-1} \cdot d\mathbf{L}^T \cdot \mathbf{F}^{-T} \right] \cdot \frac{\partial f^\star}{\partial \mathbf{X}} J dV_0 + \\ & + \int_{V_0} \left[(f - f_{\text{loc}}) f^\star + \ell^2 \frac{\partial f}{\partial \mathbf{X}} \cdot \mathbf{F}^{-1} \cdot \mathbf{F}^{-T} \cdot \frac{\partial f^\star}{\partial \mathbf{X}} \right] dD_{kk} J dV_0 \quad \Rightarrow \end{aligned}$$

$$\begin{aligned} dW_2 = & \int_{V_0} (df - df_{\text{loc}}) f^\star J dV_0 + \\ & + \int_{V_0} \ell^2 \left[\frac{\partial df}{\partial \mathbf{X}} \cdot \mathbf{F}^{-1} - \frac{\partial f}{\partial \mathbf{X}} \cdot \mathbf{F}^{-1} \cdot (d\mathbf{L} + d\mathbf{L}^T) \right] \cdot \mathbf{F}^{-T} \cdot \frac{\partial f^\star}{\partial \mathbf{X}} J dV_0 + \\ & + \int_{V_0} \left[(f - f_{\text{loc}}) f^\star + \ell^2 \frac{\partial f}{\partial \mathbf{X}} \cdot \mathbf{F}^{-1} \cdot \mathbf{F}^{-T} \cdot \frac{\partial f^\star}{\partial \mathbf{X}} \right] dD_{kk} J dV_0 \end{aligned} \tag{5.49}$$

The latter expression can be "pushed-forward" from the reference to the current configuration by making use of $(5.34)_1$ and expressions (5.45), i.e.,

$$dW_2 = \int_V (df - df_{\text{loc}}) f^\star dV + \int_V \ell^2 \left(\frac{\partial df}{\partial \mathbf{x}} - 2 \frac{\partial f}{\partial \mathbf{x}} \cdot d\mathbf{D} \right) \cdot \frac{\partial f^\star}{\partial \mathbf{x}} dV +$$
$$+ \int_V \left[(f - f_{\text{loc}}) f^\star + \ell^2 \frac{\partial f}{\partial \mathbf{x}} \cdot \frac{\partial f^\star}{\partial \mathbf{x}} \right] dD_{kk} dV \quad \Rightarrow$$

$$dW_2 = dW_2^{ss} - 2\ell^2 \int_V \boldsymbol{\nabla} f \cdot d\mathbf{D} \cdot \boldsymbol{\nabla} f^\star dV + \int_V \left[(f - f_{\text{loc}}) f^\star + \ell^2 \boldsymbol{\nabla} f \cdot \boldsymbol{\nabla} f^\star \right] dD_{kk} dV \tag{5.50}$$

$$\text{with} \quad dW_2^{ss} = \int_V \left[(df - df_{\text{loc}}) f^\star + \ell^2 \boldsymbol{\nabla}(df) \cdot \boldsymbol{\nabla} f^\star \right] dV \tag{5.51}$$

where dW_2^{ss} corresponds to the differential of dW_2 if small strains are assumed. In order to further proceed with the evaluation of dW_2, one needs to derive an explicit expression for df_{loc}. Implementation of the chain rule on $f_{\text{loc}} = f_{\text{loc}}(\mathbf{u}, f)$ yields:

$$df_{\text{loc}} = \frac{\partial f_{\text{loc}}}{\partial \mathbf{E}} : d\mathbf{E} + \frac{\partial f_{\text{loc}}}{\partial f} df = \frac{\partial f_{\text{loc}}}{\partial \mathbf{E}} : d\mathbf{D} + \frac{\partial f_{\text{loc}}}{\partial f} df \tag{5.52}$$

In (5.52), substitution of $d\mathbf{E}$ with $d\mathbf{D}$ is possible since "small strains" are assumed in the calculation of (5.51). Plugging (5.52) into the expression for dW_{ss} one gets:

$$dW_2^{ss} = \int_V \left[\left(df - \frac{\partial f_{\text{loc}}}{\partial \mathbf{E}} : d\mathbf{D} - \frac{\partial f_{\text{loc}}}{\partial f} df \right) f^\star + \ell^2 \boldsymbol{\nabla}(df) \cdot \boldsymbol{\nabla} f^\star \right] dV \tag{5.53}$$

This equation along with (5.50) now yield the desired relation for dW_2. Furthermore, consider the following tensor to matrix mappings:

$$\boldsymbol{\nabla} f \cdot d\mathbf{D} \cdot \boldsymbol{\nabla} f^\star = \boldsymbol{\nabla} f^\star \cdot d\mathbf{D} \cdot \boldsymbol{\nabla} f \;\rightarrow\; \underset{1\times M}{\lfloor \nabla f^\star \rfloor} \{ \underset{M\times 1}{dD \cdot \nabla f} \}$$

$$\text{with} \quad \{ \underset{M\times 1}{dD \cdot \nabla f} \} = \Big[\underset{M\times N}{A_{\nabla f}} \Big] \{ \underset{N\times 1}{dD} \} \tag{5.54}$$

$$\boldsymbol{\nabla} f \cdot \boldsymbol{\nabla} f^\star = \boldsymbol{\nabla} f^\star \cdot \boldsymbol{\nabla} f \;\rightarrow\; \underset{1\times M}{\lfloor \nabla f^\star \rfloor} \Big\{ \underset{M\times 1}{\nabla f} \Big\} \tag{5.55}$$

and additionally note that dD_{kk} can be written as:

$$dD_{kk} = dD_{11} + dD_{22} + dD_{33} = \underset{1\times N}{\lfloor \delta \rfloor} \{ \underset{N\times 1}{dD} \} \tag{5.56}$$

Finally, using the finite element interpolations for the quantities $\boldsymbol{\nabla} f$, $\boldsymbol{\nabla} f^\star$ given by (5.16),

utilizing (5.17) to derive interpolations for $d\mathbf{D}$ and $\boldsymbol{\nabla}(df)$ and introducing the vector form of $\frac{\partial f_{\text{loc}}}{\partial \mathbf{E}}$ as:

$$\frac{\partial f_{\text{loc}}}{\partial \mathbf{E}} \rightarrow \underset{N\times N}{\left[\frac{\partial f_{\text{loc}}}{\partial E}\right]} \tag{5.57}$$

one can write (5.50) in the following discretized form:

$$\begin{aligned} dW_2 = \lfloor D^{\star} \rfloor \underset{e}{\mathbf{A}} \Bigg\{ \int_{V^e} \Bigg[\left(1 - \frac{\partial f_{\text{loc}}}{\partial f}\right) \Big\{N_f\Big\} \lfloor N_f \rfloor - \Big\{N_f\Big\} \left[\frac{\partial f_{\text{loc}}}{\partial E}\right] \Big[B_u\Big] + \ell^2 \Big[B_f\Big]^T \Big[B_f\Big] \Bigg] dV \\ - 2\ell^2 \int_{V^e} \Big[B_f\Big]^T \Big[A_{\nabla f}\Big] \Big[B_u\Big] \, dV + \int_{V^e} \Big[(f - f_{\text{loc}}) \Big\{N_f\Big\} + \ell^2 \Big[B_f\Big]^T \Big\{\nabla f\Big\} \Big] \lfloor B_{\nu} \rfloor \, dV \Bigg\} d\Big\{D\Big\} \end{aligned} \tag{5.58}$$

Having derived explicit expressions for the differentials dW_1 and dW_2, one can now substitute the corresponding relations into (5.31), which subsequently leads to the following:

$$\begin{aligned} dW = -\lfloor D^{\star} \rfloor \underset{e}{\mathbf{A}} \Bigg\{ \int_{V^e} \Bigg[\Big[B_L\Big]^T \Bigg(\left[\frac{\partial \sigma}{\partial E}\right] + \Big[\Sigma\Big] + \Big\{\sigma\Big\} \lfloor \delta \rfloor \Bigg) \Big[B_L\Big] + \\ + \Big[B_L\Big]^T \left\{\frac{\partial \sigma}{\partial f}\right\} \lfloor N_f \rfloor \Bigg] dV + \\ + \int_{V^e} \Bigg[\left(1 - \frac{\partial f_{\text{loc}}}{\partial f}\right) \Big\{N_f\Big\} \lfloor N_f \rfloor - \Big\{N_f\Big\} \left[\frac{\partial f_{\text{loc}}}{\partial E}\right] \Big[B_u\Big] + \ell^2 \Big[B_f\Big]^T \Big[B_f\Big] \Bigg] dV - \\ - 2\ell^2 \int_{V^e} \Big[B_f\Big]^T \Big[A_{\nabla f}\Big] \Big[B_u\Big] \, dV + \int_{V^e} \Big[(f - f_{\text{loc}}) \Big\{N_f\Big\} + \ell^2 \Big[B_f\Big]^T \Big\{\nabla f\Big\} \Big] \lfloor B_{\nu} \rfloor \, dV \Bigg\} d\Big\{D\Big\} \end{aligned} \tag{5.59}$$

Equation (5.59) is of the same form as (5.30). Thus, comparing the two expressions, one can ultimately derive the local (static) Jacobian, which can be written as:

$$\boxed{\underset{n\times n}{\Big[k_{\text{S}}^{e}\Big]} = \underset{n\times n}{\Big[k_{\text{S}}^{e(ss)}\Big]} + \underset{n\times n}{\Big[k_{\text{S}}^{e(ls)}\Big]}} \tag{5.60}$$

where

$$\boxed{\begin{aligned} \underset{n\times n}{\Big[k_{\text{S}}^{e(ss)}\Big]} = \int_{V^e} \Bigg\{ \underset{n\times \bar{N}}{\Big[B_L\Big]^T} \underset{\bar{N}\times \bar{N}}{\left[\frac{\partial \sigma}{\partial E}\right]} \underset{\bar{N}\times n}{\Big[B_L\Big]} + \underset{n\times \bar{N}}{\Big[B_L\Big]^T} \underset{\bar{N}\times 1}{\left[\frac{\partial \sigma}{\partial f}\right]} \underset{1\times n}{\lfloor N_f \rfloor} - \underset{n\times 1}{\Big\{N_f\Big\}} \underset{N\times N}{\left[\frac{\partial f_{\text{loc}}}{\partial E}\right]} \underset{N\times n}{\Big[B_u\Big]} + \\ + \left(1 - \frac{\partial f_{\text{loc}}}{\partial f}\right) \underset{n\times 1}{\Big\{N_f\Big\}} \underset{1\times n}{\lfloor N_f \rfloor} + \ell^2 \underset{n\times M}{\Big[B_f\Big]^T} \underset{M\times n}{\Big[B_f\Big]} \Bigg\} dV \end{aligned}} \tag{5.61}$$

and

$$\boxed{\begin{aligned}\underset{n\times n}{\left[k_{\mathrm{S}}^{e(ls)}\right]} = \int_{V^e} \Bigg\{ \underset{n\times\bar{N}}{\left[B_L\right]}^T \Bigg(\underset{\bar{N}\times\bar{N}}{\left[\Sigma\right]} + \underset{\bar{N}\times 1}{\left\{\sigma\right\}} \underset{1\times\bar{N}}{\lfloor\delta\rfloor} \Bigg) \underset{\bar{N}\times n}{\left[B_L\right]} - 2\ell^2 \underset{n\times M}{\left[B_f\right]}^T \underset{M\times N}{\left[A_{\nabla f}\right]} \underset{N\times n}{\left[B_u\right]} + \\ + \left[(f - f_{\mathrm{loc}}) \underset{n\times 1}{\left\{N_f\right\}} + \ell^2 \underset{n\times M}{\left[B_f\right]}^T \underset{M\times 1}{\left\{\nabla f\right\}} \right] \underset{1\times n}{\lfloor B_\nu \rfloor} \Bigg\} dV\end{aligned}} \tag{5.62}$$

In (5.60)-(5.62), $\left[k_{\mathrm{S}}^{e(ss)}\right]$ denotes the corresponding local Jacobian if "small strain" hypothesis is adopted and $\left[k_{\mathrm{S}}^{e(ls)}\right]$ is the finite strain correction matrix which emerges when no restriction is placed on the magnitude of strains. With $\left[k_{\mathrm{S}}^{e}\right]$ known for all elements at the end of every increment, the global Jacobian matrix $\left[K_{\mathrm{S}}\right]$ can be evaluated in each iteration of Newton's method as:

$$\boxed{\left[K_{\mathrm{S}}\right] = \mathop{\mathbf{A}}_{e} \left[k_{\mathrm{S}}^{e}\right]} \tag{5.63}$$

Closing this section, it is useful to have in mind the following remarks:

- Expressions (5.60)-(5.62) are approximate mainly for two reasons; firstly, because of the finite element approximation which has been introduced in the weak formulation, and secondly because the tangent moduli are used instead of the linearization moduli in the evaluation of $d\boldsymbol{\sigma}$ and df_{loc}. Even though the latter take into account both the constitutive model and the corresponding integration scheme they add, nonetheless, more complexity to the computational implementation without improving the accuracy of the calculations, as explained bellow.

- As pointed out in [7], [60], the Jacobian stiffness matrix is only involved in the solution of the system (5.27) for the corrections on the global unknowns of the problem, which is solved only if (5.26) does not converge in the current iteration of the method. This in fact implies that, the accuracy of the solution depends on the accuracy of the numerical calculations which are related to the evaluation of the residual of the problem. On the other hand, any approximations on the Jacobian matrix only affect the quadratic rate of convergence of the Newton loop. For example, approximation of the moduli involved in the calculation of $\left[k_{\mathrm{S}}^{e}\right]$ with the tangent moduli of the total elastoplastic equations introduced in section 4.2 suggests a first order approximation to the linearization moduli as the time increment $\Delta t \to 0$, which nevertheless suffices an acceptable rate of convergence ([7]). In this context, one could also approximate the Jacobian given by (5.60) with the "small strain" one, thus simplifying the computational implementation.

- Evaluation of (5.60)-(5.62) require the calculation of the vector $\lfloor B_\nu \rfloor$ and the matrix $\left[A_{\nabla f}\right]$. The former can be derived from (5.56) by substituting the interpolation for $\{dD\}$, and is defined as:

$$\underset{1\times n}{\lfloor B_\nu \rfloor} = \underset{1\times N}{\lfloor\delta\rfloor} \underset{N\times n}{\left[B_u\right]} \tag{5.64}$$

The latter can be derived by explicitly calculating an expression for $\{dD \cdot \nabla f\}$ of the form (5.54). For instance, carrying out the algebra in the case of three-dimensions[8], one gets the following:

$$\underset{3\times1}{\{dD \cdot \nabla f\}} = \underset{3\times3}{\begin{bmatrix} dD_{11} & dD_{12} & dD_{13} \\ dD_{21} & dD_{22} & dD_{23} \\ dD_{31} & dD_{32} & dD_{33} \end{bmatrix}} \underset{3\times1}{\begin{Bmatrix} \frac{\partial f}{\partial x_1} \\ \frac{\partial f}{\partial x_2} \\ \frac{\partial f}{\partial x_3} \end{Bmatrix}} = \underset{3\times1}{\begin{Bmatrix} dD_{11}\frac{\partial f}{\partial x_1} + dD_{12}\frac{\partial f}{\partial x_2} + dD_{13}\frac{\partial f}{\partial x_3} \\ dD_{12}\frac{\partial f}{\partial x_1} + dD_{22}\frac{\partial f}{\partial x_2} + dD_{23}\frac{\partial f}{\partial x_3} \\ dD_{13}\frac{\partial f}{\partial x_1} + dD_{23}\frac{\partial f}{\partial x_2} + dD_{33}\frac{\partial f}{\partial x_3} \end{Bmatrix}}$$

$$\Rightarrow \underset{3\times1}{\{dD \cdot \nabla f\}} = \underset{3\times6}{\begin{bmatrix} \frac{\partial f}{\partial x_1} & 0 & 0 & \frac{\partial f}{\partial x_2} & \frac{\partial f}{\partial x_3} & 0 \\ 0 & \frac{\partial f}{\partial x_2} & 0 & \frac{\partial f}{\partial x_1} & 0 & \frac{\partial f}{\partial x_3} \\ 0 & 0 & \frac{\partial f}{\partial x_3} & 0 & \frac{\partial f}{\partial x_1} & \frac{\partial f}{\partial x_2} \end{bmatrix}} \underset{3\times1}{\begin{Bmatrix} dD_{11} \\ dD_{22} \\ dD_{33} \\ dD_{12} \\ dD_{13} \\ dD_{23} \end{Bmatrix}} \equiv \underset{3\times6}{\left[A_{\nabla f}\right]} \underset{6\times1}{\{dD\}} \tag{5.65}$$

5.4 The Role of UMAT and UEL Subroutines

Computational implementation of the finite element method presented in this chapter is realized by making use of the so-called *user subroutines* of Abaqus/Standard module of the general purpose finite element program ABAQUS ([1]). This flexible functionality enables not only the simulation of complex, nonlinear constitutive behavior and/or coupled phenomena but also lets the user create their own element type[9] for special modeling purposes. More specifically, ABAQUS allows the introduction of user-defined material behavior and user-defined element type through its *User MATerial* and *User ELement* subroutines (abbreviated as UMAT and UEL respectively), which are written in programming language such as FORTRAN. The basic ideas concerning the formulation of UMAT and UEL subroutines is briefly discussed bellow.

[8] Simplification to two- and one-dimensional problems is straightforward.

[9] A user-defined element includes the specification of the number of nodes, number of integration points, the definition of the corresponding interpolation functions, and the degrees of freedom of each node. In the most general case, degrees of freedom may also vary from node to node in an element, depending on the nature of the problem for which the corresponding element is used in.

User MATerial Subroutines

User MATerial (UMAT) subroutines are used in cases where a non-existent, user-defined constitutive model describing the behavior of the material under consideration needs to be introduced. In view of (5.26) and (5.60)-(5.62), evaluation of the residual and the Jacobian stiffness matrix of the global problem requires the calculation, in an element (local) level, of integrals involving quantities that are related to the particular constitutive model implemented, namely the stresses, strains, one or more state variables and the corresponding material moduli. Generally speaking, the latter integrals are evaluated numerically and thus, all integrands must be determined at the corresponding Gauss integration points. For this purpose, the UMAT subroutine is called by ABAQUS at every integration point for all elements where user-defined material behavior is specified. In material models involving only mechanical behavior, a UMAT must usually provide the stresses (STRESS), the local material Jacobian $\partial(\Delta\boldsymbol{\sigma})/\partial(\Delta\mathbf{E})$ (DDSDDE) and any solution-dependent state variables (STATEV)[10] at the end of the corresponding increment that it is called. Additionally, for coupled temperature-displacement problems the volumetric heat generation per unit time (RPL) has to be provided along with the variations of the latter quantity and stresses with respect to temperature and strain[11]. A typical UMAT code interface is presented bellow.

```
1         SUBROUTINE UMAT(STRESS,STATEV,DDSDDE,SSE,SPD,SCD,
2        + RPL,DDSDDT,DRPLDE,DRPLDT,
3        + STRAN,DSTRAN,TIME,DTIME,TEMP,DTEMP,PREDEF,DPRED,CMNAME,
4        + NDI,NSHR,NTENS,NSTATV,PROPS,NPROPS,COORDS,DROT,PNEWDT,
5        + CELENT,DFGRD0,DFGRD1,NOEL,NPT,LAYER,KSPT,JSTEP,KINC)
6 C
7         INCLUDE 'ABA_PARAM.INC'
8 C
9         CHARACTER*80 CMNAME
10        DIMENSION STRESS(NTENS),STATEV(NSTATV),
11       + DDSDDE(NTENS,NTENS),DDSDDT(NTENS),DRPLDE(NTENS),
12       + STRAN(NTENS),DSTRAN(NTENS),TIME(2),PREDEF(1),DPRED(1),
13       + PROPS(NPROPS),COORDS(3),DROT(3,3),DFGRD0(3,3),DFGRD1(3,3),
14       + JSTEP(4)
15
16        user coding to define DDSDDE, STRESS, STATEV, SSE, SPD, SCD
17        and, if necessary, RPL, DDSDDT, DRPLDE, DRPLDT, PNEWDT
18
19        RETURN
20        END
```

[10] Solution-dependent variables usually include the state variables of the corresponding constitutive model, other variables whose values must be stores for future calculations and variables whose values are needed for post-processing purposes.

[11] i.e. the quantities $\partial(\Delta\boldsymbol{\sigma})/\partial(\Delta T)$ (DDSDDT), $\partial r_{pl}/\partial(\Delta\mathbf{E})$ (DRPLDE) and $\partial r_{pl}/\partial(\Delta T)$ (DRPLDT).

User ELement Subroutines

User ELement (UEL) subroutines are usually developed to deal with problems where descretization of the corresponding BVP describing one (or more than one -coupled-) physical phenomenon(a) results in additional degrees of freedom other than the classical displacement-rotation ones. As it can be seen from the finite element formulation of the mixed BVP presented in this chapter, in such cases, more nodal unknowns arise, additional interpolations may need to be introduced. Additionally, element calculations involve the evaluation of the residual and the Jacobian stiffness matrix, which are then used in the assembled into the corresponding global matrices that are used for the solution of the system (5.27). For the latter calculations, the UEL subroutine is called by ABAQUS for all elements where user-defined element type is specified. Again, considering only mechanical constitutive behavior, UEL subroutine should provide the local residual vector (RHS), the local Jacobian matrix (AMATRX) and any solution-dependent variables (SVARS)[12] at the end of the increment it is called. Furthermore, since visualization of user element output is not directly supported by ABAQUS, a UVARM subroutine is included for the extraction of all the relevant output variables. Finally, if user-defined material behavior is also implemented, a UMAT-like subroutine (abbreviated for distinction purposes as KUMAT) also needs to be incorporated into UEL, which will be called for material calculations[13] at each integration point of the element. A typical UEL code interface is presented bellow.

```
1         SUBROUTINE UEL(RHS,AMATRX,SVARS,ENERGY,NDOFEL,NRHS,NSVARS,
2        + PROPS,NPROPS,COORDS,MCRD,NNODE,U,DU,V,A,JTYPE,TIME,DTIME,
3        + KSTEP,KINC,JELEM,PARAMS,NDLOAD,JDLTYP,ADLMAG,PREDEF,NPREDF,
4        + LFLAGS,MLVARX,DDLMAG,MDLOAD,PNEWDT,JPROPS,NJPROP,PERIOD)
5  C
6         INCLUDE 'ABA_PARAM.INC'
7  C
8         DIMENSION RHS(MLVARX,*),AMATRX(NDOFEL,NDOFEL),PROPS(*),
9        + SVARS(*),ENERGY(8),COORDS(MCRD,NNODE),U(NDOFEL),
10       + DU(MLVARX,*),V(NDOFEL),A(NDOFEL),TIME(2),PARAMS(*),
11       + JDLTYP(MDLOAD,*),ADLMAG(MDLOAD,*),DDLMAG(MDLOAD,*),
12       + PREDEF(2,NPREDF,NNODE),LFLAGS(*),JPROPS(*)
13
14        user coding to define RHS, AMATRX, SVARS, ENERGY, and PNEWDT
15
16        RETURN
17        END
```

[12] In the context of UEL subroutines, solution-dependent state variables now also include stresses, strains or other variables which in the context of UMAT are stored separately.

[13] It should be noted here that if a user-defined element is introduced that also incorporates user-defined material behavior, additional quantities related to material behavior might need to be calculated for the evaluation the AMATRX. For instance, for the constitutive model presented in this thesis, $\partial(\Delta\boldsymbol{\sigma})/\partial f$ (DDSDF), $\partial(\Delta f_{\text{loc}})/\partial(\Delta\mathbf{E})$ (DDFLOCDDE) and $\partial(\Delta f_{\text{loc}})/\partial f$ (DDFLOCDF) have to be calculated in addition to $\partial(\Delta\boldsymbol{\sigma})/\partial(\Delta\mathbf{E})$.

The algorithmic procedure implemented by both the UEL and the corresponding UMAT, are presented in the following flowcharts.

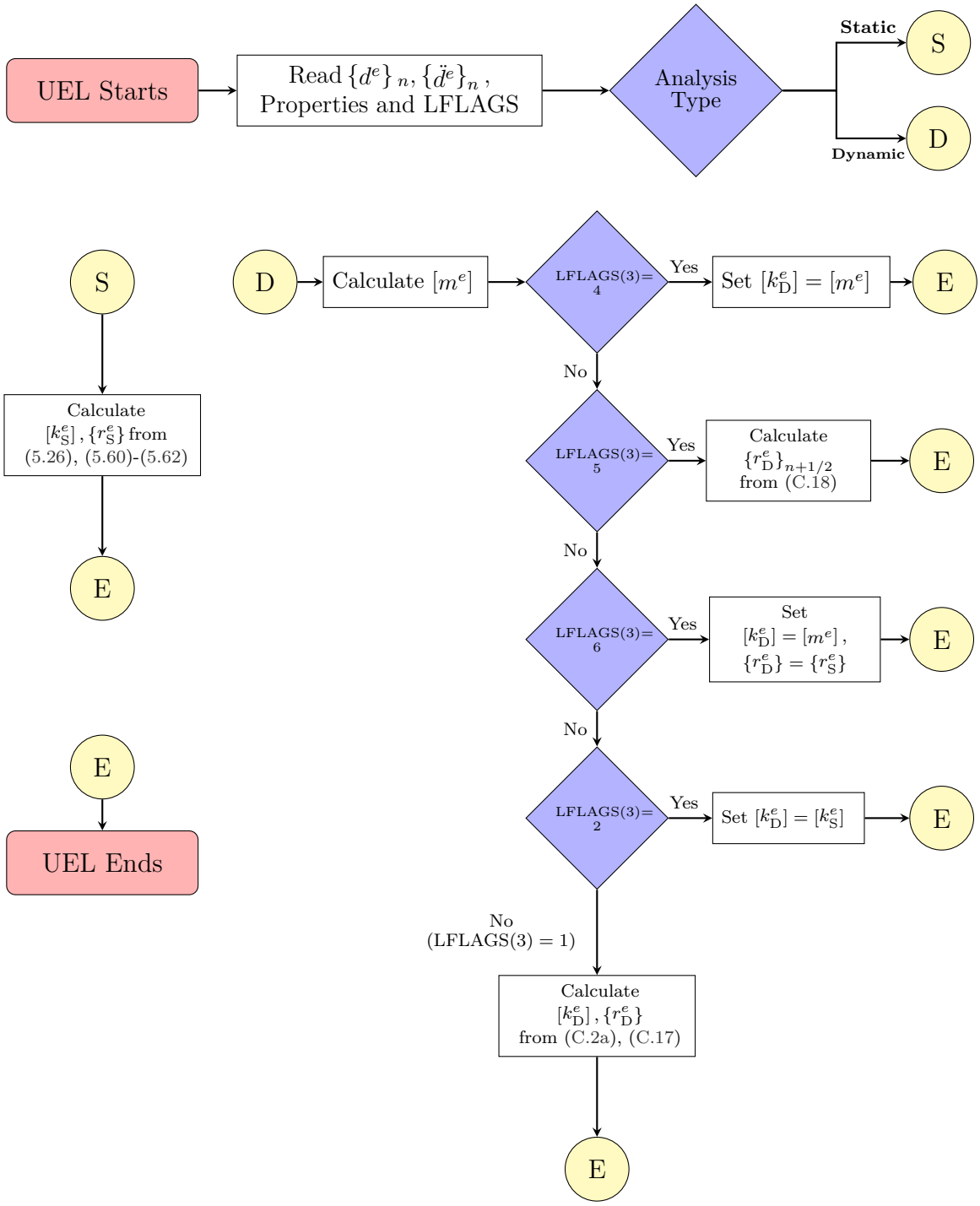

Figure 5.1: Flowchart of the UEL developed for the implementation of the gradient anisotropic model. LFLAGS denotes the array containing information about the corresponding procedure type.

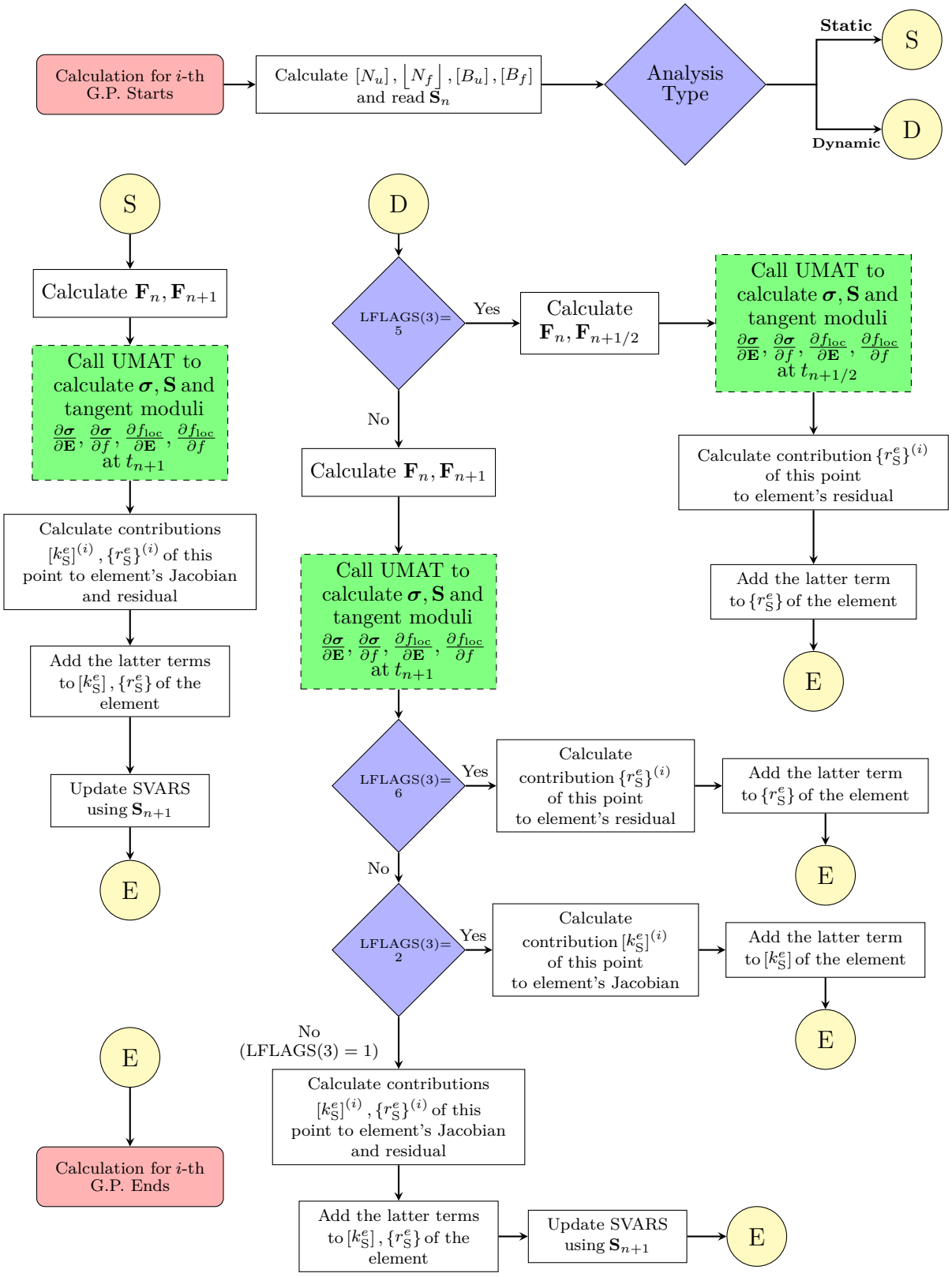

Figure 5.2: Internal flowchart displaying calculations for each Gauss integration point. The quantity $\mathbf{S}$ denotes the array of the solution dependent variables defined for the specific problem.

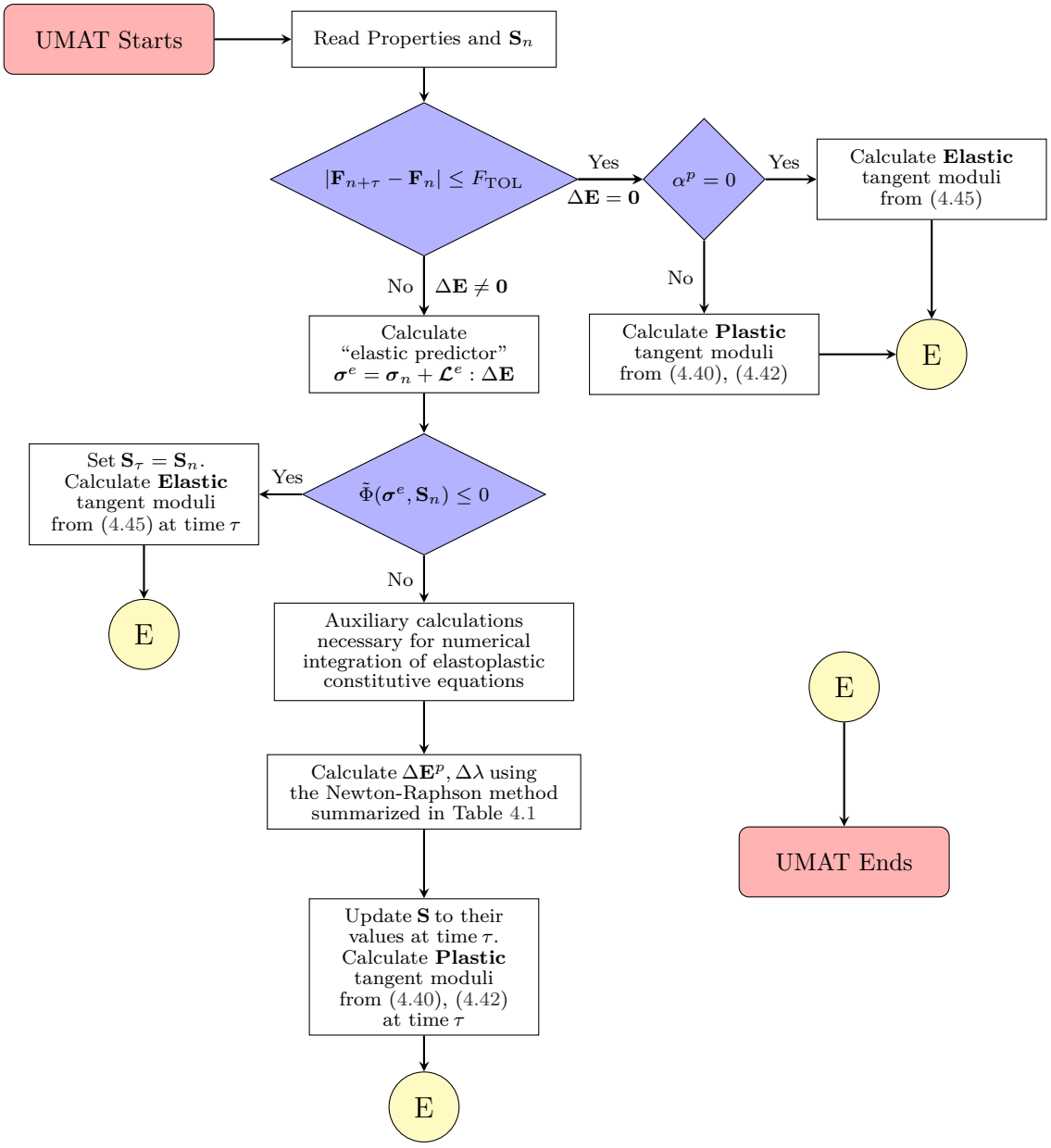

Figure 5.3: Internal flowchart of the UMAT developed for the implementation of the anisotropic model. Time τ may refer to either the end of the increment ($\tau = t_{n+1}$) or at the middle of the increment ($\tau = t_{n+1/2}$) if the "half increment residual" is evaluated (see Appendix C).

Chapter 6

Applications

In this chapter, the finite element results from implementation of the model developed in Chapter 4 are presented. More specifically, the effect of the gradient enhancement was investigated with a series of simulations concerning the following benchmark problems:

- *Localization of deformation during plain-strain tension.*
- *The problem of plain-strain ductile fraction under 'small scale yielding conditions'.*
- *Damage propagation during the Charpy V-notch test in plain-strain conditions.*

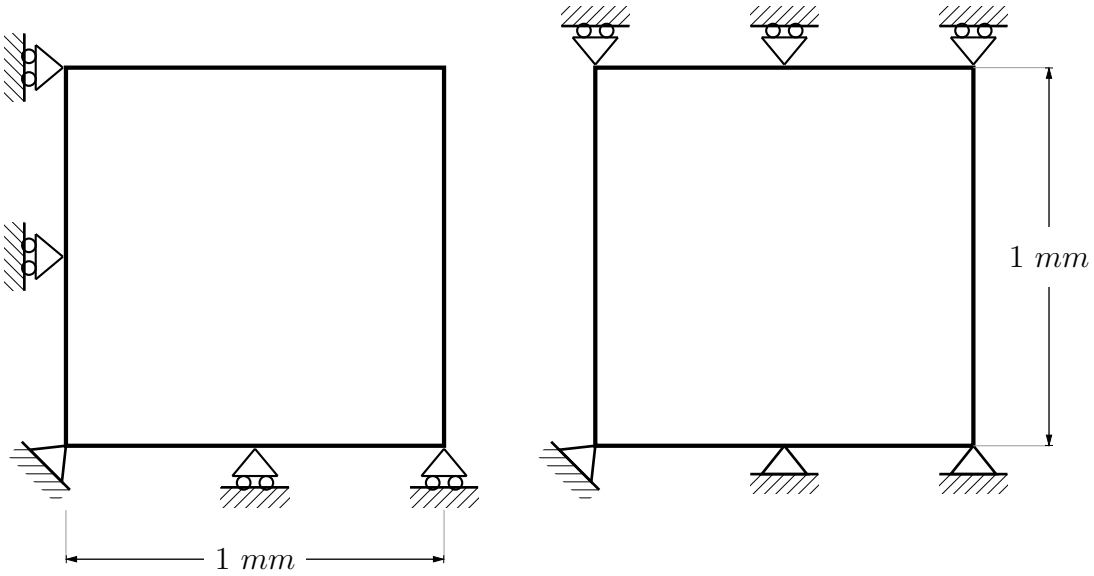

Figure 6.1: Single quadrilateral elements of unit length that were used in various code validations. Boundary conditions (a) for plane strain tension and (b) for simple shear are also depicted.

For this purpose, a UEL subroutine for the gradient anisotropic model was initially developed in the context of this diploma thesis, capable of being used in both static and dynamic finite

element analyses. Moreover, for comparison purposes, a "nonlocal UMAT", fully equivalent to the aforementioned UEL, was also developed, which significantly simplified the procedures. This UMAT, which takes advantage of the similarity between the steady state heat transfer PDE and equation 4.4, is formulated in such a way so that the temperature degrees of freedom correspond to the nonlocal porosity f. The Abaqus/Standard module of the general purpose finite element program ABAQUS ([2]) was used as a solver for the global discretized equations in conjunction with the latter FORTRAN subroutines, which are called at every element for local calculations at every integration point. Most code validations were carried out using series of benchmark one element tests, as the ones depicted in Figure 6.1, under plain-strain conditions.

Furthermore, calculations for the second and third of the problems mentioned above were also carried out using the well-known Gurson's pressure dependent isotropic model[1] [31], the yield function of which is given as:

$$\Phi(\sigma_e, p, \bar{\varepsilon}^p, f) = \left[\frac{\sigma_e}{\sigma_y(\bar{\varepsilon}^p)}\right]^2 + 2q_1 f \cosh\left[\frac{3q_2}{2}\frac{p}{\sigma_y(\bar{\varepsilon}^p)}\right] - (1 + q_3 f^2) \tag{6.1}$$

where $\sigma_e \equiv \sigma_e^{vM} = \sqrt{3(\mathbf{s} : \mathbf{s})/2}$ is the von Mises equivalent stress, $\mathbf{s} = \boldsymbol{\sigma} - p\boldsymbol{\delta}$ and $p = \sigma_{kk}/3$ denote the deviatoric stress tensor and the hydrostatic stress respectively, and q_1, q_2, q_3 are parameters first introduced by Tvergaard in [77] in an effort to make Gurson's model predictions agree with simulations of materials containing periodically distributed circular cylindrical voids. For the series of calculations presented herein, $q_1 = q_2 = q_3 = 1$ are chosen so that (6.1) reduces to the classical yield function introduced by Gurson. For this model, the finite element formulation is identical to the one presented in Chapter 5 and the evolution equations along with the corresponding consistent "linearization moduli" of the material model can be found in [5], [30].

Finally, for all applications, the matrix material, with Young's modulus E and Poisson's ratio ν, exhibits isotropic hardening of the form:

$$\sigma_y = \sigma_0\left(1 + \frac{\bar{\varepsilon}^p}{\varepsilon_0}\right)^{1/n}, \quad \varepsilon_0 = \frac{\sigma_0}{E} \tag{6.2}$$

where $n \geq 1$ is the hardening exponent and σ_0 is the yield stress in tension. Moreover, keeping in mind that the length units used here are mm, E, σ_y are normalized by the yield stress σ_0 and so, all corresponding results (stresses, reaction forces etc.) presented in the following sections are in this sense normalized as well by the initial yield strength. Also, for the anisotropic model, it assumed that the porous material initially consists of a statistically isotropic distribution of spherical voids, i.e., the initial aspect ratios of the RLEV are $w_1|_0 = w_2|_0 = 1$.

[1] Both the local and a gradient enhanced version, in the sense of the mixed BVP formulation presented in Chapter 5, were used in the corresponding analyses.

6.1 Localization under Plain Strain Tension

Before proceeding with the application of the gradient anisotropic model to benchmark problems found in literature, it is was of great importance to verify the proper functionality of the nonlocal enhancement in the alleviation of the mesh-dependent behavior of the corresponding local model. For this purpose, a series of finite element analysis was conducted for various meshes, both for the local and for the nonlocal model, the results of which are presented in this section. More precisely, a series of plain strain tension tests of a 2-dimensional, rectangular block were carried out using the classical anisotropic model and its gradient counterpart, with the latter being implemented via the developed nonlocal UMAT. As in Anand *et al.* [4], the ratio of the the specimen's edges H/L is held constant at 1.5. Dimensions for the specimen used in the aforementioned calculations are presented in Figure 6.2.

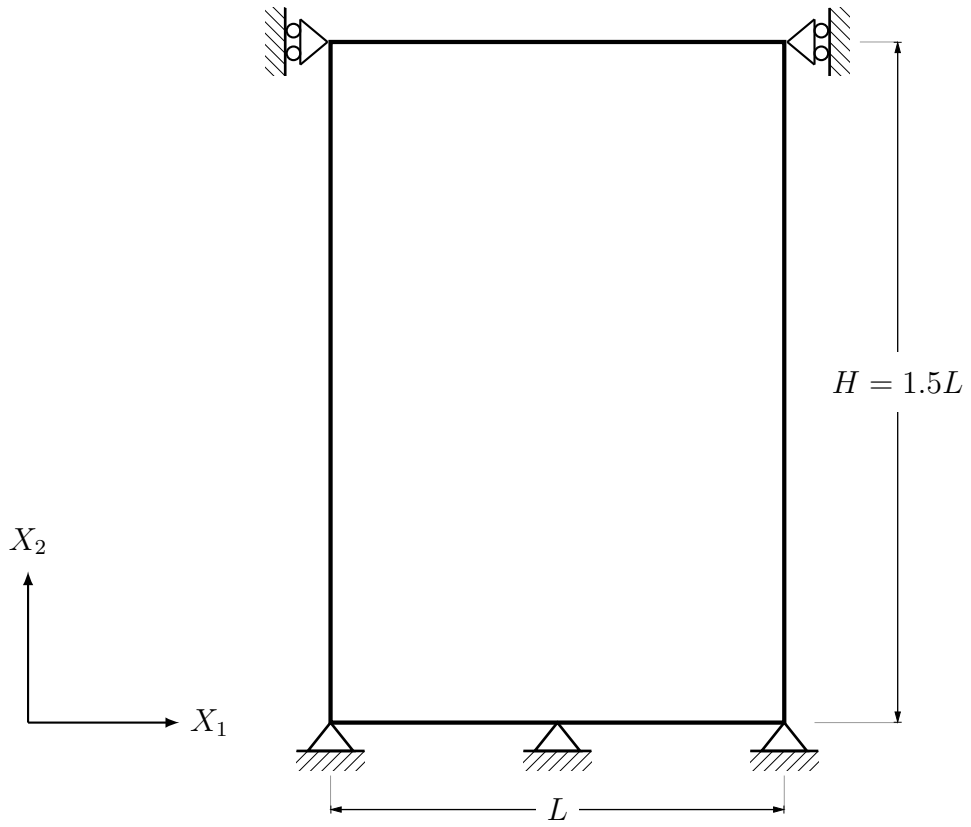

Figure 6.2: Geometry and boundary conditions for the localization specimen. For this series of calculations $L = 20\,mm$, $H = 30\,mm$. No imperfections are introduced since the boundary conditions are sufficient to trigger the occurence of the localized shear band mode.

Regarding boundary conditions, the bottom face of the specimen at $X_2 = 0$ is held fixed (i.e., $\mathbf{u}(X_1, X_2 = 0) = \mathbf{0}$), the top face at $X_2 = H$ is restricted to move in the direction of loading (i.e. $u_1(X_1, X_2 = H) = 0$) and the lateral faces, at $X_1 = 0, X_1 = L$ are kept traction-free. All analyses are displacement controlled and are driven by the prescribed displacement of the top face $u_2(X_1, X_2 = H) = \hat{u}_2$ in the loading direction X_2. The imposed boundary conditions

described above are such that may lead to the rise of a non-homogeneous deformation pattern without the introduction of any additional material or geometrical imperfections.

Table 6.1: Normalized material properties used for the localization problem.

E	ν	σ_0	n	f_N	ϵ_N	s_N
$300\sigma_0$	0.3	1	10	0.04	0.4	0.1

The mesh-sensitivity analysis is realized for three different meshes that consist of 5400, 8000 and 15000 elements respectively. The four-node, bilinear, isoparamentric plain strain elements CPE4 and CPE4T, with 2×2 Gauss integration points from the general purpose, continuum element library of Abaqus/Standard [1] are used for the local and nonlocal calculations respectively. The material properties used in both sets of calculations are summarized in Table 6.1. Initial porosity is selected as 4% and the nonlocal analyses are carried out for an $\ell = 0.05L = 1\ mm$.

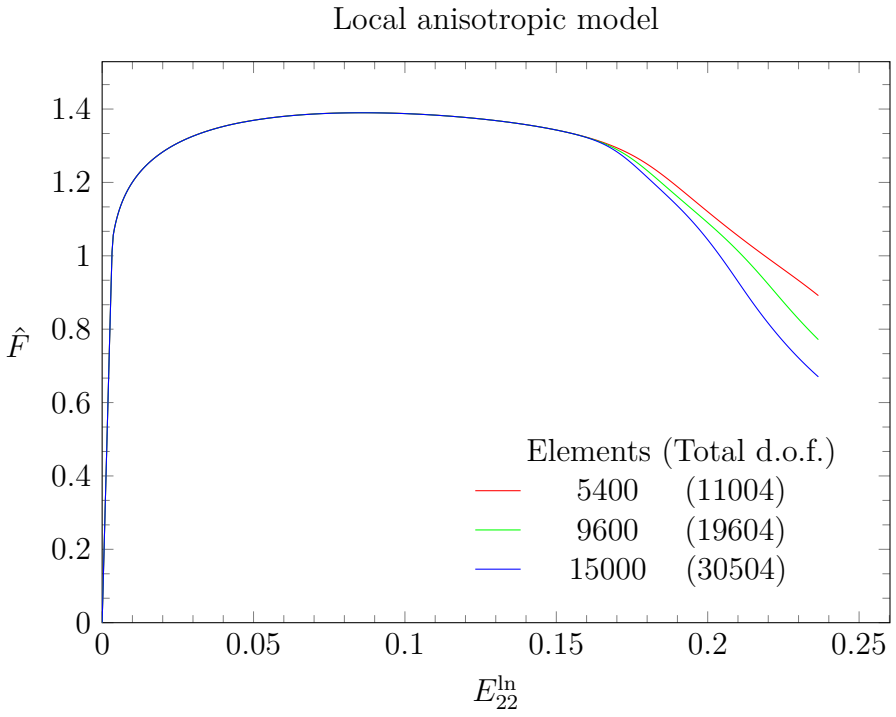

Figure 6.3: Normalized load vs 'macroscopic axial strain' curve for the local ($\ell = 0$) anisotropic model for a strain level up to $E_{22}^{\ln} \approx 0.236$.

The finite element results for the local series of simulations ($\ell = 0$) can be seen in Figures 6.3-6.5. To begin with, Figure 6.3 depicts the normalized load-extension curves of the specimen as calculated for the three different meshes that consist of 5400, 9600 and 15000 elements,

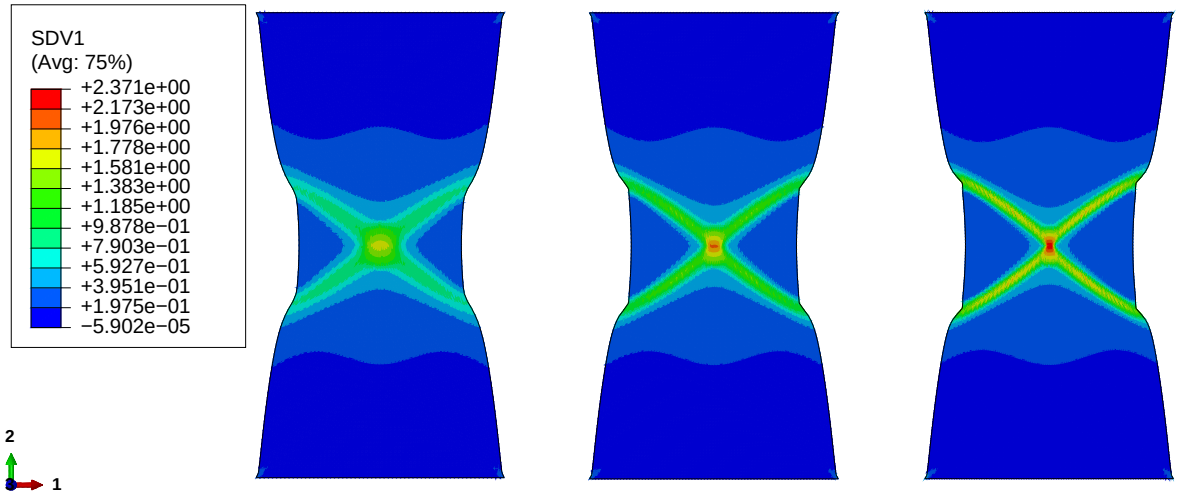

(a) 5400 elements (b) 9600 elements (c) 15000 elements

Figure 6.4: Contour Plots of $\bar{\varepsilon}^p$ at a strain level $E_{22}^{\ln} = 0.223$, for the local anisotropic model.

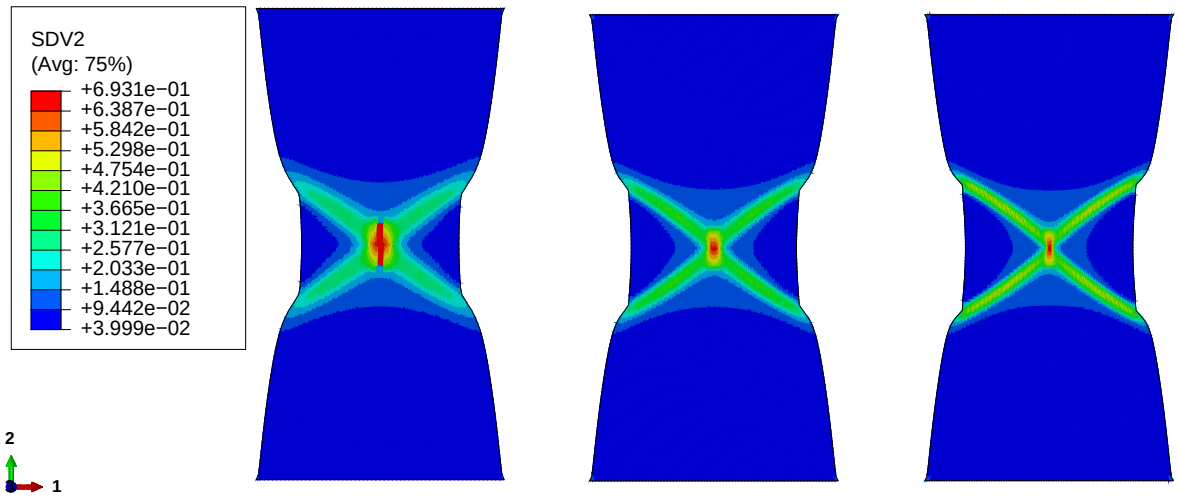

(a) 5400 elements (b) 9600 elements (c) 15000 elements

Figure 6.5: Contour Plots of f_{loc} at a strain level $E_{22}^{\ln} = 0.223$, for the local anisotropic model.

where the corresponding normalized load and logarithmic axial strain $\hat{F}$ and $E_{22}^{\ln}$ are defined as:

$$\hat{F} = \frac{F_2}{\sigma_0 A} \quad \text{and} \quad E_{22}^{\ln} = \ln\left(1 + \frac{\hat{u}_2}{H}\right) \tag{6.3}$$

with F_2 being the total force in direction X_2 evaluated in the analysis and $A = Lt$ is the corresponding loading area, where the thickness t of the cross-section is selected as unity for the sake of simplicity. One can observe that up to a strain level $E_{22}^{\ln} \approx= 0.16$, the numerical solutions coincide for all meshes and no deviations are exhibited as the discretization becomes

finer. Nevertheless, this is not the case for deformations beyond the latter critical point. More specifically, as strains grow larger than the aforementioned critical strain level, the solution is no longer homogeneous and all deformation progressively localizes into narrow shear bands as the ones shown in Figure 6.4. As a consequence, damage initiation and propagation also concentrate in these bands of severe plastic deformation, a fact which is verified by the the increased values of the local porosity illustrated in Figure 6.5. However, in contrast to what one would intuitively expect, the non-convergence of the curves in Figure 6.3 as the mesh is refined reveals the strong mesh-dependency of the solution if no regularization is introduced in the problem. Moreover, the ill-posedness of the problem is also justified by taking into consideration that, as the mesh becomes more dense, the width of the shear bands presented above is reduced, tending to zero so that, for the same level of strain and a different discretization scheme, more than one failure pattern are admitted. This evidence leads to the deduction that the local problem is non-objective with respect to mesh refinement and the local anisotropic model is insufficient to provide a unique solution.

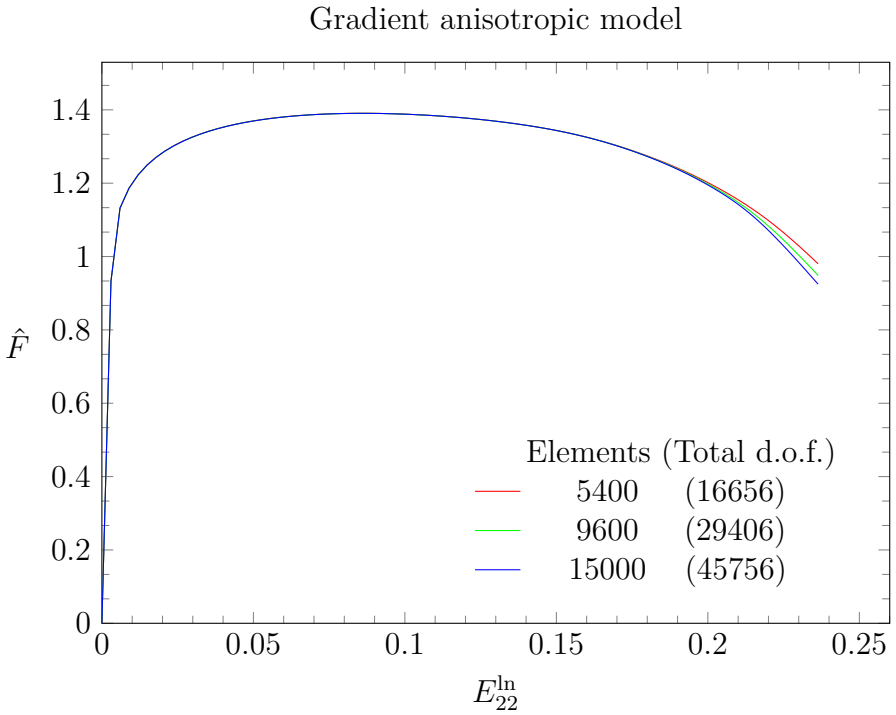

Figure 6.6: Normalized load vs 'macroscopic axial strain' curve for the nonlocal ($\ell = 0.05L$) anisotropic model for a strain level up to $E_{22}^{\ln} \approx 0.236$.

On the other hand, the situation is entirely different for the gradient anisotropic model. Numerical results in this case are shown in Figures 6.6-6.9. Figure 6.6 illustrates the normalized load-displacement curves for the anisotropic model with regularization. Obviously, as the mesh is systematically refined, the curves converge into a single response indicating that a unique solution is now admitted by the problem. Moreover, Figures 6.7, 6.8 make clear that the shear bands, which emerge yet again due to localization of deformation, remain finite as the discretization becomes more dense, and their size now depends on the characteristic length of the material. Comparison of the distribution of the nonlocal porosity f, which is

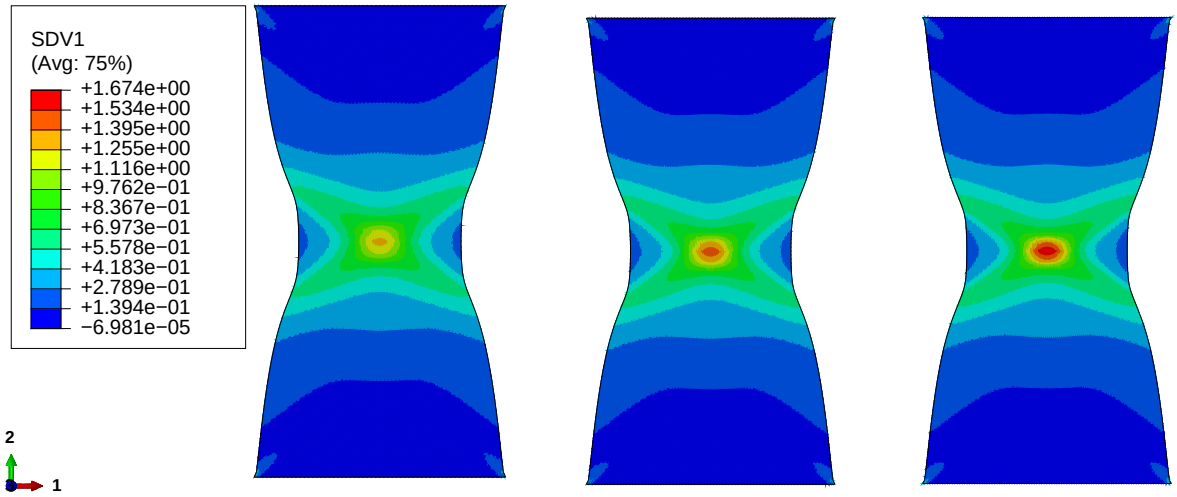

(a) 5400 elements (b) 9600 elements (c) 15000 elements

Figure 6.7: Contour Plots of $\bar{\varepsilon}^p$ at a strain level $E_{22}^{\ln} = 0.223$, for the nonlocal anisotropic model.

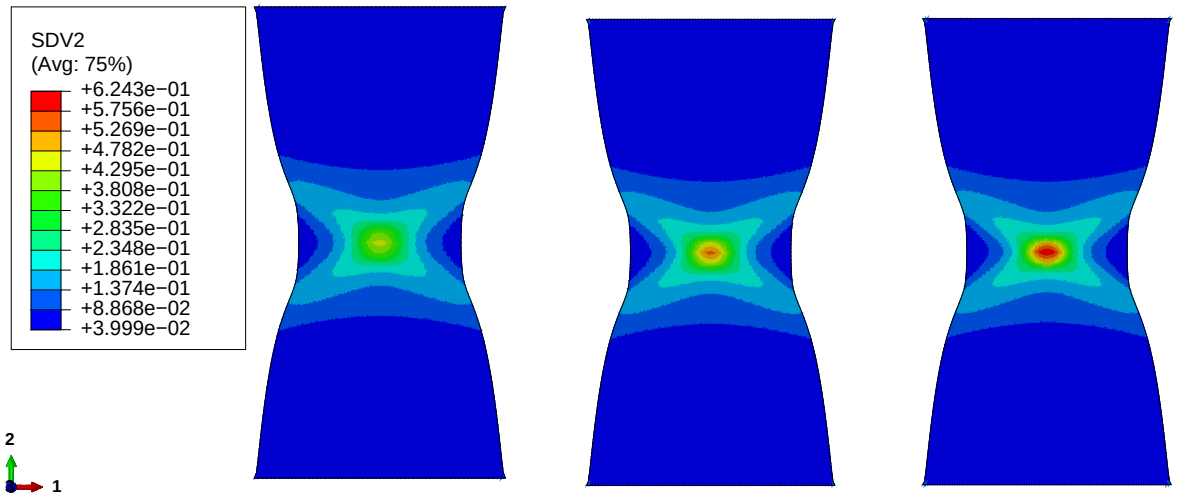

(a) 5400 elements (b) 9600 elements (c) 15000 elements

Figure 6.8: Contour Plots of f_{loc} at a strain level $E_{22}^{\ln} = 0.223$, for the nonlocal anisotropic model.

depicted in Figure 6.9, with its corresponding local counterpart confirms that the former tends to be more smooth than the latter and, literally being a volume average of the porosity over a region dictated by the intrinsic material length ℓ, takes smaller values as expected.

It should also be noted here that the gradient anisotropic model predicts, in contrast to the corresponding local model, 'less severe' concentration of deformation and porosity in the localization region which may be interpreted as a result of the regularization effect introduced

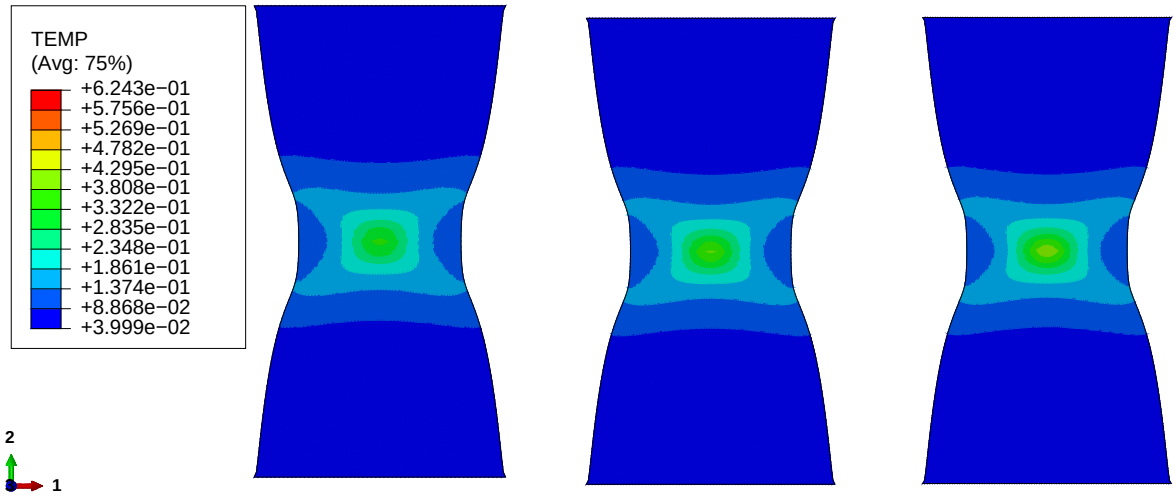

(a) 5400 elements (b) 9600 elements (c) 15000 elements

Figure 6.9: Contour Plots of f at a strain level $E_{22}^{\ln} = 0.223$, for the nonlocal anisotropic model.

by the nonlocal enhancement to the original BVP, an observation which is in accordance with numerical results presented, for instance, by Ramaswamy and Aravas in [69] for a gradient Gurson model with a similar enhancement of higher porosity gradients.

6.2 Plain Strain Ductile Fracture

In this application, the effect of the nonlocal enhancement to the classical anisotropic model is investigated in the problem of ductile fracture of a homogeneous porous elastic-plastic material under plain strain conditions. More specifically, the problem of mode-I blunt crack under 'small scale yielding' conditions (see [70], [71]) is treated for both the local and the nonlocal model and the results are compared in a similar fashion as was done in [7] for the same problem. For the sake of completeness, the latter series of calculations were also carried out using both the classical (local) and a nonlocal version of Gurson's model with a nonlocal porosity enhancement of the gradient type, similar to the one described in Chapter 5. A boundary layer formulation of an infinite body with a semi-infinite, semicircular notch at the crack's tip is used in order to study the near tip material response and, due to symmetry, only the upper half region is analysed. As shown in Figure 6.10, the crack's face is traction free and it is constrained to move in the direction X_1, perpendicular to the direction of the external loading. Moreover, displacement boundary conditions at the outer boundary of the region under examination are applied incrementally, via a user defined MPC subroutine[2], to

[2]Multi Point Constraints (MPCs) can be used to impose, linear or nonlinear, constraints between different degrees of freedom within a model. For highly complex MPCs that cannot be defined by the predefined types provided by Abaqus/Standard [1], the latter provides the capability of the desired MPC to be implemented thorough the corresponding user-specified MPC subroutine.

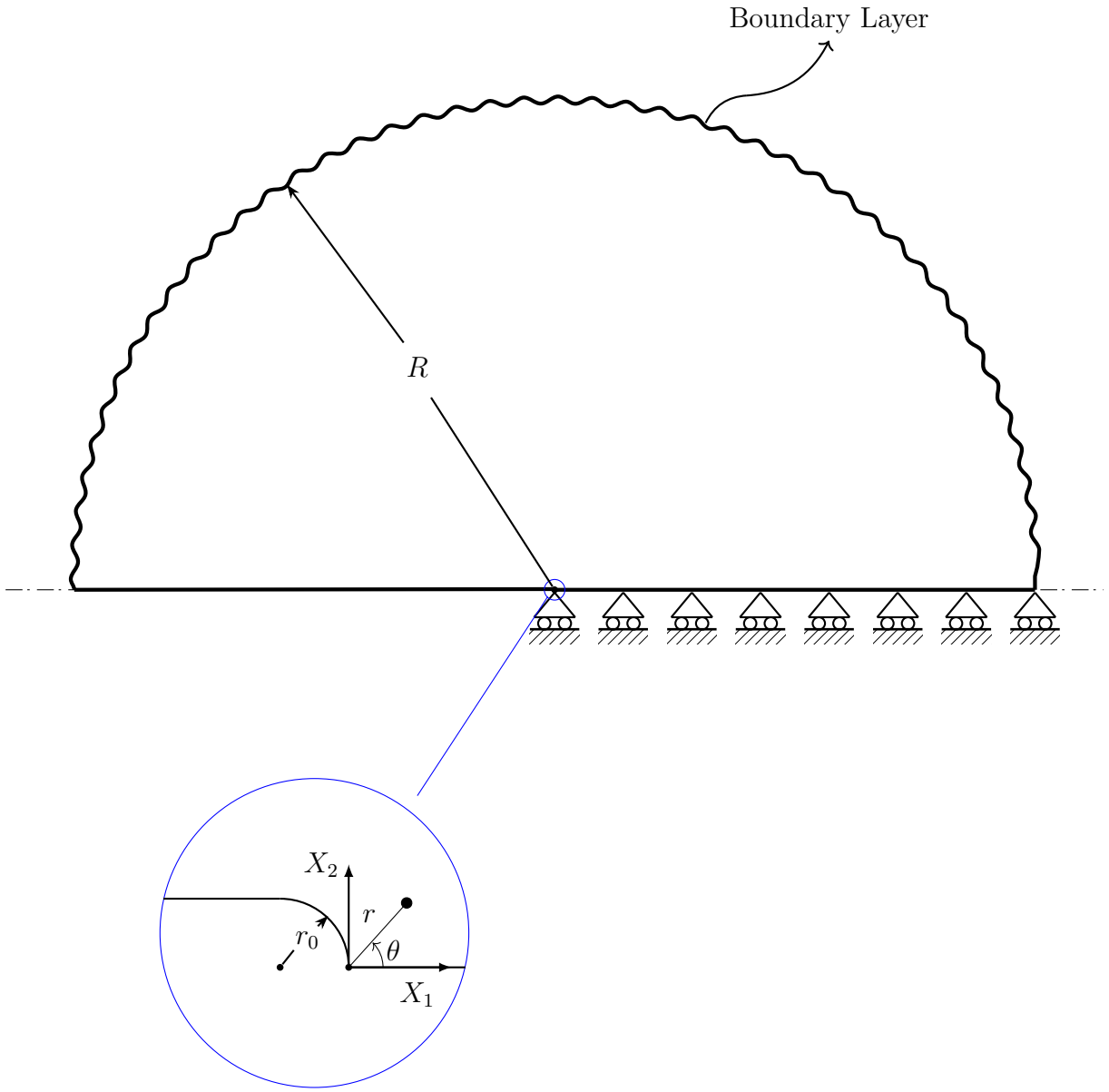

Figure 6.10: Geometry and boundary conditions for near-tip area of the crack. The outermost radius of the area under examination is $R \approx 1.2 \times 10^3 r_0$, where r_0 is the initial radius of the semicircular notch at the tip of the crack. For this series of numerical calculations $r_0 = 1\ mm$.

impose an asymptotic dependence on the mode-I elastic solution for classical crack problems, and are of the form:

$$\left\{ \begin{array}{c} u_1 \\ u_2 \end{array} \right\} = \frac{K_I}{2\mu}\sqrt{\frac{r}{2\pi}}(3 - 4\nu - \cos\theta) \left\{ \begin{array}{c} \cos(\theta/2) \\ \sin(\theta/2) \end{array} \right\} \tag{6.4}$$

where u_i are the components of the displacement field, K_I is the mode-I stress intensity factor, X_1, X_2 are the axis of symmetry and the direction of mode-I loading respectively which define the Cartesian coordinate system that is also depicted in the figure above and

r, θ are the polar coordinates initiating from the crack-tip.

Table 6.2: Normalized material properties used for the crack problem simulations.

E	ν	σ_0	n	f_N	ϵ_N	s_N
$300\sigma_0$	0.3	1	10	0.04	0.4	0.1

Once again, the four-node, bilinear, isoparamentric plain strain elements CPE4 and CPE4T, with 2×2 Gauss integration points from the general purpose, continuum element library of Abaqus/Standard [1] are used for the local and nonlocal calculations respectively. As in [7], a total of 1658 elements are used in the simulations and the corresponding finite element mesh near the crack's tip is shown in Figure 6.11. The material properties used in both sets of calculations are summarized in Table 6.2. Initial porosity is selected as 4% and the nonlocal analyses are carried out for an $\ell = 1\ mm$. In all cases, results are presented for various normalized load levels $K1 \equiv K_I/(\sigma_0\sqrt{r_0})$.

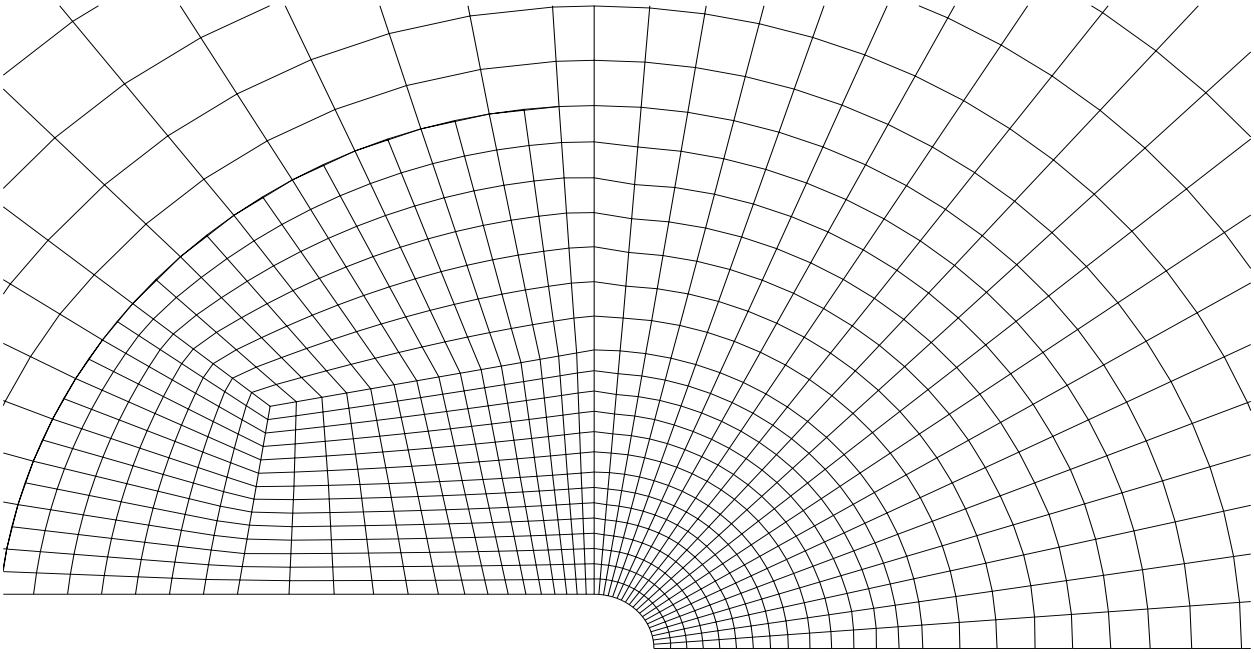

Figure 6.11: The finite element discretization used for the near-tip region of the semi-infinite notch.

To start with, finite element results concerning the local models are illustrated in Figures 6.12 through 6.19. Figures 6.12 - 6.16 showcase the distributions of the normalized stress σ_{22}, the hydrostatic stress p, the equivalent plastic strain $\bar{\varepsilon}^p$ and the (local) porosity f_{loc} along the path ahead of the semicircular crack's tip, for a range of normalized load levels $K1$ up to $K1 = 36.11$, with x_1 denoting the distance of any point along the path from the root of the crack. All calculations are restricted to the aforementioned load level range due to the numerical difficulties encountered by the Gurson's model, which predicts severe loss

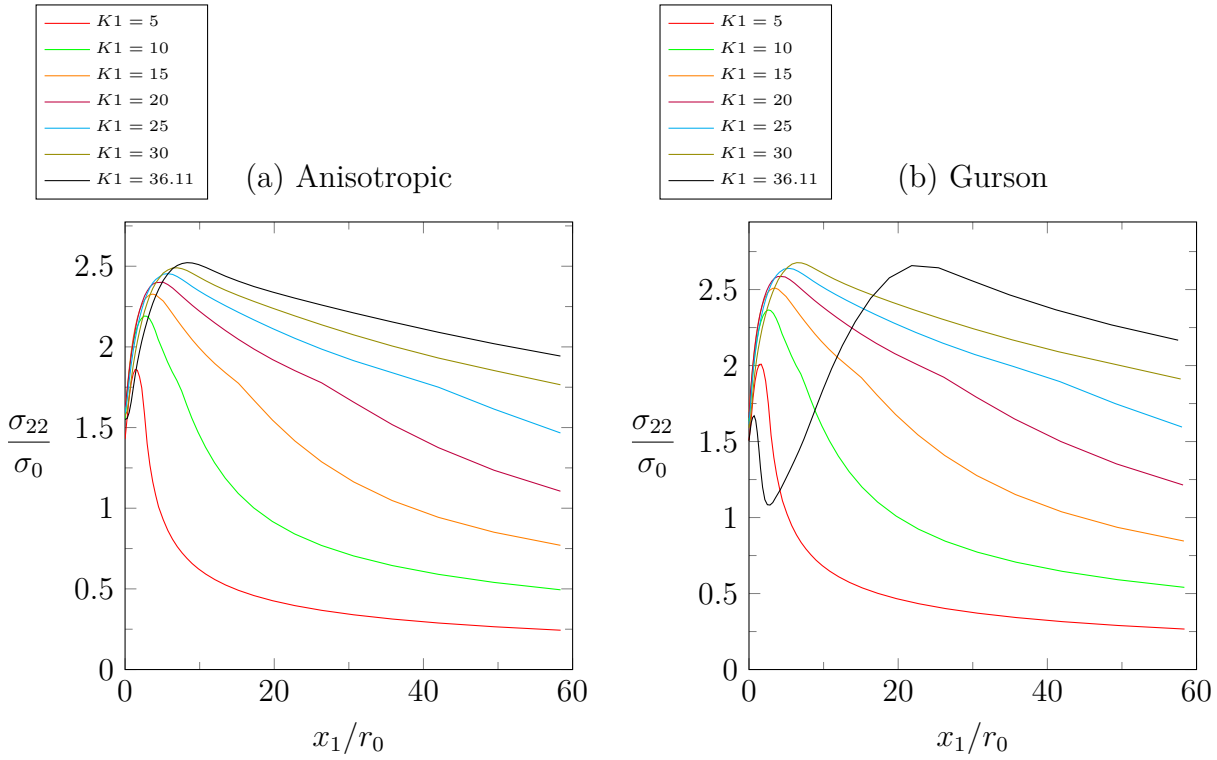

Figure 6.12: Normalized σ_{22} distribution ahead of the crack's tip for different load levels (a) Anisotropic, (b) Gurson's model.

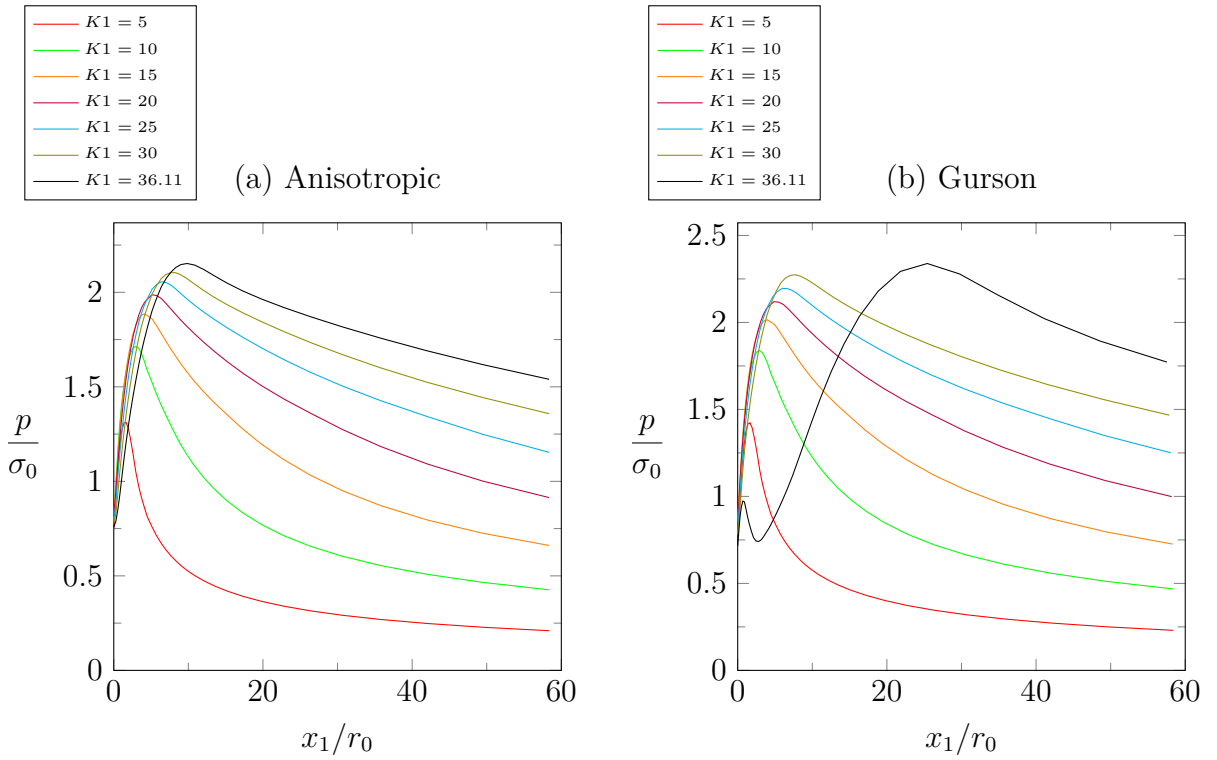

Figure 6.13: Normalized p distribution ahead of the crack's tip for different load levels (a) Anisotropic, (b) Gurson's model.

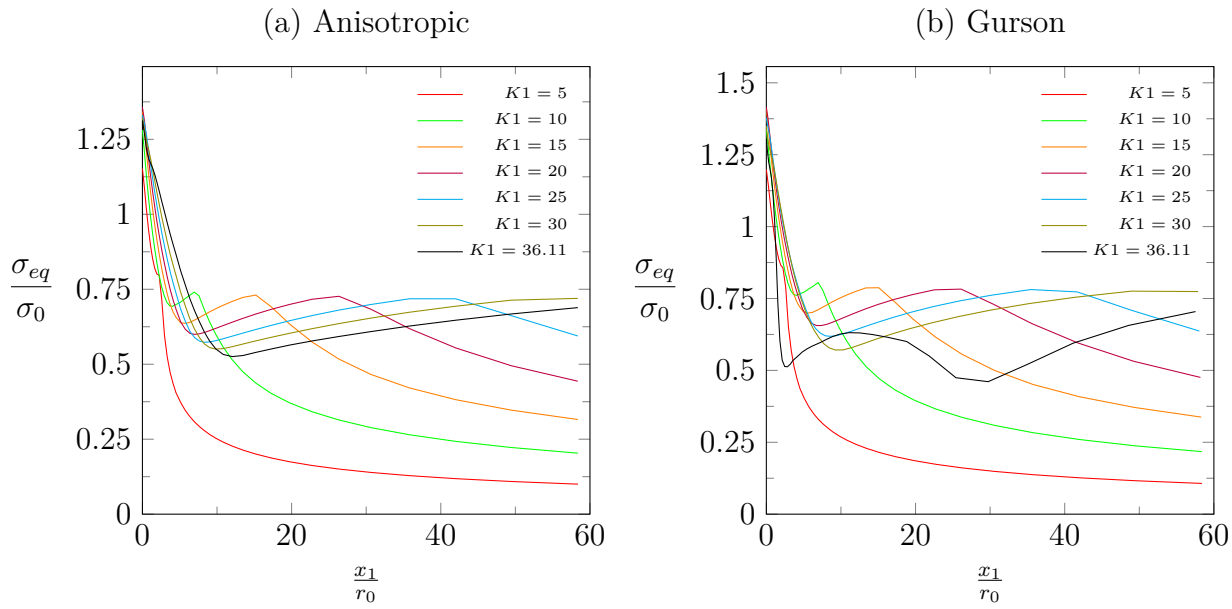

Figure 6.14: Normalized von Mises equivalent stress distribution ahead of the crack's tip for different load levels (a) Anisotropic, (b) Gurson's model.

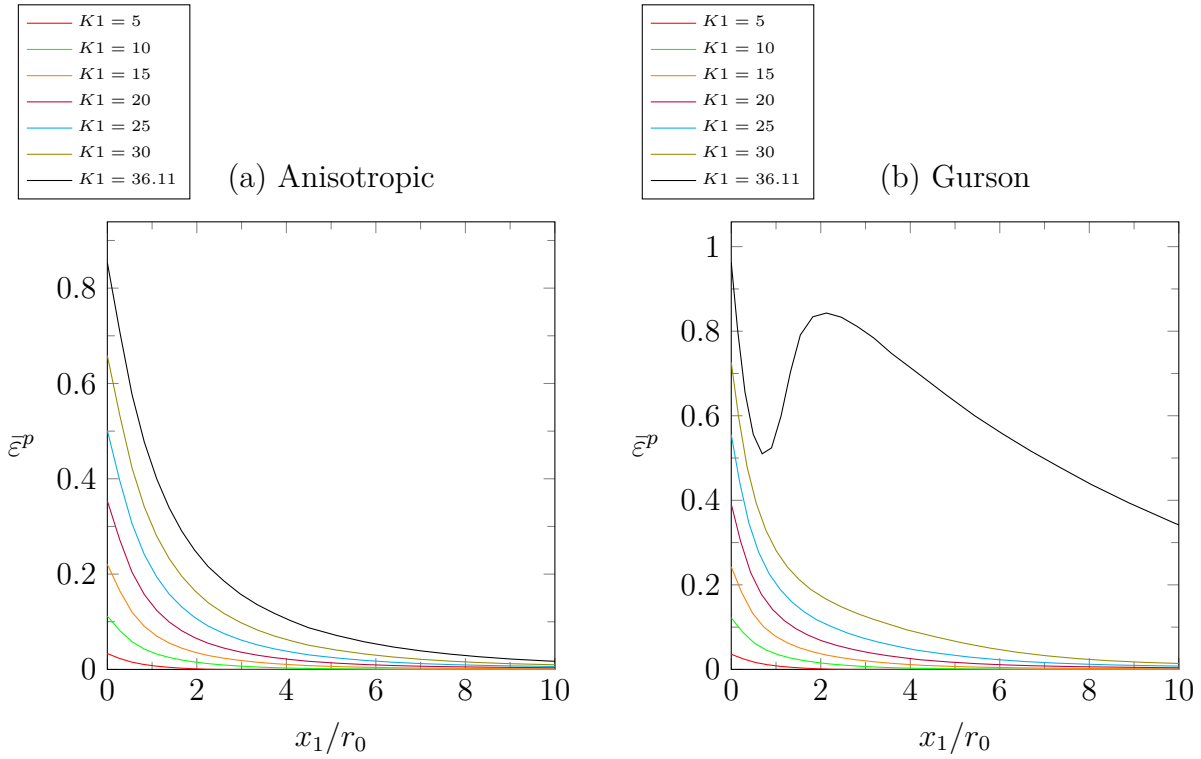

Figure 6.15: $\bar{\varepsilon}^p$ distribution along the path ahead of the crack's tip for different load levels (a) Anisotropic, (b) Gurson's model.

of stress- carrying capacity of the material for loads higher than $K1 = 36.11$. Regarding the material response for load levels up to $K1 = 30$, one can observe that the anisotropic model seems to be in agreement with Gurson's model, both in the stress-strain states and in the

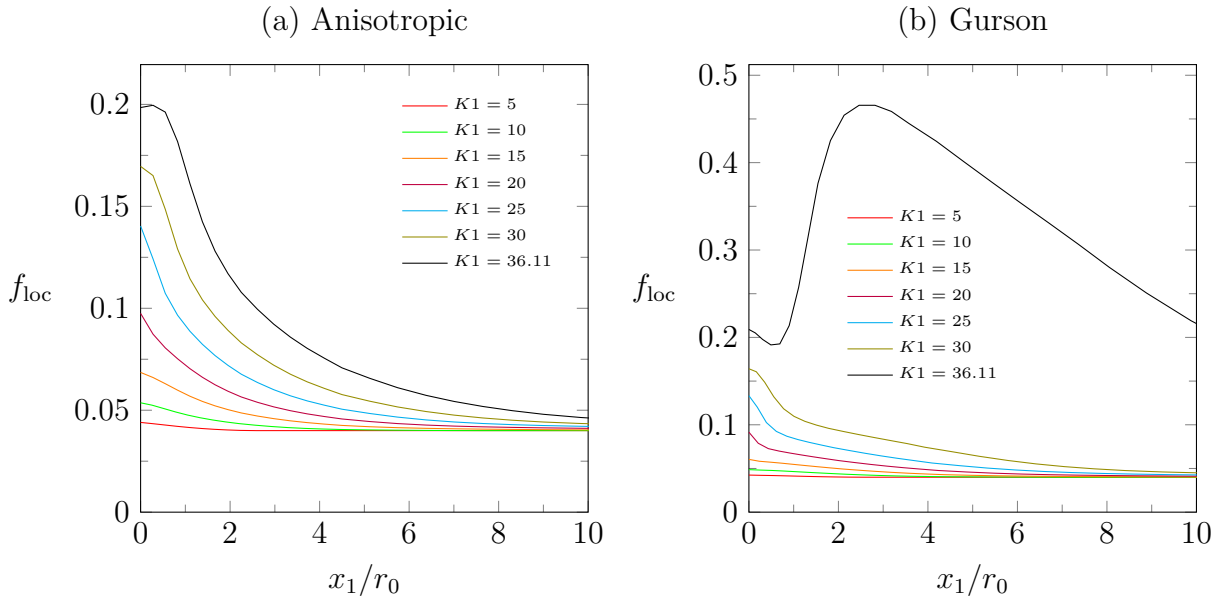

Figure 6.16: f_{loc} distribution along the path ahead of the crack's tip for different load levels (a) Anisotropic, (b) Gurson's model.

damage development predictions at the near-tip region. However, this is not the case for higher load levels. More specifically, finite element analyses carried out for the local Gurson model in the load range between $K1 = 30$ and $K1 = 36.11$ reveal that the solution exhibits a transition at a load $K1 \approx 32.5$ (see Figure 6.17) from the monotonically decreasing one to the mode corresponding to $K1 = 36.11$. As a consequence of this deviation, the crack propagation mechanism is substantially different between the local anisotropic and Gurson

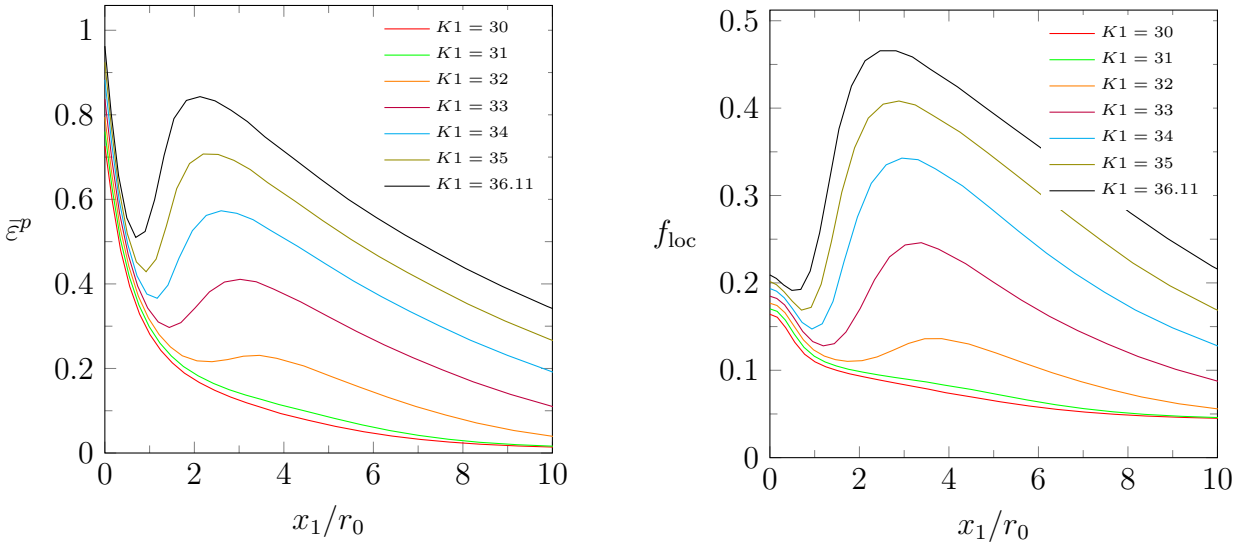

Figure 6.17: $\bar{\varepsilon}^p$ and f_{loc} distributions along the path ahead of the crack's tip for the local Gurson model in the range $K1 = 30$ - $K1 = 36.11$.

(a) Anisotropic

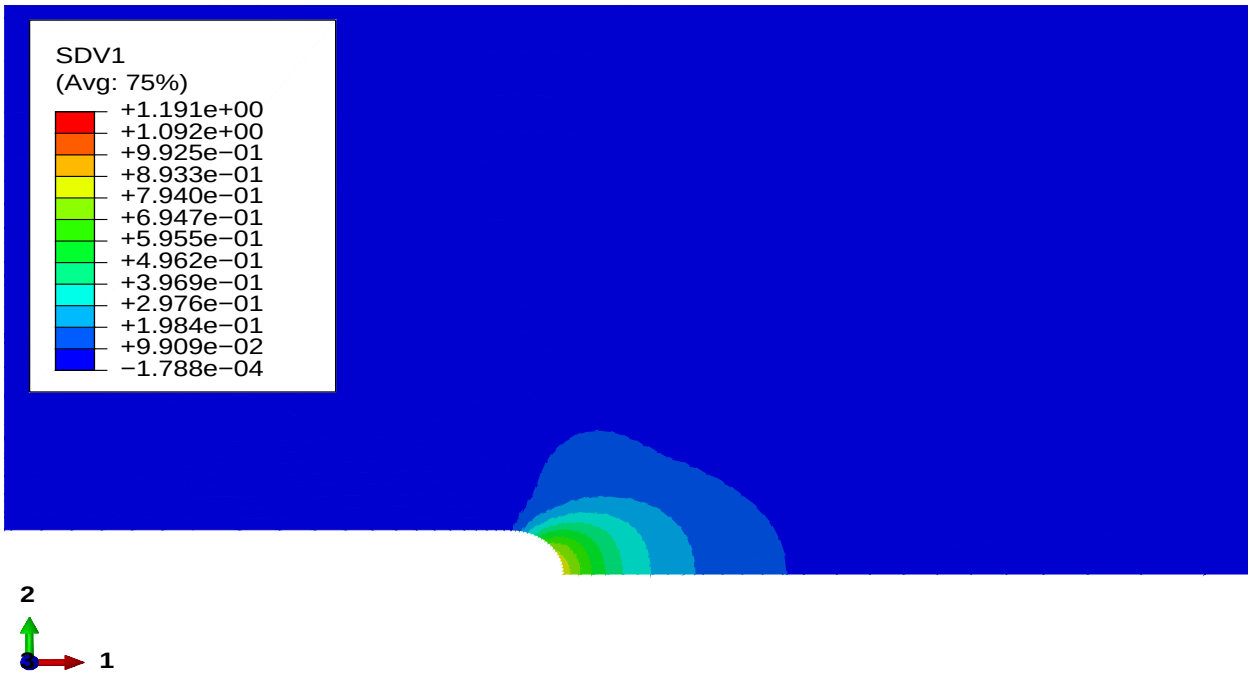

(b) Gurson

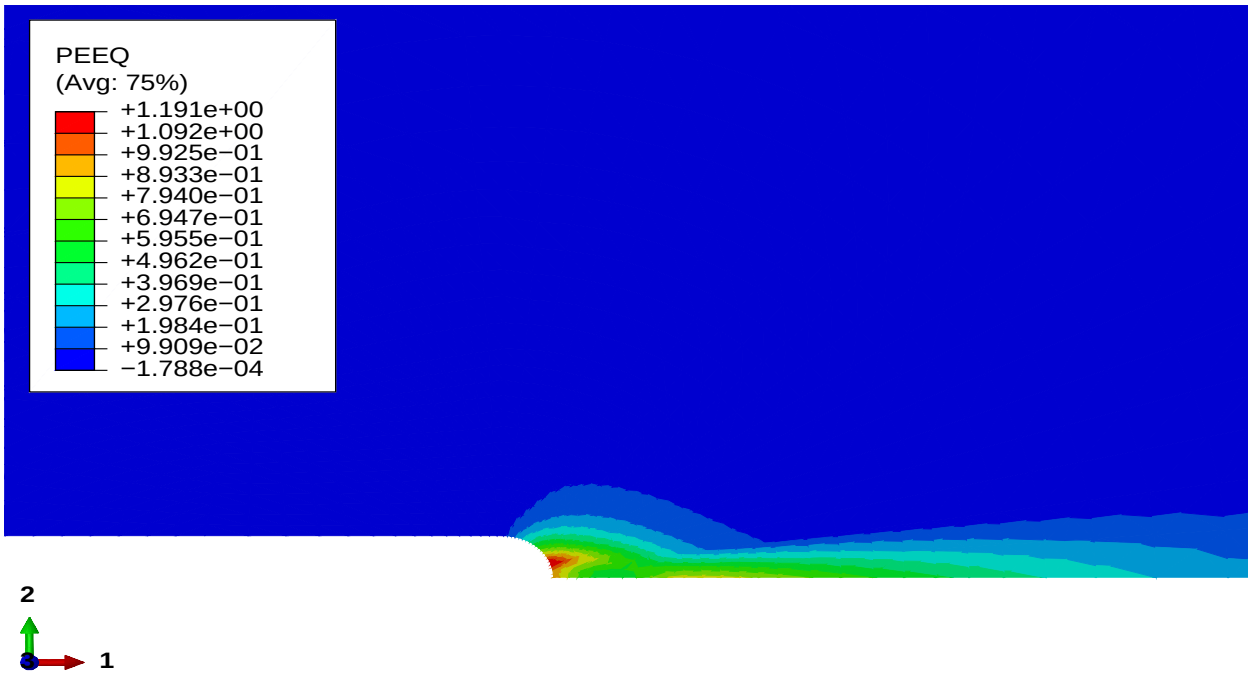

Figure 6.18: Contour plots of the equivalent plastic strain $\bar{\varepsilon}^p$ for both local models at the maximum load level $K1 = 36.11$.

(a) Anisotropic

(b) Gurson

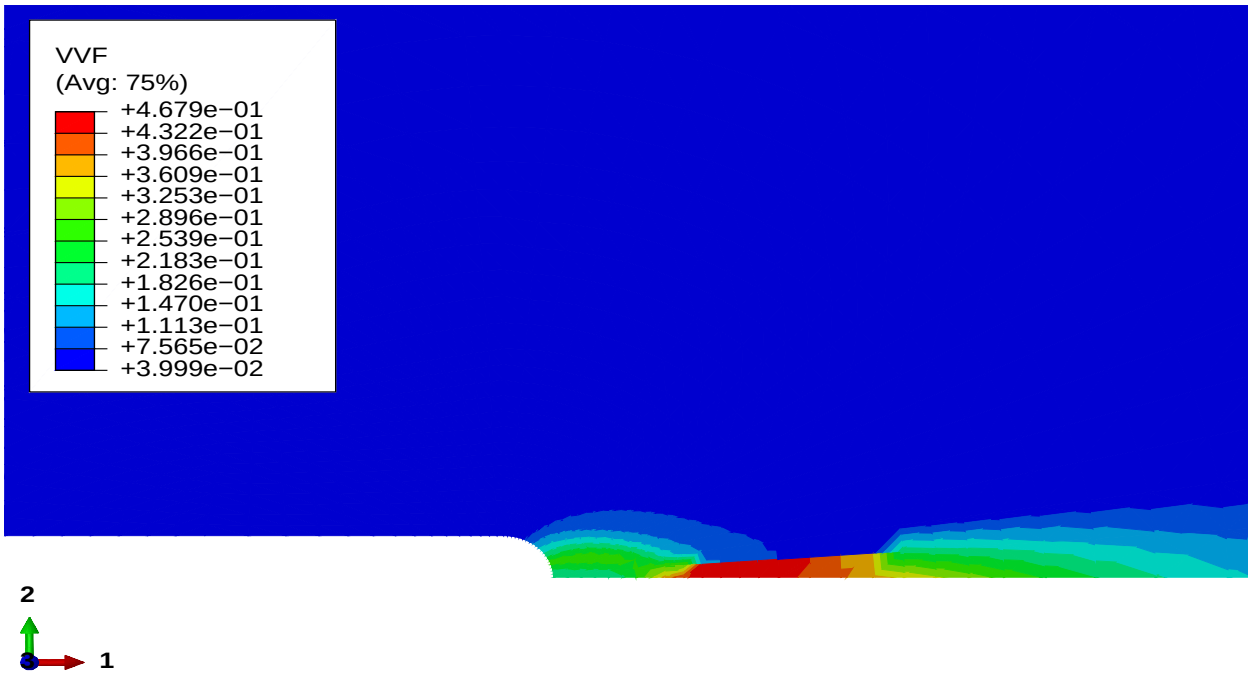

Figure 6.19: Contour plots of the local porosity f_{loc} for both local models at the maximum load level $K1 = 36.11$.

models, and is in qualitative agreement with the results obtained by Aravas and Ponte Castañeda in [7]. As Figures 6.12a-6.16a suggest, the former model predicts that the most critical stress state is at a close distance from the tip of the crack while porosity and plastic deformation are at their maximum precisely at the crack's root for all load levels. This implies that damage initiation will take place at the beginning of the semi-circular notch and will propagate along the path ahead of the blunt crack. On the other hand, Figures 6.12b-6.16b show that the corresponding crack initiation and propagation mechanism is different for the local Gurson model. In that case, at maximum load level, porosity reaches a peak close but ahead of the crack's tip while $\bar{\varepsilon}^p$ also increases in the region as a consequence of the severe plastic deformation that emerges. Moreover, both pressure and σ_{22} undergo a major decrease at the area due to loss of a portion of the stress-carrying capacity of the material while the critical stress state now develops at some distance from the crack's root. This severe local increase in pressure combined with a drastic drop of σ_{eq} create high stress triaxiality conditions[3] in the region, an observation which implies that a secondary crack might emerge ahead of the initial crack. Thus, the local Gurson model predicts that damage propagation will take place by a multiple crack initiation and coalescence mechanism. The aforementioned differences in material response between the local models can also be verified from the contours of the equivalent plastic strain $\bar{\varepsilon}^p$ and local f_{loc}, for the region near the root of the semi-circular notch, which are shown in Figures 6.18, 6.19.

The situation is entirely different for the nonlocal anisotropic and Gurson models where

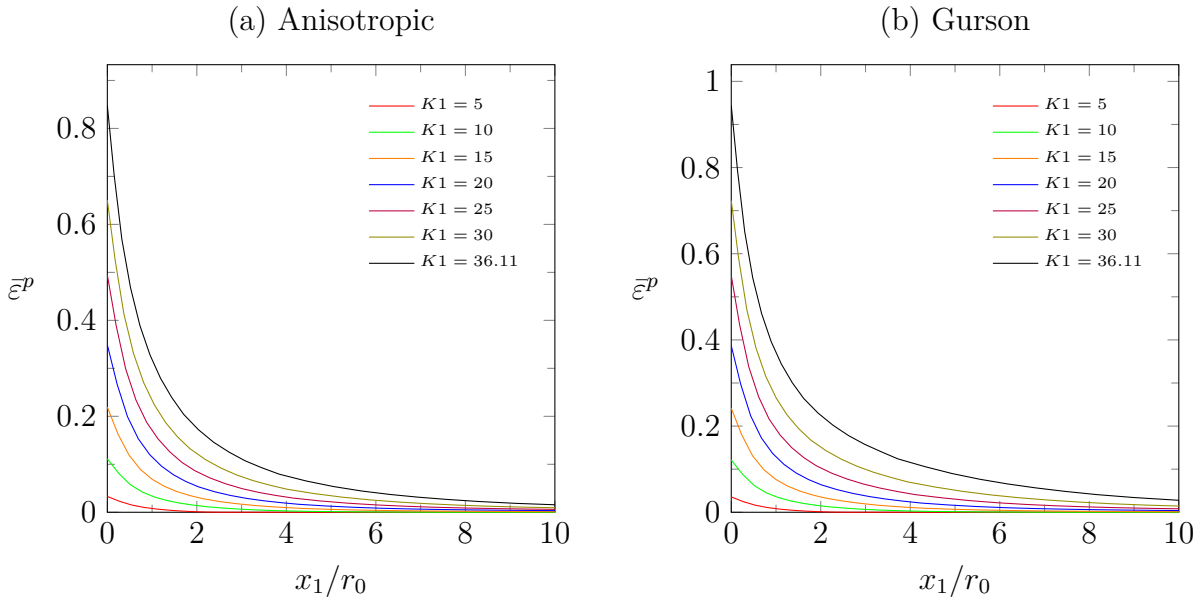

Figure 6.20: $\bar{\varepsilon}^p$ distribution ahead of the crack's tip at different load levels for the nonlocal (a) Anisotropic, (b) Gurson model.

[3]Recall here that the stress triaxiality factor X_Σ, which is defined as the quotient of hydrostatic stress and an appropriate stress norm (usually the von Mises equivalent stress), gives a qualitative estimate about the stress state at a specific point.

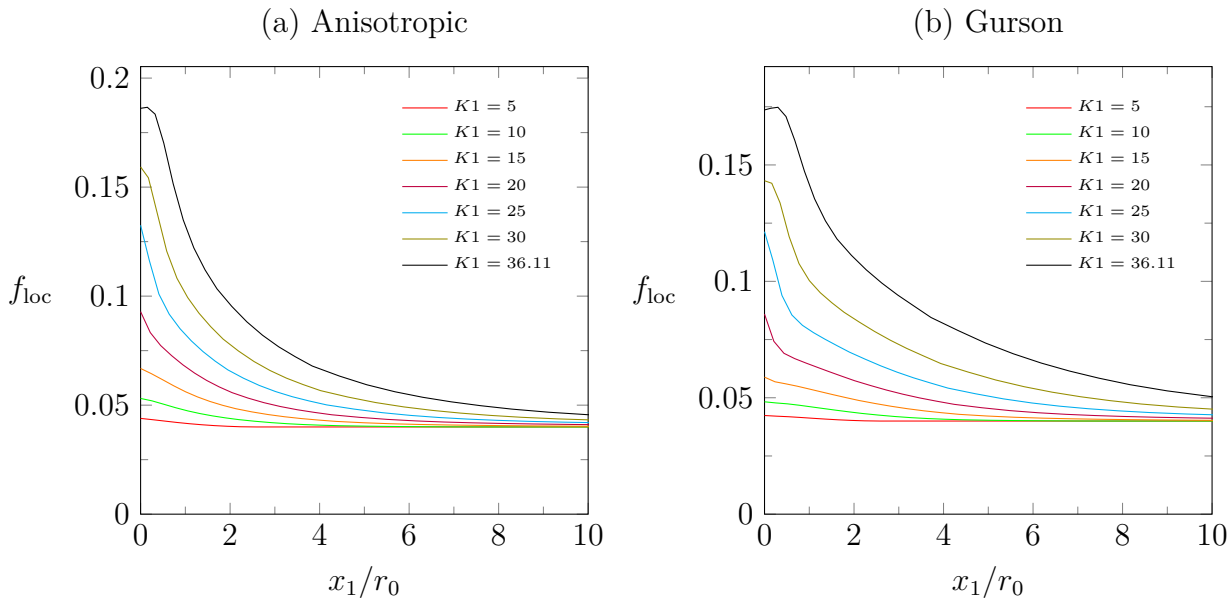

Figure 6.21: f_{loc} distribution ahead of the crack face at different load levels for the nonlocal (a) Anisotropic, (b) Gurson model.

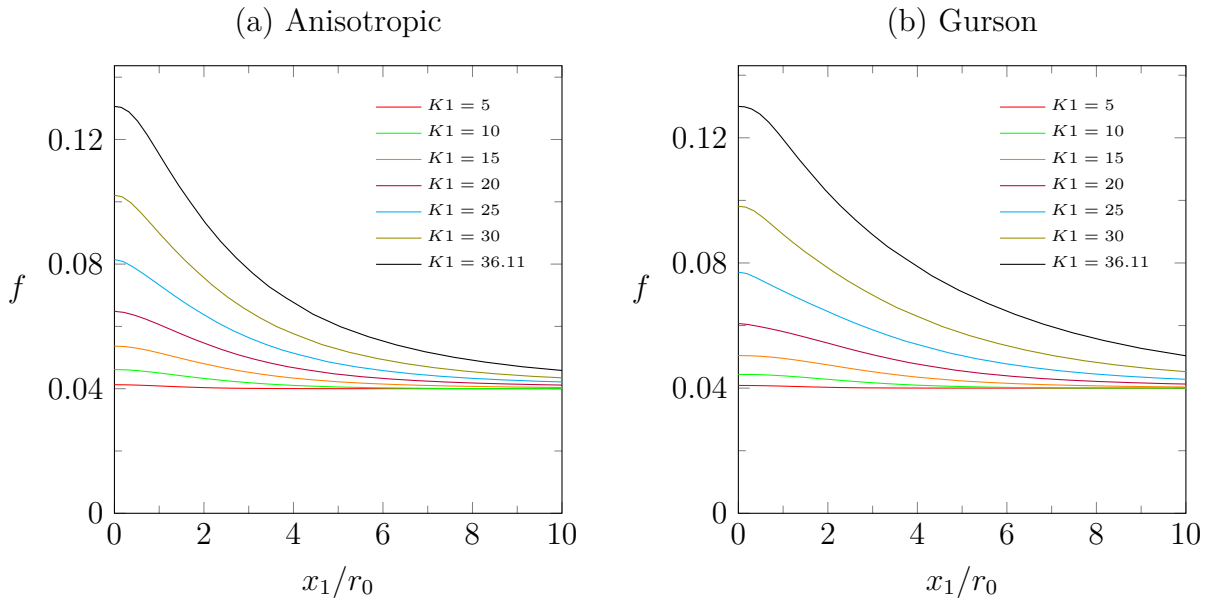

Figure 6.22: f distribution ahead of the crack face at different load levels for the nonlocal (a) Anisotropic, (b) Gurson model.

regularization has been used. The corresponding results are shown in Figures 6.20 through 6.28. Again, Figures 6.20-6.25 illustrate the plots along the path ahead of the blunt crack's root for the same variables as with the local models, with the addition of the 'path plot' for the distribution of the nonlocal porosity f. The first important thing one can observe here is that now, there exists a qualitative agreement in the form of the solution, which is similar for both models and for all load levels. To be precise, both the gradient anisotropic and the gradient Gurson model predict that porosity reaches its maximum value at the tip of the

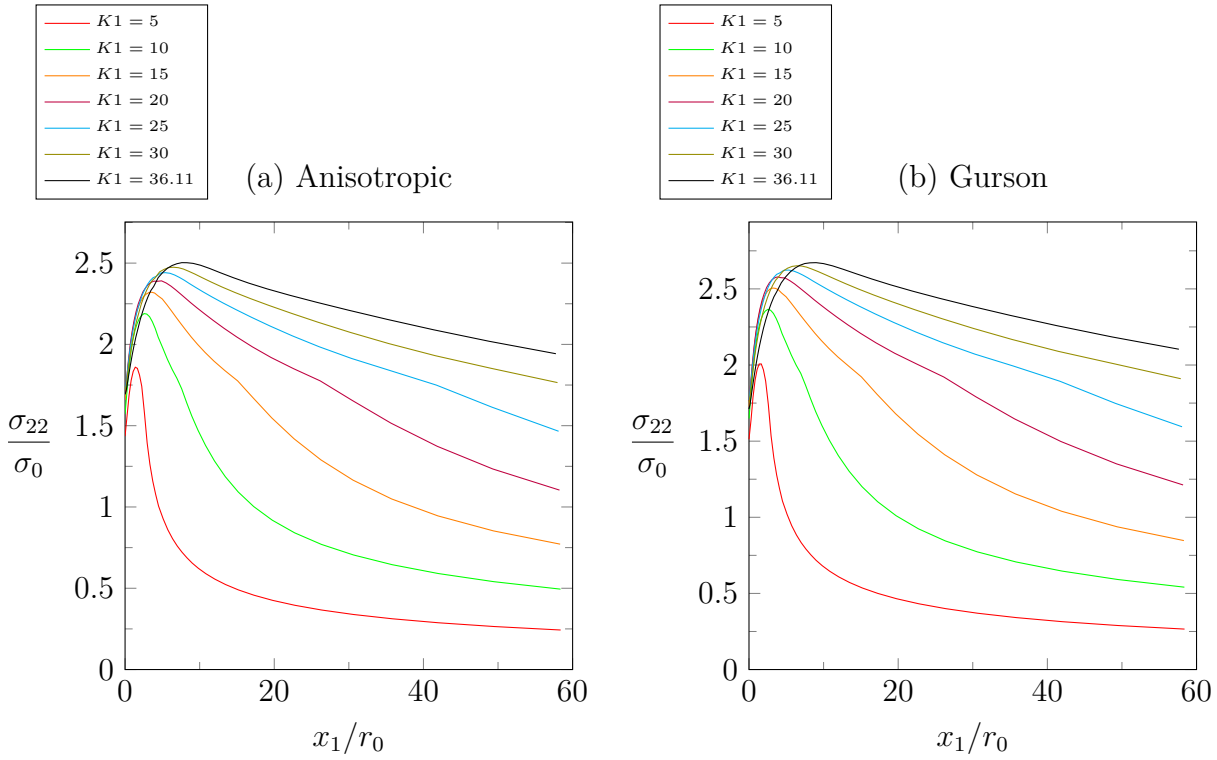

Figure 6.23: Normalized σ_{22} stress distribution ahead of the crack face at different load levels for the nonlocal (a) Anisotropic, (b) Gurson model.

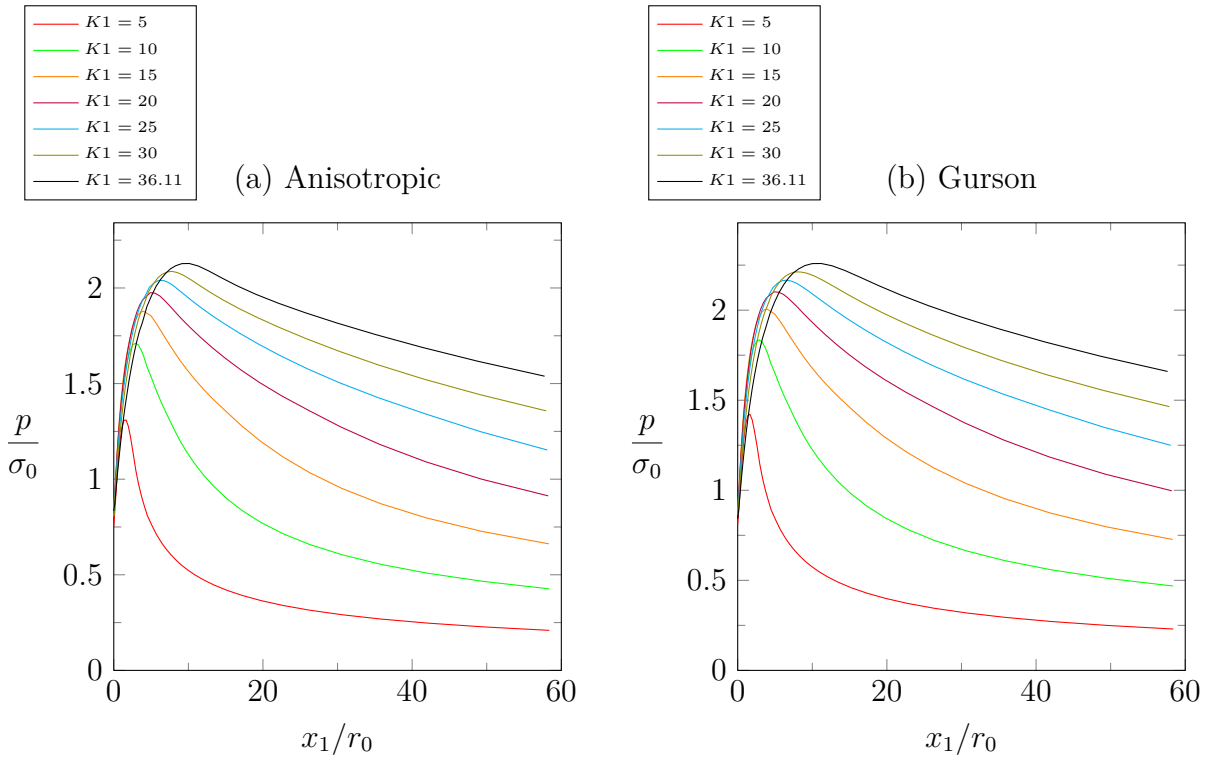

Figure 6.24: Normalized pressure distribution ahead of the crack face at different load levels for the nonlocal (a) Anisotropic, (b) Gurson model.

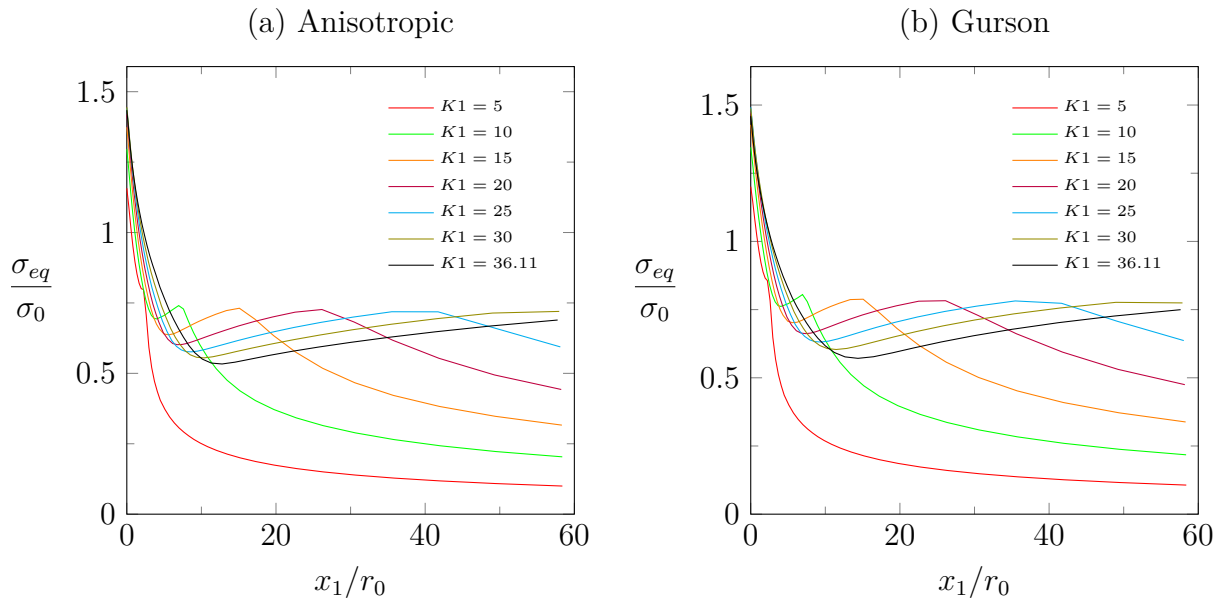

Figure 6.25: Normalized von Mises equivalent stress distribution ahead of the crack face at different load levels for the nonlocal (a) Anisotropic, (b) Gurson model.

crack where, as a consequence, the equivalent plastic strain $\bar{\varepsilon}^p$ is also maximum. Additionally, in view of the values of p and σ_{eq} at a short distance ahead of the crack, one can also deduce that high triaxiality conditions are present near the crack's root. Finite element analyses carried out for values of ℓ higher than unity also exhibited the same qualitative behavior. Thus, the regularized models predict that damage will initiate from the crack's root and will propagate ahead of the crack in similar manner, which is in fact a more realistic prediction of the procedure of ductile fraction compared to the one given by the local Gurson model. This can be attributed to the fact that, since regularized models are objective, in the sense that a sufficient and proper discretization will lead to the unique solution, predictions made by such models can be considered more valid compared to any local model. The corresponding contour plots for $\bar{\varepsilon}^p$, f_{loc} and f at the tip's region that verify the aforementioned remarks are presented in Figures 6.26-6.28. Furthermore, proper functionality of the gradient models can be verified from the fact that the nonlocal porosity f takes lower values compared to f_{loc} as expected, since the nonlocal variable f takes into account not only the high levels of porosity near the crack's tip but values of f_{loc} in a region determined by the characteristic length ℓ of the material. Also, comparison of the f_{loc} distributions between the corresponding local and nonlocal models reveals that the gradient models predict in general lower porosity values than their local counterparts, an observation which is probably a result of the more smooth solution predicted through regularization.

Finally, the assumption of 'small scale yielding' is validated, for the analyses presented above, from the contour plots shown in Figure 6.29 which illustrate the size of the plastic region at the maximum load, for the nonlocal models (the plastic zone is of the same size in the local models as well), since they reveal that the length of the plastic zone, in both planar directions, is smaller than 10% of the outer radius R of the boundary layer.

(a) Anisotropic

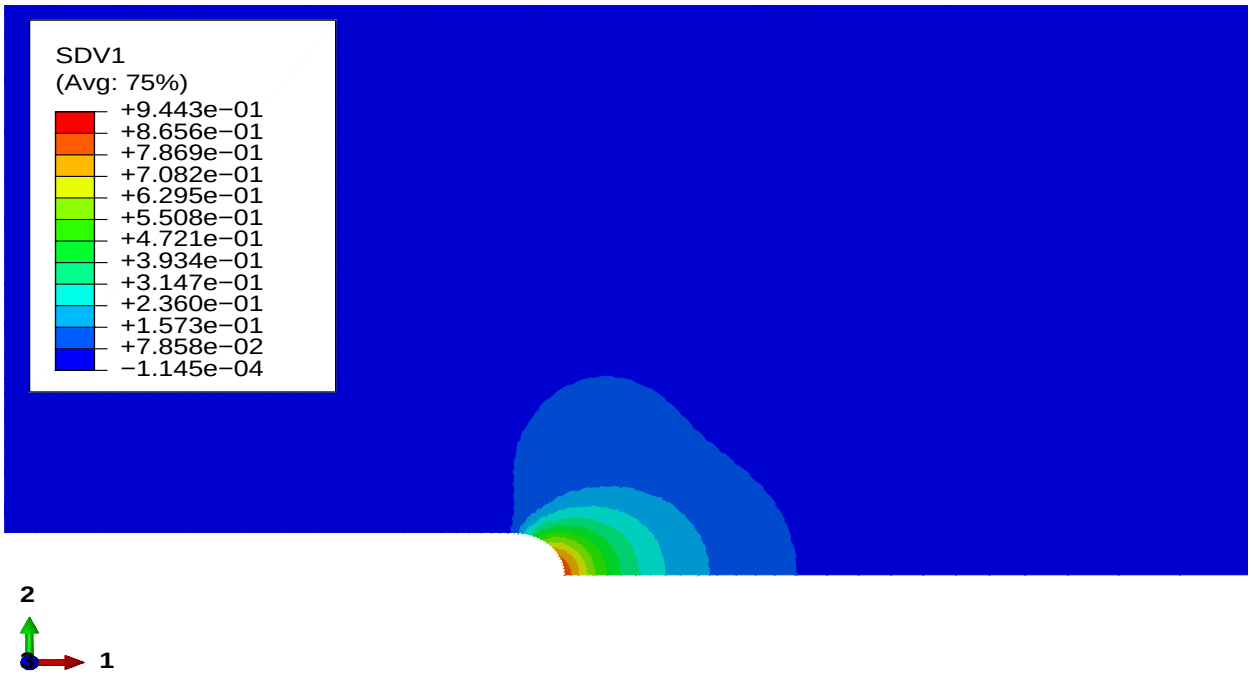

(b) Gurson

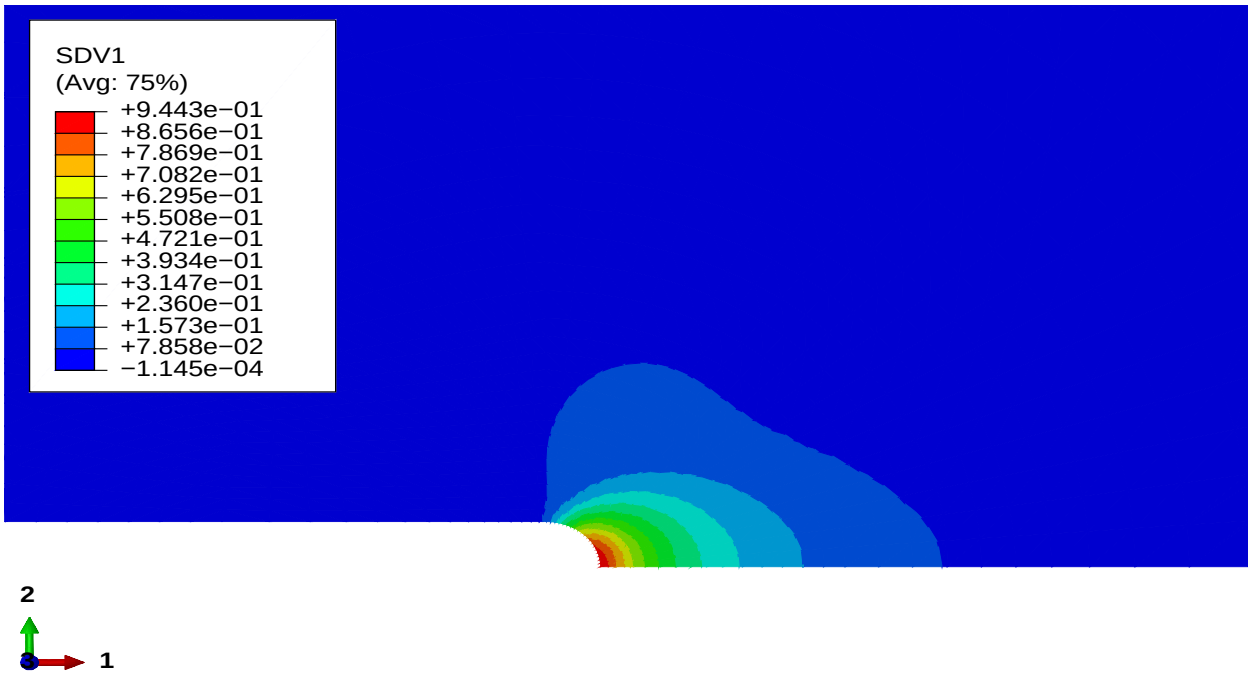

Figure 6.26: Contour plots of the equivalent plastic strain $\bar{\varepsilon}^p$ for both nonlocal models at the maximum load level $K1 = 36.11$.

(a) Anisotropic

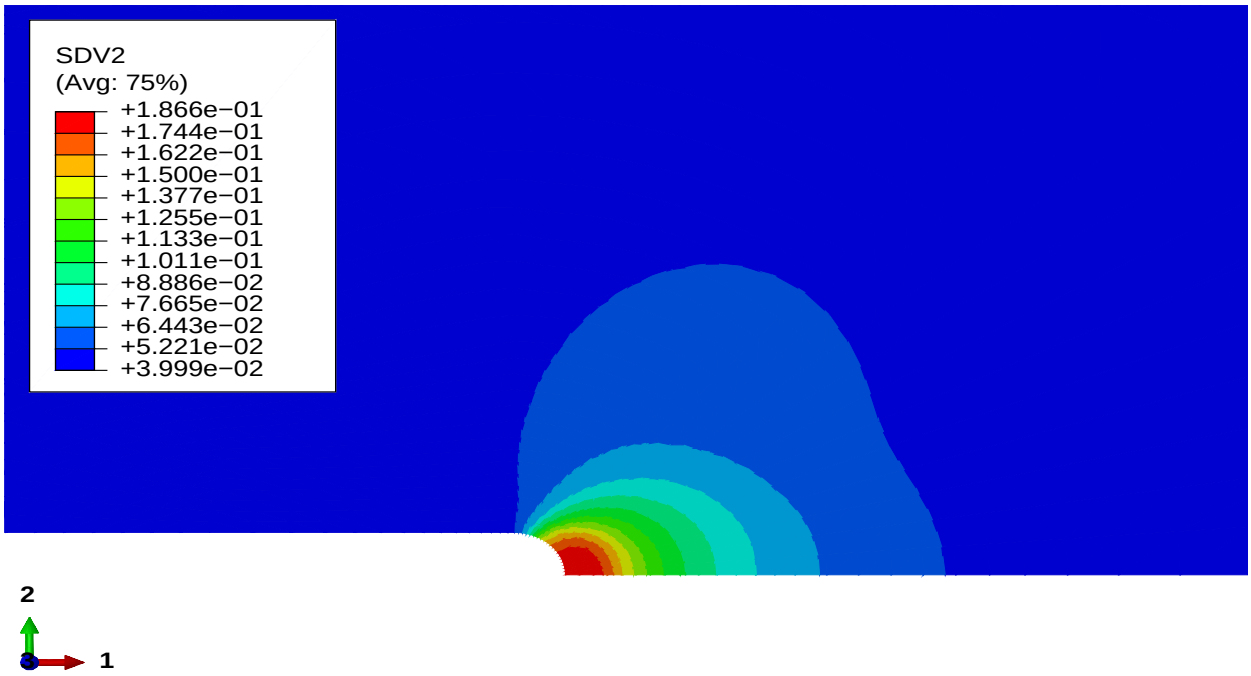

(b) Gurson

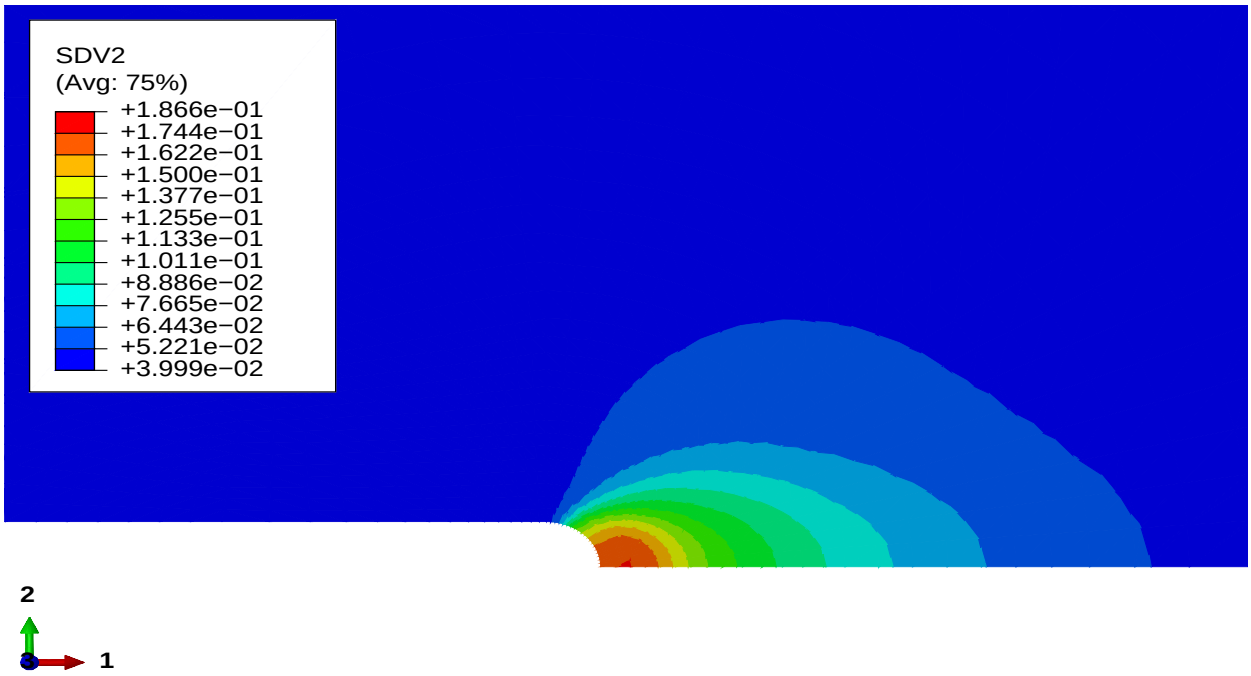

Figure 6.27: Contour plots of the local porosity f_{loc} for both nonlocal models at the maximum load level $K1 = 36.11$.

(a) Anisotropic

(b) Gurson

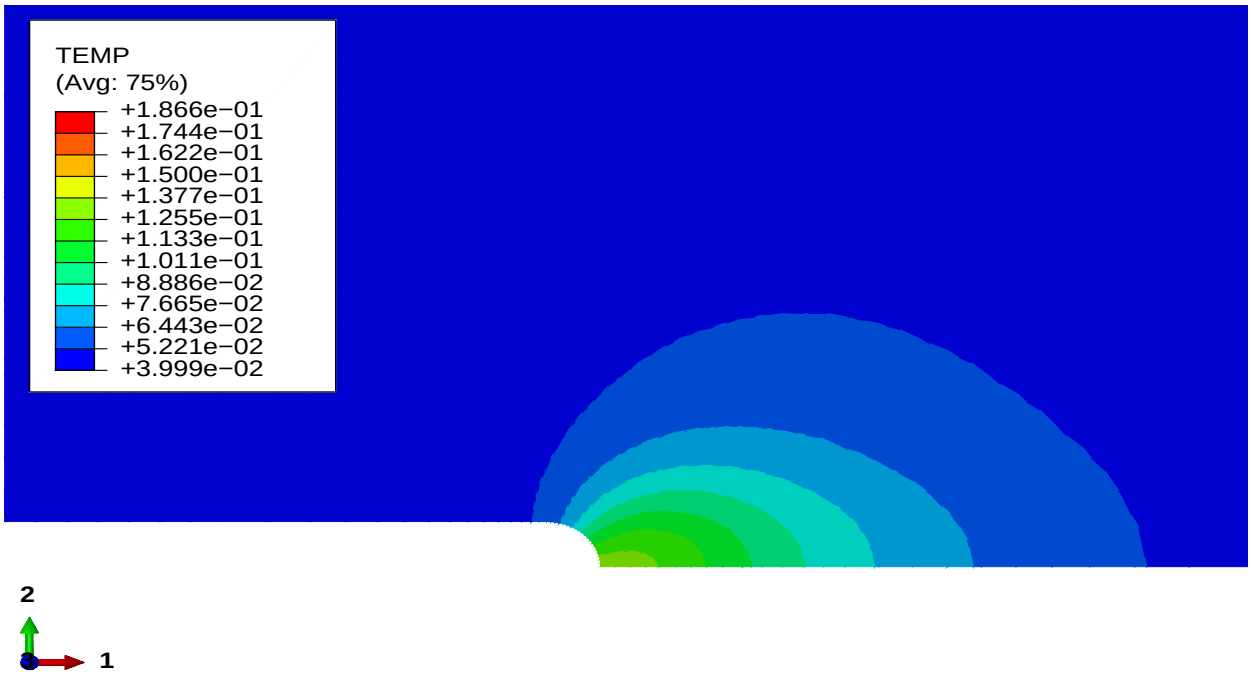

Figure 6.28: Contour plots of the nonlocal porosity f for both nonlocal models at the maximum load level $K1 = 36.11$.

(a) Anisotropic

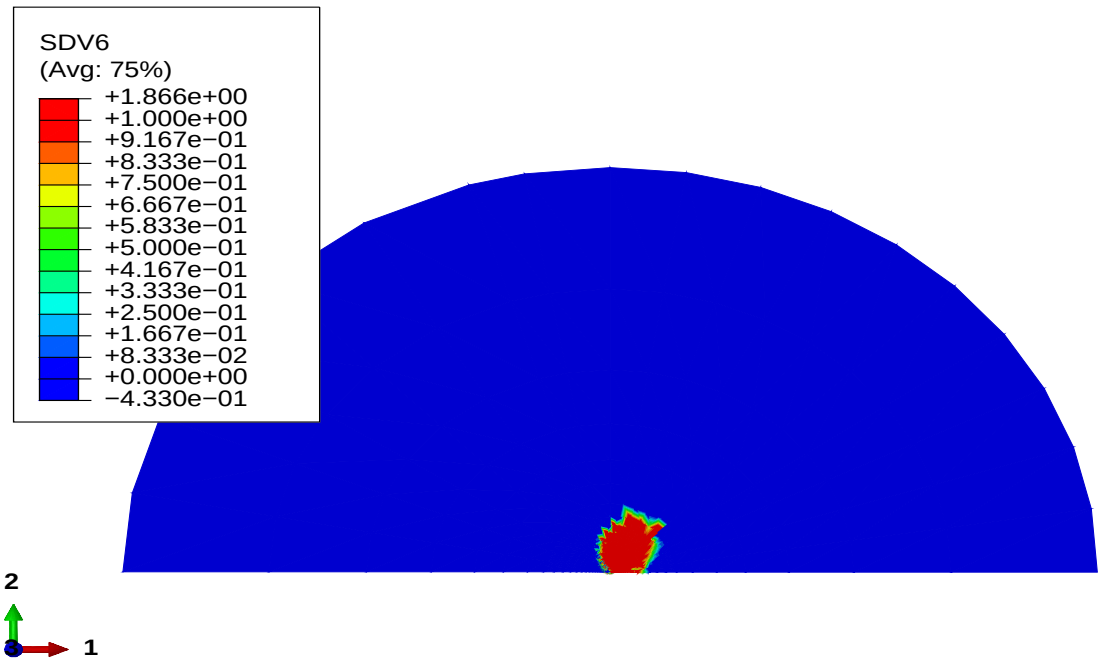

(b) Gurson

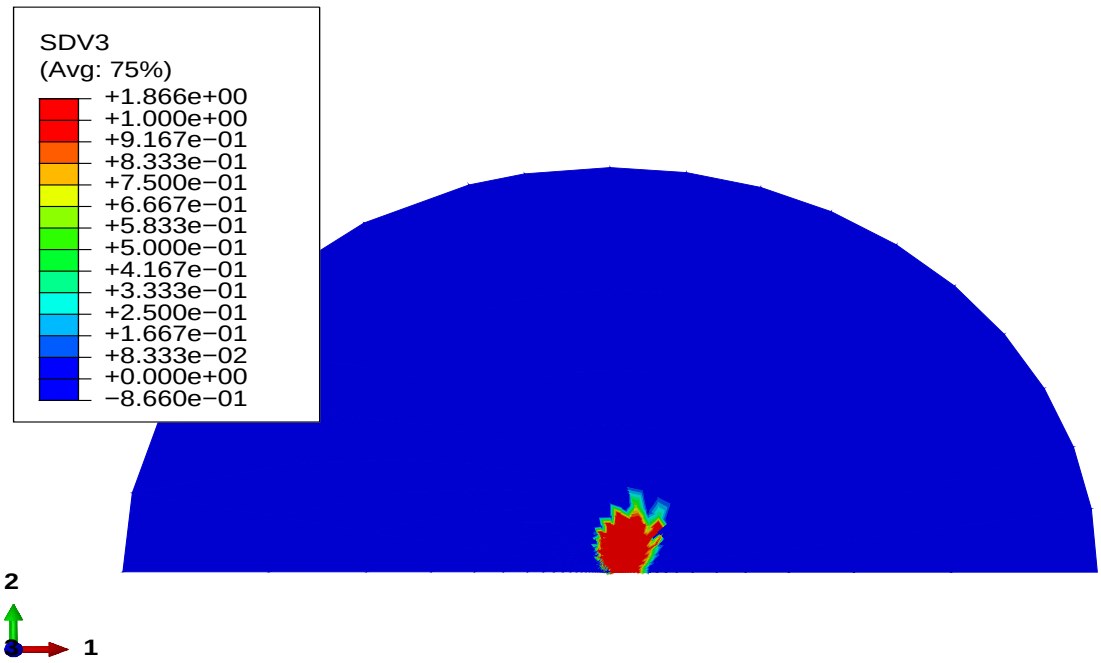

Figure 6.29: Contour plots of the plastic zone (red region) for both nonlocal models at the maximum load level $K1 = 36.11$.

6.3 The Charpy V-notch Test

In this section, a series of finite element analyses were carried out for the simulation of the well known Charpy V-notch energy (CVN) test. The CVN impact test is an experimental method that is usually utilized, among other methods, for the approximate evaluation of the

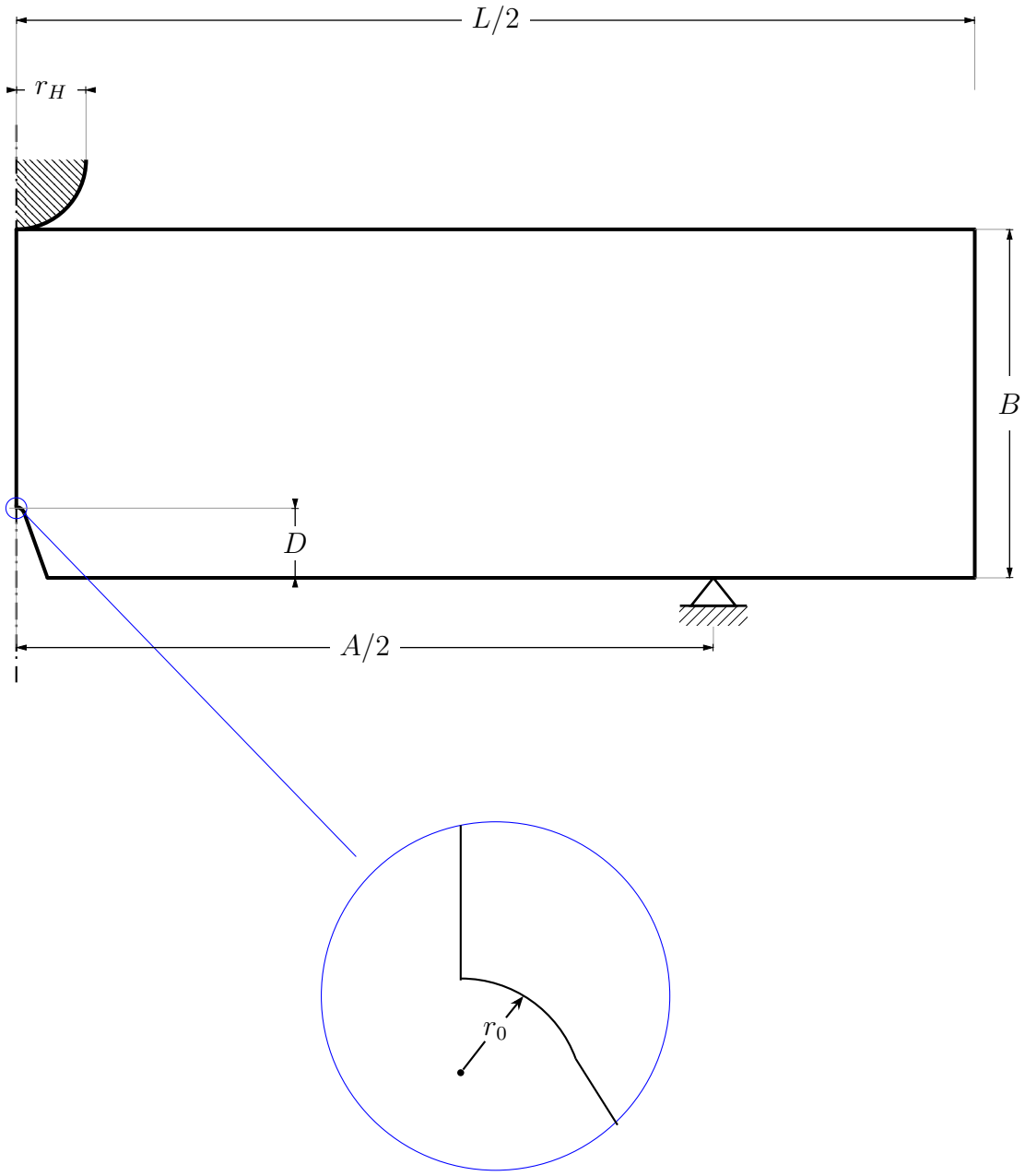

Figure 6.30: Dimensions, geometry and boundary conditions of the Charpy test specimen and the 'hammer' used in the simulations. For this series of numerical calculations $L = 55\ mm$, $B = 10\ mm$, $A = 40\ mm$, $D = 2\ mm$, $r_0 = 0.25\ mm$ and $r_H = 2\ mm$. Due to symmetry, only half of the billet is analysed.

toughness as well as the ductile-brittle transition temperature of a given material. To be precise, the test involves striking a notched specimen of standardized dimensions with a

swinging pendulum of known mass and length that has a sharp edge, which is also known as the 'hammer'. Although the method is cost efficient and relatively easy to implement, nonetheless, mostly rough qualitative results can be deduced and no theoretical correlation between the mechanisms of crack initiation and propagation and structural design parameters can be established [74]. The problem of ductile fracture under plain strain conditions is once more studied by conducting a series of finite element analyses using both the classical and the nonlocal anisotropic model. Additionally, since the actual CVN may be conducted both in a quasi-static (slow-bending loading) or dynamic (fast hammer impact) manner, both static and dynamic analyses were performed for the investigation of the inertial term's effect on the process. Some calculations were also carried out by using the corresponding local and nonlocal Gurson models. Geometry and dimensions of the Charpy specimen that was used herein as well as the material constants that were employed for all relevant calculations are illustrated in Figure 6.30 and Table 6.3 respectively, and are the same as the ones used by Tvergaard and Needleman in [85].

Table 6.3: Normalized material properties used for the Charpy problem simulations.

E	ν	σ_0	n	f_N	ϵ_N	s_N
$500\sigma_0$	0.3	1	10	0.04	0.3	0.1

The finite element mesh that was used for all simulations consists of 4732 elements and is presented in Figure 6.31. Initially, the specimen was intended to be void free (i.e., $f_{\text{loc}}|_0=$

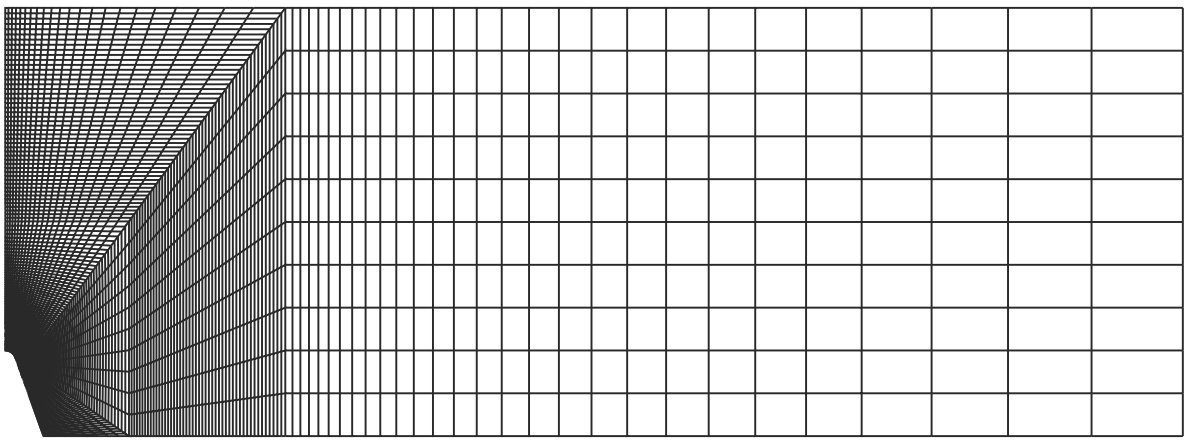

(a)

$f_0 = 0$) but due to numerical issues in view of division with zero in the evaluation of 4.6, initial porosity was set to the very small value of 5×10^{-4}. Furthermore, in order to account for the final material failure, the modification for the local porosity first introduced by

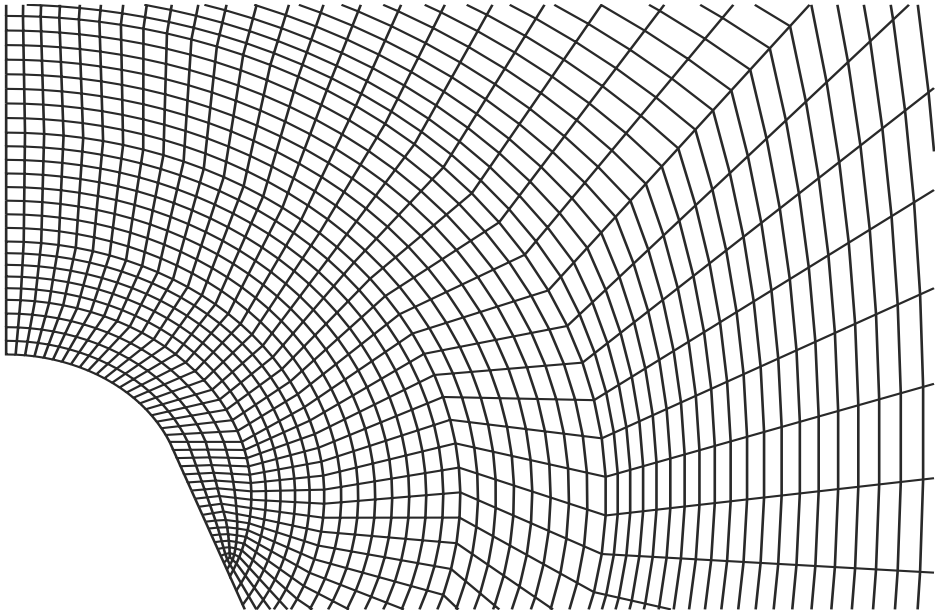

(b)

Figure 6.31: Finite element mesh used for the Charpy test; (a) Discretization for the whole specimen that was analyzed, (b) Near-notch mesh.

Tvergaard and Needleman in [82] is used in the calculations, i.e.,

$$f^{\star}_{\text{loc}}(f_{\text{loc}}) = \begin{cases} f_{\text{loc}} & , \text{ for } f_{\text{loc}} \leq f_C \\ f_C + \dfrac{f^{\star}_U - f_C}{f_F - f_C}(f_{\text{loc}} - f_C) & , \text{ for } f_{\text{loc}} > f_C \end{cases} \tag{6.5}$$

where f_C is the critical porosity value after which the modification is physically relevant, $f^{\star}_U$ is the ultimate value at which all stress-capacity of the material is lost and f_F is the void volume fraction at fracture. For this series of calculations $f_C = 0.15$, $f_F = 0.25$ and $f^{\star}_U = 0.67$ are selected.

6.3.1 Effect of Nonlocality for the Quasi-Static CVN Test

In this section, finite element results for the quasi-static analyses that were carried out both for the anisotropic and Gurson's models are examined. A characteristic length $\ell = 1$ was selected for all analyses concerning the nonlocal models.

To begin with, results concerning the local models are presented in Figures 6.32 through 6.37. Figure 6.32 shows the normalized load - nominal 'axial' strain curve for both local models, where the normalized load is defined as in 6.3_1 with $A = Ht$ and the nominal strain is given as $\varepsilon = u_2/H$, with u_2 being the vertical displacement of the 'hammer'. The thickness of the specimen t is once again unity for the plain strain condition problem. Although the direction of loading, and the corresponding displacement, are in the opposite direction of the positive X_2-axis, absolute values are presented herein as a matter of convenience. It is

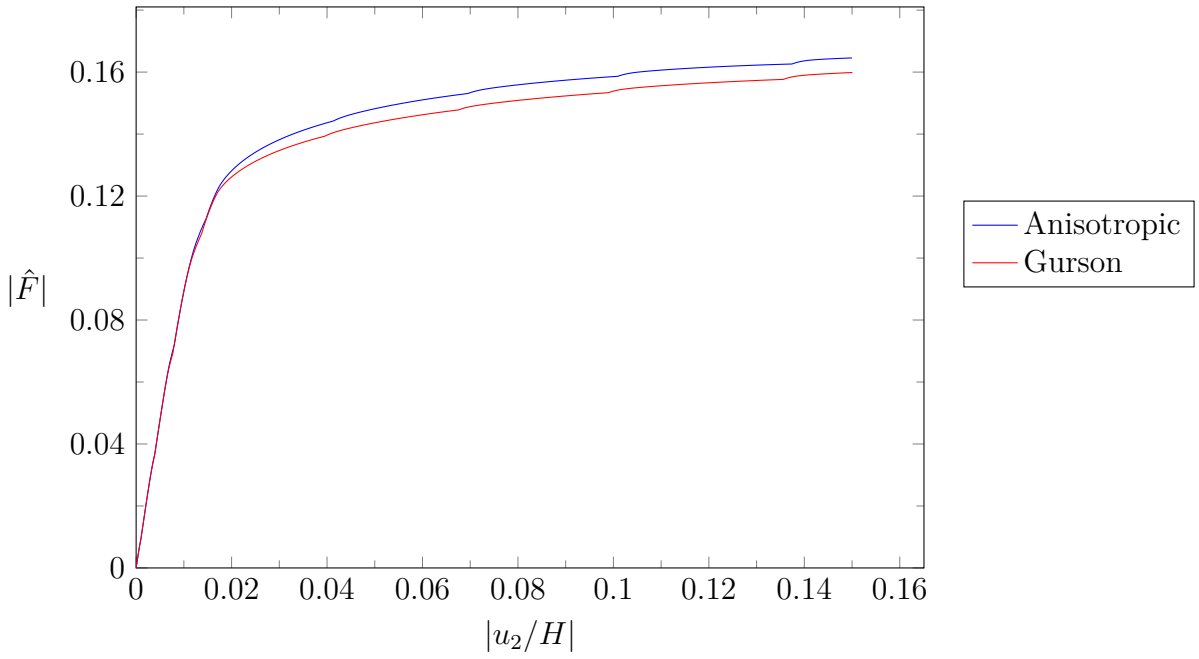

Figure 6.32: Normalized load vs nominal 'axial' strain for the local ($\ell = 0$) models up to a nominal strain $|\varepsilon| = 0.15$

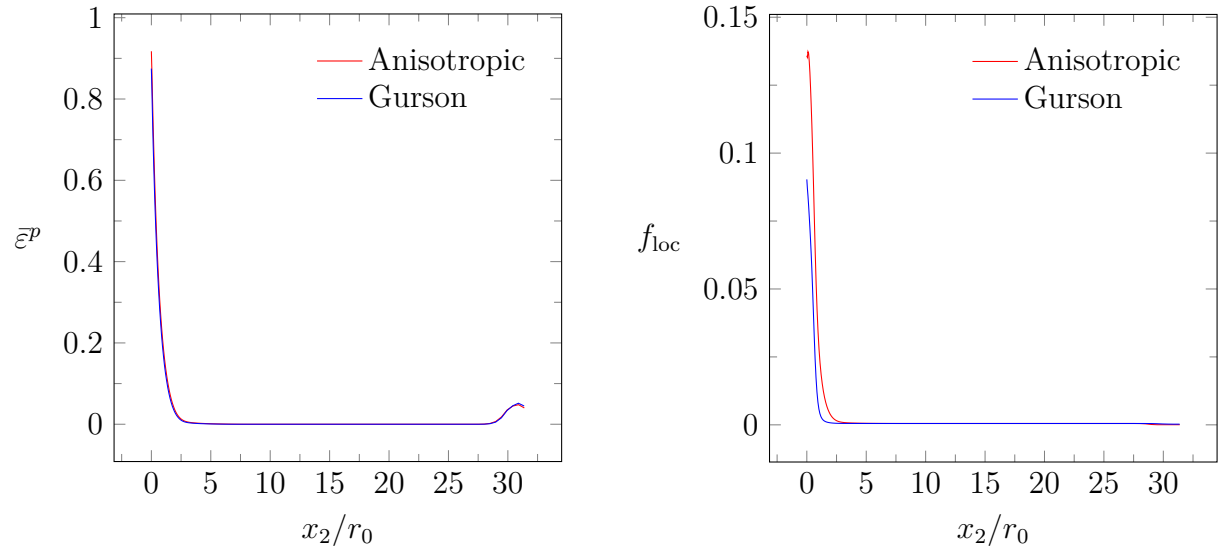

Figure 6.33: $\bar{\varepsilon}^p$ and f_{loc} distributions along the left side of the specimen at a nominal strain of 9%.

interesting to note here that the local anisotropic model seems to predict a more 'stiff' material behavior compared to the local Gurson model, which in turn implies that slightly higher loads are necessary for the initiation and propagation of the fracture mechanism. From an energetic perspective, one can also postulate that since the area under the anisotropic curve is slightly larger than the corresponding one of Gurson's model, the material governed by the anisotropic model can absorb slightly more energy before fracture occurs. Figures 6.33, 6.34 illustrate the variation of equivalent plastic strain $\bar{\varepsilon}^p$, local porosity f_{loc}, hydrostatic stress

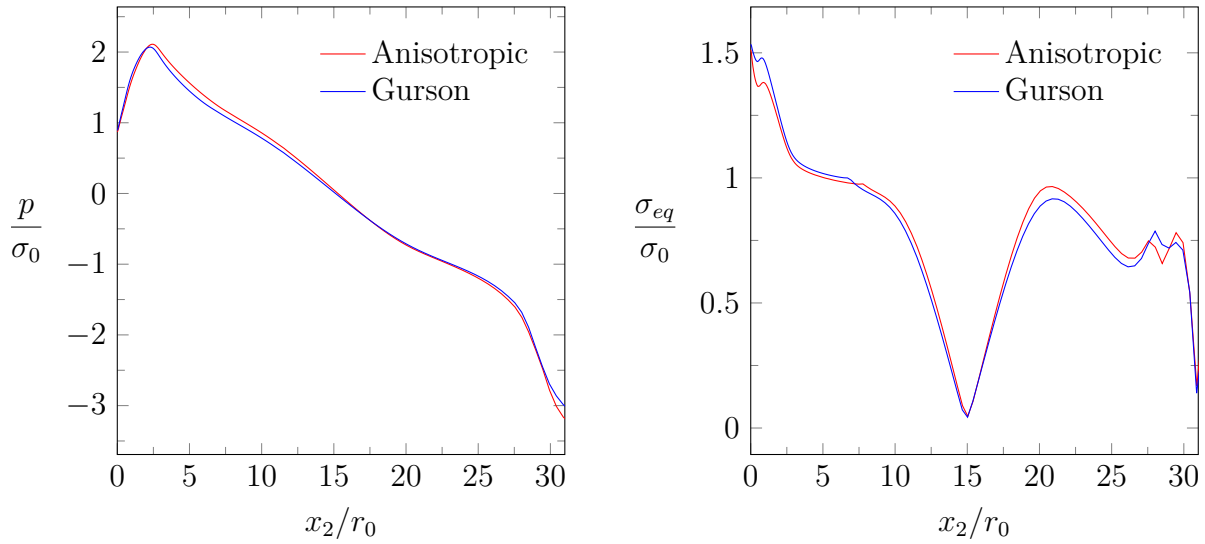

Figure 6.34: Normalized hydrostatic and von Mises equivalent stress distributions along the left side of the specimen at a nominal strain of 9%.

p and von Mises equivalent stress σ_{eq} along the crack's edge, where x_2 denotes the distance of a material point from the root of the notch. Up to this point of deformation, predictions of both models concerning the stress state that develops, seem to agree. A difference can be found in the porosity distribution at the crack's tip, which is higher for the anisotropic rather than the Gurson's model. Moreover, $\bar{\varepsilon}^p$ is also slightly higher for the anisotropic model at the beginning of the crack, which is intuitively expected as the region of higher porosity is consequently characterized by higher plastic strain levels. Nevertheless, in view of the difference in the distribution of f_{loc}, this behavior is, at least partly, in qualitative agreement with the results obtained for the local models in the case of the mode-I blunt crack problem examined in the previous section, for lower load levels. In contrast however to the aforementioned problem, where the local models predict a different damage inititiation and propagation mechanism, in this problem, crack initiation is predicted to begin at the tip of the notch for both models. The latter remarks are also validated in view of the contours of $\bar{\varepsilon}^p$ and f_{loc}, as shown in Figures 6.35, 6.36 for the area near the crack tip. Furthermore, contours of the aspect ratios w_1, w_2 for the anisotropic model shown in Figure 6.37 reveal that, at the tip of the notch, the initially spherical voids tend to become ellipsoids whose major axis is in the X_2-direction, an observation which is intuitively expected since the lower part of the specimen. due to the bending character of the loading, can be considered to be under tension.

The corresponding finite element results for the nonlocal anisotropic and Gurson models are presented in Figures 6.38-6.45. Figure 6.38 shows the normalized load-nominal strain curve for the nonlocal models up to a strain level of 15%. In this case, it is clear that the overall response predicted by the enhanced models is essentially the same for both material models. Moreover, Figures 6.39-6.41 illustrate the 'path plots' along the left edge of the specimen for all relevant variables in a similar manner as for the corresponding local models, with the addition of the plot for the nonlocal porosity f. Firstly, one can note that stress

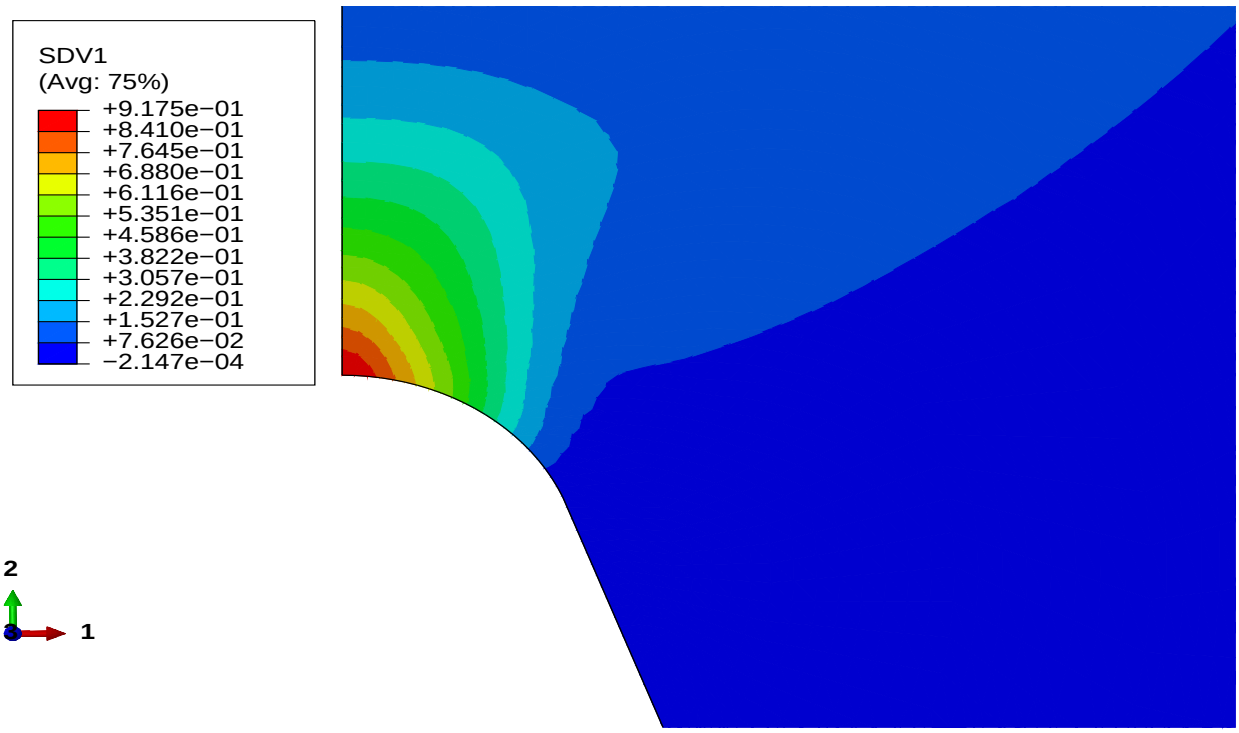

(a) Anisotropic

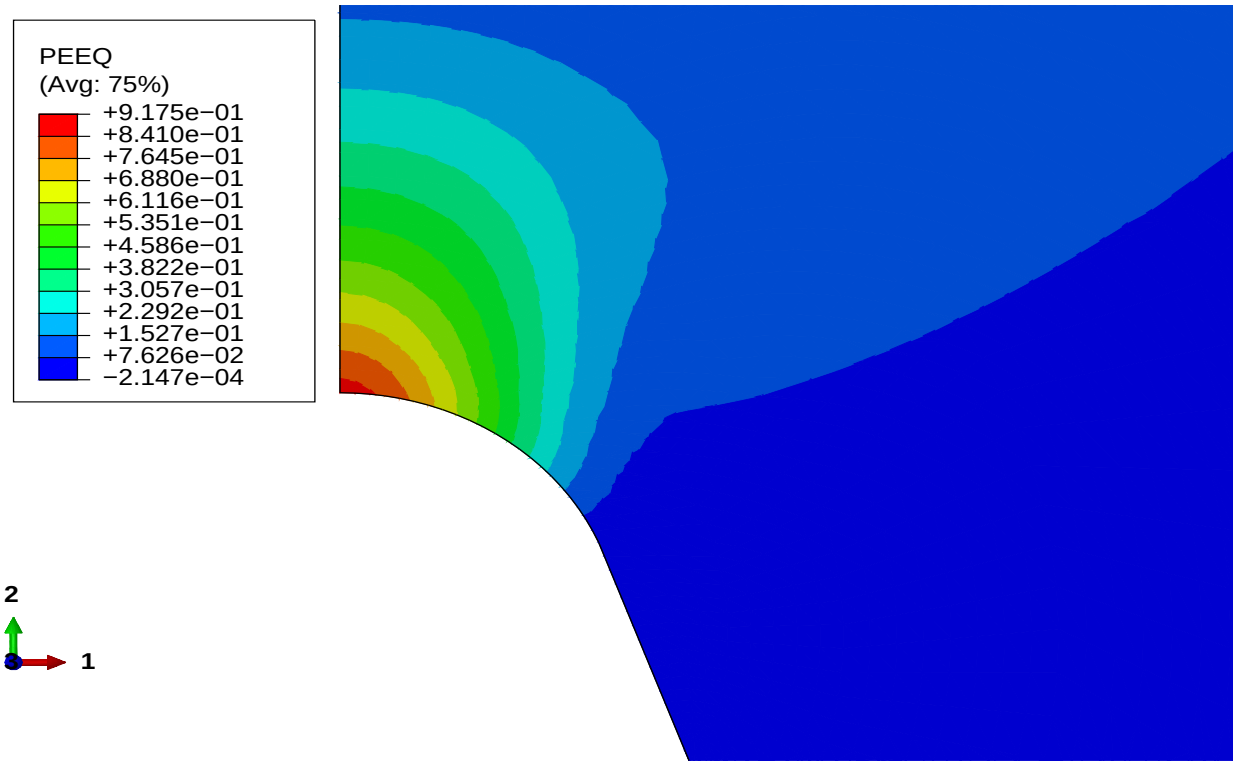

(b) Gurson

Figure 6.35: Contour plots of the equivalent plastic strain $\bar{\varepsilon}^p$ for both local models at a nominal strain of 9%.

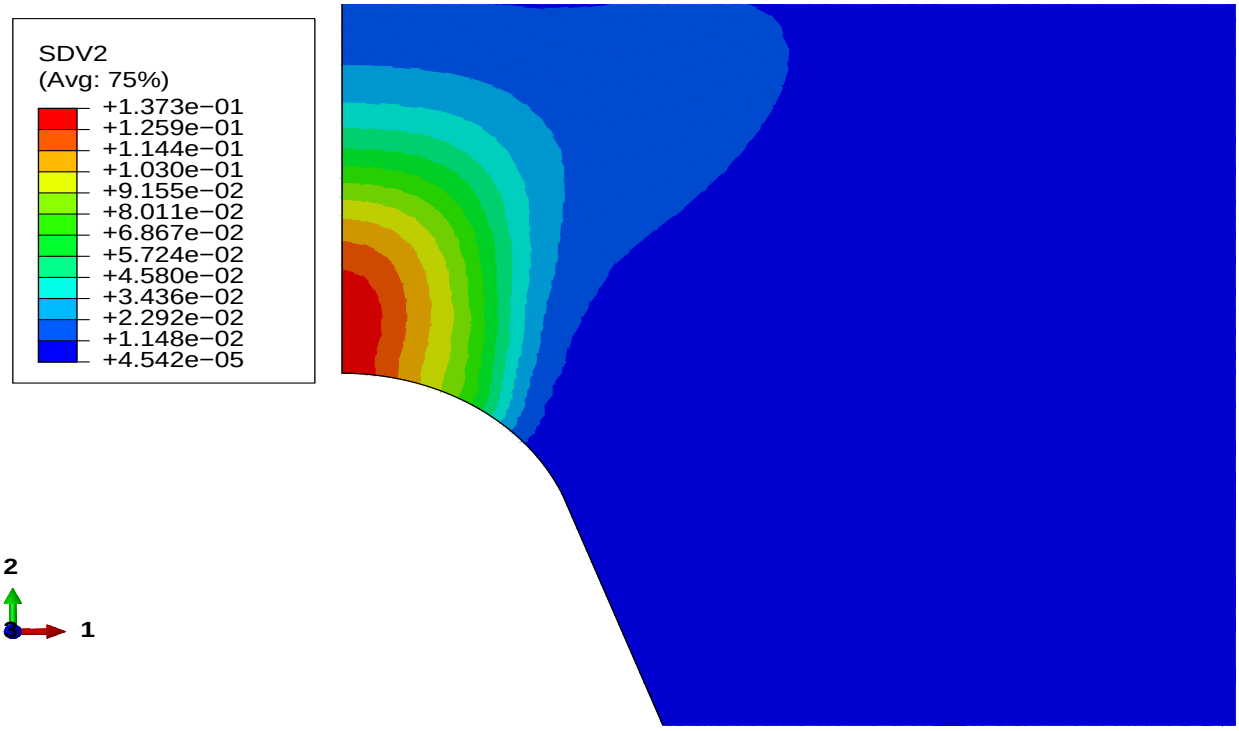

(a) Anisotropic

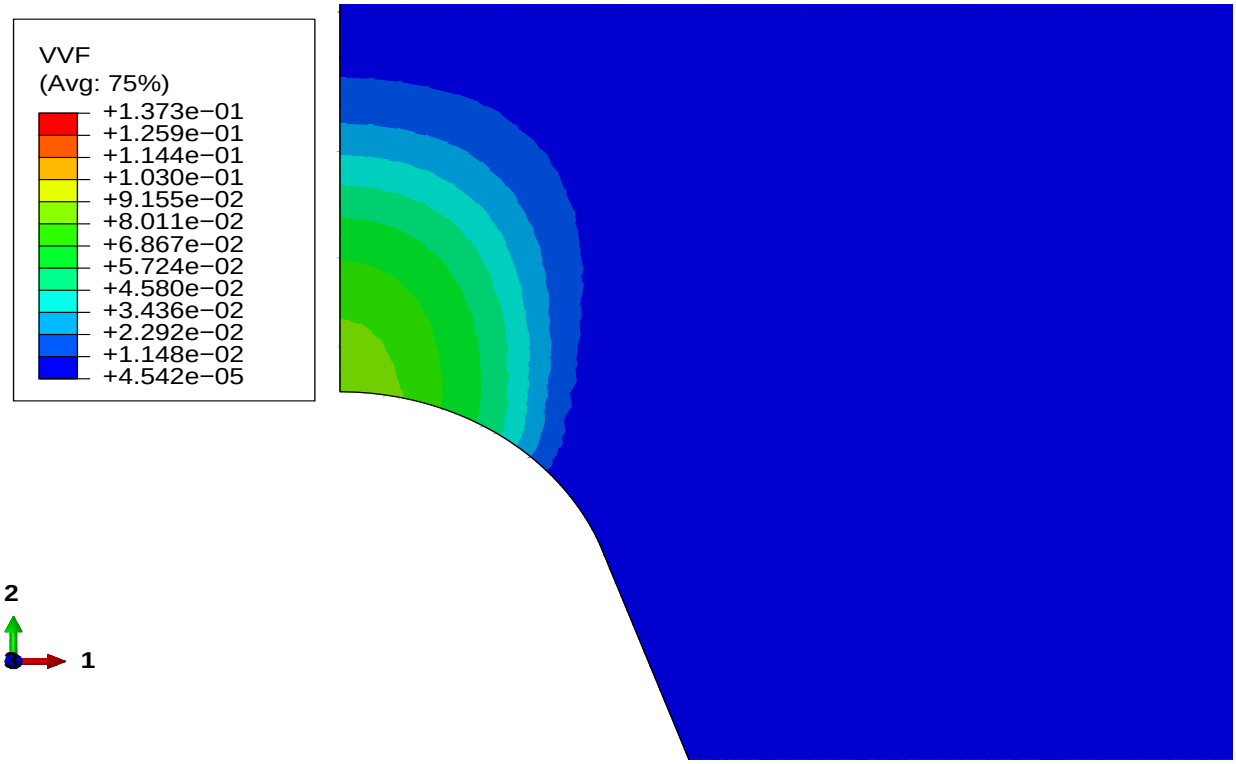

(b) Gurson

Figure 6.36: Contour plots of the local porosity f_{loc} for both local models at a nominal strain of 9%.

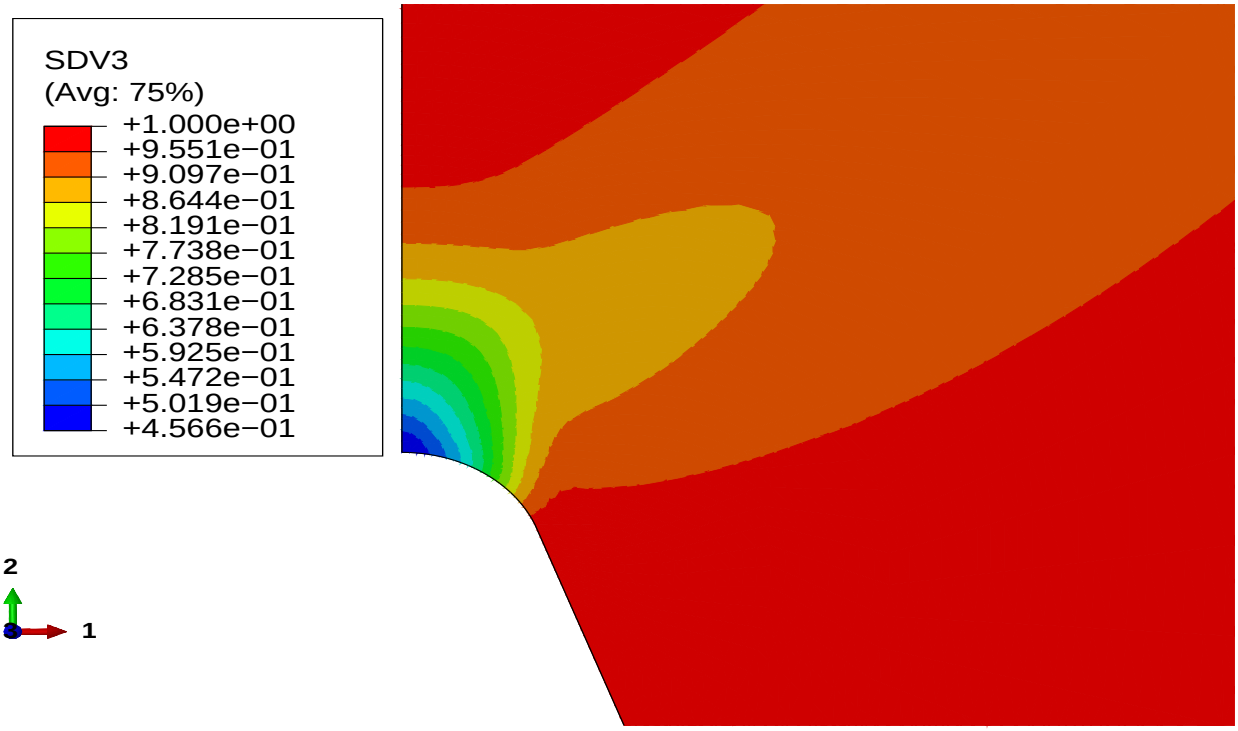

(a) w_1

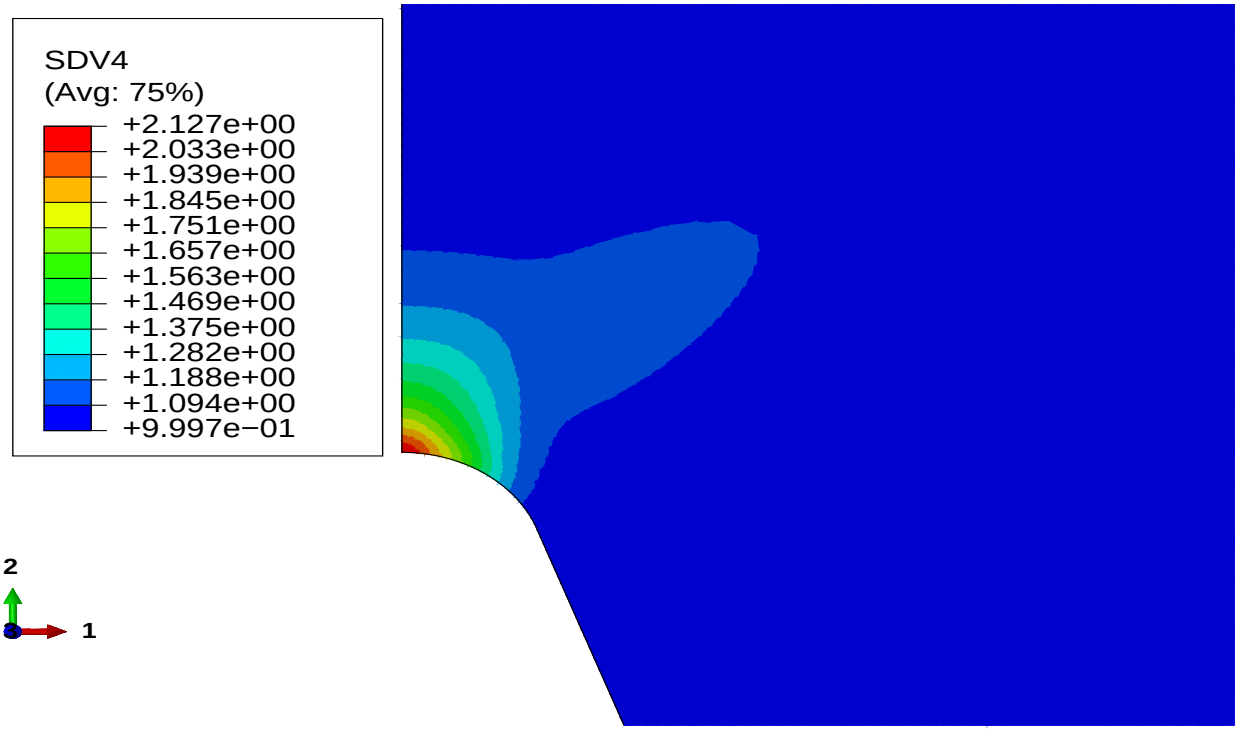

(b) w_2

Figure 6.37: Contour plots of the aspect ratios w_1, w_2 for the local anisotropic model at a nominal strain of 9%.

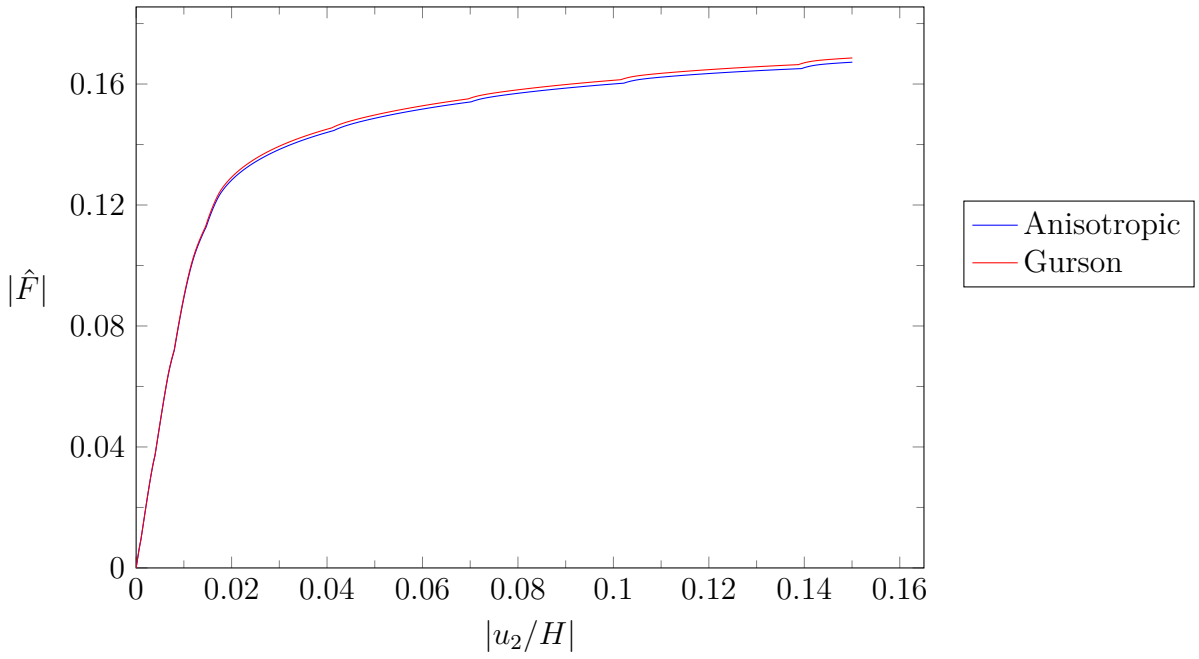

Figure 6.38: Normalized load vs nominal 'axial' strain for the nonlocal ($\ell = 1$) models up to a nominal strain $|\varepsilon| = 0.15$

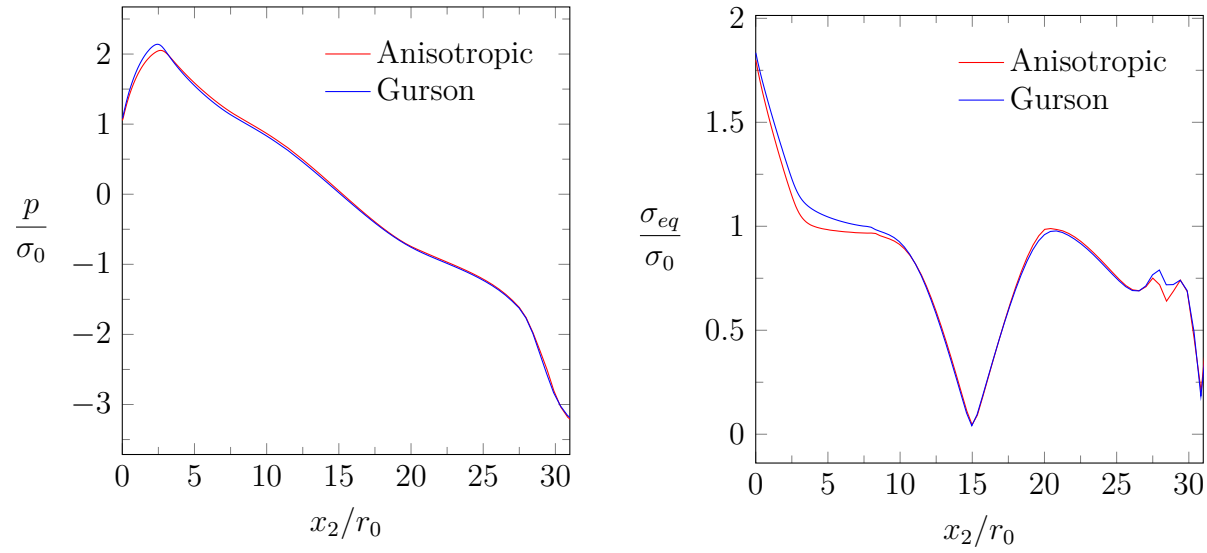

Figure 6.39: Normalized hydrostatic and von Mises equivalent stress distributions along the left side of the specimen at a nominal strain of 10% for the nonlocal models.

and strain states that develop near the crack's tip are once again in agreement, predicting a peak in pressure at a short distance from the notch's root. Furthermore, local porosity distributions reveal that maximum values are attained at the crack's tip, with the nonlocal anisotropic model predicting a higher peak value compared to Gurson's model. This observation is in accordance with the results for the nonlocal models concerning the mode-I blunt crack fracture problem, where f_{loc} takes slightly higher values for all load-levels.

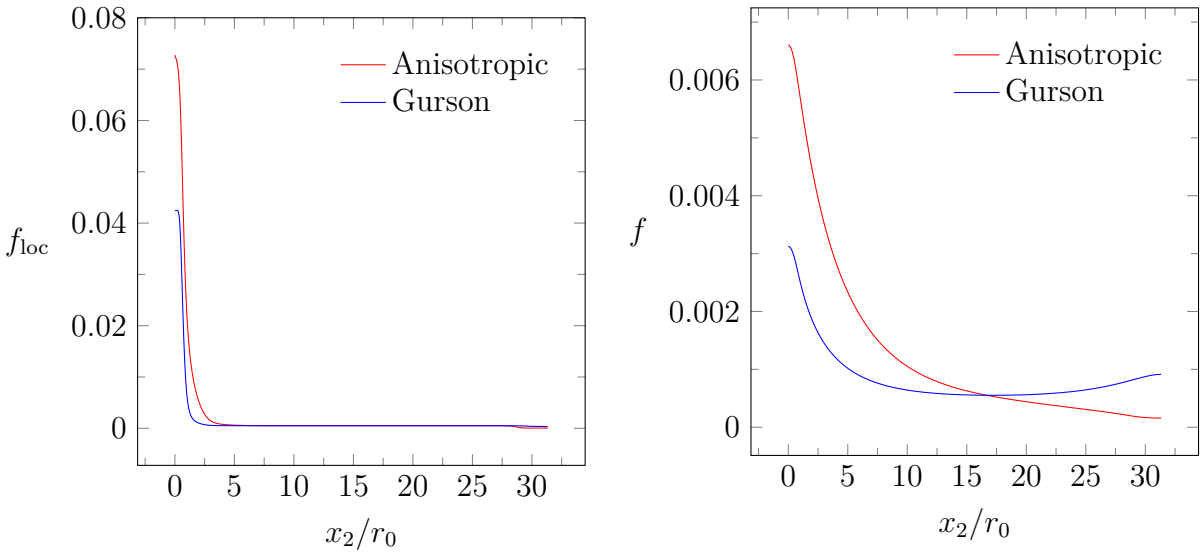

Figure 6.40: Local and nonlocal porosity distributions along the left side of the specimen at a nominal strain of 10% for the nonlocal models.

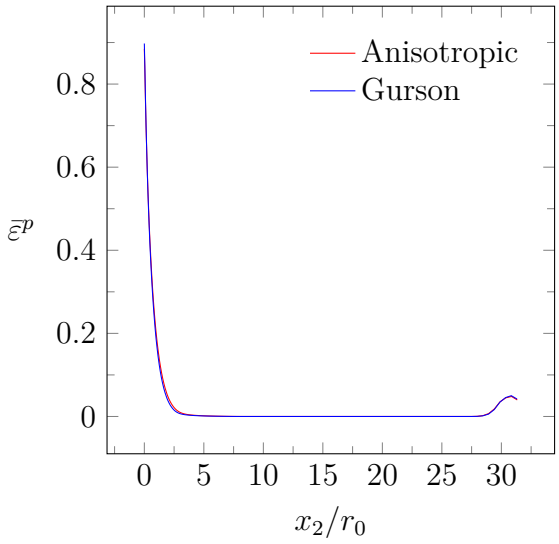

Figure 6.41: $\bar{\varepsilon}^p$ distribution along the left side of the specimen at a nominal strain of 10%, for the nonlocal models.

The situation is the same for the distribution of the nonlocal porosity f as seen in Figure 6.40b, with the nonlocal variable taking lower values compared to its local counterpart, as expected. In addition, another common characteristic between the nonlocal results of this problem with the one examined in the previous section is that f_{loc} takes lower values compared to the corresponding variable in the local model, which one can postulate is due to the effect of regularization to the solution. The aforementioned observations are also clearly depicted in Figures 6.42-6.44, which illustrate the contours of $\bar{\varepsilon}^p$, f_{loc} and f for both models, in the near-tip region of the specimen. Finally, regarding the shape of the of the pores for the nonlocal anisotropic model, Figure 6.45 shows the contours of the aspect ratios w_1 and w_2 for the region near the root of the semicircular notch. These reveal, as with the corresponding

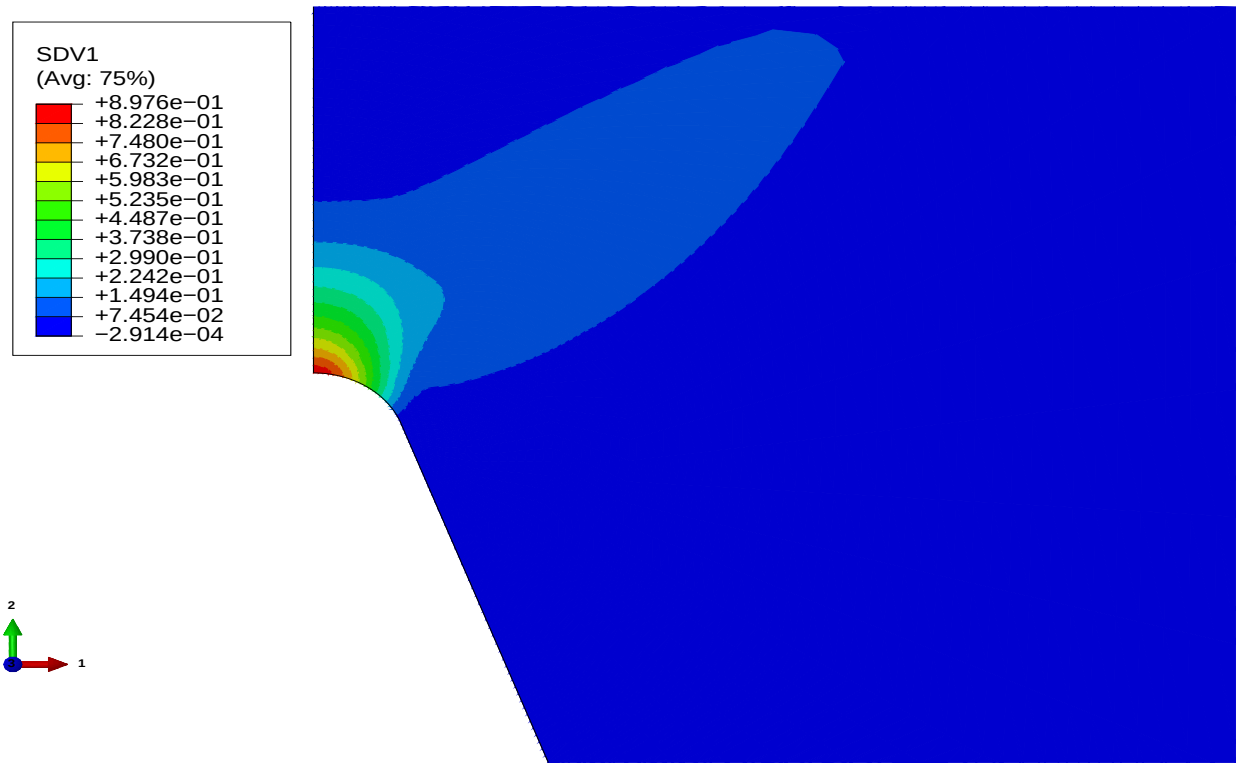

(a) Anisotropic

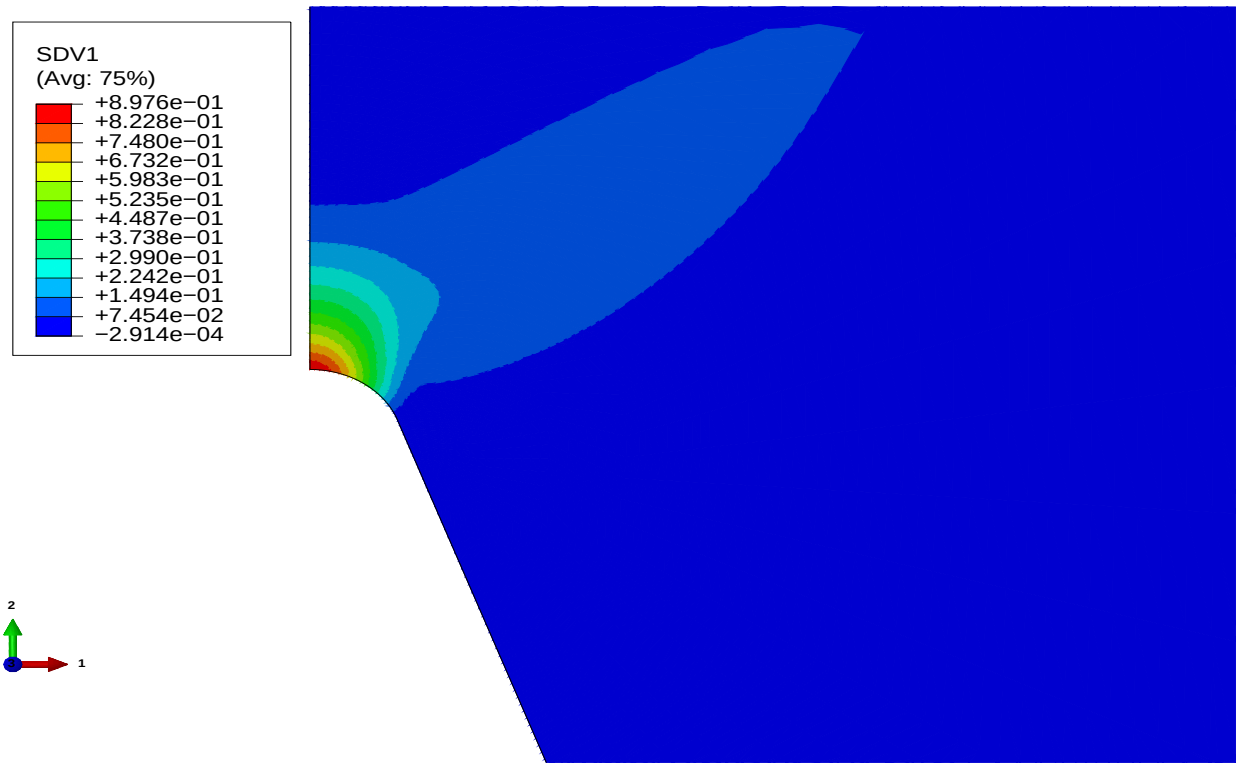

(b) Gurson

Figure 6.42: Contour plots of the equivalent plastic strain $\bar{\varepsilon}^p$ for both nonlocal models at a nominal strain of 10%.

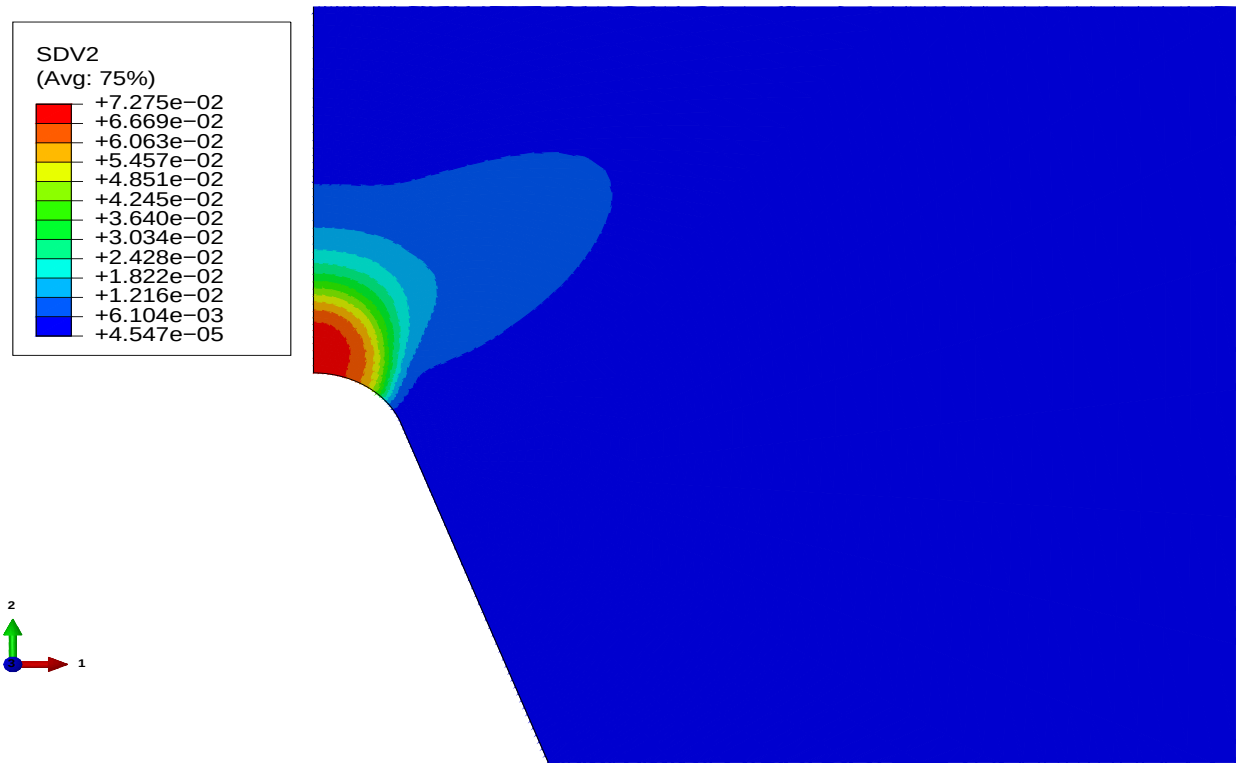

(a) Anisotropic

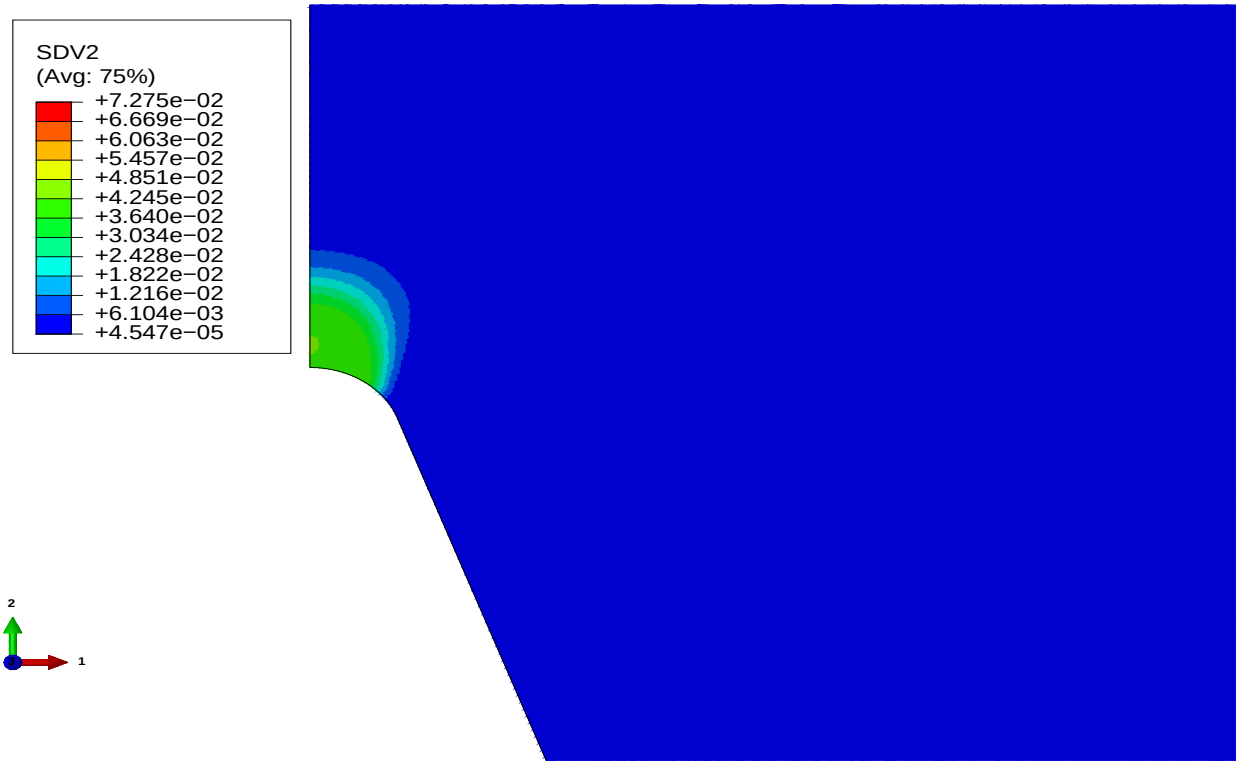

(b) Gurson

Figure 6.43: Contour plots of the local porosity f_{loc} for both nonlocal models at a nominal strain of 10%.

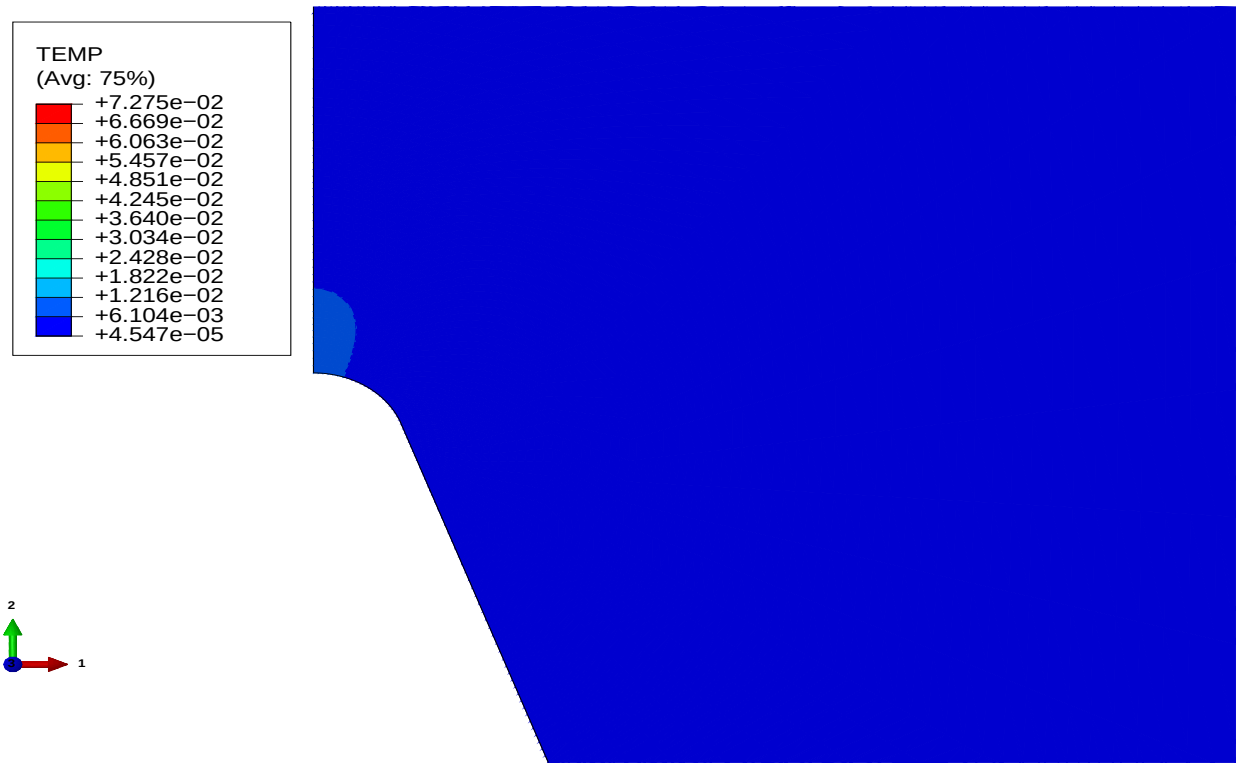

(a) Anisotropic

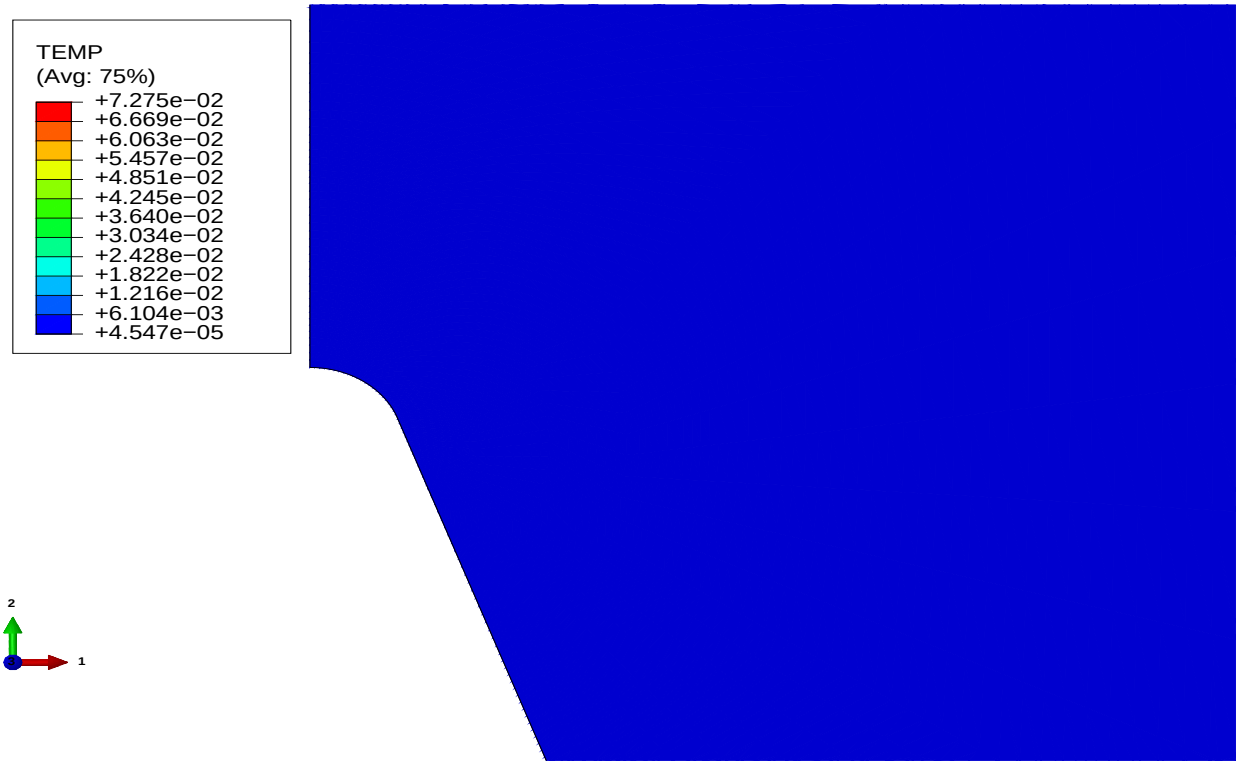

(b) Gurson

Figure 6.44: Contour plots of the nonlocal porosity f for both nonlocal models at a nominal strain of 10%. Notice that the legend limits are the same with the corresponding local porosity for comparison purposes.

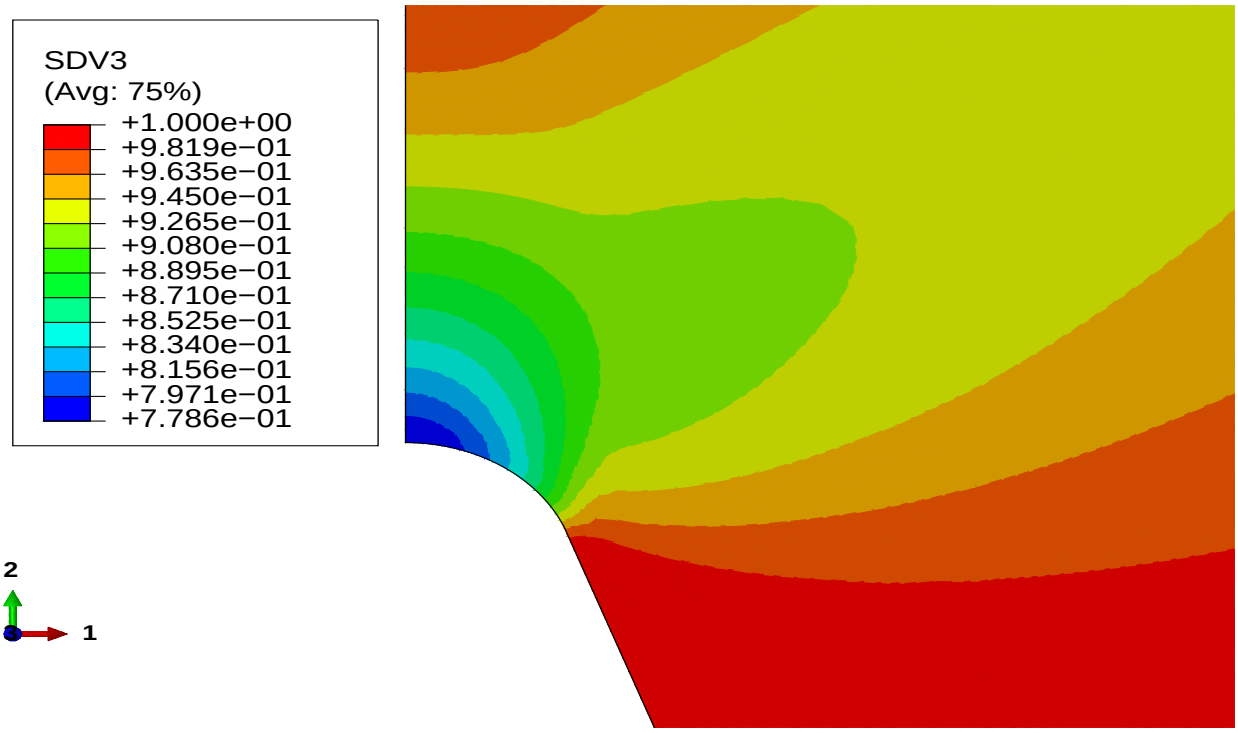

(a) w_1

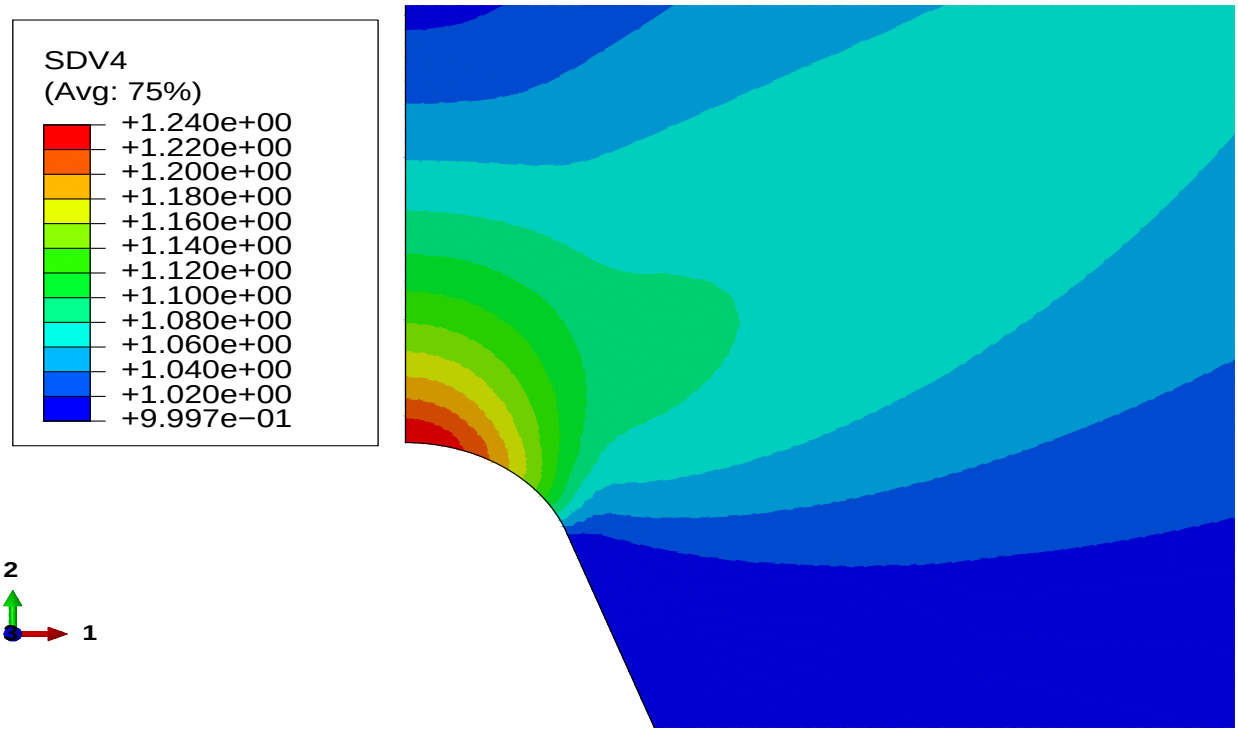

(b) w_2

Figure 6.45: Contour plots of the aspect ratios w_1, w_2 for the nonlocal anisotropic model at a nominal strain of 10%.

local model, the tendency of the pores at the tip to become elongated ellipsoids with major axis in the direction of loading. Another interesting thing to note here, in view of the values of w_2 for the nonlocal compared to the local model, is that once again the distribution of the variable is more smooth in the nonlocal case, which is in accordance with the overall 'smoother behavior' predicted, in general, by the regularized models.

6.3.2 Dynamic vs Quasi-Static Loading in the CVN Test

As mentioned earlier, for the sake of completeness, an investigation was also carried out in order to examine whether or not the dynamic response of the structure differs significantly from the previously assumed quasi-static behavior. For this purpose, the same specimen was used with the difference that now, a prescribed velocity boundary condition for the rigid hammer was imposed instead of a static displacement boundary condition. Based on the range of strain rates used in [85], a fairly high strain rate of $\dot{\varepsilon}_2 = \dot{u}_2/H = 100\ s^{-1}$ was used in the simulations. Initial mass density[4], which is used in the calculation of the mass matrix in the discretized equations of motion, is that of common steel (i.e. $\rho_0 = 7.85\ g/cm^3$) with a normalized value $\bar{\rho_0} = \rho_0/\sigma_0 = 0.0187 \times 10^{-9}\ s^2/mm^2$.

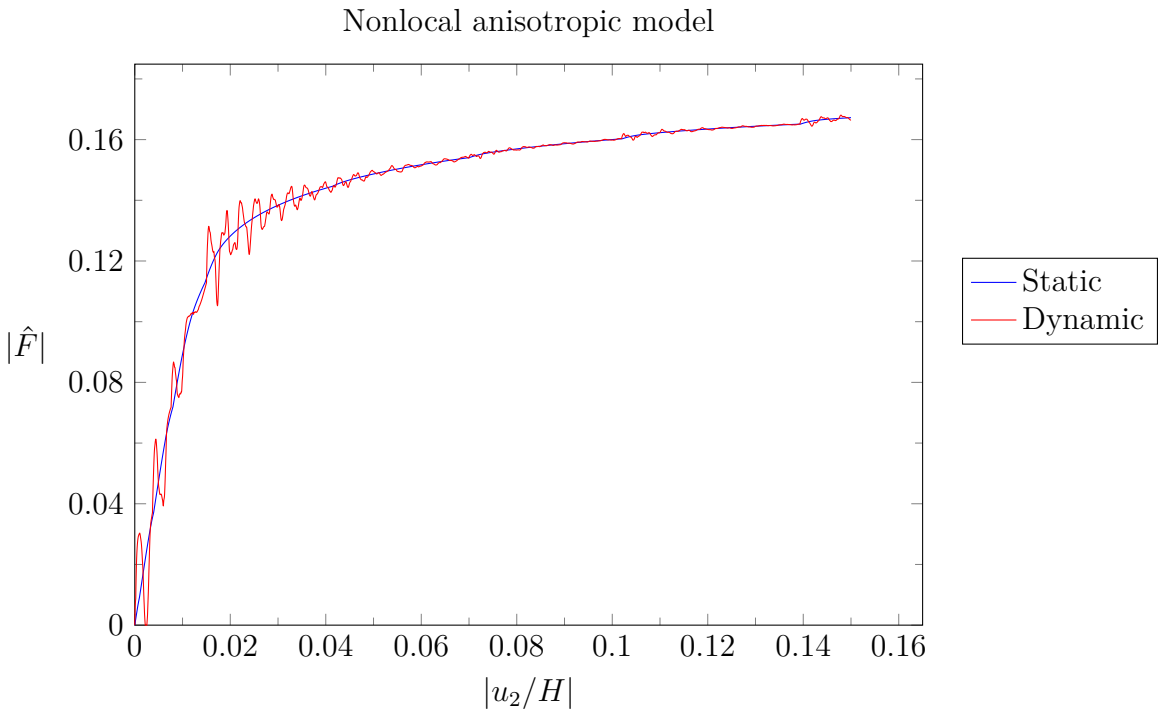

Figure 6.46: Normalized load vs nominal 'axial' strain for the static and dynamic problem, for the nonlocal ($\ell = 1$) anisotropic model up to a nominal strain $|\varepsilon| = 0.15$.

With no loss of generality, the analyses were carried out for the nonlocal anisotropic model and the behavior is expected to be the same for the corresponding local one since the regularization parameter does not affect the dynamic response of the material. The latter

[4] i.e. the mass density of the material in the undeformed configuration.

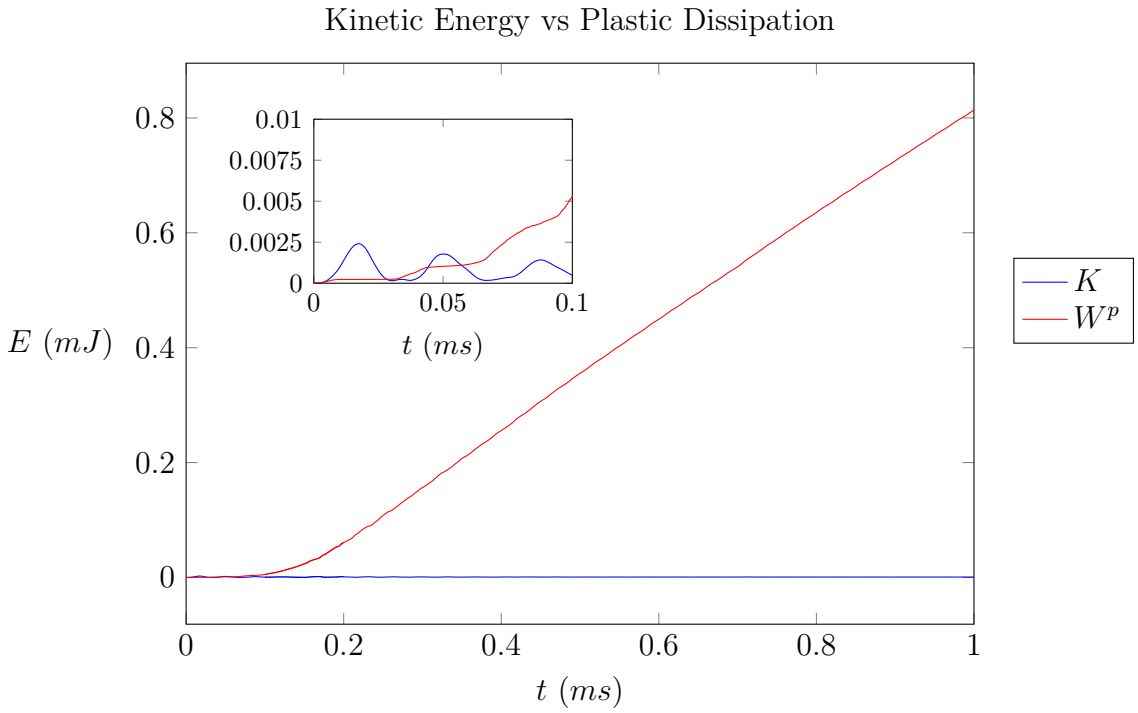

Figure 6.47: Kinetic energy versus plastic dissipation up to a nominal strain of 10%.

calculations were realized once again for $\ell = 1\ mm$. The results are as follows. Figure 6.46 illustrates the normalized load-nomal 'axial' strain curves for the static and dynamic problems, for the aforementioned characteristic length. Due to the presence of weak stress waves in smaller deformations, the dynamic solution naturally fluctuates around the corresponding static solution and as deformation progresses, the dynamic solution concides with the quasi-static one. Moreover, comparison for all relevant field variables revealed that, the dynamic solution is essentially the same as the static one in 'large times', justifying the prediction indicated, for the overall behavior, by the latter normalized load-strain curves. Finally, for the sake of completeness, the kinetic energy, K, and the plastic dissipation, W^p, which are defined as:

$$K = \frac{1}{2}\int_V \rho \boldsymbol{v} \cdot \boldsymbol{v} dV \quad , \quad W^p = \boldsymbol{\sigma} : \mathbf{D}^p \tag{6.6}$$

were also calculated for the dynamic problem, and the results are presented in Figure 6.47. Obviously, it is clear that kinetic energy, which briefly surpasses plastic power dissipation at the very beginning stages of deformation, soon becomes negligible, an observation which suggests that plastic deformation due to the static stress distribution in the material is the mechanism that dominates the solution. With all these in mind, one can postulate that the quasi-static approach that was adopted in the investigation of the effect of regularization in the CVN test is indeed valid.

Discussion and Conclusions

Modeling of materials exhibiting various instabilities due to large deformations suggests, in general, a challenging problem from the computational point of view due to the limitations of the classical, local models to provide an objective description of phenomena that take place in length scales comparable to the size of the underlying microstructure. Calibration of the regularization method, experimental evaluation of the intrinsic material length, and selection of the proper constitutive model in order to accurately describe the physics of the real material behavior are only some of the critical issues that have to be considered, determination of which is by no means trivial.

In the present work, a rate-independent, implicit nonlocal model of the gradient type was developed for the case of two-phase porous metals, which also takes into account the anisotropic characteristics of the corresponding microstructure. The classical anisotropic constitutive model previously developed by Aravas and Ponte Castañeda in [7] was re-established in order to account for the nonlocal porosity introduced as a part of the regularization process. Furthermore, additional modifications both in the mathematical formulation and in the numerical integration procedure of the evolution equations were realized, in an effort to improve the accuracy and the computational efficiency of the model. Thereafter, a detailed insight on the discretization of the problem in view of the finite element method was given. Regarding the applications of this model, at first, a series of finite element analyses for a benchmark localization problem have been carried out while the effect of the regularization imposed by the nonlocal model has been investigated, in a comparative manner with the corresponding Gurson model, for two different variations of the problem of ductile fracture. Results deduced from the finite element calculations, can be summarized as follows:

- Concerning the fundamental desired property of any regularizing model, i.e. the alleviation of the pathological mesh-dependency exhibited by the respective local model, it was validated that the model presented herein is capable of successfully tackling the deficiency while possessing a more realistic material behavior compared, for instance, to the isotropic Gurson's model. Moreover, in all cases, the nonlocal porosity was found to be lower than the local one as expected, with the two being closer to each other as the intrinsic length was reduced, in other words as the nonlocal model approached the limiting case of the local one.

- The gradient anisotropic model was found to be in qualitative agreement with the corresponding gradient Gurson in the problem of 'small scale yielding' of a mode-I

crack while on the other hand, differences between the porosity distribution at the tip of the crack were noticed in the Charpy V-notch test. This can be possibly attributed to the different stress and strain conditions developed at the crack's tip, which in turn is due to the difference in the loading conditions of the two cases.

- A common feauture observed in both cases of ductile fracture is that both gradient models, in general, predict less severe 'concentration' of stresses, plastic deformation and porosity (i.e. damage) compared to the local counterparts. This can probably be interpreted as an effect of the regularization, which smooths out the solution predicted by the local models.

- Another interesting result is that for intermediate to higher loads, in view of the comparison of the local-nonlocal Gurson model for the blunt crack problem, the latter tends to severely overestimate loss of stress-carrying capacity of the material by artificially introducing a sudden rise to the evolution of porosity at some distance from the crack's root, a property which is in contrast both with the predictions of the local anisotropic and the gradient counterparts of the models.

- Results of the dynamic anlyses for the CVN test revealed that, even for considerably high strain rates and different values of the localization limiter, the inertial term's contribution to the solution is of negligible size, thus indicating that a quasi-static approach does not affect the accuracy of the predictions of the nonlocal model for the problem of ductile fracture, at least in a rate-independent formulation.

In any case however, the complexity of both the constitutive model involved and the necessity for deeper comprehension of the regularization's effect on the mechanism of initiation and propagation of damage in porous metals, suggest that further investigation should take place. For instance, and due to computational issues experienced by the implicit solver for higher deformations in both problems of ductile fracture, an explicit solving scheme for the discretized equations could be developed and tested for the simulation of damage propagation. Furthermore, although two-dimensional problems are able, under certain conditions, to give fairly good results, the effect of regularization could be more realistically investigated by using fully three-dimensional models, which of course are considerably more complex and difficult to construct. Finally, another possibility could be the development of a rate-dependent nonlocal model and the investigation of its corresponding predictions to both static and dynamic problems.

Bibliography

[1] ABAQUS/Standard, Version 6.14, © Dassault Systémes, 2014

[2] ABAQUS, Analysis User's Manual, Version 6.14, © Dassault Systémes, 2014

[3] Agmon S., 'Lectures on Elliptic Boundary Value Problems', Van Nostrand, Princeton, (1965)

[4] Anand L., Aslan O., Chester S. A., 'A large-deformation gradient theory for elastic-plastic materials: Strain softening and regularization of shear bands', *Int. J. Plast.*, **30-31**, (2012), 116–143

[5] Aravas N., 'On the numerical integration of a class of pressure-dependent plasticity models', *Int. J. Numer. Methods Eng.*, **24**(7), (1987), 1395–1416

[6] Aravas N., Aifantis E. C., 'On the geometry of slip and spin in finite plastic deformation', *Int. J. Plast.*, **7**(3), (1991), 141–160

[7] Aravas N. and Ponte Castañeda P., 'Numerical methods for porous metals with deformation-induced anisotropy', *Comput. Methods Appl. Mech. Engrg.*, **193**, (2004), 3767–3805.

[8] Aravas N., 'Finite elastoplastic transformations of transversely isotropic materials', *Int. J. Solids Struct.*, **29**(17), (1992), 2137–2157

[9] Aravas N., 'Cartesian Tensors', University of Thessaly Publications, (2005).

[10] Aravas N., 'Mechanics of Materials Volume I', Tziolas Publications, (2014).

[11] Benallal A., Tvergaard V., 'Nonlocal continuum effects on bifurcation in the plane strain tension-compression test', *J. Mech. Phys. Solids*, **43**(5), (1995), 741–770

[12] Bassi A., 'Bifurcation problems in finite strain elastoplasticity', *Ph.D. Thesis, Politecnico di Milano*, (2002).

[13] Bažant Z. P., 'Instability, ductility and size effect in strain-softening concrete', *ASCE J. Eng. Mech. Div.*, **102**(2), (1976), 331–344

[14] Chadwick P., 'Continuum Mechanics: Concise Theory and Problems', Dover Publications (1999).

[15] Chandrasekharaiah D. S., Debnath L., 'Continuum Mechanics', Academic Press, Inc., (1994).

[16] Chu C. C., Needleman A., 'Void Nucleation Effects in Biaxially Stretched Sheets', *J. Eng. Matl. Tech.*, **102**(3), (1980), 249–256

[17] Crisfield M.A., 'A fast incremental/iterative solution procedure that handles snap-through', *Computers & Structures*, **13**, (1983), 55–62

[18] Dafalias Y. F., 'The plastic spin concept and a simple illustration of its role in finite plastic transformations', *Mech. Mater.*, **3**(3), (1984), 223–233

[19] Dafalias Y. F., 'The plastic spin', *J. Appl. Mech.*, **52**(4), (1985), 865–871

[20] Danas K., 'Numerical Methods for the study of Anisotropy in Porous Metals due to Finite Plastic Deformations', *Diploma Thesis, University of Thessaly.*, (2002).

[21] Danas K., 'Porous materials with evolving microstructure: constitutive modeling, numerical implementation and applications', *Phd Thesis, École Polytechnique.*, (2008).

[22] Danas K., Aravas N., 'Numerical modeling of elasto-plastic porous materials with void shape effects at finite deformations', *Compos. B Eng.*, **43**(6), (2012), 2544–2559

[23] de Borst. R., 'Stability and uniqueness in numerical modeling of concrete structures', *IABSE Rep.*, **54**, (1987), 161–176

[24] de Borst. R., Sluys L. J., Mühlhaus, Pamin A. J., 'Fundamental issues in finite element analyses of localization of deformation', *Engineering Computations*, **10**(2), (1993), 99–121

[25] Drucker, D.C., 'A definition of a stable inelastic material', *ASME J. Appl. Mech.*, **26**, (1959), 101–106

[26] Engelen R. A. B., Geers M. G. D., Baaijens F. P. T., 'Nonlocal implicit gradient-enhanced elasto-plasticity for the modeling of softening behaviour', *Int. J. Plast.*, **19**, (2003), 403–433

[27] Eshelby J. D., 'The determination of the elastic field of an ellipsoidal inclusion, and related problems', *Proc. R. Soc. London A*, **241**, (1957), 376–396

[28] Eshelby J. D., 'Elastic inclusions and inhomogeneities', in: I.N. Sneddon, R. Hill (Eds.) *Progress in Solid Mechanics*, **vol II**, (1961), 87–140

[29] Fish J., Shek K., 'Finite deformation plasticity based on the additive split of the rate of deformation and hyperelasticity', *Comp. Methods Appl. Mech. Eng.*, **190**, (2000), 75–93

[30] Govindarajan R. M., Aravas N., 'Pressure-dependent plasticity models: Loading-unloading criteria and the consistent linearization of an integration algorithm', *Comm. Numer. Meth. Eng.*, **11**(4), (1995), 339–345

[31] Gurson A. L., 'Continuum Theory of Ductile Rupture by Void Nucleation and Growth: Part 1–Yield Criteria and Flow Rules for Porous Ductile Media', *J. Eng. Matl. Tech.*, **99**(1), (1977), 2–15

[32] Hashiguchi K., Yamakawa Y., Introduction to finite strain theory for continuum elasto-plasticity, John Wiley & Sons Ltd, (2013).

[33] Hibbitt H. D., Karlsson B. I., 'Analysis of Pipe Whip', EPRI, Report NP–1208, (1979),

[34] Hilber H. M., Hughes T. J. R., Taylor R. L., 'Improved numerical dissipation for time integration algorithms in structural dynamics', *Earthq. Eng. Struct. Dyn.*, **5**, (1977), 283 –292

[35] Hill R., 'On uniqueness and stability in the theory of finite elastic strain', *J. Mech. Phys. Solids*, **5**(4), (1957), 229–241

[36] Hill R., 'A general theory of uniqueness and stability in elastic-plastic solids', *J. Mech. Phys. Solids*, **6**(3), (1958), 236–249

[37] Hill R., 'Acceleration waves in solids', *J. Mech. Phys. Solids*, **10**(1), (1962), 1–16

[38] Hill R., 'Aspects of invariance in solid mechanics', in: C.-S. Yih (Ed.), *Adv. Appl. Mech.*, **18**, (1979), 1–75

[39] Hughes T. J. R., 'Generalizing of selective integration procedures to anisotropic and non-linear media', *Int. J. Numer. Methods Eng.*, **15**(9), (1980), 1413–1418

[40] Hutchinson J. W., Tvergaard V., 'Shear band formation in plane strain', *Int. J. Solids Struct.*, **17**(5), (1981), 451–470

[41] Hutchinson J. W., 'Post bifurcation bahavior in the plastic range', *J. Mech. Phys. Solids*, **21**(3), (1973), 163–190

[42] Hutchinson J. W., 'Bifurcation analysis of the onset of necking in an elastic/plastic cylinder under uniaxial tension', *J. Mech. Phys. Solids*, **22**(1), (1974), 61–71

[43] Hutchinson J. W., 'Plastic Buckling', *Adv. Appl. Mech.*, **14**, (1974), 67–144

[44] Jirásek M., Bažant Z. P., 'Inelastic Analysis of Structures', John Wiley & Sons Ltd, (2002).

[45] Kailasam M., Ponte Castañeda P., Willis J. R. 'The effect of particle size, shape, distribution and their evolution on the constitutive response of nonlinearly viscous composites. I. Theory', *Philo. Tran. R. Soc. London A*, **355**(1730), (1997), 1835–1852

[46] Kailasam M., Ponte Castañeda P., Willis J. R. 'The effect of particle size, shape, distribution and their evolution on the constitutive response of nonlinearly viscous composites. II. Examples', *Philo. Tran. R. Soc. London A*, **355**(1730), (1997), 1853–1872

[47] Kailasam M., Ponte Castañeda P., 'A general constitutive theory for linear and nonlinear particulate media with microstructure evolution', *J. Mech. Phys. Solids*, **46**(3), (1998), 427–465

[48] Kailasam M., Aravas N., Ponte Castañeda P., 'Porous metals with developing anisotropy: constitutive models, computational issues and applications to deformation processing', *Comput. Model. Engrg. Sci*, **1**, (2000), 105–118

[49] Koplik J., Needleman A., 'Void growth and coalescence in porous plastic solids', *Int. J. Solids Struct.*, **24**(8), (1988), 835–853

[50] Lee E. H., 'Elastic-Plastic Deformation at Finite Strains', *J. Appl. Mech.*, **36**(1), (1969), 1–6

[51] Liu I-S., 'Continuum Mechanics', Springer Science & Business Media, (2002).

[52] Liu I-S., 'On Euclidean objectivity and the principle of material frame-indifference', *Continuum Mech. Thermodyn.*, **16**(1-2), (2004), 177–183

[53] Lubliner J., 'Plasticity Theory', Dover Publications (2008).

[54] Nadeau J. C., Ferrari M., 'Invariant tensor-to-matrix mappings for evaluation of tensorial expressions', *J. Elast.*, **52**(1), (1998), 43–61

[55] Nagtegaal J.C., Veldpaus F.E., 'On the implementation of finite strain plasticity equations in a numerical model', in: J.F.T. Pitman (Ed.) *Numerical methods in industrial forming processes*, John Wiley & Sons, New York, (1984), 351–371

[56] Needleman A., Rice J. R., 'Limits to Ductility Set by Plastic Flow Localization', in: D.P. Koistinen, N.-M. Wang (Eds.), Mechanics of Sheet Metal Forming, Plenum Press, New York, London, (1978), 237–267

[57] Nemat-Nasser S., 'A Treatise on Finite Deformation Heterogeneous Inelastic Materials', Cambridge University Press, (2004).

[58] Ogden R. W., 'Non-Linear Elastic Deformations', Dover Publications (1997).

[59] Ortiz M., E. P. Popov, 'Accuracy and stability of integration algorithms for elastoplastic constitutive relations', *Int. J. Numer. Methods Engrg.*, **21**, (1985), 1561–1576

[60] Papatriantafillou I. C., 'Trip steels: constitutive modeling and computational Issues ', *Phd Thesis, University of Thessaly*, (2005).

[61] Peerlings R. H. J., Geers M. G. D., Borst R. de, Brekelmans W. A. M., 'A critical comparison of nonlocal and gradient-enhanced softening continua', *Int. J. Solids Struct.*, **38**(44-45), (2001), 7723–7746

[62] Pijaudier-Cabot G., Bažant Z. P., 'Nonlocal Damage Theory', *ASCE J. Eng. Mech.*, **113**(10), (1987), 1512–1533

[63] Ponte Castañeda P., 'Heterogeneous Materials', Lecture Notes, École Polytechnique, Department of Mechanis (2005).

[64] Ponte Castañeda P., 'The effective mechanical properties of nonlinear isotropic composites', *J. Mech. Phys. Solids*, **39**(1), (1991), 45–71

[65] Ponte Castañeda P., Willis J. R., 'The effect of spatial distribution on the effective behavior of composite materials and cracked media', *J. Mech. Phys. Solids*, **43** (1995), 1919–1951

[66] Ponte Castañeda P., Zaidman M., 'Constitutive models for porous materials with evolving microstructure', *J. Mech. Phys. Solids*, **42**(9), (1994), 1459–1497

[67] Ponte Castañeda P., Zaidman M., 'The finite deformation of nonlinear composite materialsâĂŤI. Instantaneous constitutive relations', *Int. J. Solids Struct*, **33**(9), (1996), 1271–1286

[68] Ramaswamy S., Aravas N., 'Finite element implementation of gradient plasticity models âĹŠ Part I: Gradient-dependent yield functions', *Comp. Methods Appl. Mech. Eng.*, **163**, (1998), 11–32

[69] Ramaswamy S., Aravas N., 'Finite element implementation of gradient plasticity models âĹŠ Part I: Gradient-dependent yield functions', *Comp. Methods Appl. Mech. Eng.*, **163**, (1998), 33–53

[70] Rice J. R., 'Mechanics of crack tip deformation and extension by fatigue', *Fatigue Crack Propagation, ASTM STP 415* (1967), 247–309

[71] Rice J.R., 'A path independent integral and the approximate analysis of strain concentration by notches and cracks', *J. Appl. Mech.*, **35**, (1968), 379–386

[72] Rice J. R., 'The localization of plastic deformation', in: W.T. Koiter (Ed.), *Proceedings of the 14th International Congress on Theoretical and Applied Mechanics*, **vol I**, North-Holland Publishing Corporation, (1976), 207–220

[73] Riks E., 'An incremental approach to the solution of buckling snapping problems', *Int. J. Solids Struct.*, **15**, (1979), 524–551

[74] Ritchie R. O., 'On the Relationship between Fracture Toughness and Charpy V-Notch Energy in Ultra-High Strength Steel', in: Rosenfield A. R., et al. (eds.), *Proceedings of a symposium held at the annual meeting of the American Institute of Mining, Metallurgical and Petroleum Engineers 1978:What Does the Charpy Test Really Tell Us?*, American Society for Metals, Metals Park, OH, (1978), 54–73

[75] Rolshoven S., 'Nonlocal plasticity models for localized failure', *Phd Thesis, École Polytechnique Fédérale de Lausanne*, (2003).

[76] Tekoğlu C., Hutchinson J.W. and Pardoen T., 'On localization and void coalescence as a precursor to ductile fracture', *Philo. Tran. R. Soc. London A*, **373**(2038), (2015), 20140121

[77] Tvergaard V., 'Influence of Voids on Shear Band Instabilities under Plane Strain Conditions', *Int. J. Fract.*, **17**(4), (1981), 389–407

[78] Tvergaard V., 'Influence of void nucleation on ductile shear fracture at a free surface', *J. Mech. Phys. Solids*, **30**(6), (1982), 399–425

[79] Tvergaard V., 'On localization in ductile materials containing spherical voids', *Int. J. Fract.*, **18**(4), (1982), 237–252

[80] Tvergaard V., 'Ductile fracture by cavity nucleation between larger voids', *J. Mech. Phys. Solids*, **30**(4), (1982), 265–286

[81] Tvergaard V., 'Effect of anisotropic hardening on ductile failure of material containing two-size scales of particles', *Yielding, Damage, and Failure of Anisotropic Solids*, (EGF Publication 5), Mechanical Engineering Publications, (1990), 695–709

[82] Tvergaard V. and Needleman A., 'Analysis of the cup-cone fracture in a round tensile bar', *Acta Metall.*, **32**(1), (1984), 157–169

[83] Tvergaard V. and Needleman A., 'Effects of nonlocal damage in porous plastic solids', *Int. J. Solids Struct.*, **32**(8-9), (1995), 1063–1077

[84] Tvergaard V. and Needleman A., 'Nonlocal effects on localization in a void-sheet', *Int. J. Solids Struct.*, **34**(18), (1997), 2221–2238

[85] Tvergaard V. and Needleman A., 'Effect of material rate sensitivity on failure modes in the Charpy V-notch test', *J. Mech. Phys. Solids*, **34**(3), (1986), 213–241

[86] Willis J. R., 'Bounds and self-consistent estimates for the overall moduli of anisotropic composites', *J. Mech. Phys. Solids*, **25**, (1977), 185–202

[87] Willis J. R., 'Variational principles and bounds for the overall properties of composites', in: J.W. Prowan (Ed.), *Continuum Models for Discrete Systems, University of Waterloo Press*, (1978), 185–215

[88] Willis J. R., 'Variational and related methods for the overall properties of composites', in: C.-S. Yih (Ed.), *Adv. Appl. Mech.*, **21**, (1981), 2–74

Appendicies

Appendix A

Calculation of tensors $\mathcal{S}$, $\mathbf{\Pi}$ and $\mathcal{Q}$

The formulation of the gradient anisotropic model thoroughly described in Chapter 4 involves calculations which, among other quantities, require the evaluation of the Eshelby tensors $\boldsymbol{\mathcal{S}}$, $\mathbf{\Pi}$ and the tensor $\boldsymbol{\mathcal{Q}}$, which is a forth order tensor associated with the microstructure. The two different approaches for the latter calculations and the corresponding computational issues that emerge, as presented in [7] and [20], are summarized in the following.

Method I : Willis expressions

The first method is based on the works of Willis [86], [88] who proved that, the Eshelby tensors $\boldsymbol{\mathcal{S}}$ and $\mathbf{\Pi}$ can be written in terms of the forth order tensors $\boldsymbol{\mathcal{P}}$ and $\boldsymbol{\mathcal{R}}$ respectively as:

$$\boldsymbol{\mathcal{S}} = \boldsymbol{\mathcal{P}} : \boldsymbol{\mathcal{M}}^{-1} \quad \text{and} \quad \mathbf{\Pi} = \boldsymbol{\mathcal{R}} : \boldsymbol{\mathcal{M}}^{-1} \tag{A.1}$$

where $\boldsymbol{\mathcal{M}}^{-1} = \boldsymbol{\mathcal{L}}$ is the elastic tensor of the matrix and

$$\boldsymbol{\mathcal{P}} = \frac{1}{4\pi \det(\mathbf{Z})} \int\limits_{|\boldsymbol{\xi}|=1} \boldsymbol{\mathcal{H}}(\boldsymbol{\xi}) \frac{1}{|\mathbf{Z}^{-1} \cdot \boldsymbol{\xi}|^3} dS(\boldsymbol{\xi}) \quad \text{and} \quad \boldsymbol{\mathcal{R}} = \frac{1}{4\pi \det(\mathbf{Z})} \int\limits_{|\boldsymbol{\xi}|=1} \hat{\boldsymbol{\mathcal{H}}}(\boldsymbol{\xi}) \frac{1}{|\mathbf{Z}^{-1} \cdot \boldsymbol{\xi}|^3} dS(\boldsymbol{\xi}) \tag{A.2}$$

Using (A.2), (A.1) yields the following expressions for $\boldsymbol{\mathcal{S}}$ and $\mathbf{\Pi}$:

$$\boxed{\boldsymbol{\mathcal{S}} = \frac{1}{4\pi \det(\mathbf{Z})} \int\limits_{|\boldsymbol{\xi}|=1} \boldsymbol{\mathcal{H}}(\boldsymbol{\xi}) : \boldsymbol{\mathcal{L}} \frac{1}{|\mathbf{Z}^{-1} \cdot \boldsymbol{\xi}|^3} dS(\boldsymbol{\xi})} \tag{A.3}$$

$$\boxed{\mathbf{\Pi} = \frac{1}{4\pi \det(\mathbf{Z})} \int\limits_{|\boldsymbol{\xi}|=1} \hat{\boldsymbol{\mathcal{H}}}(\boldsymbol{\xi}) : \boldsymbol{\mathcal{L}} \frac{1}{|\mathbf{Z}^{-1} \cdot \boldsymbol{\xi}|^3} dS(\boldsymbol{\xi})} \tag{A.4}$$

Furthermore, a similar expression has been derived by Kailasam *et al.* in [48] for the microstructural tensor $\boldsymbol{\mathcal{Q}}$ which can be written as:

$$\boxed{\boldsymbol{\mathcal{Q}} = \frac{\mu}{4\pi \det(\mathbf{Z})} \int\limits_{|\boldsymbol{\xi}|=1} \boldsymbol{\mathcal{E}}(\boldsymbol{\xi}) \frac{1}{|\mathbf{Z}^{-1} \cdot \boldsymbol{\xi}|^3} dS(\boldsymbol{\xi})} \tag{A.5}$$

In (A.3)-(A.5), μ is the shear modulus of the matrix material and $\boldsymbol{\xi}$ is the outward-pointing normal vector to the infinitesimal surface $dS(\boldsymbol{\xi})$ on which the corresponding surface integrals are calculated. Moreover, $\mathbf{Z}$ is a second order tensor containing the information about the shape and orientation of the local ellipsoid, i.e.,

$$\mathbf{Z} = w_1 \mathbf{n}^{(1)}\mathbf{n}^{(1)} + w_2 \mathbf{n}^{(2)}\mathbf{n}^{(2)} + \mathbf{n}^{(3)}\mathbf{n}^{(3)} \quad , \quad \det(\mathbf{Z}) = w_1 w_2 \tag{A.6}$$

$\boldsymbol{\mathcal{H}}(\boldsymbol{\xi})$, $\hat{\boldsymbol{\mathcal{H}}}(\boldsymbol{\xi})$ are forth order (fully) symmetric and antisymmetric in the first two indices tensors respectively[1], which are defined in terms of the well known acoustic tensor $\mathbf{K}$ as:

$$[\boldsymbol{\mathcal{H}}(\boldsymbol{\xi})]_{ijkl} = [\mathbf{K}^{-1}(\boldsymbol{\xi})]_{ik}\xi_j\xi_l|_{(ij)(kl)} \quad , \quad [\hat{\boldsymbol{\mathcal{H}}}(\boldsymbol{\xi})](\boldsymbol{\xi})_{ijkl} = [\mathbf{K}^{-1}(\boldsymbol{\xi})]_{ik}\xi_j\xi_l|_{[ij](kl)} \tag{A.7a}$$

$$\text{with} \quad [\mathbf{K}(\boldsymbol{\xi})]_{ik} = \mathcal{L}_{ijkl}\xi_j\xi_l \tag{A.7b}$$

and $\boldsymbol{\mathcal{E}}(\boldsymbol{\xi})$ is a forth order tensor defined as:

$$\boldsymbol{\mathcal{E}}(\boldsymbol{\xi}) = \boldsymbol{\mathcal{L}} - \boldsymbol{\mathcal{L}} : \boldsymbol{\mathcal{H}}(\boldsymbol{\xi}) : \boldsymbol{\mathcal{L}} \tag{A.8}$$

For isotropic matrix material, i.e., $\boldsymbol{\mathcal{L}} = 2\mu\boldsymbol{\mathcal{K}} + 3\nu\boldsymbol{\mathcal{J}}$, expressions (A.7a)-(A.8) can be significantly simplified, leading to:

$$\begin{aligned}[\boldsymbol{\mathcal{H}}(\boldsymbol{\xi}) : \boldsymbol{\mathcal{L}}]_{ijkl}(\boldsymbol{\xi}, \nu) = {} & \frac{1}{2|\boldsymbol{\xi}|^2}(\delta_{ik}\xi_j\xi_l + \delta_{jk}\xi_i\xi_l + \delta_{il}\xi_j\xi_k + \delta_{jl}\xi_i\xi_k) \\ & - \frac{1}{|\boldsymbol{\xi}|^4}\frac{1}{1-\nu}\xi_i\xi_j\xi_k\xi_l + \frac{1}{|\boldsymbol{\xi}|^2}\frac{\nu}{1-\nu}\xi_i\xi_j\delta_{kl}\end{aligned} \tag{A.9}$$

$$[\hat{\boldsymbol{\mathcal{H}}}(\boldsymbol{\xi}) : \boldsymbol{\mathcal{L}}]_{ijkl}(\boldsymbol{\xi}) = \frac{1}{2|\boldsymbol{\xi}|^2}(\delta_{ik}\xi_j\xi_l - \delta_{jk}\xi_i\xi_l + \delta_{il}\xi_j\xi_k - \delta_{jl}\xi_i\xi_k) \tag{A.10}$$

and

$$\begin{aligned}[\boldsymbol{\mathcal{E}}(\boldsymbol{\xi})]_{ijkl}(\boldsymbol{\xi}, \nu) = {} & \delta_{ik}\delta_{jl} + \delta_{il}\delta_{jk} - \frac{1}{|\boldsymbol{\xi}|^2}(\delta_{ik}\xi_j\xi_l + \delta_{il}\xi_j\xi_k + \delta_{jk}\xi_i\xi_l + \delta_{jl}\xi_i\xi_k) \\ & + \frac{2\nu}{1-\nu}\left[\delta_{ij}\delta_{kl} - \frac{1}{|\boldsymbol{\xi}|^2}(\delta_{ij}\xi_k\xi_l + \delta_{kl}\xi_i\xi_j)\right] + \frac{2}{|\boldsymbol{\xi}|^4}\frac{1}{1-\nu}\xi_i\xi_j\xi_k\xi_l\end{aligned} \tag{A.11}$$

It should be noted that evaluation of the expressions (A.3)-(A.5) involves double (surface) integrals of the form:

[1] The notation $A_{(ij)(kl)} = \frac{1}{4}(A_{ijkl} + A_{ijlk} + A_{jikl} + A_{jilk})$ and $A_{[ij](kl)} = \frac{1}{4}(A_{ijkl} + A_{ijlk} - A_{jikl} - A_{jilk})$ is used to indicate these symmetries and antisymmetries

$$I = \int\limits_{|\boldsymbol{\xi}|=1} A(\boldsymbol{\xi}) dS(\boldsymbol{\xi}) = \int\limits_{\phi=0}^{\pi} \int\limits_{\theta=0}^{2\pi} A(\boldsymbol{\xi}(\theta,\phi)) \sin\phi d\theta d\phi \tag{A.12}$$

where $\boldsymbol{\xi} = (\sin\phi\cos\theta, \sin\phi\sin\theta, \cos\phi)$. Using the transformations $\theta(r) = (r+1)\pi$, $\phi(s) = (s+1)\pi/2$, the latter integral is now evaluated in the interval $[-1,1]$ and thus, it can be numerically integrated using Gauss-quadrature, i.e.,

$$I = \frac{\pi^2}{2} \int\limits_{-1}^{1} \int\limits_{-1}^{1} A(\boldsymbol{\xi}(\theta(r),\phi(s))) \sin\phi(s) dr ds \approx \frac{\pi^2}{2} \sum_{i=1}^{\mathrm{NG}} \sum_{j=1}^{\mathrm{NG}} W_i W_j A(\boldsymbol{\xi}(\theta_i,\phi_i)) \sin\phi_j \tag{A.13}$$

where $\theta_i = \theta(r_i)$ and $\phi_j = \phi(s_j)$, r_i and s_j are the Gauss integration points, W_i and W_j are the corresponding weights and NG is the number of integration points in each direction. Although implementation of the procedure presented above is straightforward, accuracy issues emerge when the aspect ratios w_1, w_2 significantly differ from unity. In this case, a large number of Gauss points is required for acceptable accuracy, rendering the method computationally cost prohibitive. For this reason, the second method presented in the following, is preferred in the computations.

Method II : Eshelby expressions

An alternative approach[2] for the calculation of $\boldsymbol{\mathcal{S}}$, $\boldsymbol{\Pi}$ and $\boldsymbol{\mathcal{Q}}$ is based both on the original expressions derived by Eshelby in [27], [28] for the components $\mathcal{S}'_{ijkl}$, $\mathit{\Pi}'_{ijkl}$ of $\boldsymbol{\mathcal{S}}$ and $\boldsymbol{\Pi}$, and on the evaluation of explicit expressions for the components $\mathcal{Q}'_{ijkl}$ using the corresponding relations presented in the previous section. Primed quantities are used to indicate that the corresponding components are calculated with respect to a coordinate system which is instantaneously aligned with the principal directions $\mathbf{n}^{(i)}$ of the RLEV. With latter components at hand, one can readily calculate the corresponding components with respect to the global coordinate system by using the standard tensor transformation relations. Moreover, the expressions presented in the following have been derived by assuming that the principal lengths of the local ellipsoid, hereafter denoted as $2a \equiv 2a_1$, $2b \equiv 2a_2$ and $2c \equiv 2a_3$ are such so the inequality $a > b > c$ is satisfied at all times.

To begin with, taking into consideration the corresponding symmetries mentioned in Chapter 4, the matrix mappings of tensors $\boldsymbol{\mathcal{S}}$, $\boldsymbol{\Pi}$ and $\boldsymbol{\mathcal{Q}}$ with respect to a coordinate system, which momentarily coincides with the orientation vectors $\mathbf{n}^{(i)}$, are given as:

$$\boldsymbol{\mathcal{S}}' \rightarrow \underset{n\times n}{\left[\mathcal{S}'\right]} \quad , \quad \boldsymbol{\Pi}' \rightarrow \underset{n\times n}{\left[\mathit{\Pi}'\right]} \quad , \quad \boldsymbol{\mathcal{Q}}' \rightarrow \underset{n\times n}{\left[\mathcal{Q}'\right]} \tag{A.14}$$

where $n = 1$, $n = 4$ and $n = 6$ for one-, two- and three-dimensional problems respectively[3].

[2] Which has indeed proved to be much faster and, in this sense, more computationally efficient.

[3] Here, the component mapping is of the form $\square'_{ijkl} \rightarrow \left[\square'\right]_{IJ}$, $I, J = 1, \cdots, n$, where $1 \rightarrow \{11\}$, $2 \rightarrow \{22\}$, $3 \rightarrow \{33\}$, $4 \rightarrow \{12\}$, $5 \rightarrow \{13\}$, $6 \rightarrow \{23\}$ is the correspondence between major and minor index pair.

The components of the latter matrix representations are given bellow. For the forth order tensor $\boldsymbol{\mathcal{S}}$ one has:

$$\mathcal{S}'_{11} = \mathcal{S}'_{1111} = Pa^2 I_{11} + RI_1\,, \quad \mathcal{S}'_{22} = \mathcal{S}'_{2222} = Pb^2 I_{22} + RI_2\,, \quad \mathcal{S}'_{33} = \mathcal{S}'_{3333} = Pc^2 I_{33} + RI_3$$

$$\mathcal{S}'_{12} = \mathcal{S}'_{1122} = Pb^2 I_{12} - RI_1\,, \quad \mathcal{S}'_{13} = \mathcal{S}'_{1133} = Pc^2 I_{13} - RI_1\,, \quad \mathcal{S}'_{21} = \mathcal{S}'_{2211} = Pa^2 I_{21} - RI_2$$

$$\mathcal{S}'_{23} = \mathcal{S}'_{2233} = Pc^2 I_{23} - RI_2\,, \quad \mathcal{S}'_{31} = \mathcal{S}'_{3311} = Pa^2 I_{13} - RI_3\,, \quad \mathcal{S}'_{32} = \mathcal{S}'_{3322} = Pb^2 I_{23} - RI_3$$

$$\mathcal{S}'_{44} = \mathcal{S}'_{1212} = \frac{P}{2}(a^2+b^2)I_{12} + \frac{R}{2}(I_1+I_2)\,, \quad \mathcal{S}'_{55} = \mathcal{S}'_{1313} = \frac{P}{2}(a^2+c^2)I_{13} + \frac{R}{2}(I_1+I_3)$$

$$\mathcal{S}'_{66} = \mathcal{S}'_{2323} = \frac{P}{2}(b^2+c^2)I_{23} + \frac{R}{2}(I_2+I_3) \tag{A.15}$$

$$\text{where} \quad P = \frac{3}{8\pi(1-\nu)} \quad \text{and} \quad R = \frac{1-2\nu}{8\pi(1-\nu)} \tag{A.16}$$

For tensor $\boldsymbol{\Pi}$ the only non-vanishing components are Π'_{1212}, Π'_{2323}, Π'_{3131} and those that occur from permutations of indices belonging in the first and second index pairs respectively (i.e., Π'_{2112}, Π'_{2121} etc.). Thus, since $\boldsymbol{\Pi}$ is antisymmetric in the first two and symmetric in the last two indices, the corresponding independent components that fully determine the latter tensor are:

$$\Pi'_{2121} = \frac{I_1 - I_2}{8\pi} \quad \text{and} \quad \Pi'_{3131} = \frac{I_1 - I_3}{8\pi} \tag{A.17}$$

Finally, for tensor $\boldsymbol{\mathcal{Q}}$ one has the following:

$$\mathcal{Q}'_{11} = \mathcal{Q}'_{1111} = \frac{\mu}{2\pi(1-\nu)}\left(4\pi - \frac{1}{2}I_1 - \frac{3a^2}{2}I_{11}\right)$$

$$\mathcal{Q}'_{22} = \mathcal{Q}'_{2222} = \frac{\mu}{2\pi(1-\nu)}\left(4\pi - \frac{1}{2}I_2 - \frac{3b^2}{2}I_{22}\right)$$

$$\mathcal{Q}'_{33} = \mathcal{Q}'_{3333} = \frac{\mu}{2\pi(1-\nu)}\left(4\pi - \frac{1}{2}I_3 - \frac{3c^2}{2}I_{33}\right)$$

$$\mathcal{Q}'_{12} = \mathcal{Q}'_{21} = \mathcal{Q}'_{1122} = \frac{\mu}{8\pi(1-\nu)}\Big[16\pi\nu + (1-4\nu)(I_1+I_2) - 3(a^2+b^2)I_{12}\Big]$$

$$\mathcal{Q}'_{13} = \mathcal{Q}'_{31} = \mathcal{Q}'_{1133} = \frac{\mu}{8\pi(1-\nu)}\Big[16\pi\nu + (1-4\nu)(I_1+I_3) - 3(a^2+c^2)I_{13}\Big]$$

$$\mathcal{Q}'_{23} = \mathcal{Q}'_{32} = \mathcal{Q}'_{2233} = \frac{\mu}{8\pi(1-\nu)}\Big[16\pi\nu + (1-4\nu)(I_2+I_3) - 3(b^2+c^2)I_{23}\Big]$$

$$\mathcal{Q}'_{44} = \mathcal{Q}'_{1212} = \mu - \frac{\mu}{8\pi(1-\nu)}\Big[(1-2\nu)(I_1+I_2) + 3(a^2+b^2)I_{12}\Big]$$

$$\mathcal{Q}'_{55} = \mathcal{Q}'_{1313} = \mu - \frac{\mu}{8\pi(1-\nu)}\Big[(1-2\nu)(I_1+I_3) + 3(a^2+c^2)I_{13}\Big]$$

$$\mathcal{Q}'_{66} = \mathcal{Q}'_{2323} = \mu - \frac{\mu}{8\pi(1-\nu)}\Big[(1-2\nu)(I_2+I_3) + 3(b^2+c^2)I_{23}\Big] \tag{A.18}$$

In (A.15) through (A.18), μ, ν denote the shear modulus and Poisson's ratio of the matrix respectively and the quantities I depend on the relative values between a, b and c as presented in the original work of Eshelby ([27]). Herein, the corresponding expressions for the parameters I are summarized once again, for the sake of completeness:

- $a > b > c$:

$$I_1 = \frac{4\pi abc}{(a^2-b^2)\sqrt{a^2-c^2}}\Big[F(\theta,k) - E(\theta,k)\Big]$$

$$I_2 = 4\pi - I_1 - I_3$$

$$I_3 = \frac{4\pi abc}{(b^2-c^2)\sqrt{a^2-c^2}}\left[\frac{b\sqrt{a^2-c^2}}{ac} - E(\theta,k)\right]$$

$$I_{12} = \frac{I_2-I_1}{3(a^2-b^2)}\,, \quad I_{13} = \frac{I_3-I_1}{3(a^2-c^2)}\,, \quad I_{23} = \frac{I_3-I_2}{3(b^2-c^2)}$$

$$I_{11} = \frac{4\pi}{3a^2} - I_{12} - I_{13}\,, \quad I_{22} = \frac{4\pi}{3b^2} - I_{12} - I_{23}\,, \quad I_{33} = \frac{4\pi}{3c^2} - I_{13} - I_{23} \tag{A.19}$$

- **Special Case I :** $a = b > c$:

$$I_1 = I_2 = \frac{2\pi a^2 c}{(a^2-c^2)^{3/2}}\left[\cos^{-1}\left(\frac{c}{a}\right) - \frac{c}{a}\sqrt{1-\frac{c^2}{a^2}}\right]$$

$$I_3 = 4\pi - 2I_1$$

$$I_{13} = I_{23} = \frac{I_3-I_1}{3(a^2-c^2)}\ ,\ I_{12} = \frac{\pi}{3a^2} - \frac{I_{13}}{4}$$

$$I_{11} = I_{22} = 3I_{12}\ ,\ I_{33} = \frac{4\pi}{3c^2} - I_{13} - I_{23} \tag{A.20}$$

- **Special Case II :** $a > b = c$:

$$I_1 = 4\pi - 2I_2$$

$$I_2 = I_3 = \frac{2\pi a c^2}{(a^2-c^2)^{3/2}}\left[\frac{a}{c}\sqrt{\frac{a^2}{c^2}-1} - \cosh^{-1}\left(\frac{a}{c}\right)\right]$$

$$I_{12} = I_{13} = \frac{I_2-I_1}{3(a^2-b^2)}\ ,\ I_{23} = \frac{\pi}{3b^2} - \frac{I_{12}}{4}$$

$$I_{11} = \frac{4\pi}{3a^2} - I_{12} - I_{13} \ , \ I_{22} = I_{33} = 3I_{23} \tag{A.21}$$

- **Special Case III :** $a = b = c$:

$$I_1 = I_2 = I_3 = \frac{4\pi}{3} \ , \quad I_{11} = I_{22} = I_{33} = \frac{4\pi}{5a^2} \ , \quad I_{12} = I_{13} = I_{23} = \frac{I_{11}}{3} \tag{A.22}$$

where

$$F(\theta, k) = \int_0^\theta \frac{1}{\sqrt{1 - k^2 \sin^2 \phi}} d\phi \quad , \quad E(\theta, k) = \int_0^\theta \sqrt{1 - k^2 \sin^2 \phi} d\phi$$

$$\text{with} \quad \theta = \sin^{-1} \sqrt{1 - \frac{c^2}{a^2}} \quad , \quad k = \frac{\sqrt{a^2 - b^2}}{\sqrt{a^2 - c^2}} \tag{A.23}$$

are elliptic integrals of the first and second kind respectively. Closing this summary, it is important to recall here, as pointed out in [20], that the latter procedure exhibits computational difficulties when a, b and c are simultaneously very close to unity. In this situation , a linear interpolation between the cases presented above is implemented for the calculation of the tensors $\boldsymbol{\mathcal{S}}$, $\boldsymbol{\Pi}$ and $\boldsymbol{\mathcal{Q}}$ in the following sense[4]:

- For $a = 1$ and b, $c \in [0.99, 1]$

$$\square(b, c) = \sum_{i=1}^{3} \square^{(i)} \cdot N_i(b, c)$$

$$N_1(b, c) = \frac{c - 0.99}{0.01} \ , \quad N_2(b, c) = \frac{b - c}{0.01} \ , \quad N_3(b, c) = \frac{1 - b}{0.01} \tag{A.24}$$

- For $1.01 > a > b = 1 > c > 0.99$

$$\square(a, c) = \sum_{i=1}^{4} \square^{(i)} \cdot N_i(a, c)$$

$$N_1(a, c) = \frac{(c - 0.99)(1.01 - a)}{0.0001} \ , \quad N_2(a, c) = \frac{(c - 0.99)(a - 1)}{0.0001}$$

$$N_3(a, c) = \frac{(1 - c)(a - 1)}{0.0001} \ , \quad N_4(a, c) = \frac{(1 - c)(1.01 - a)}{0.0001} \tag{A.25}$$

- For $a = 1$ and b, $c \in [0.99, 1]$

$$\square(a, b) = \sum_{i=1}^{3} \square^{(i)} \cdot N_i(a, b)$$

[4] In these expressions $\square$ denotes any of $\boldsymbol{\mathcal{S}}$, $\boldsymbol{\Pi}$ or $\boldsymbol{\mathcal{Q}}$

$$N_1(a,b) = \frac{1.01 - a}{0.01}\,, \quad N_2(a,b) = \frac{a - b}{0.01}\,, \quad N_3(a,b) = \frac{b - 1}{0.01} \tag{A.26}$$

Appendix B

Gradient Anisotropic Model: Complementary Calculations

B.1 Solution of the ODE for $\mathbf{F}^{\mathrm{v}}$

As mentioned in the description of the gradient anisotropic model presented in Chapter 4, update of the aspect ratios w_α, $\alpha = 1, 2$, and the orientation vectors $\mathbf{n}^{(i)}$, $i = 1, 2, 3$, of the representative local ellipsoid in the corresponding incremental procedure requires the solution of an initial value problem described by the ODE (4.31), which is once again recalled here for convenience:

$$\dot{\mathbf{F}}^{\mathrm{v}}(t) \cdot \mathbf{F}^{\mathrm{v}-1}(t) = (\boldsymbol{\mathcal{A}}(t) - \boldsymbol{\mathcal{C}}(t)) : \mathbf{D}^p(t) + \mathbf{W}(t) \tag{B.1a}$$

$$\text{I.C.} \quad \mathbf{F}^{\mathrm{v}}(0) = \mathbf{F}_0^{\mathrm{v}} = a_0 \mathbf{n}_0^{(1)} \mathbf{e}_1 + b_0 \mathbf{n}_0^{(2)} \mathbf{e}_2 + c_0 \mathbf{n}_0^{(3)} \mathbf{e}_3 \ , \ w_1|_0 = \frac{c_0}{a_0} \ , \ w_2|_0 = \frac{c_0}{b_0} \tag{B.1b}$$

where $(a_0,\ b_0,\ c_0)$, $(w_1|_0,\ w_2|_0)$ and $(\mathbf{n}_0^{(1)},\ \mathbf{n}_0^{(2)},\ \mathbf{n}_0^{(3)})$ are the semi-axes, aspect ratios and orientation vectors respectively of the initial ellipsoidal void and $(\mathbf{e}_1,\ \mathbf{e}_2,\ \mathbf{e}_3)$ are the unit vectors of the global Cartesian coordinate system. In following, in order to simplify the notation, all quantities are assumed to depend on t unless otherwise specified, and explicit reference to this dependence is dropped. Adopting the hypothesis that the Lagrangian triad is fixed within each increment of deformation, then according to (1.69) $\mathbf{D}^p = \mathbf{R} \cdot \dot{\mathbf{E}}^p \cdot \mathbf{R}^T$ and $\mathbf{W} = \dot{\mathbf{R}} \cdot \mathbf{R}^T$ hold and one can also define the rotation neutralized form of $\mathbf{F}^{\mathrm{v}}$ as:

$$\hat{\mathbf{F}}^{\mathrm{v}} = \mathbf{R}^T \cdot \mathbf{F}^{\mathrm{v}} \quad \Rightarrow \quad \mathbf{F}^{\mathrm{v}} = \mathbf{R} \cdot \hat{\mathbf{F}}^{\mathrm{v}} \tag{B.2}$$

where $\mathbf{R}$ is the rotation tensor associated with the right polar decomposition of $\Delta\mathbf{F}$ within each increment, which is defined by (4.46). Substitution of the latter expressions for $\mathbf{F}^{\mathrm{v}}$, $\mathbf{D}^p$ and $\mathbf{W}$ in (B.1a), now yields :

$$\left(\dot{\mathbf{R}} \cdot \hat{\mathbf{F}}^{\mathrm{v}} + \mathbf{R} \cdot \dot{\hat{\mathbf{F}}}^{\mathrm{v}}\right) \cdot \hat{\mathbf{F}}^{\mathrm{v}-1} \cdot \mathbf{R}^T = \dot{\mathbf{R}} \cdot \mathbf{R}^T + (\boldsymbol{\mathcal{A}} - \boldsymbol{\mathcal{C}}) : (\mathbf{R} \cdot \dot{\mathbf{E}}^p \cdot \mathbf{R}^T) \Rightarrow$$

$$\Rightarrow \dot{\mathbf{R}}\cdot\mathbf{R}^T+\mathbf{R}\cdot\dot{\hat{\mathbf{F}}}^{\mathrm{v}}\cdot\hat{\mathbf{F}}^{\mathrm{v}-1}\cdot\mathbf{R}^T=\dot{\mathbf{R}}\cdot\mathbf{R}^T+(\boldsymbol{\mathcal{A}}-\boldsymbol{\mathcal{C}}):(\mathbf{R}\cdot\dot{\mathbf{E}}^p\cdot\mathbf{R}^T)\Rightarrow$$
$$\Rightarrow \mathbf{R}\cdot\dot{\hat{\mathbf{F}}}^{\mathrm{v}}\cdot\hat{\mathbf{F}}^{\mathrm{v}-1}\cdot\mathbf{R}^T=(\boldsymbol{\mathcal{A}}-\boldsymbol{\mathcal{C}}):(\mathbf{R}\cdot\dot{\mathbf{E}}^p\cdot\mathbf{R}^T)$$

Pre and post multiplying last expression with $\mathbf{R}^T$ and $\mathbf{R}$ respectively one gets:

$$\dot{\hat{\mathbf{F}}}^{\mathrm{v}}\cdot\hat{\mathbf{F}}^{\mathrm{v}-1}=\mathbf{R}^T\cdot\Big[(\boldsymbol{\mathcal{A}}-\boldsymbol{\mathcal{C}}):(\mathbf{R}\cdot\dot{\mathbf{E}}^p\cdot\mathbf{R}^T)\Big]\cdot\mathbf{R} \tag{B.3}$$

In order to further proceed, one needs to reduce (B.3) to a more straight forward integrable form. As is readily shown bellow, this can be achieved by taking advantage of the mathematical isotropy of $\boldsymbol{\mathcal{A}}$ and $\boldsymbol{\mathcal{C}}$. Indeed, with no loss of generality, consider the evaluation of the first term of the right hand side of (B.3) involving $\boldsymbol{\mathcal{A}}$, by employing indicial notation:

$$\Big\{\mathbf{R}^T\cdot\Big[\boldsymbol{\mathcal{A}}:(\mathbf{R}\cdot\dot{\mathbf{E}}^p\cdot\mathbf{R}^T)\Big]\cdot\mathbf{R}\Big\}_{ij}=R^T_{ik}\Big[\boldsymbol{\mathcal{A}}:(\mathbf{R}\cdot\dot{\mathbf{E}}^p\cdot\mathbf{R}^T)\Big]_{kl}R_{lj}=$$
$$=R^T_{ik}\mathcal{A}_{klmn}(\mathbf{R}\cdot\dot{\mathbf{E}}^p\cdot\mathbf{R}^T)_{mn}R_{lj}=R^T_{ik}\mathcal{A}_{klmn}(R_{mp}\dot{E}^p_{pq}R^T_{qn})R_{lj}=R_{ki}R_{lj}R_{mp}R_{nq}\mathcal{A}_{klmn}\dot{E}^p_{pq}=$$
$$=R^T_{ik}R^T_{jl}R^T_{pm}R^T_{qn}\mathcal{A}_{klmn}\dot{E}^p_{pq}=\hat{\mathcal{A}}_{ijpq}\dot{E}^p_{pq} \tag{B.4}$$

Equation (B.4) implies that $\boldsymbol{\mathcal{A}}$ is an isotropic function of its arguments with $\hat{\mathcal{A}}_{ijpq}=R^T_{ik}R^T_{jl}R^T_{pm}R^T_{qn}\mathcal{A}_{klmn}$. Similarly, it can be proved that $\boldsymbol{\mathcal{C}}$ is also an isotropic function so that $\hat{\mathcal{C}}_{ijpq}=R^T_{ik}R^T_{jl}R^T_{pm}R^T_{qn}\mathcal{C}_{klmn}$. Then, equation (B.3) can now be written as:

$$\dot{\hat{\mathbf{F}}}^{\mathrm{v}}\cdot\hat{\mathbf{F}}^{\mathrm{v}-1}=(\hat{\boldsymbol{\mathcal{A}}}-\hat{\boldsymbol{\mathcal{C}}}):\dot{\mathbf{E}}^p\Rightarrow\dot{\hat{\mathbf{F}}}^{\mathrm{v}}=\Big[(\hat{\boldsymbol{\mathcal{A}}}-\hat{\boldsymbol{\mathcal{C}}}):\dot{\mathbf{E}}^p\Big]\cdot\mathbf{F}^{\mathrm{v}}\Rightarrow$$
$$\Rightarrow\ \frac{d\hat{\mathbf{F}}^{\mathrm{v}}}{dt}-\mathbf{H}\cdot\hat{\mathbf{F}}^{\mathrm{v}}=\mathbf{0}\ \text{ with }\ \mathbf{H}=(\hat{\boldsymbol{\mathcal{A}}}-\hat{\boldsymbol{\mathcal{C}}}):\dot{\mathbf{E}}^p \tag{B.5}$$

Although no approximations have been made so far for the derivation of (B.5), integration of the latter, homogeneous 1st order tensorial ODE for $\hat{\mathbf{F}}^{\mathrm{v}}$ over the increment $[t_n,t_{n+1}]$ can be carried out exactly only if the second order tensor $\mathbf{H}$ is constant. Assuming that $\dot{\mathbf{E}}^p$ is constant over the increment and approximating $\mathbf{H}$ with its value at the beginning of the increment[1], i.e., $\mathbf{H}\approx\mathbf{H}_n=(\boldsymbol{\mathcal{A}}_n-\boldsymbol{\mathcal{C}}_n):\dot{\mathbf{E}}^p=ct$, the general solution of the (B.5) is given as (see [9]):

$$\hat{\mathbf{F}}^{\mathrm{v}}(t)=\Big[\exp\Big((t-t_n)(\boldsymbol{\mathcal{A}}_n-\boldsymbol{\mathcal{C}}_n):\dot{\mathbf{E}}^p\Big)\Big]\cdot\hat{\mathbf{F}}^{\mathrm{v}}_n\ ,\ t\in[t_n,t_{n+1}] \tag{B.6}$$

Taking into account that over the increment $\Delta\mathbf{E}^p=(t_{n+1}-t_n)\dot{\mathbf{E}}^p$, evaluation of (B.6) at the end of the increment yields:

$$\boxed{\hat{\mathbf{F}}^{\mathrm{v}}_{n+1}=\hat{\mathbf{F}}^{\mathrm{v}}(t_{n+1})=\Big[\exp(\mathbf{M})\Big]\cdot\hat{\mathbf{F}}^{\mathrm{v}}_n\quad\text{where}\quad\mathbf{M}=(\boldsymbol{\mathcal{A}}_n-\boldsymbol{\mathcal{C}}_n):\Delta\mathbf{E}^p} \tag{B.7}$$

[1]Recalling that $\hat{\boldsymbol{\mathcal{A}}}_n=\boldsymbol{\mathcal{A}}_n$ and $\hat{\boldsymbol{\mathcal{C}}}_n=\boldsymbol{\mathcal{C}}_n$.

Furthermore, as stated in Section 1.3 for the polar decomposition of the deformation gradient, the principal directions and the corresponding principal lengths, at the current configuration, of any material point of the continuum body coincide with the eigenvectors and eigenvalues respectively of the Eulerian stretch tensor $\mathbf{V}$, which in turn is associated with the left Cauchy-Green tensor $\mathbf{B}$ by (1.26). Then, in a similar manner, the principal directions and the corresponding semi-lengths[2] of the local ellipsoid, i.e., ($\hat{\mathbf{n}}^{(1)}_{n+1}$, $\hat{\mathbf{n}}^{(2)}_{n+1}$, $\hat{\mathbf{n}}^{(3)}_{n+1}$) and ($a_{n+1}$, b_{n+1}, c_{n+1}), instantaneously coincide with the eigenvectors and eigenvalues of the left Cauchy-Green tensor $\hat{\mathbf{B}}^{\mathrm{v}}_{n+1}$ associated with the corresponding deformation gradient of the voids $\hat{\mathbf{F}}^{\mathrm{v}}_{n+1}$ at the end of the increment (i.e., at the current configuration). The latter observation implies that the shape and orientation of the RLEV can be updated by solving the corresponding eigenvalue problem associated with tensor $\hat{\mathbf{B}}^{\mathrm{v}}_{n+1}$, which can then be written in the following spectral representation:

$$\hat{\mathbf{B}}^{\mathrm{v}}_{n+1} = \hat{\mathbf{F}}^{\mathrm{v}}_{n+1} \cdot (\hat{\mathbf{F}}^{\mathrm{v}}_{n+1})^T = a^2_{n+1}\hat{\mathbf{n}}^{(1)}_{n+1}\hat{\mathbf{n}}^{(1)}_{n+1} + b^2_{n+1}\hat{\mathbf{n}}^{(2)}_{n+1}\hat{\mathbf{n}}^{(2)}_{n+1} + c^2_{n+1}\hat{\mathbf{n}}^{(3)}_{n+1}\hat{\mathbf{n}}^{(3)}_{n+1}$$

$$\text{and} \qquad \boxed{w_1|_{n+1} = \frac{c_{n+1}}{a_{n+1}} \quad , \quad w_2|_{n+1} = \frac{c_{n+1}}{b_{n+1}}} \tag{B.8}$$

With ($\hat{\mathbf{n}}^{(1)}_{n+1}$, $\hat{\mathbf{n}}^{(2)}_{n+1}$, $\hat{\mathbf{n}}^{(3)}_{n+1}$) and $\hat{\mathbf{F}}^{\mathrm{v}}_{n+1}$ known, one can now calculate $\mathbf{n}^{(i)}_{n+1}$ and $\mathbf{F}^{\mathrm{v}}_{n+1}$ using (4.90) and (B.2). What is important to note here is that calculation of $\hat{\mathbf{F}}^{\mathrm{v}}_{n+1}$ by (B.7) requires information about $\hat{\mathbf{F}}^{\mathrm{v}}$ at the start of the increment, i.e., about $\hat{\mathbf{F}}^{\mathrm{v}}_{n}$, and this suggests that $\mathbf{F}^{\mathrm{v}}$ should also be stored as a state variable in the material calculations at the end of every increment. In addition, the exponential of the second order tensor $\mathbf{M}$ is required for the calculation of $\hat{\mathbf{F}}^{\mathrm{v}}_{n+1}$ in (B.7), which is defined by the expression ([9]):

$$\boxed{\exp(\mathbf{M}) = \boldsymbol{\delta} + \mathbf{M} + \frac{1}{2!}\mathbf{M}^2 + \frac{1}{3!}\mathbf{M}^3 + \cdots = \sum_{n=0}^{\infty}\frac{1}{n!}\mathbf{M}^n} \tag{B.9}$$

[2] Or more precisely their squared values.

B.2 Newton Loop for $\Delta\bar{\varepsilon}^p$ and Δf_{loc}

Solution of the system of nonlinear equations (4.77) for the corrections $\Delta(\Delta\lambda)$ and $\Delta(\Delta\mathbf{E}^p)$ at every iteration requires the calculation of $\tilde{\Phi}$ and $\mathbf{G}$ at the end of the corresponding increment. For this purpose, among other quantities, one needs to calculate $\bar{\varepsilon}^p_{n+1}$ and $f_{\text{loc}}|_{n+1}$ from (4.69) and (4.70). Since information at the start of the increment is known (i.e., $\bar{\varepsilon}^p_n$ and $f_{\text{loc}}|_n$ are known), the updating procedure of f_{loc} and $\bar{\varepsilon}^p$ is ultimately reduced to the calculation of the corresponding variations $\Delta\bar{\varepsilon}^p$ and Δf_{loc}, which are given as:

$$\Delta\bar{\varepsilon}^p = \frac{A_{n+1}}{(1-f)\sigma_y(\bar{\varepsilon}^p_n + \Delta\bar{\varepsilon}^p)}, \quad A_{n+1}(\Delta\lambda, \Delta\mathbf{E}^p) = \hat{\boldsymbol{\sigma}}_{n+1}(\Delta\lambda, \Delta\mathbf{E}^p) : \Delta\mathbf{E}^p \tag{B.10a}$$

$$\hat{\boldsymbol{\sigma}}_{n+1} = \boldsymbol{\sigma}^e - \boldsymbol{\mathcal{L}}^e_n : \Delta\mathbf{E}^p + \Delta\lambda\mathbf{R}_1, \quad \mathbf{R}_1 = \boldsymbol{\sigma}_n \cdot \boldsymbol{\Omega}^p_n - \boldsymbol{\Omega}^p_n \cdot \boldsymbol{\sigma}_n \tag{B.10b}$$

$$\Delta f_{\text{loc}} = (1-f)\boldsymbol{\delta} : \Delta\mathbf{E}^p + \mathcal{T}(\bar{\varepsilon}^p_n + \Delta\bar{\varepsilon}^p)\Delta\bar{\varepsilon}^p \tag{B.10c}$$

where $\Delta\lambda$, $\Delta\mathbf{E}^p$ are known for the current iteration. Notice that, due the fact that backward Euler integration is used for the evolution equations of $\bar{\varepsilon}^p$ and f_{loc}, the corresponding expression (B.10a) is nonlinear in $\Delta\bar{\varepsilon}^p$ and thus, a numerical method is implemented for its evaluation. More specifically, a Newton-Raphson iterative procedure is used for the solution of the following nonlinear equation for $\Delta\bar{\varepsilon}^p$:

$$F(\Delta\bar{\varepsilon}^p) = \Delta\bar{\varepsilon}^p - \frac{A_{n+1}}{(1-f)\sigma_y(\bar{\varepsilon}^p_n + \Delta\bar{\varepsilon}^p)} = 0 \tag{B.11}$$

Assuming that at any iteration of the method $\Delta\bar{\varepsilon}^p$ is known from the previous, non-converged iteration, one can calculate $\hat{\boldsymbol{\sigma}}_{n+1}$ and A_{n+1} from (B.10a), (B.10b) and (B.11) is checked for convergence. If convergence is not achieved, the correction for $\Delta\bar{\varepsilon}^p$ can be calculated from:

$$\Delta(\Delta\bar{\varepsilon}^p) = -\left(\frac{dF}{d(\Delta\bar{\varepsilon}^p)}\right)^{-1} F(\Delta\bar{\varepsilon}^p) \tag{B.12}$$

where $\frac{dF}{d(\Delta\bar{\varepsilon}^p)}$ is the jacobian of the method which is calculated as follows:

$$\begin{aligned}
\frac{dF}{d(\Delta\bar{\varepsilon}^p)} \equiv \frac{dF}{d\bar{\varepsilon}^p} &= 1 - \frac{\frac{dA_{n+1}}{\bar{\varepsilon}^p}(1-f)\sigma_y(\bar{\varepsilon}^p_n + \Delta\bar{\varepsilon}^p) - A_{n+1}\frac{d}{d\bar{\varepsilon}^p}[(1-f)\sigma_y(\bar{\varepsilon}^p_n + \Delta\bar{\varepsilon}^p)]}{(1-f)^2\sigma_y^2(\bar{\varepsilon}^p_n + \Delta\bar{\varepsilon}^p)} = \\
&= 1 + \frac{A_{n+1}(1-f)\frac{d\sigma_y}{d\bar{\varepsilon}^p}}{(1-f)^2\sigma_y^2} \Rightarrow \\
&\Rightarrow \boxed{\frac{dF}{d(\Delta\bar{\varepsilon}^p)} = 1 + \frac{A_{n+1}}{(1-f)\sigma_y^2}\frac{d\sigma_y}{d\bar{\varepsilon}^p}}
\end{aligned} \tag{B.13}$$

With the correction $\Delta(\Delta\bar{\varepsilon}^p)$ known, $\Delta\bar{\varepsilon}^p$ is updated to its new value and the procedure is

repeated until convergence is achieved. The algorithm described above is summarized in Table B.1.

Table B.1: The Newton-Raphson algorithm for the iterative calculation of $\Delta\bar{\varepsilon}^p$

1. Set $k = 0$.

2. Given $(\Delta\bar{\varepsilon}^p)^{(k)}$, calculate $F[(\Delta\bar{\varepsilon}^p)^{(k)}]$ from (B.11).

3. If $F[(\Delta\bar{\varepsilon}^p)^{(k)}] \leq \text{TOL}$, then GOTO **4.** Else GOTO **i.**

- **i.** Calculate $(\frac{dF}{d(\Delta\bar{\varepsilon}^p)})^{(k)}$ from (B.13).
- **ii.** Solve equation (B.12) for the correction $\Delta(\Delta\bar{\varepsilon}^p)$
- **iii.** Calculate $(\Delta\bar{\varepsilon}^p)^{(k+1)} = (\Delta\bar{\varepsilon}^p)^{(k)} + \Delta(\Delta\bar{\varepsilon}^p)$.
- **iv.** Set $k \leftarrow k + 1$ and GOTO **2.**.

4. Solution has converged. Set $\Delta\bar{\varepsilon}^p = (\Delta\bar{\varepsilon}^p)^{(k)}$ and exit.

After convergence is achieved, Δf_{loc} can also be calculated using (B.10c). It is important to point out here that in order to initiate the method, a first estimate for $\Delta\bar{\varepsilon}^p$ needs to be selected. One can always use the $\Delta\bar{\varepsilon}^p$ derived from the forward Euler integration of $\dot{\bar{\varepsilon}}^p$ but an alternative choice is the one that emerges from the linearization of (B.10a). In this direction, one can rewrite the latter equation in the form:

$$\Delta\bar{\varepsilon}^p = \frac{\hat{\boldsymbol{\sigma}}_{n+1} : \Delta\mathbf{E}^p}{(1-f)\sigma_y(\bar{\varepsilon}^p_n + \Delta\bar{\varepsilon}^p)} \equiv \frac{B}{\sigma_y(\bar{\varepsilon}^p_n + \Delta\bar{\varepsilon}^p)} \quad \text{where} \quad B = \frac{\hat{\boldsymbol{\sigma}}_{n+1} : \Delta\mathbf{E}^p}{(1-f)} \tag{B.14}$$

Linearization of the term $1/\sigma_y(\bar{\varepsilon}^p_n + \Delta\bar{\varepsilon}^p)$ yields:

$$\frac{1}{\sigma_y(\bar{\varepsilon}^p_n + \Delta\bar{\varepsilon}^p)} \approx \frac{1}{\sigma_y|_n + h_n\Delta\bar{\varepsilon}^p} = \frac{1}{\sigma_y|_n}\frac{1}{1+\frac{h_n}{\sigma_y|_n}\Delta\bar{\varepsilon}^p} \approx \frac{1}{\sigma_y|_n}\left(1 - \frac{h_n}{\sigma_y|_n}\Delta\bar{\varepsilon}^p\right) \tag{B.15}$$

where a Taylor expansion of σ_y around $\Delta\bar{\varepsilon}^p$ and the property $\frac{1}{1+\varepsilon} \approx 1 - \varepsilon$ where used. Substitution of (B.15) to (B.14) leads to the following first estimate for $\Delta\bar{\varepsilon}^p$:

$$\Delta\bar{\varepsilon}^p = \frac{1}{\frac{\sigma_y|_n}{B} + \frac{h_n}{\sigma_y|_n}} \quad \text{with} \quad h_n = \left.\frac{d\sigma_y}{d\bar{\varepsilon}^p}\right|_n \tag{B.16}$$

Appendix C

FEM for Dynamic Analysis

As pointed out in Chapter 5, in the general case where dynamic phenomena are to be taken into account, the equations of motion need to be integrated instead of the usual equilibrium equations. Depending on the nature and physics of the underlying problem, i.e., depending on whether or not inertial phenomena[1] are important compared to static ones, an appropriate dynamic integration operator ([2]) has to be selected for the solution of the equations of motion. Dynamic integration operators can generally be subdivided into two major categories, namely the *implicit* and *explicit* operators. In the former case, the integration scheme implemented is uncondionally stable but, due to the fact that dynamic quantities at t_{n+1} depend on the same quantites which are also evaluated time t_{n+1}, nonlinear equations which need to be solved iteratively emerge, resulting in high computational costs. On the other hand, although explicit schemes used for the evaluation of quantities at time t_{n+1} require information of the involving quantities solely at time t_n (a fact that implies improved computational efficiency) they are, nonetheless, conditionally stable[2]. In structural applications[3], such as the ones examined in Chapter 6, implicit schemes can give acceptable solutions, if relatively small increments are selected. Thus, in the context of an implicit scheme, discretization of the corresponding dynamic mixed BVP using the finite element approximation, leads to the derivation of the nonlinear system of algebraic equations (5.25), which is restated bellow in its global form:

$$\Big\{R_{\mathrm{D}}(\Big\{D\Big\})\Big\}_{n+1} = -\Big[M\Big]_{n+1}\Big\{\ddot{D}\Big\}_{n+1} + \Big\{R_{\mathrm{S}}(\Big\{D\Big\})\Big\}_{n+1} = \Big\{0\Big\} \tag{C.1a}$$

$$\text{with} \quad \Big\{R_{\mathrm{S}}(\Big\{D\Big\})\Big\}_{n+1} = \Big\{F_{\mathrm{ext}}\Big\}_{n+1} - \Big\{F_{\mathrm{int}}(\Big\{D\Big\})\Big\}_{n+1} \tag{C.1b}$$

[1] Such phenomena are related to acceleration wave propagation within the continuum body.

[2] This suggests that the effectiveness of the method severely depends on the size of the selected time increment which may result in even heavier computational costs compared to implicit methods if a very small time increment must be used. However, problems with a significant number of degrees of freedom with relatively short dynamic response times can only be efficiently approached using explicit schemes due to the large number of equations that would need to be solved in an iterative implicit scheme.

[3] i.e., applications where external loads are applied statically or quasi-statically.

where $\left\{\ddot{D}\right\}$ is the global acceleration vector. Herein, the solution procedure is based on the implicit Hilber-Hughes-Taylor (HHT) operator[4] first proposed in [34] which substitutes the static residual in (C.1a) at the end of the increment with a weighted average of the latter at the beginning and end of time step, controlled by the damping parameter α, i.e.,

$$\left\{R_{\mathrm{D}}(\left\{D\right\})\right\}_{n+1} = -\left[M\right]_{n+1}\left\{\ddot{D}\right\}_{n+1} + (1+\alpha)\left\{R_{\mathrm{S}}(\left\{D\right\})\right\}_{n+1} - \alpha\left\{R_{\mathrm{S}}(\left\{D\right\})\right\}_{n} = \left\{0\right\} \tag{C.2a}$$

$$\text{with I.C.} \qquad \left\{D\right\}(t_0) = \left\{D\right\}_0 \tag{C.2b}$$

$$\left\{\dot{D}\right\}(t_0) = \left\{\dot{D}\right\}_0 \tag{C.2c}$$

$$\text{and} \quad \left\{\ddot{D}\right\}(t_0) \;:\; \left[M\right]\left\{\ddot{D}\right\}_0 = \left\{R_{\mathrm{S}}\right\}_0 \tag{C.2d}$$

Solution of the system of nonlinear equations (C.2a) is carried out using the Newton-Raphson method and the corresponding acceleration vector can then be calculated from the HHT approach. Implementation of the method is as follows.

To begin with, consider the Taylor expansions of $\left\{D\right\}_{n+1}, \left\{\dot{D}\right\}_{n+1}$ and $\left\{\ddot{D}\right\}_{n+1}$ as:

$$\left\{D\right\}_{n+1} = \left\{D\right\}_{n} + \left\{\dot{D}\right\}_{n}\Delta t + \left\{\ddot{D}\right\}_{n}\frac{\Delta t^2}{2} + \left\{\dddot{D}\right\}_{n}\frac{\Delta t^3}{6} + \cdots \tag{C.3}$$

$$\left\{\dot{D}\right\}_{n+1} = \left\{\dot{D}\right\}_{n} + \left\{\ddot{D}\right\}_{n}\Delta t + \left\{\dddot{D}\right\}_{n}\frac{\Delta t^2}{2} + \cdots \tag{C.4}$$

$$\left\{\ddot{D}\right\}_{n+1} = \left\{\ddot{D}\right\}_{n} + \left\{\dddot{D}\right\}_{n}\Delta t + \left\{\overset{(4)}{D}\right\}_{n}\frac{\Delta t^2}{2} + \cdots \tag{C.5}$$

Neglecting higher order terms in (C.5), $\left\{\dddot{D}\right\}_n$ can be approximated as:

$$\left\{\dddot{D}\right\}_{n} \approx \frac{\left\{\ddot{D}\right\}_{n+1} - \left\{\dot{D}\right\}_{n}}{\Delta t} \tag{C.6}$$

Moreover, introducing the so-called Newmark parameters β and γ, one can truncate the series (C.3) and (C.4) to get:

$$\left\{D\right\}_{n+1} \approx \left\{D\right\}_{n} + \left\{\dot{D}\right\}_{n}\Delta t + \left\{\ddot{D}\right\}_{n}\frac{\Delta t^2}{2} + \left\{\dddot{D}\right\}_{n}\beta\Delta t^3 \tag{C.7}$$

$$\left\{\dot{D}\right\}_{n+1} \approx \left\{\dot{D}\right\}_{n} + \left\{\ddot{D}\right\}_{n}\Delta t + \left\{\dddot{D}\right\}_{n}\gamma\Delta t^2 \tag{C.8}$$

[4]It should be mentioned that this operator is second order accurate and also introduces controllable numerical damping of high frequency numerical "noise" which may enter the solution due to accumulation of round-off errors or due to automatic time increment changes.

Substituting (C.6) into (C.7), (C.8) and grouping the corresponding terms, one can arrive to the following expressions for $\left\{D\right\}_{n+1}, \left\{\dot{D}\right\}_{n+1}$:

$$\left\{D\right\}_{n+1} = \left\{D\right\}_{n} + \left\{\dot{D}\right\}_{n} \Delta t + \left[\left(\frac{1}{2} - \beta\right)\left\{\ddot{D}\right\}_{n} + \beta\left\{\ddot{D}\right\}_{n+1}\right]\Delta t^2 \tag{C.9}$$

$$\left\{\dot{D}\right\}_{n+1} \approx \left\{\dot{D}\right\}_{n} + \left[(1-\gamma)\left\{\ddot{D}\right\}_{n} + \gamma\left\{\ddot{D}\right\}_{n+1}\right]\Delta t \tag{C.10}$$

where, in view of the HHT method, Newmark's parameters β, γ are related to the numerical damping parameter α as:

$$\beta = \frac{1}{4}(1-\alpha)^2 \ , \ \gamma = \frac{1}{2} - \alpha, \quad \text{with} \quad -\frac{1}{2} \leq \alpha \leq 0 \tag{C.11}$$

Linearization of (C.9), (C.10) also yields:

$$d\left\{D\right\}_{n+1} = \beta\Delta t^2 \, d\left\{\ddot{D}\right\}_{n+1} \quad \text{and} \quad d\left\{\dot{D}\right\}_{n+1} = \gamma\Delta t \, d\left\{\ddot{D}\right\}_{n+1} \tag{C.12}$$

Back to the Newton-Raphson method, if k is the previous unconverged iteration, the dynamic residual $\left\{R_{\mathrm{D}}\right\}_{n+1}^{(k+1)}$ at $k+1$ can be expanded in an infinite series as:

$$\left\{R_{\mathrm{D}}\right\}_{n+1}^{(k+1)} = \left\{R_{\mathrm{D}}\right\}_{n+1}^{(k)} + \left.\frac{\partial\left\{R_{\mathrm{D}}\right\}_{n+1}}{\partial\left\{D\right\}_{n+1}}\right|_{\left\{D\right\}_{n+1}^{(k)}} \left(\left\{D\right\}_{n+1}^{(k+1)} - \left\{D\right\}_{n+1}^{(k)}\right) + O\left[\left(\left\{D\right\}_{n+1}^{(k+1)} - \left\{D\right\}_{n+1}^{(k)}\right)^2\right] \Rightarrow$$

$$\Rightarrow \left\{R_{\mathrm{D}}\right\}_{n+1}^{(k+1)} \approx \left\{R_{\mathrm{D}}\right\}_{n+1}^{(k)} + \left.\frac{\partial\left\{R_{\mathrm{D}}\right\}_{n+1}}{\partial\left\{D\right\}_{n+1}}\right|_{\left\{D\right\}_{n+1}^{(k)}} \left\{\Delta D\right\} \tag{C.13}$$

with the latter suggesting a first order approximation for the residual at $k+1$. Now, for convergence of the solution at $k+1$ iteration, $\left\{R_{\mathrm{D}}\right\}_{n+1}^{(k+1)} = \left\{0\right\}$ must hold, which implies that the latter equation leads to:

$$\left\{R_{\mathrm{D}}\right\}_{n+1}^{(k)} = -\left.\frac{\partial\left\{R_{\mathrm{D}}\right\}_{n+1}}{\partial\left\{D\right\}_{n+1}}\right|_{\left\{D\right\}_{n+1}^{(k)}} \left\{\Delta D\right\} \equiv \left[K_{\mathrm{D}}\right]_{n+1}^{(k)} \left\{\Delta D\right\} \tag{C.14}$$

where $\left[K_{\mathrm{D}}\right]$ is the dynamic Jacobian matrix. For the derivation of the latter Jacobian, one first has to differentiate (C.2a) with respect to $\left\{D\right\}_{n+1}$ to get:

$$\frac{\partial\{R_{\mathrm{D}}\}_{n+1}}{\partial\{D\}_{n+1}} = -[M]_{n+1}\frac{\partial\{\ddot{D}\}_{n+1}}{\partial\{D\}_{n+1}} + (1+\alpha)\frac{\partial\{R_{\mathrm{S}}\}_{n+1}}{\partial\{D\}_{n+1}} \tag{C.15}$$

Using $(C.12)_1$ and recalling the definition of the static Jacobian matrix (see (5.28)), (C.15) becomes:

$$\frac{\partial\{R_{\mathrm{D}}\}_{n+1}}{\partial\{D\}_{n+1}} = -[M]_{n+1}\frac{1}{\beta\Delta t^2} - (1+\alpha)[K_{\mathrm{S}}]_{n+1} \tag{C.16}$$

Finally, by combining (C.14), (C.16) ,the linear system that has to be solved for the corrections $\{\Delta D\}$ of the global unknown vector can be written in the following form:

$$\boxed{\begin{gathered}[K_{\mathrm{D}}]^{(k)}_{n+1}\{\Delta D\} = \{R_{\mathrm{D}}\}^{(k)}_{n+1} \\ [K_{\mathrm{D}}]^{(k)}_{n+1} = [M]_{n+1}\frac{1}{\beta\Delta t^2} + (1+\alpha)[K_{\mathrm{S}}]^{(k)}_{n+1} \\ [K_{\mathrm{D}}]^{(k)}_{n+1} = \mathop{\mathsf{A}}_{e}[k^e_{\mathrm{D}}]^{(k)}_{n+1}\ ,\ \{R_{\mathrm{D}}\}^{(k)}_{n+1} = \mathop{\mathsf{A}}_{e}\{r^e_{\mathrm{D}}\}^{(k)}_{n+1}\ , \\ [M]_{n+1} = \mathop{\mathsf{A}}_{e}[m^e]_{n+1}\end{gathered}} \tag{C.17}$$

The Newton-Raphson procedure presented above for the solution of dynamic problems is summarized in Table C.1.

Table C.1: Summary of the Newton-Raphson algorithm for the solution of transient problems

1. Set $k = 0$.

2. Given $\{D\}^{(k)}_{n+1}, \{\ddot{D}\}^{(k)}_{n+1}$, calculate $\{R_{\mathrm{D}}\}^{(k)}_{n+1}$ from (C.2a).

3. If $\{R_{\mathrm{D}}\}^{(k)}_{n+1} \leq$ TOL, then GOTO **4.** Else GOTO **i.**

- **i.** Calculate $[K_{\mathrm{D}}]^{(k)}_{n+1}$ from $(C.17)_1$
- **ii.** Solve the system (C.17) for the corrections $\{\Delta D\}$
- **iii.** Calculate $\{D\}^{(k+1)}_{n+1}, \{\ddot{D}\}^{(k+1)}_{n+1}$ using (C.12)
- **iv.** Set $k \leftarrow k+1$ and GOTO **2.**

4. Solution has converged. Set $\{D\}_{n+1} = \{D\}^{(k+1)}_{n+1}$, $\{\ddot{D}\}_{n+1} = \{\ddot{D}\}^{(k+1)}_{n+1}$ and exit.

As already mentioned, although implicit methods are unconditionally stable and relatively larger (compared to explicit schemes) time increments can be used, accuracy problems may appear as the solution of the problem progresses. For this purpose, the "half-increment residual" method described in [33] for adaptive time incrementation may be used in order to constantly properly adjust the time increment, depending on the "quality of equilibrium" at the duration of the increment ([2]). To be precise, after normal calculations concerning the derivation of the solution at t_{n+1} are carried out, one can calculate the "half-increment residual" as:

$$\boxed{\left\{R_{\mathrm{D}}\right\}_{n+1/2} = \left[M\right]\left\{\ddot{D}\right\}_{n+1/2} + (1+\alpha)\left\{R_{\mathrm{S}}\right\}_{n+1/2} - \frac{\alpha}{2}\left(\left\{R_{\mathrm{S}}\right\}_{n} + \left\{R_{\mathrm{S}}\right\}_{n-1}\right)} \tag{C.18}$$

where $n-1$ denotes the time at the start of the previous step and $\left\{D\right\}_{n+1/2}, \left\{\ddot{D}\right\}_{n+1/2}$ can be calculated by using (C.9), (C.10) and assuming linear variation of acceleration within the time increment. The time step of the next increment is then adjusted depending on the value of $\max_{i=1,\cdots,\mathrm{TDOF}} |\left\{R_{\mathrm{D}}\right\}_{n+1/2}|$, where TDOF is the number of the total degrees of freedom of the problem.